

# UC Irvine

## UC Irvine Electronic Theses and Dissertations

### Title

Mesenchymal Stem Cell Applications to Treat Inflammatory Diseases and Cancer

### Permalink

<https://escholarship.org/uc/item/5539h8v3>

### Author

Farhoodi, Henry Patrick

### Publication Date

2021

### Copyright Information

This work is made available under the terms of a Creative Commons Attribution License, available at <https://creativecommons.org/licenses/by/4.0/>

Peer reviewed|Thesis/dissertation

UNIVERSITY OF CALIFORNIA, IRVINE

Mesenchymal Stem Cell Applications to Treat

Inflammatory Diseases and Cancer

DISSERTATION

submitted in partial satisfaction of the requirements for the degree of

DOCTOR OF PHILOSOPHY

in Pharmaceutical Sciences

By

Henry Farhoodi

Dissertation Committee:  
Associate Professor Weian Zhao, Chair  
Professor Young-Jik Kwon  
Professor Andrej Luptak

Figure 1.1 of Chapter 1 © 2019 The Authors. Published by Springer Nature.  
An elastic-net logistic regression approach to generate classifiers and gene signatures for types of immune cells and T helper cell subsets.  
Author: Arezo Torang et al.  
Publication: BMC Bioinformatics  
Publisher: Springer Nature  
Date: Aug 2019  
**Note:** This is an open access article distributed under the terms of the Creative Commons CC-BY license, which permits unrestricted use, distribution, and reproduction in any medium, provided the original work is properly cited.

Figure 1.2 of Chapter 1 © 2014 The Authors. Published by Frontiers.  
The role of the immune response in Chlamydia trachomatis infection of the male genital tract: a double-edged sword.  
Author: Kate A. Redgrove and Eileen A. McLaughlin  
Publication: Frontiers in Immunology  
Publisher: Frontiers  
Date: Oct 2014  
**Note:** This is an open access article distributed under the terms of the Creative Commons CC-BY license, which permits unrestricted use, distribution, and reproduction in any medium, provided the original work is properly cited.

Figure 1.3 of Chapter 1 © 2013 by Elsevier Inc. All rights reserved.  
Genetic Variants Regulating Immune Cell Levels in Health and Disease  
Author: Valeria Orru et al.  
Publication: Cell  
Publisher: Elsevier  
Date: Sept. 2013  
**Note:** Permission obtained for this content by Copywrite Clearance Center.

Chapter 2 and part of Chapter 7 © 2020 The Authors. Published by Elsevier.  
Optimization of a syngeneic murine model of bone metastasis.  
Author: Henry P. Farhoodi, Aude I. Segaliny, Zachary W. Wagoner, Jason L. Cheng, Linan Liu, Weian Zhao.  
Publication: Journal of Bone Oncology  
Publisher: Elsevier  
Date: August 2020  
**Note:** This is an open access article distributed under the terms of the Creative Commons CC-BY license, which permits unrestricted use, distribution, and reproduction in any medium, provided the original work is properly cited.

Chapter 3 and part of Chapter 7 © 2019 The Authors. Published by Elsevier B.V.  
Combinatorial targeting of cancer bone metastasis using mRNA engineered stem cells.  
Author: Aude I. Segaliny, Jason L. Cheng, Henry P. Farhoodi, Michael Toledano, Chih Chun Yu, Beatrice Tierra, Leanne Hildebrand, Linan Liu, Michael J. Liao, Jaedu Cho, Dongxu Liu, Lizhi Sun, Gultekin Gulsen, Min-Ying Su, Robert L. Sah, Weian Zhao.  
Publication: EBioMedicine  
Publisher: Elsevier  
Date: July 2019  
**Note:** This article is available under the Creative Commons CC-BY-NC-ND license and permits non-commercial use of the work as published, without adaptation or alteration provided the work is fully attributed.

Chapter 5 and part of Chapter 7 © 2019 The Authors. Published by Elsevier B.V.  
Meta-analysis of preclinical studies of mesenchymal stromal cells to treat rheumatoid arthritis.  
Author: Linan Liu, Chi W. Wong, Menglu Han, Henry P. Farhoodi, Guangyang Liu, Yongjun Liu, Wenbin Liao, Weian Zhao.  
Publication: EBioMedicine  
Publisher: Elsevier  
Date: September 2019  
**Note:** This article is available under the Creative Commons CC-BY-NC-ND license and permits non-commercial use of the work as published, without adaptation or alteration provided the work is fully attributed.

Chapter 6 and part of Chapter 7 © The Authors 2020. Published by SAGE Publications.  
Preclinical Evaluation of a Single Intravenous Infusion of hUC-MSC (BX-U001) in Rheumatoid Arthritis.  
Author: Linan Liu, Henry P. Farhoodi, Menglu Han, et al  
Publication: Cell Transplantation  
Publisher: SAGE Publications  
Date: January 2020  
**Note:** This article is available under the Creative Commons CC-BY-NC-ND license and permits non-commercial use of the work as published, without adaptation or alteration provided the work is fully attributed.

All other materials © 2021 Henry P. Farhoodi. Published by ProQuest.

# DEDICATION

To:

My mother Jane, who's unconditional support gave me the strength to overcome my challenges, and to my father Faramarz, who taught me science as a young child and guided me to live in the interests of bettering humanity.



# TABLE OF CONTENTS

|  | Page       |
|--|------------|
| <b>LIST OF FIGURES</b>   | v- vii     |
| <b>LIST OF TABLES</b>  | viii       |
| <b>ACKNOWLEDGEMENTS</b>  | ix – x     |
| <b>CURRICULUM VITAE</b>  | xi – xv    |
| <b>ABSTRACT OF THE DISSERTATION</b>  | xvi – xvii |
| <b>CHAPTER 1: Introduction</b>   | 1 – 7      |
| 1.1 Inflammation   | 1 – 5      |
| 1.2 Cancer   | 6          |
| 1.3 References   | 6 – 7      |
| <b>CHAPTER 2: Optimization of a syngeneic model of bone metastasis</b>   | 8 – 33     |
| 2.1 Abstract   | 9          |
| 2.2 Introduction   | 10 – 12    |
| 2.3 Results  | 12 – 24    |
| 2.3.1 In vivo selection for bone localizing 4T1 cells  | 15 – 16    |
| 2.3.2 Comparison of caudal artery injection route to other standard bone metastasis inducing cell delivery methods                         | 17 – 18    |
| 2.3.3 Optimizing 4T1-CLL1 caudal artery injection for desired growth rates and consistency   | 18 – 21    |
| 2.4 Discussion   | 22 – 24    |
| 2.5 Materials and Methods  | 24 – 30    |
| 2.6 Author Contributions   | 31         |
| 2.7 Acknowledgments  | 31         |
| 2.8 References   | 31 – 33    |
| <b>CHAPTER 3: Combinatorial targeting of cancer bone metastasis using mRNA engineered MSC</b>  | 34 – 103   |
| 3.1 Abstract   | 35         |
| 3.2 Introduction   | 36 – 38    |
| 3.3 Results  | 38 – 60    |
| 3.3.1 MSC engineering using mRNA and <i>in vitro</i> functional validation   | 38 – 43    |
| 3.3.2 Enhanced homing of engineered MSC to breast cancer bone metastases <i>in vivo</i>  | 43 – 47    |
| 3.3.3 Engineered MSC with both CD and OPG exhibit therapeutic effects in treating bone metastases in MDA-MB231 xenograft intratibial model | 47 – 56    |
| 3.3.4 Engineered MSC with both CD and OPG exhibit superior therapeutic effects in a syngeneic model of spontaneous bone metastases         | 56 – 60    |
| 3.4 Discussion   | 60 – 65    |
| 3.5 Materials and Methods  | 65 – 83    |
| 3.6 Supplemental Materials   | 83 – 98    |
| 3.7 Acknowledgements   | 98         |
| 3.8 Author Contributions   | 98         |
| 3.9 References   | 99 – 103   |
| <b>CHAPTER 4: Preclinical Evaluation of hUC-MSC (BX-U001) to treat Inflammatory Bowel Disease</b>  | 104 – 132  |
| 4.1 Abstract   | 105 – 106  |
| 4.2 Introduction   | 106 – 109  |
| 4.3 Results  | 109 – 119  |
| 4.4 Discussion   | 119 – 125  |
| 4.5 Materials and Methods  | 125 – 129  |
| 4.6 Acknowledgements   | 129        |
| 4.7 References   | 129 – 132  |
| <b>CHAPTER 5: Meta-analysis of preclinical studies of MSC to treat rheumatoid arthritis</b>  | 133 – 180  |
| 5.1 Abstract   | 134        |
| 5.2 Introduction   | 135 – 136  |

|   |           |
|---|-----------|
| 5.3 Materials and methods   | 136 – 138 |
| 5.4 Results   | 138 – 155 |
| 5.4.1 Study characteristics   | 138 – 141 |
| 5.4.2 Quality of included studies   | 141       |
| 5.4.3 Effect size   | 141 – 145 |
| 5.4.4 Subgroup analysis   | 145 – 153 |
| 5.4.5 Meta-regression of effect size  | 153 – 154 |
| 5.4.6 Evaluation of publication bias  | 154 – 155 |
| 5.5 Discussion  | 155 – 159 |
| 5.6 Supplemental Materials  | 160 – 177 |
| 5.7 Author contributions  | 177       |
| 5.8 Acknowledgments   | 177       |
| 5.9 References  | 178 – 180 |
| <b>CHAPTER 6: Preclinical Evaluation of hUC-MSC (BX-U001) to treat Rheumatoid Arthritis</b> | 181 – 207 |
| 6.1 Abstract  | 182       |
| 6.2 Introduction  | 183 – 184 |
| 6.3 Materials and Methods   | 184 – 188 |
| 6.4 Results   | 189 – 197 |
| 6.4.1 Generation and <i>in vitro</i> characterization of hUC-MSC                            | 189       |
| 6.4.2 hUC-MSC improved arthritis assessment outcomes  | 190 – 193 |
| 6.4.3 Microscopic joint inflammation was reduced after hUC-MSC treatment                    | 193       |
| 6.4.4 IL-6 level was declined by hUC-MSC treatment  | 194 – 196 |
| 6.4.5 No side effect was observed after hUC-MSC administration                              | 196 – 197 |
| 6.5 Discussion  | 197 – 199 |
| 6.6 Supplemental Materials  | 200 – 204 |
| 6.7 Acknowledgements  | 204       |
| 6.8 References  | 204 – 206 |
| <b>CHAPTER 7: Summary</b>   | 207 – 209 |

# LIST OF FIGURES

| Figure | Title   | Page       |
|--------|---|------------|
| 1.1    | Components of the innate and adaptive immune system phylogeny   | 2          |
| 1.2    | Immune response to pathogens  | 3          |
| 1.3    | Complexity of T cell and dendritic cell phenotypes and their relationships within the immune system   | 4          |
| 2.1    | Schematic of method to induce consistent syngeneic bone metastasis.   | 13         |
| 2.2    | The 4T1-CLL1 line shows some phenotypic differences to 4T1 cells.   | 15         |
| 2.3    | 4T1-CLL1 delivered via caudal artery produce invasive and destructive bone metastases.  | 16         |
| 2.4    | Graphical comparison of 4T1 breast cancer metastasis locations for different routes of cancer cell injection.   | 18         |
| 2.5    | Quantity of cells injected alters pattern of 4T1-CLL1 metastasis.   | 21         |
| S2.1   | Important landmarks in mice for a 4T1 caudal artery bone metastasis model.  | 25         |
| S2.2   | Example ex vivo bioluminescent imaging to confirm bone presence of in vivo signals.   | 26         |
| S2.3   | Demonstration of caudal artery injection with comments.   | 28         |
| S2.4   | 4T1-CLL1 tumor growth over time is not sufficiently inhibited by 5-fluorouracil.  | 29         |
| S2.5   | Methodology for identifying metastasis location.  | 30         |
| 3.1    | Combinatorial targeting of cancer bone metastasis using mRNA engineered mesenchymal stem cells.   | 38         |
| 3.2    | MSC engineering using mRNA and in vitro functional validation.  | 32         |
| 3.3    | P-selectin is highly expressed in the bone metastatic niche.  | 33         |
| 3.4    | Enhanced homing of engineered MSC to breast cancer bone metastases in vivo in the MDA-MB231 intratibial model.  | 45         |
| 3.5    | Engineered MSC exhibit therapeutic effects in treating bone metastases in vivo in the MDA-MB231 intratibial model.  | 48 –<br>49 |
| 3.6    | Systemic infusion of PSGL-1/SLEX/CD/OPG MSC improves animal survival without inducing systemic toxicity in the MDA-MB231 intratibial model.   | 53 –<br>54 |
| 3.7    | CD/OPG MSC exhibit therapeutic effects and minimal toxicity in a syngeneic mouse model of spontaneous bone metastases.  | 57 –<br>58 |
| S3.1   | PSGL-1/SLEX/CD/OPG MSC conserve their differentiation abilities after mRNA engineering.   | 83         |
| S3.2   | Example of gating strategies used to analyze bone marrow cells  | 84         |
| S3.3   | The conversion of 5-Fluorocytosine (5-FC) pro-drug into 5-Fluorouracil (5-FU) by PSGL-1/SLEX/CD/OPG MSC were measured by mass spectrometry.   | 85         |
| S3.4   | In vitro functional validation of PSGL-1/SLEX expression by engineered MSC.   | 86         |
| S3.5   | In vitro functional validation of OPG secreted by engineered MSC.   | 87         |
| S3.6   | In vitro functional validation of CD expression by engineered MSC.  | 88         |
| S3.7   | P-selectin expression within the bone marrow was increased around the tumor area.   | 89         |
| S3.8   | MSC entrapped into the lungs following i.v. injection, in the MDA- MB231 intratibial model, and were mostly cleared out by 48 hours post-transplantation.   | 90         |
| S3.9   | PSGL-1/SLEX/CD/OPG MSC display more effective homing than Native MSC to the bone marrow, in particular to bone metastatic tumors, in the immunocompromised intratibial model (a-c) and in the syngeneic model of spontaneous bone metastasis (d,e). | 91         |
| S3.10  | Representative techniques to monitor and characterize engineered MSC's tumor killing efficacy in the MDA-MB231 intratibial model.   | 92         |
| S3.11  | Representative in vivo imaging data demonstrate the inhibition by engineered MSC treatment on MDA-MB231 tumor growth in the tibias of Nude mice in the MDA-MB231 intratibial immunocompromised model.   | 93         |
| S3.12  | PSGL-1/SLEX/OPG MSC inhibit tumor-induced osteoclast activity in the MDA-MB231 intratibial model, thus preventing bone loss.  | 94         |
| S3.13  | MDA-MB231 intratibial model mice infused with PSGL-1/SLEX/CD/OPG MSC via i.v. injection exhibited minimal toxicity.   | 95         |
| S3.14  | MDA-MB231 intratibial model mice infused with PSGL-1/SLEX/CD/OPG MSC via i.v. injection exhibited minimal toxicity.   | 96         |

|              |  |                               |
|--------------|--|-------------------------------|
| <b>S3.15</b> | Illustrative bone integrity analyses following systemic i.v. infusion of PSGL- 1/SLEX/CD/OPG MSC in MDA-MB231 intratibial model mice.  | <b>96</b>                     |
| <b>S3.16</b> | PSGL-1/SLEX/CD/OPG MSC exhibit therapeutic effects and minimal toxicity in a syngeneic mouse model of spontaneous bone metastasis.   | <b>97 – 98</b>                |
| <b>4.1</b>   | hUC-MSC are characterized by standard MSC phenotypes established by the International Society for Cellular Therapy (ISCT).   | <b>110</b>                    |
| <b>4.2</b>   | Relative Fluc signal in colons of healthy mice (Green line, n=3) and IBD mice (Red, n=3) after infusion with 1 million Luc-MSC. Normalized to 6hr fluorescent signal.  | <b>111</b>                    |
| <b>4.3</b>   | Experimental timetable for establishing TNBS animal model and treatment with hUC-MSC.  | <b>112</b>                    |
| <b>4.4</b>   | hUC-MSC treatment significantly reduced the body weight change of TNBS-induced mice (T vs V: *p< 0.05).  | <b>112</b>                    |
| <b>4.5</b>   | hUC-MSC treatment reduces mean DAI of T Group (T vs V: *p< 0.05).  | <b>113</b>                    |
| <b>4.7</b>   | Representative pictures of colons.   | <b>115</b>                    |
| <b>4.8</b>   | hUC-MSC treatment reduced macroscopic damage to IBD mouse colons.  | <b>116</b>                    |
| <b>4.9</b>   | hUC-MSC infusion significantly reduced colon weight gain from TNBS model.  | <b>117</b>                    |
| <b>4.10</b>  | Representative pictures of histological exam.  | <b>118</b>                    |
| <b>4.11</b>  | hUC-MSC infusion significantly improved survival from TNBS Model over 8 days (p< 0.01).  | <b>119</b>                    |
| <b>4.12</b>  | Proposed mechanism of action for hUC-MSC in IBD.   | <b>123</b>                    |
| <b>5.1</b>   | Forest plots showing the normalized mean difference (MD) and 95% CI of the clinical score for each study included in the meta-analysis.  | <b>143</b><br>–<br><b>144</b> |
| <b>5.2</b>   | Forest plots showing the normalized mean difference (MD) and 95% CI of (a) histological score, (b) paw thickness for each study included in the meta-analysis.   | <b>144</b>                    |
| <b>5.3</b>   | Forest plots showing normalized mean difference (MD) of clinical score changes and 95% CI for the subgroup of MSC donor species.   | <b>146</b><br>–<br><b>147</b> |
| <b>5.4</b>   | Forest plots showing normalized mean difference (MD) of clinical score changes and 95% CI for the subgroup of transplant types.  | <b>148</b>                    |
| <b>5.5</b>   | Forest plots showing normalized mean difference (MD) of clinical score changes and 95% CI for the subgroup MSC tissue of origin.   | <b>149</b><br>–<br><b>150</b> |
| <b>5.6</b>   | Forest plots showing normalized mean difference (MD) of clinical score changes and 95% CI for the subgroup of routes of administration.  | <b>150</b><br>–<br><b>151</b> |
| <b>5.7</b>   | Regression model with regression line is shown in (a) single MSC injection treatment, (b) multiple MSC injections treatment (linear regression), and (c) multiple MSC injections treatment (quadratic regression). | <b>152</b>                    |
| <b>5.8</b>   | Funnel plot for (a) clinical score, (b) histological score, and (c) paw thickness.   | <b>155</b>                    |
| <b>S5.1</b>  | Flowchart of meta-analysis search and review process.  | <b>162</b>                    |
| <b>S5.2</b>  | Quality assessment of literature.  | <b>163</b>                    |
| <b>S5.3</b>  | Forest plots showing the normalized mean difference (MD) and 95% CI for histological scores with a subgroup of (a) bone erosion; (b) cartilage damage; (c)inflammation.  | <b>164</b><br>–<br><b>165</b> |
| <b>S5.4</b>  | Forest plots showing the standardized mean difference (SMD) and 95% CI for (a) clinical score, (b) histological score, (c) paw thickness for each study included in the meta-analysis.                             | <b>165</b><br>–<br><b>166</b> |
| <b>S5.5</b>  | Forest plots showing the normalized mean difference (MD) and 95% CI for two important MSC donor species, human and mouse, and tissue of origin.  | <b>167</b><br>–<br><b>168</b> |
| <b>S5.6</b>  | A forest plot showing the normalized mean difference (MD) and 95% CI of histological score of MSC tissue of origin.  | <b>168</b><br>–<br><b>169</b> |
| <b>S5.7</b>  | Funnel plot for (a) clinical score, (b) histological score and (c) paw thickness, after trim-and-fill correction.  | <b>170</b><br>–               |

|             |   |            |
|-------------|---|------------|
|             |   | <b>171</b> |
| <b>S5.8</b> | Forest plots showing the normalized mean difference (MD) and 95% CI for clinical scores with a subgroup of autoantibody levels (IgG).   | <b>172</b> |
| <b>S5.9</b> | Forest plots showing the standardized mean difference (SMD) and 95% CI for clinical score, for each study included with subgroup of autoantibody levels (IgG) in the meta-analysis. | <b>173</b> |
| <b>6.1</b>  | Timeline of using hUC-MSC to treat CIA-induced RA.  | <b>187</b> |
| <b>6.2</b>  | In vitro characterization of hUC-MSC.   | <b>189</b> |
| <b>6.3</b>  | Average clinical score and model-based rate of change for each experimental group from Day20 to Day42 (two batches combined).   | <b>191</b> |
| <b>6.4</b>  | CA group mice had significantly better histological scores than those of TA group.  | <b>194</b> |
| <b>6.5</b>  | Concentrations of pro-inflammatory cytokines (IL-6, IFN- $\gamma$ , TNF- $\alpha$ and IL-1 $\beta$ ) in each experimental group at baseline, Day 22, Day 26 and endpoint (Day 42).  | <b>196</b> |
| <b>S6.1</b> | Mean body weight of each experimental group from Day 20 to Day 42.  | <b>200</b> |
| <b>S6.2</b> | Average clinical score of each experimental group from Day20 to Day42 (two batches combined).   | <b>200</b> |
| <b>S6.3</b> | Representative pictures of mouse paws from each experimental group.   | <b>201</b> |
| <b>S6.4</b> | Paw thickness of front and hind legs for each experimental group (two batches combined).  | <b>201</b> |
|             |   |            |

# LIST OF TABLES

| Table | Title   | Page      |
|-------|---|-----------|
| 2.1   | Percentage of mice showing 4T1 breast cancer metastases to significant locations for different routes of cancer cell injection. | 14        |
| 4.1   | Body Weight Change Percentage (BWC%, Mean $\pm$ SEM).   | 112 – 113 |
| 4.2   | Disease Activity Index (DAI, Mean $\pm$ SEM).   | 114       |
| 4.3   | Macroscopic scores (Mean $\pm$ SEM).  | 115       |
| 4.4   | Important cytokines relating to IBD and MSC treatment.  | 118       |
| 4.5   | Previous and ongoing clinical trials using MSC to treat IBD.  | 123 – 125 |
| 4.6   | Animal grouping for efficacy studies.   | 126       |
| 4.7   | Animal grouping for survival study.   | 126       |
| S4.1  | TNBS model mice exhibiting diarrhea and/or rectal bleeding with corresponding scores.   | 127       |
| 5.1   | Pre-clinical studies using MSC to treat RA included in this study.  | 139 – 140 |
| 5.2   | Study arms categorized by experimental variables of interest and their qualitative effect size.                                 | 142       |
| S5.1  | Autoantibodies summary of the pre-clinical studies using MSC to treat RA in this study.   | 174 – 175 |
| S5.2  | Summary of meta-regression statistics.  | 175       |
| S5.3  | Meta-regression of the effect of treatment dosage with subgroup of number of injections.  | 175 – 176 |
| S5.4  | Results of clinical studies using MSC to treat RA.  | 176 - 177 |
| 6.1   | Animal Grouping.  | 186       |
| 6.2   | Clinical scores after hUC-MSC infusion (Combined batches; Mean and 95% CI).   | 191       |
| 6.3   | Comparison (TA vs. CA) on clinical score between Day 24 and Day 42 (Estimate = TA - CA).  | 192       |
| 6.4   | Changes of clinical score between Day 24 and Day 42 (Estimate = Day 42 - Day 24).   | 192       |
| 6.5   | Histological scores (Day 42, Mean $\pm$ SEM).   | 193       |
| 6.6   | Relative concentrations of cytokines (%; Mean $\pm$ SEM).   | 195       |
| S6.1  | Comparison (TA vs. CA) on clinical score on Day 24 (Estimate = TA - CA).  | 202       |
| S6.2  | Batch 1 Clinical scores (Mean $\pm$ SD).  | 202       |
| S6.3  | Batch 2 Clinical scores (Mean $\pm$ SD).  | 202       |
| S6.4  | Paw thickness (front vs. hind) after hUC-MSC infusion (Mean and 95% CI).  | 203       |
| S6.5  | Paw thickness after hUC-MSC infusion (Mean and 95% CI).   | 203       |
| S6.6  | Difference in TA vs TA mean body weights prior to CIA induction (Day 24).   | 204       |
| S6.7  | Comparison of body weight in TA and CA groups after hUC-MSC infusion (Mean and 95% CI).   | 204       |

# ACKNOWLEDGEMENTS

In my time as a graduate student, I have had a lot of mentors and advice, without which I could not have learned enough or gained the skills to finish this work. Dr. Weian Zhao has been my P.I. and mentor for the last five years, and has transformed me from an inexperienced student, to being comfortable with all aspects of research. I was so impressed by the innovative approach of his research in the stem cell class he was teaching, that I decided I needed to work with him. It was intimidating attending that first lab meeting and seeing so many diverse projects and great ideas being discussed, making me think I was out of my league, but I also appreciated this was an opportunity to learn from the many talented people in the lab, on many subjects. I have grown so much from years in Dr. Zhao's lab, and from his inciteful comments and demand for solid scientific grounds underlying every experiment. Thank you for your guidance, positivity, friendship, and the learning experience you gave me the opportunity to take part in.

I would also like to thank Dr. Young Jik Kwon, and Dr. Andrej Luptak for serving on my defense committee and the lessons they taught me, both as a student in their classrooms and later as their teaching assistant. I thank Dr. Craig Walsh, Dr. Claudia Benavente, Dr. Mahtab Jafari, and Dr. Xiangmin Xu for serving on my qualifying exam committee and giving excellent advice on the future of my graduate studies. I greatly appreciate the mentorship and guidance of Dr. Peter Donovan and Dr. Leslie Thompson, as well as for the awarding of the prestigious NIH NINDS fellowship, which gave me the freedom to perform my research without constraint. I also thank Dr. Michael Cumsky and Dr. Elizabeth Eldon, who gave me a foundation in research, without which I could not have attempted doctoral studies.

One of the great things working in such a diverse lab, was the number of different subjects I could learn from a collection of great scientific minds. While I am grateful for all the great scientific discussions, I have had with members of the Zhao Lab, I am especially grateful to those who directly mentored me, or who allowed me to act as their mentor. Dr. Linan (Jerry) Liu has been instrumental to my productivity and ability to develop as a graduate student and scientist. His constant feedback and was priceless, as well the advice he gave me. Dr. Shirley Zhang was a great teacher, coworker, and friend since I joined the Zhao lab, and along with Menglu Han, was

always a great confidant when times were tough. Menglu has learned and grown alongside me as we started and end our doctoral studies together, and I appreciate working together on many projects. Dr. Aude Segaliny gave me the chance to study bone metastasis under her guidance and has been a great friend and mentor throughout my dissertation work. Dr. Jenu Chacko taught me the power of advanced microscopic techniques, which allowed me to study in detail the structural effects of cancer. Dr. Jan Zimak was always available to bounce ideas off and was an excellent scientific resource throughout my doctoral studies, particularly in molecular biology. Brenda Nguyen, Artin Ziary, Zachary Wagoner, and Anhad Sarang were all outstanding students and allowed me to grow as a team leader and mentor while working with great people who were as passionate as I was about the work we did together.

Additionally, I thank Dr. Matthew Luderer, who gave me a second chance in my first semester of college, incentivizing me to work harder to understand science. I also thank Renee Hodgkinson who taught me how to visualize scientific problems in high school, a skill which I still use daily. My experiences learning from my mentors and teaching my mentees indicate to me that teaching is the greatest impact a person can have regardless of other achievements, because the knowledge and experience will continue to be passed on to others with incalculable long-term impact.

All achievements and contributions I make are and will be a result of my family, who gave my life a purpose and meaning. My parents who gave me a head start on my education by teaching me to read, write, mathematics, and science long before I started school. My parents gave me advantages they did not have themselves and supported me in every way possible. I thank my brother Charlie, who I always aspired to be like and has always been there when I needed him. I thank my brother Chris and sister Natasha for providing me constant intellectual challenges, helping me grow my problem-solving skills, and giving me a chance to practice responsibility for others from an early age.

Permission to use all copyrighted materials has been obtained from the copywrite holders.



# CURRICULUM VITAE

Henry Farhoodi

## EDUCATION

University of California Irvine – Irvine, CA

2020

PhD Pharmaceutical Sciences

University of California Irvine – Irvine, CA

2016

Master of Science in Biotechnology

California State University Long Beach – Long Beach, CA

2014

Post-Baccalaureate Certificate in Biotechnology

University of Florida – Gainesville, FL

2008

Bachelor of Science in Botany

## RESEARCH EXPERIENCE

University of California Irvine – Irvine, CA – *P.I. Dr. Weian Zhao*

4/2015 – 12/2020

Developing/evaluating engineered stem cell treatments for human breast cancer, liver fibrosis, and melanoma. Evaluating stem cell treatments for autoimmune diseases, cancer, and traumatic brain injury *in vitro* and *in vivo*. Performing pre-clinical studies for several successful FDA IND submissions resulting in clinical trials of stem cell treatments. Developing new methods to model disease in rodents. Developing new methods to analyze cancer tissue.

Amberstone Biosciences – Laguna Hills, CA – *P.I. Dr. George Wu*

8/2020 – 11/2020

Developing new methods to identify therapeutic antibodies from animal tissues and blood.

City of Hope – Duarte, CA – *P.I. Dr. Qiang Lu*

9/2013 - 7/2014

Tracking cortical neuron development and migration *in vivo*, in response to miRNA silencing of selected genes. Engineering DNA constructs and testing binding affinity of various proteins in mouse and human neural stem cells to determine their roles in asymmetric cell division resulting in publication.

California State University – Long Beach, CA – *P.I. Dr. Elizabeth Eldon*

8/2012 – 9/2013

Generating and analyzing an antibody that can bind to the TIR domain of the 18-Wheeler protein to better understand the protein's role in immunology and development.

University of Florida – Gainesville, FL – *P.I. Dr. Fredy Altpeter*

8/2008 – 1/2009

Plant tissue culture and growing transgenic organisms from undifferentiated callous cells for improving crop tolerance to harsh conditions.

## ACHIEVEMENTS & MAJOR CONTRIBUTIONS

**Zhao Lab:** Completed several pre-clinical studies of stem cell therapies in rodents, which were used in two FDA IND packages resulting in approval of clinical trials. Wrote several grants including successful award from the NIH National Institute for Neurological Disorders and Stroke to study stem cell treatments for neurological diseases. Established several animal models in mice for autoimmune diseases, and cancer, including writing a new method to increase bone metastasis rates. Wrote and managed 4 independent IACUC animal protocols. Evaluated human stem cells for treatment and study of many diseases, including rheumatoid arthritis, various cancers, ulcerative colitis, Crohn's disease, liver fibrosis, and traumatic brain injury. Produced state of the art, 3D cancer structural images to identify *in vivo* efficacy and mechanism of stem cell therapy. Determined route of passage of exosomes passing through the blood brain barrier. Developed new technique for structural analysis of cancer tissue sections. Managed lab safety affairs, reducing safety incidents to 0 for 4 years while in charge. Directly mentored and taught 7 undergraduate students and two technicians resulting in significant career progression for all of them. Negotiated prices of large equipment purchases from retailers, saving lab tens of thousands of dollars.

**Amberstone Biosciences:** Increased yield of antibody secreting plasma cells from rodent tissues by 10%. Developed new methods of isolating and enhancing antibody secreting cells from mouse tissues. Developed and tested novel methods to isolate antibody secreting cells from camelids, resulting in a multi-fold increase in purity.

**Lu Lab:** Developed strategies to clone many large genes into human cell lines over a six-month period. Gave experimental evidence to support universality of lab asymmetric cell division model.

**Eldon Lab:** Given leadership of major lab project. Troubleshoot what was wrong with project and designed method to progress.

## PUBLICATIONS & CONFERENCE PRESENTATIONS

### *Publications:*

**Farhoodi H.P.\***, Liu L.\*, Nguyen B., Ziary A., Han M., Liao W., Zhao W. Human Umbilical Cord MSC Reduce Inflammation in Inflammatory Bowel Disease. Manuscript in preparation (2020).

**Farhoodi H.P.**, Ségaliny A.I., Wagoner Z.W., Cheng J.L., Liu L., Zhao W. Optimization of a syngeneic murine model of bone metastasis. *Journal of Bone Oncology*. 2020, 23, 100298, Doi: 10.1016/j.jbo.2020.100298. (2020).

**Farhoodi H.P.\***, Liu L\*, Han M, Liu G, Yu J, Nguyen L, Nguyen B, Nguyen A, Liao W, Zhao W. Preclinical Evaluation of a Single Intravenous Infusion of hUC-MSC (BX-U001) in Rheumatoid Arthritis. *Cell Transplant*. 2020 Jan-Dec;29:963689720965896. Doi: 10.1177/0963689720965896. (2020).

Liu L., Wong C.W., Han M., **Farhoodi H.P.**, Liu G., Liu Y., Liao W. & Zhao W. Meta-analysis of Preclinical Studies of Mesenchymal Stromal Cells for Rheumatoid Arthritis. *EBioMedicine* 2019;47:563-577. Doi:10.1016/j.ebiom.2019.08.073 (2019).

Ségaliny A.I., Cheng J., **Farhoodi H.P.**, Toledano M., Yu C.C., Tierra B., Hildebrand L., Liu L., Liao M., Cho J., Liu D., Sun L., Gulsen G., Su M.Y., Sah R., & Zhao W. Combinatorial Targeting of Cancer Bone Metastasis Using mRNA Engineered Stem Cells. *EBioMedicine* Vol. 45, 39-57. Doi.org/10.1016/j.ebiom.2019.06.047 (2019).

Geng, A., Qiu, R., Murai, K., Liu, J., Wu, X., Zhang, H., **Farhoodi, H.**, Duong, N., Jiang, M., Jiing-kuan, Y., Tsark, W. & Lu, Q. KIF20A/MKLP2 regulates the division modes of neural progenitor cells during cortical development. *Nature Communications*, 9, 2707. Doi: 10.1038/s41467-018-05152-1 (2018).

Liu L., Zhang S.X., Liao W., **Farhoodi H.P.**, Wong C.W., Chen C.C., Ségaliny A.I., Chacko J.V., Nguyen L.P., Lu M., Polovin G.P., Pone E.J., Downing T.L., Lawson D.A., Digman M.A., & Zhao W. Mechanoresponsive stem cells to target

cancer metastases through biophysical cues. *Science translational medicine* 9, doi:10.1126/scitranslmed.aan2966 (2017).

Chen C.C., Liu L., Ma F., Wong C.W., Guo X.E., Chacko J.V., **Farhoodi H.P.**, Zhang S.X., Zimak J., Ségaliny A., Riazifar M., Pham V., Digman M.A., Pone E.J., & Zhao W. Elucidation of Exosome Migration Across the Blood–Brain Barrier Model In Vitro. *Cellular and Molecular Bioengineering*:1-21. (2016).

**Presentations:**

Oral presentation: **Henry Farhoodi**, Alleviating Symptoms of Traumatic Brain Injury Using Mesenchymal Stem Cells. NIH NINDS Training Director Visitation, University of California, Irvine, CA, October 20, 2020.

Oral presentation: **Henry Farhoodi**. Using Stem Cells to Treat Cancer. UCI An Lanh Free Clinic - Project Summer Research Enrichment Institute, University of California, Irvine, CA, July 24, 2019.

Oral presentation: **Henry Farhoodi**. Personalized MSC Treatment of Inflammatory Bowel Disease. PhD Advancement to Candidacy Oral Exam, University of California, Irvine, CA, July 9, 2019.

Oral presentation: **Henry Farhoodi**. Mesenchymal Stem Cells as a Multiplex Treatment for Inflammatory Bowel Disease. Pharmaceutical Sciences Department Research in Progress Seminar, University of California, Irvine, CA, March 6, 2019.

Oral presentation: **Farhoodi H.P.**, Liu L., Nguyen L., Liu G., Sarang A., & Zhao W. Mesenchymal Stem Cells in the Treatment of Autoimmune Diseases. Vertex Day Research Symposium, Department of Pharmaceutical Sciences, University of California, Irvine, CA, March 8, 2018.

Oral presentation: **Farhoodi H.P.**, Liu L. & Zhao W. The Mechanosensation of Metastatic Cancer. Biotechnology Program Graduate Symposium, Department of Molecular Biology and Biochemistry, University of California, Irvine, CA, May 31, 2016.

Poster Presentations: “Human Mesenchymal Stem Cells to Treat Inflammatory Bowel Disease.”

**Henry Farhoodi**, Linan Liu, and Weian Zhao.

UC Irvine Biomedical Engineering Department PhD Recruitment Day (02/07/2019)

UC Irvine Cell & Molecular Biosciences Department PhD Recruitment Day (01/25/2019)

UC Irvine Immunology Fair (12/07/2018)

Poster Presentations: “Mechano-Responsive Stem Cells to Target Cancer Metastasis through Biophysical Cues”

Linan Liu, Shirley X. Zhang, **Henry Farhoodi**, Wenbin Liao, Egest J. Pone, & Weian Zhao

SABPA 12<sup>th</sup> annual biomedical forum (2<sup>nd</sup> prize for presentation) (04/29/2017)

UCI Pharmaceutical Sciences Department Poster Session (05/23/2016)

2<sup>nd</sup> Annual Ewha-UCI Joint Symposium (01/25/2016)

UCI Stem Cell Awareness Research Symposium (10/27/2015-10/28/2015)

Poster Presentation: “Regulation of neurogenesis by ephrin-B/RGS and G protein signaling”

**Henry Farhoodi**, Runxiang Qiu, and Qiang Lu.

CIRM Bridges Meeting 2014 San Francisco (7/27/14-7/29/2014)

## TECHNIQUES

**Animal:** Mouse intraperitoneal/retro-orbital/colonic/subcutaneous/intradermal/intratibial/intracaudal arterial/intracardiac/ tail vein/hepatic portal vein/fat pad Injections, enema drug delivery, and mouse sedation. Rodent invasive survival surgery including organ manipulations, tumor extraction, and limb amputation. Rodent euthanization and organ harvest (all organs). Rodent blood and bone marrow collection, tissue homogenization and single tissue cell isolation. IVIS live animal and *ex vivo* organ imaging. Experienced in animal overall health evaluation, and clinical scoring for multiple disease phenotypes. Animal models including: Collagen induced arthritis, liver fibrosis, subdermal immunization, TNBS induced colitis, DSS induced colitis, Oxazolone induce colitis, spontaneous metastatic cancer models, patient derived xenograft cancer model, spontaneous bone metastasis models.

**Cell Culture/histology:** Cell culture maintenance, cell freezing/thawing, cell transfection, lentiviral transduction, electroporation, flow cytometry, immunocytochemistry, primary cell culture (T cells, macrophages, B cells, plasma cells, mesenchymal stem cells), mesenchymal stem cell isolation, trans-well assay, cell microvesicle/exosome isolation, various cell viability assays, T regulatory cell identification from blood, cell bioluminescence quantification, antibody secretion quantification, immunohistochemistry, trichrome/H&E staining, tissue processing (frozen and paraffin embed), tissue sectioning/mounting.

**Molecular:** Gel electrophoresis, Western blots, molecular cloning, q/RT/PCR, bacterial and mammalian protein and DNA extraction, E. coli transformation and culture, DNA ligation, plasmid design, X-ray crystallography crystal screening, FPLC protein purification, polymerase activity assay, co-immuno-precipitation, ligation-mediated PCR, Alu qPCR, DNA extraction from mouse tissue, fluorescent microscopy, ELISA, BSA/BCA curves, HPLC, mass spec (MALDI-TOF), isoelectric focusing, nanoparticle tracking analysis (NTA), Second Harmonic Generation (SHG), Atomic Force Microscopy (AFM), Confocal microscopy, Luminex blood cytokine assay, Myeloperoxidase assay.

**Data Analysis Software:** GraphPad Prism, ImageJ, Excel, PowerPoint, Nikon Elements.

## TRAINING & AWARDS

- 2018-2020 NIH T32 Fellowship in Stem Cell Translational Research from the National Institute for Neurological Disorders and Stroke (NINDS/NIH)
- 2016-2020 EH&S Safety coordinator (Stem Cell Research Institute)
- 2016 UCI Pharmaceutical Sciences Graduate Student Fellowship
- UCI Graduate Division Certificate in Teaching Excellence
- Scientist to CSO Leadership Training Certificate
- UCI Animal Research Training Certificate
- UCI Teaching Assistant Professional Development Program Certificate
- CIRM Bridges Stem Cell Research Internship Grant
- University of Southern California Human Embryonic Stem Cell Training Certificate
- CSULB Biotechnology Certificate
- CSULB/UCI/City of Hope Laboratory safety/Autoclave/Gas cylinder training
- UCI TANGO to Safety Training Certificate
- California State University Long Beach Stem cell training

## EMPLOYMENT HISTORY

**University of California Irvine – Irvine, CA – Graduate Student Research Assistant** **9/2016 – 12/2020**

- Managing multiple projects as lead and secondary researcher
- Researching, planning, executing, and analyzing experiments
- Writing grants, research manuscripts, and protocols
- Managing IACUC animal protocols
- Managing safety affairs
- Mentoring junior researchers

**Amberstone Biosciences – Laguna Hills, CA – Research Intern** **8/2020 – 11/2020**

- Designed and executed experiments, researched and conceptualized new methods to identify antibodies and antibody producing cells from a diverse population

**University of California Irvine – Irvine, CA – Pharmaceutical Sciences Teaching Assistant** **9/2017 – 12/2017**

- Taught and administered lectures, discussions, and labs – aided professors – graded papers

**University of California Irvine – Irvine, CA – Molecular Biology Teaching Assistant** **9/2015 – 09/2017**

- Taught and administered lectures, discussions, and labs – aided professors – graded papers

**University of California Irvine – Irvine, CA – Graduate Research Lab Associate** **5/2015 – 9/2016**

- Performed *in vitro*, *in-vivo* and *ex-vivo* experiments to prove lab treatment efficacy, developing ideas for projects

**California Institute for Regenerative Medicine – Duarte, CA – Stem Cell Intern** **9/2013 – 7/2014**

- As part of the City of Hope Beckman Research Institute, planned and generated over 50 molecular clones for electroporation/lentiviral vector transduction of human cell lines for live cell imaging
- Used engineered cells to provide evidence that lab model of cell division is universal in stem cell biology

**Cal State Long Beach – Long Beach, CA – Graduate Student Research Assistant** **9/2012 – 9/2013**

- Generated plasmids for developing antibodies to study embryonic development and immune function
- Managed fruit fly stocks

## RELEVANT SPECIAL SKILLS & LANGUAGES

- PADI Certified Advanced Deep-Water Diver
- Extensive experience with computer hardware assembly, C++, Python, GraphPad Prism, Image J, Microsoft Office
- Adept in animal handling (rodents, larger mammals, reptiles, amphibians)
- Working knowledge of Spanish

# ABSTRACT OF THE DISSERTATION

Despite decades of research and advancement in cancer therapeutics, metastases continue to be challenging to treat using traditional highly toxic drugs. Metastases can be too small to identify by the traditional electromagnetic scans used for identifying large tumors, and thus go undiagnosed and untreated until they have spread beyond the ability of drugs to stop them. Cancer bone metastases are especially problematic to treat due to their ability to degrade bone tissue and invade into the damaged bone. The discovery that stem cells may have a propensity to home toward tumors, implies they may be able to identify features of the tumor micro-environment, which traditional small molecule drugs are not specific enough to distinguish from healthy tissue. MSC (mesenchymal stromal/stem cells) are particularly useful because they have far lower immunogenicity than other allogeneic cell or tissue transplants. We developed several systems using MSC as vectors to deliver therapeutics more specifically to the tumor microenvironment, with far lower toxicity than standard chemotherapy. Unfortunately, animal models of bone metastasis leave much to be desired, and a new method using a combination of *in vivo* selection and intra-arterial delivery of cancer cells, was developed to study our cancer bone metastasis treatment in mice. One novel treatment system we developed and tested involves the multipotent mRNA transfection of MSC with P-selectin glycoprotein ligand-1 and Sialyl-Lewis X to improve homing capabilities of the MSC, osteoprotegerin to reduce bone resorption, and cytosine deaminase to convert injected prodrug to potent anti-cancer drug specifically in the locale of the tumors. This treatment was shown to both reduce tumor growth and to impair the destruction of bone caused by the metastatic invasion of bone tissue.

Additionally, MSC are well known to have strong immunomodulatory capabilities. We performed a meta-analysis of preclinical and clinical studies using MSC to treat Rheumatoid arthritis (RA), and

found that significant work still needs to be done to evaluate the effects of MSC transplantation on inflammatory diseases, such as RA. Using what was learned from the meta-analysis MSC were evaluated in their ability to treat two prevalent auto-immune diseases: RA and inflammatory bowel disease (IBD). The MSC therapy significantly reduced inflammation in both RA and IBD when given as systemic injections. These studies were the basis of IND applications to the US FDA for a new MSC therapeutic product (BX-U001), which were approved to be further evaluated in clinical trials in the coming years. There are many more possible applications of MSC to treat disease because they have low immunogenicity and minimal safety concerns (considered by many to be the safest allogeneic stem cell transplant option), they can be easily mass produced (despite being primary cells), their ability to be engineered to carry many therapeutics (due to the complexity and modularity of cells), and their innate homing towards sites of inflammation and cancer. The combination of many different tools and abilities, make MSC like the Swiss Army knife of cell therapies, capable of tackling challenges which single target small molecule drugs cannot.

# CHAPTER 1

## Introduction

### 1.1 Inflammation

The immune system can be the cause of, and solution to, many non-congenital diseases. The severity of pathogenic infections, cardiovascular disease, cancer, and autoimmune disorder heavily depends on the activity of immune cells. Recent advances in cell therapies using immune cells to fight disease (ex. CAR-T) have highlighted the power of immune cells to fight diseases when harnessed and focused. Additionally, the complexity of the immune system, and our relatively poor understanding of its workings makes developing immunotherapy for disease challenging. Here I describe how the immune system functions in terms of inflammatory responses, and how stem cells could be used to treat both cancer and auto immune disease.

The immune system is comprised of innate immune cells, which are responsive to general features of pathogens, and adaptive immune cells which are activated to respond to specific target antigens. Innate immune cells include macrophages, neutrophils, basophils, dendritic cells, natural killer cells, and monocytes, whereas adaptive immune cells include T cells, and B cells (Figures 1.1,1.2) [1,2]. Some immune cells are present within specific tissues, so that they can respond quickly to pathogens, or serve tissue specific functions, and some immune cells circulate in the blood and lymph vessels, so that they can be omnipresent in the entire organism [3]. This combination of innate and adaptive, with local and systemic distribution makes the immune system flexible enough to deal with the almost infinite number of potential pathogens they might have to deal with [3].

Inflammation is the biological mechanism of defense from the immune system, in response to certain molecules such as dead or damaged cells, pathogens, or toxic compounds [4.5]. Inflammatory responses to these triggers can be either acute or chronic and vary in intensity. The complexity of the immune system can be attributed to the number of different cell types and molecules they produce, which interact to induce and resolve inflammation at the right time and location. The diversity and complexity of immunity is exemplified by T cells and dendritic cells,



which have very variable cell subtypes (Figure 1.3) [4].

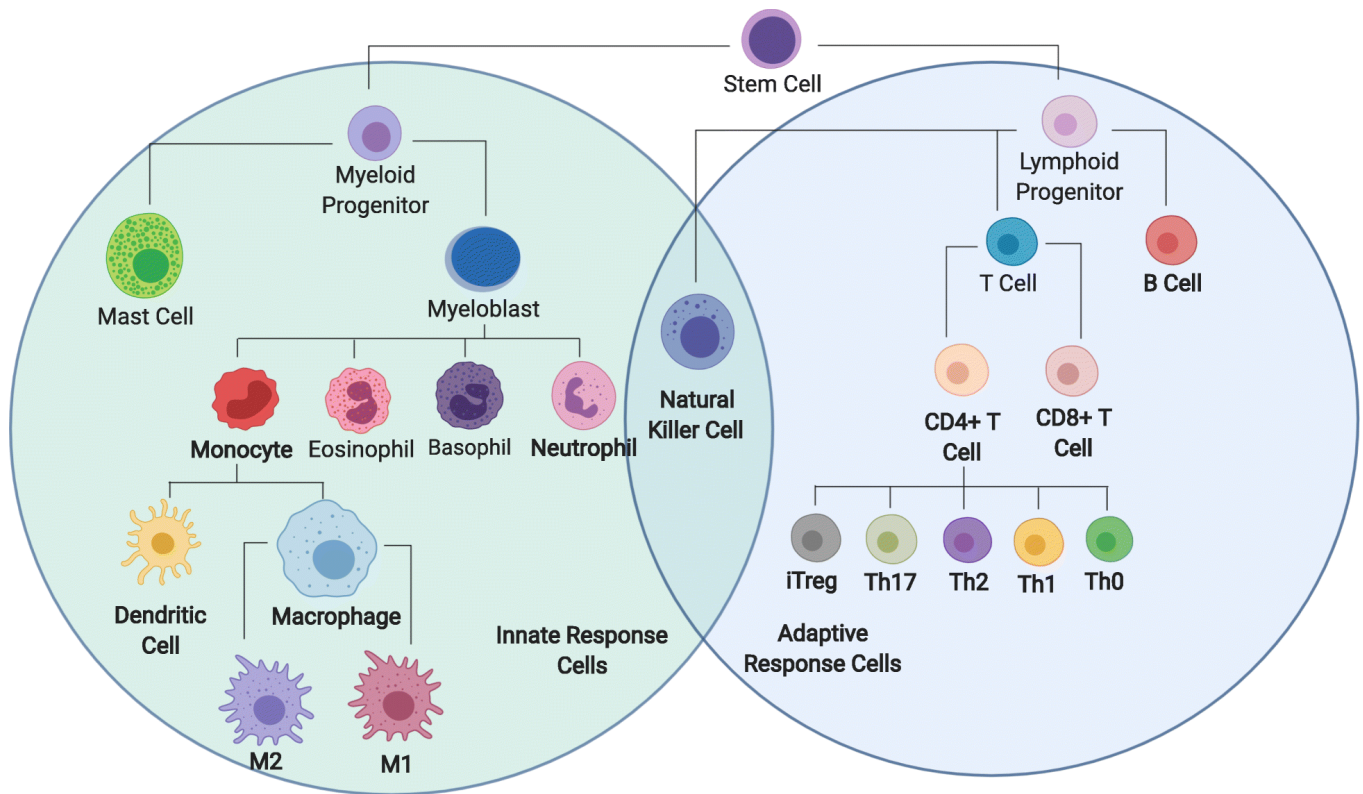


**Figure 1.1.** Components of the innate and adaptive immune systems phylogeny [1].

When a disruption in any of the protective barriers within the body (skin, gastrointestinal lining, lung epithelia) occurs, pathogens interact with tissue resident immune cells and their antigens are endocytosed by antigen presenting cells, such as dendritic cells and macrophages (Figure 1.2) [2]. Additionally, macrophages secrete  $TNF\alpha$ ,  $IFN-\gamma$  and  $IL-12$ , which promote differentiation of naïve T cells to pro inflammatory  $CD4^+$  and  $CD8^+$  T cells. Dendritic cells migrate to the lymph system to present antigens to the adaptive immune cells in lymph nodes and the spleen. Any pathogenic antigen receptive lymphocytes respond by rapidly dividing and entering circulation [3]. Proteins in the blood plasma promote vasodilation of the vessels at the site of injury and increase vascular permeability, which allows more immune cells to enter the region of damaged tissue [3]. Endothelial cells of the blood vessels at sites of injury are activated to promote adherence of circulating leukocytes, further promoting leukocytic invasion of the

damaged tissue. This increase in volume caused by leaky blood vessels and invading leukocytes causes swelling known as inflammation [3]. The invading leukocytes secrete cytokines, prostaglandins, and leukotrienes, which serve to recruit more immune cells to the area and activate them to pro inflammatory states [3].

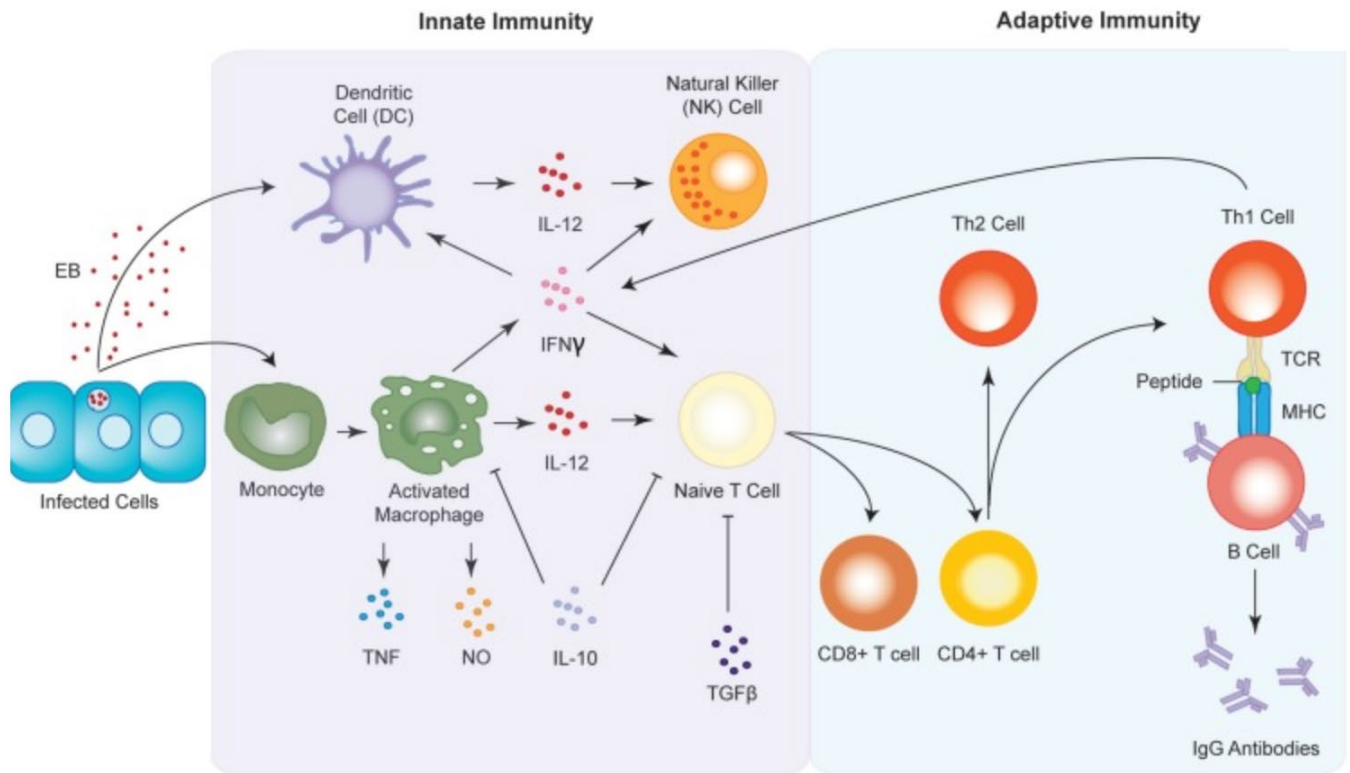


**Figure 1.2.** The immune system responds to pathogens via resident monocytes, macrophages, and dendritic cells and proceeds to induce adaptive immunity via cytokines (small colored particles) [2].

Cytokines are small proteins secreted by cells to interact with other cells [6]. Cytokines are used by the immune system to promote or reduce inflammatory responses in other immune cells, or in some cases on themselves (autocrine action) [7]. Cytokines allow both local interactions, and long-distance interactions, so that immune cells at a site of injury can send signals to immunocytes in other areas of the body that further inflammatory response is needed [7]. Cytokines can act as switches to turn certain immune functions on or off, depending on their locations and their local concentration in the vicinity of the effector site [7]. Additionally, cytokines play major roles in angiogenesis, tumorigenesis, stem cell differentiation, and apoptosis [7].

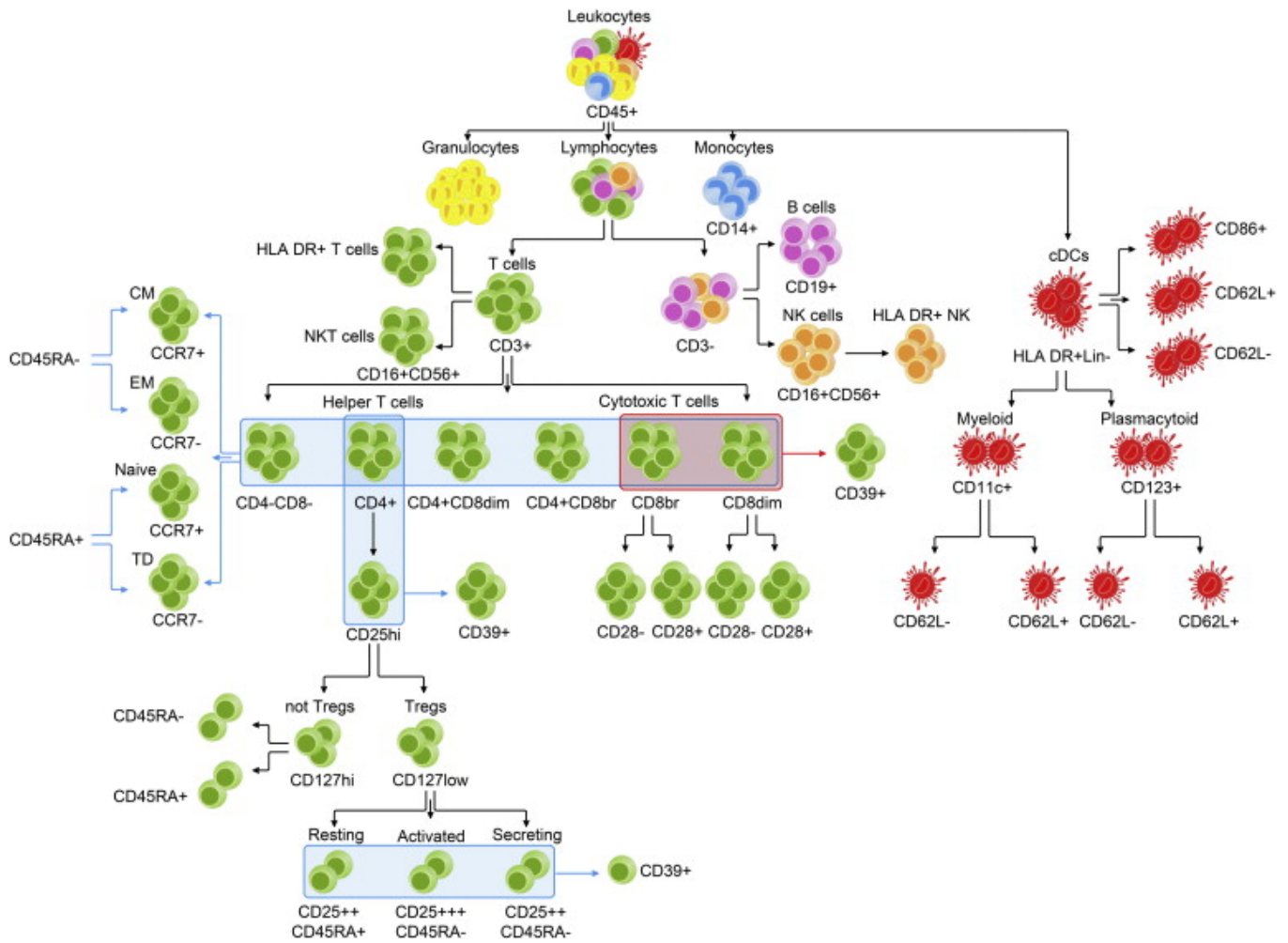


**Figure 1.3.** Complexity of T cell and dendritic cell phenotypes and their relationships within the immune system [4].

The immune system has mechanisms to promote inflammation, which are self-propagating, potentially resulting in too much inflammation and damage to healthy tissues. Conversely, there are mechanisms to reduce inflammation and restore balance to a damaged tissue so that it can be prepared [8]. The ratio of certain cytokines and certain immune cells which produce them is crucial to the whether the balance of inflammation swings toward inflammation or away from it [8,9].

Macrophages are large cells with the capacity to perform many functions and secrete large quantities of cytokines. Macrophages were previously categorized as either M1 or pro inflammatory phenotype, or M2 anti-

inflammatory phenotype [3]. While it has been argued that this is an oversimplification of a complex array of macrophage phenotypes, for the purpose of explanation I will continue to refer to M1 and M2 macrophages as examples of pro and anti-inflammatory. The balance of M1 to M2 macrophages can determine whether the inflammatory cascade continues or stops [3,9]. Additionally, M2 macrophages can induce a significant increase the numbers of T regulatory cells, which are also anti-inflammatory [9]. T regulatory cells are powerful modulators of immunity because they can induce apoptosis of pro-inflammatory CD4<sup>+</sup> and CD8<sup>+</sup> T Cells [3,5,8,9].

Promoting the prevalence and activity of M2 macrophages and FoxP3<sup>+</sup> T regulatory cells is thought to be a potent method of regulating excessive inflammation and a potential treatment for chronic inflammatory diseases [10,11]. Promoting systemic changes in the ratios of immune cells such as these, without significant immunosuppression is challenging with small molecule drugs [12]. Cell therapies have the potential to act on many pathways of the immune system simultaneously, and are more flexible than small molecule drugs, because they can alter their therapeutic potential in response to their environment [11,12].

Mesenchymal Stromal Cells (also know as Mesenchymal Stem Cells or MSC) are multipotent cells which are abundant in adult humans. MSC are easily expandable and can be sourced from donors without invasive procedures [12,13]. One important feature of MSC, which makes them an excellent choice for a cell therapy, is their low immunogenicity as allogeneic transplants, compared to most other cell types [13]. These properties combined; mean cells taken from a single donor can be used to treat many thousands of patients with minimal donor to recipient matching. The therapeutic potential of MSC treatments has been thoroughly explored over the last decade [11-16]. MSC have been shown to home to sites of inflammation and cancer, which means they can more specifically target these sites than small molecule drugs which have limited or no homing capabilities [11]. MSC are known to possess potent immunoregulatory capabilities, which involve effects on macrophage phenotypes and lineage determination, and promotion of FoxP3<sup>+</sup> T regulatory cells. In this dissertation, I present evidence to support the claim that MSC are potent therapeutics to treat autoimmune disorders, and that human umbilical cord derived MSC are particularly good for this purpose.

## 1.2 Cancer

Cancer is characterized as cells which resist cell death, sustain proliferation, evade growth suppressors, promote angiogenesis, obtain replicative immortality, and actively invade the surround tissue [16]. Metastases or cancer which spreads to other locations in the body, are responsible for over 90% of cancer related deaths [17]. Metastases are particularly hard to treat, and many standard treatments are extremely toxic to patients [11,17,18]. Treatments include surgery to remove the primary tumor, radiation, chemotherapy, and hormone modulation therapy [19]. The toxicity of cancer treatments is attributable to their non-specific activity, causing significant damage to rapidly dividing cells, which includes both cancer cells and healthy stem cells in the patient [19,20]. Cell therapies aim to use natural cancer homing capabilities of cells to target cancer and metastases more specifically [20-23]. CAR-T and adoptive T cell treatments for cancer are becoming increasingly popular, but have had serious side effects in some patients, resulting in death [23]. MSC offer great potential for treatment of cancer metastases due to their low toxicity relative to other cell therapies and small molecule drugs [11,20-22]. During my doctoral research I worked to develop several MSC based treatments for breast cancer metastasis [11,14]. The following chapters describe in detail a novel method to generate bone metastases in mice, and the treatment of those bone metastases using MSC as a vector to deliver small molecule drugs.

## 1.3 References

- 1) Torang, A., Gupta, P. & Klinke, D.J. An elastic-net logistic regression approach to generate classifiers and gene signatures for types of immune cells and T helper cell subsets. *BMC Bioinformatics* **20**, 433 (2019). [10.1186/s12859-019-2994-z](https://doi.org/10.1186/s12859-019-2994-z)
- 2) Redgrove KA, McLaughlin EA. The Role of the Immune Response in Chlamydia trachomatis Infection of the Male Genital Tract: A Double-Edged Sword. *Front Immunol.* 2014;5:534. Published 2014 Oct 27. [doi:10.3389/fimmu.2014.00534](https://doi.org/10.3389/fimmu.2014.00534)
- 3) DeFranco, Anthony L. *Immunity: Primers in Biology*. 1<sup>st</sup> ed., New Science Press Ltd, 2007.
- 4) Orru, V. et al. Genetic variants regulating immune cell levels in health and disease. *Cell* **155**, 242–256 (2013).
- 5) Chen L, Deng H, Cui H, et al. Inflammatory responses and inflammation-associated diseases in organs. *Oncotarget.* 2017;9(6):7204-7218. Published 2017 Dec 14. [doi:10.18632/oncotarget.23208](https://doi.org/10.18632/oncotarget.23208).
- 6) Zhang JM, An J. Cytokines, inflammation, and pain. *Int Anesthesiol Clin.* 2007;45(2):27-37. [doi:10.1097/AIA.0b013e318034194e](https://doi.org/10.1097/AIA.0b013e318034194e).
- 7) García-Lloret MI, Ignacio Santos J. Las citocinas y su papel como mediadores de salud y enfermedad.

- Nuevos enfoques para viejos problemas [Cytokines and their role as health and disease mediators. New approaches to old problems]. *Bol Med Hosp Infant Mex.* 1990;47(12):797-808.
- 8) Whiteside TL. The role of regulatory T cells in cancer immunology. *Immunotargets Ther.* 2015;4:159-171. Published 2015 Aug 5. doi:10.2147/ITT.S55415
  - 9) Kang, H., Yang, B., Zhang, K. et al. Immunoregulation of macrophages by dynamic ligand presentation via ligand–cation coordination. *Nat Commun* 10, 1696 (2019). <https://doi.org/10.1038/s41467-019-09733-6>
  - 10) Kumar, V. Macrophages: The potent immunoregulatory innate immune cells. In: Bhat, KH (ed.). *In macrophage activation-biology and disease.* London, UK: IntechOpen, 2020.
  - 11) Ségaliny A.I., Cheng J., Farhoodi H.P., Toledano M., Yu C.C., Tierra B., Hildebrand L., Liu L., Liao M., Cho J., Liu D., Sun L., Gulsen G., Su M.Y., Sah R., & Zhao W. Combinatorial Targeting of Cancer Bone Metastasis Using mRNA Engineered Stem Cells. *EBioMedicine* Vol. 45, 39-57. Doi.org/10.1016/j.ebiom.2019.06.047 (2019).
  - 12) Farhoodi H.P.\*, Liu L\*, Han M, Liu G, Yu J, Nguyen L, Nguyen B, Nguyen A, Liao W, Zhao W. Preclinical Evaluation of a Single Intravenous Infusion of hUC-MSC (BX-U001) in Rheumatoid Arthritis. *Cell Transplant.* 2020 Jan-Dec;29:963689720965896. Doi: 10.1177/0963689720965896. (2020).
  - 13) Liu L., Wong C.W., Han M., Farhoodi H.P., Liu G., Liu Y., Liao W. & Zhao W. Meta-analysis of Preclinical Studies of Mesenchymal Stromal Cells for Rheumatoid Arthritis. *EBioMedicine* 2019;47:563-577. Doi:10.1016/j.ebiom.2019.08.073 (2019).
  - 14) Liu L., Zhang S.X., Liao W., Farhoodi H.P., Wong C.W., Chen C.C., Ségaliny A.I., Chacko J.V., Nguyen L.P., Lu M., Polovin G.P., Pone E.J., Downing T.L., Lawson D.A., Digman M.A., & Zhao W. Mechanoresponsive stem cells to target cancer metastases through biophysical cues. *Science translational medicine* 9, doi:10.1126/scitranslmed.aan2966 (2017).
  - 15) Chen C.C., Liu L., Ma F., Wong C.W., Guo X.E., Chacko J.V., Farhoodi H.P., Zhang S.X., Zimak J., Ségaliny A., Riazifar M., Pham V., Digman M.A., Pone E.J., & Zhao W. Elucidation of Exosome Migration Across the Blood–Brain Barrier Model In Vitro. *Cellular and Molecular Bioengineering*:1-21. (2016).
  - 16) Mei SH, Haitzma JJ, Dos Santos CC, Deng Y, Lai PF, Slutsky AS, Liles WC, Stewart DJ. Mesenchymal stem cells reduce inflammation while enhancing bacterial clearance and improving survival in sepsis. *Am J Respir Crit Care Med.* 2010 Oct 15;182(8):1047-57. doi: 10.1164/rccm.201001-0010OC. Epub 2010 Jun 17. PMID: 20558630. Hanahan D, Weinberg RA. The hallmarks of cancer. *Cell.* 2000 Jan 7;100(1):57-70. doi: 10.1016/s0092-8674(00)81683-9. PMID: 10647931.
  - 17) Chaffer CL, Weinberg RA. A perspective on cancer cell metastasis. *Science* (80- ). 2011. doi:10.1126/science.1203543
  - 18) Farhoodi H.P., Ségaliny A.I., Wagoner Z.W., Cheng J.L., Liu L., Zhao W. Optimization of a syngeneic murine model of bone metastasis. *Journal of Bone Oncology.* 2020, 23, 100298, Doi: 10.1016/j.jbo.2020.100298. (2020).
  - 19) Coleman RE. Management of bone metastases. *Oncologist.* 2000;5(6):463-470.
  - 20) Higgs JT, Jarboe JS, Lee JH, Chanda D, Lee CM, Deivanayagam C, et al. Variants of Osteoprotegerin Lacking TRAIL Binding for Therapeutic Bone Remodeling in Osteolytic Malignancies. *Mol Cancer Res.* 2015;13(5):819-827.
  - 21) NguyenThai QA, Sharma N, Luong do H, Sodhi SS, Kim JH, Kim N, et al. Targeted inhibition of osteosarcoma tumor growth by bone marrow-derived mesenchymal stem cells expressing cytosine deaminase/5-fluorocytosine in tumor-bearing mice. *J Gene Med.* 2015;17(3-5):87-99.
  - 22) Qiao B, Shui W, Cai L, Guo SQ, Jiang DM. Human mesenchymal stem cells as delivery of osteoprotegerin gene: homing and therapeutic effect for osteosarcoma. *Drug Des Dev Ther.* 2015;9:969-976.
  - 23) Leen AM, Rooney CM, Foster AE. Improving T cell therapy for cancer. *Annu Rev Immunol.* 2007;25:243-65. doi: 10.1146/annurev.immunol.25.022106.141527. PMID: 17129181.

# CHAPTER 2

## Optimization of a Syngeneic Murine Model of Bone Metastasis

**Authors:** Henry P. Farhoodi<sup>1-3</sup>, Aude I. Segaliny<sup>1-3</sup>, Zachary W. Wagoner<sup>1-3</sup>, Jason L. Cheng<sup>1-3</sup>, Linan Liu<sup>1-3</sup>, and Weian Zhao<sup>1-6</sup>

<sup>1</sup> Sue and Bill Gross Stem Cell Research Center, University of California, Irvine, Irvine, CA 92697, USA;

<sup>2</sup> Department of Pharmaceutical Sciences, University of California, Irvine, Irvine, CA 92697, USA;

<sup>3</sup> Chao Family Comprehensive Cancer Center, University of California, Irvine, Irvine, CA 92697, USA;

<sup>4</sup> Edwards Life Sciences Center for Advanced Cardiovascular Technology, University of California, Irvine, Irvine, CA 92697, USA;

<sup>5</sup> Department of Biomedical Engineering, University of California, Irvine, Irvine, CA 92697, USA;

<sup>6</sup> Department of Biological Chemistry, University of California, Irvine, Irvine, CA 92697, USA;

## 2.1 Abstract

Many cancers metastasize to the bones, particularly in cases of breast and prostate cancers. Due to the “vicious cycle” of cancer cells inducing bone resorption, which promotes further tumor growth, they are difficult to treat and may lead to extreme pain. These factors increase the urgency for emerging therapeutics that target bone metastases more specifically and effectively. Animal studies are essential to the development of any therapeutics, but also require robust animal models of human diseases. Robust animal models are often challenging to develop in the case of bone metastasis studies. Previous methods to induce bone metastasis include intracardiac, intravenous, subcutaneous via mammary fat pad, and intraosseous cancer cell injections, but these methods all have limitations. By contrast, the caudal artery route of injection offers more robust bone metastasis, while also resulting in a lower rate of vital organ metastases than that of other routes of tumor implantation. A syngeneic animal model of bone metastasis is necessary in many cancer studies, because it allows the use of immunocompetent animals, which more accurately mimic cancer development observed in immunocompetent humans. Here we present a detailed method to generate robust and easily monitored 4T1-CLL1 syngeneic bone metastases with over 95% occurrence in BALB/c mice, within two weeks. This method can potentially increase consistency between animals in bone cancer metastasis studies and reduce the number of animals needed for studying bone metastases in mice.

**Keywords:** Cancer; animal models; bone metastasis; intra-arterial, caudal artery; 4T1



## 2.2 Introduction

Over 90% of cancer mortalities can be attributed to metastasis, the dissemination of cancer cells from the primary tumor site to other tissues in the body [1,2]. Bone metastases are frequent, occurring in up to 70% of patients with advanced breast or prostate cancers and in approximately 15 to 30% of patients with cancers of the lung, colon, stomach, bladder, uterus, rectum, thyroid, or kidney [3,4]. A consistent and efficient animal model is necessary to study the mechanisms of bone cancer metastasis and develop novel treatments for these bone metastases. Unfortunately, the current standard model, using intracardiac injection of cancer cells, is not easy to perform, nor does it produce metastases specific to bone [5,6]. Other implantation routes for establishing bone metastasis are not optimal for varying reasons. Intravenous injections (IV) tend to produce lung tumors that can metastasize to bones, but also commonly metastasize to the liver, spleen, or brain. Another pitfall of IV injections is that the relatively large lung tumors, that inevitably develop, can mask weaker signals located in other parts of the body, due to signal detector saturation. This issue is exaggerated for subcutaneous injections to the mammary fat pads (subsequently referred to as just “fat pads”) due to the large primary tumors which form before metastasis, and the fact that the fat pads are in close proximity to the bones of the leg, pelvis, and spine. Fat pad injections also rely on spontaneous dissemination of cancer cells which results in low rates of metastasis to bones, increasing the number of animals needed for experiments, and makes it difficult to establish consistent timelines in experiments. Intraosseous (also known as intratibial) injections are consistent and well controlled in terms of cell quantity/growth but require an invasive bone drilling procedure that creates local inflammation and fails to accurately mimic the natural cancer bone metastatic process from the circulatory system [7,8]. The methods mentioned above result in tumors formed at the vital organs, causing high

animal mortality rates, which impede the study and development of targeted treatments for bone metastasis in animal models [9].

Due to ethical and financial constraints, the number of animals used in an experiment needs to be limited, and an efficient rate of bone metastasis decreases the number of animals needed to complete a study [10,11]. In recent work, we required a robust syngeneic cancer model to evaluate our cell therapy for treating bone metastasis and the resulting damage caused to bones [12]. We tested each of the previously mentioned models and were unsatisfied with their rates of bone specific metastasis despite using *in vivo* selection to improve bone homing.

Intra-arterial injections are sometimes used to generate bone metastases in mice, as described by Wright et al. [9]. This method was recently expanded upon by Kuchimaru et al. to improve bone metastasis in rodents using the caudal artery of the tail. This injection route produces consistent and efficient distribution of cancer cells localized in the leg bones, via the blood distributed to the lower body. Caudal-artery injections are easier to perform than tail vein injections, a common technique used for *in vivo* studies, and result in few complications. In addition, the frequency of metastases to the vital organs is remarkably low, with most tumors establishing themselves in the bone, allowing the majority of mice to survive to the experimental endpoint [13].

Most bone metastasis studies use human cancer lines xenotransplanted to animal models, and thus require immunocompromised animals for the human cancer cells to produce detectable tumors [14]. This immunocompromised system does not accurately mimic the conditions of cancer development and treatment in humans. A syngeneic cancer model enables the study of cancer treatments in an immunocompetent system and can give additional information about the efficacy of an anticancer therapy not possible in immuno-compromised models alone [8]. The 4T1 cell line (ATCC® CRL-2539™) is a

murine breast cancer that produces metastatic growth equivalent to human breast cancer metastasis, when given to BALB/c mice [15]. While these cells are excellent for mimicking general metastasis, the rates of bone specific metastasis can be improved by *in vivo* selection for cells that prefer to metastasize to bones [16-21]. *In vivo* selection was originally developed by the Clézardin lab to generate far higher rates of bone metastasis, using a fluorescence-based reporter system [20]. The use of *in vivo* selection for bone homing cells can be further enhanced by engineering cells to express luciferase. This enables the concurrent selection of cells that luminesce more stably and brightly *in vivo*, grow faster within the bone, and produce a more identifiable bone tumor from which to select cells [21].

Although the caudal artery method (Kuchimaru et al.) is an outstanding effort to improve bone metastatic rates, the previously described method has a broad scope using many cell lines (mostly xenogenic), and it was necessary to optimize specifics of the protocol for syngeneic experiments [13]. Here, we describe details and comments to establishing robust and consistent 4T1 breast cancer bone metastasis in a syngeneic BALB/cJ mouse model.

### **2.3 Results**

A bone localizing murine breast cancer cell line (4T1-CLL1) was derived from 4T1 cells engineered to express luciferase (Luc) and red fluorescent protein (RFP) by several rounds of *in vivo* selection and used to generate a consistent and robust bone metastasis rate in BALBc mice (Figure 2.1). We then compared standard cancer cell injection routes to the recently described caudal artery injection route. The caudal artery injection method combined with 4T1-CLL1 bone localizing cells produced higher rates of bone metastasis and generally lower rates of vital organ metastasis than other standard methods (Table 2.2).

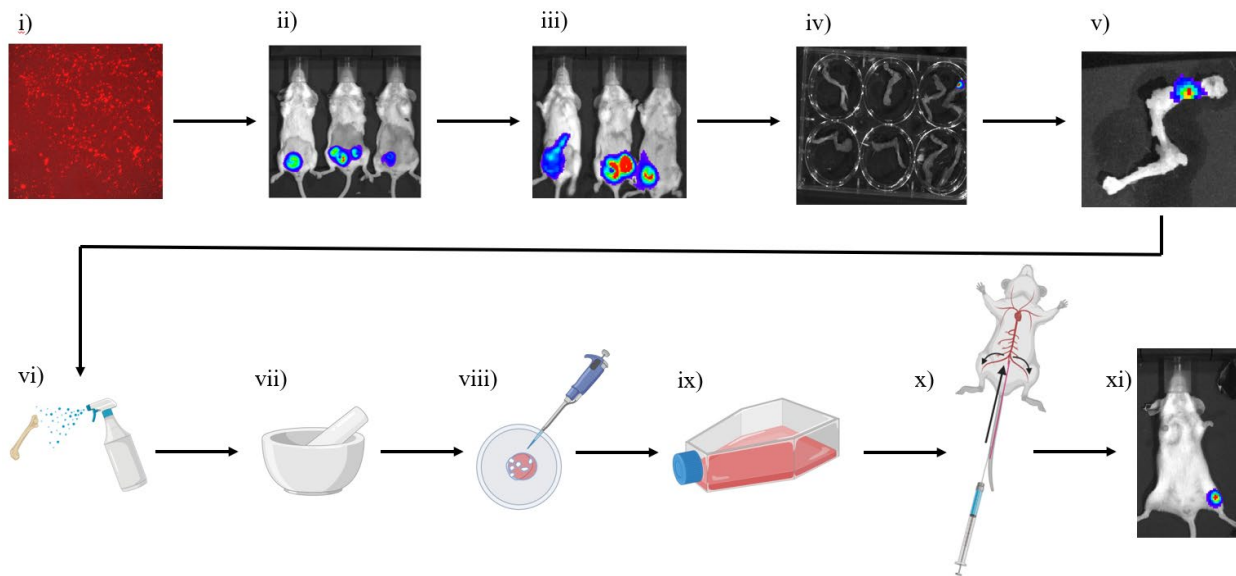


**Figure 2.1** Schematic of method to induce consistent syngeneic bone metastasis. i) Engineer cancer cells to express RFP and luciferase. ii) Inject engineered cells to lower inguinal fat pad of 5-week-old female BALB/c mice. iii) Monitor mice with *in vivo* bioluminescent imaging until fat pad tumor appears to show bone metastasis. iv) Harvest legs of mice and place in a well plate to confirm bone metastasis via *ex vivo* bioluminescent imaging. v) Select bones showing positive *ex vivo* bioluminescent signal. iv) Wash bones with ethanol. vii) Grind up bones with mortar and pestle. viii) Wash ground bones with growth media, pass through a cell strainer to remove bone fragments, then transfer to flask for culture. ix) Culture cells to expand *in vitro*. x) Inject 5 to 8-week-old female BALB/c mice with cultured cells via caudal artery route. xi) Monitor mice with *in vivo* bioluminescent imaging and identify bone metastases. See “Methods” for detailed protocols.

**Table 2.1. Percentage of mice showing 4T1 breast cancer metastases to significant locations for different routes of cancer cell injection.**

| Metastasis Model           | Fat pad      | IV           | IC           | CA 1wk       | CA 2wk       | CA 1wk (cancer only) | CA 2wk (cancer only) | CA 1wk (PI only) | CA 2wk (PI only) | CA 2wk (PI + cancer only) |
|----------------------------|--------------|--------------|--------------|--------------|--------------|----------------------|----------------------|------------------|------------------|---------------------------|
| Number of mice             | 12           | 3            | 3            | 93           | 92           | 68                   | 82                   | 32               | 31               | 30                        |
| Any cancer development (%) | 100          | 100          | 100          | 73.12        | 89.13        | 100                  | 100                  | 31.18            | 96.77            | 100                       |
| <b>Any bone (%)</b>        | <b>16.67</b> | <b>66.67</b> | <b>66.67</b> | <b>67.74</b> | <b>85.87</b> | <b>92.65</b>         | <b>96.34</b>         | <b>29.03</b>     | <b>96.77</b>     | <b>100</b>                |
| Any leg (%)                | 16.67        | 0            | 33.33        | 49.46        | 83.7         | 67.65                | 93.9                 | 20.43            | 93.55            | 96.67                     |
| Spine (%)                  | 0            | 33.33        | 66.67        | 44.09        | 77.17        | 60.29                | 86.59                | 20.43            | 93.55            | 96.67                     |
| Pelvis (%)                 | 0            | 0            | 66.67        | 21.51        | 43.48        | 29.41                | 48.78                | 7.527            | 0                | 0                         |
| Any fat pad (%)            | 100          | 33.33        | 100          | 46.24        | 75           | 63.24                | 84.15                | 18.28            | 9.68             | 10                        |
| <b>Any vital organ (%)</b> | <b>8.333</b> | <b>100</b>   | <b>100</b>   | <b>4.301</b> | <b>21.74</b> | <b>5.882</b>         | <b>24.39</b>         | <b>0</b>         | <b>12.9</b>      | <b>13.33</b>              |
| Lung (%)                   | 0            | 100          | 100          | 4.301        | 14.13        | 5.882                | 15.85                | 0                | 9.68             | 10                        |
| Brain (%)                  | 0            | 33.33        | 66.67        | 0            | 3.261        | 0                    | 3.659                | 0                | 3.226            | 3.333                     |
| Liver (%)                  | 8.333        | 33.33        | 33.33        | 0            | 7.609        | 0                    | 8.537                | 0                | 0                | 0                         |
| Kidney (%)                 | 0            | 33.33        | 66.67        | 0            | 5.435        | 0                    | 6.098                | 0                | 12.9             | 13.33                     |
| 2 wk mortality (%)         | 0            | 100          | 100          | 1.075        | 1.09         | 1.471                | 1.22                 | 1.075            | 3.226            | 3.333                     |

*Abbreviations: IV: intravenous injection, IC: Intracardiac injection, CA: Caudal artery injection, 1wk: After one week of growth. The “cancer only” group is a subset of the CA group and includes only CA animals that showed any detectable tumor growth up to that point. The “PI” group is a subset of the CA group and includes only CA mice that received perfect injections (100% of cells were delivered into the caudal artery). Any cancer development refers to the tumor take rate for the specified group. The Intravenous model established with a single injection to the tail vein with 500,000 Luc-RFP cells and bioluminescent imaging performed 11 days post cell injection, the Intracardiac model established by injection to left ventricle of 200,000 Luc-RFP cells and bioluminescent imaging performed 11 days post-injection, the Fat pad model established by subcutaneous injection on top of one or both of the lower inguinal mammary fat pads (Supplemental Figure 2.1a “#5”) of 100,000 Luc-RFP cells mixed with 50% Matrigel™ and bioluminescent imaging performed 14 days post cell injection, the Caudal artery (1 wk) model established by intra-arterial injections of 10,000 to 20,000 Luc-RFP cells imaged after 7 days post cell injection, Caudal artery (2 wk) model contains the same animals as “Caudal artery (1 wk)” and bioluminescent imaging was performed 14 days post cell injection. Bioluminescent images (front and back) were exposed for 1 second, 60 seconds, and auto exposed to get high sensitivity for weak signals and minimize saturation caused by strong signals.*

### 2.3.1 *In vivo* selection for bone localizing 4T1 cells

One important aspect of many murine cancer studies is the ability to track cancer growth *in vivo*. Using lentiviral particles (GenTarget Inc. LVP324), 4T1 cells were engineered to express RFP and luciferase, which enables tracking of cancer cells both *in vivo* and within post-mortem tissues (Figure 2.1i). While 4T1 cells can produce bone metastases, they also frequently create primary tumors in non-bone organs, particularly the mammary fat pads. To increase the rate of bone specific metastases, we used *in vivo* selection. Two rounds of *in vivo* selection were used to produce a 4T1 derivative cell line “4T1-CLL1” (Figure 2.1ii-1ix), which we have shown can generate bone metastasis at high rates when used in combination with a caudal artery injection, in BALB/cJ mice (Table 2.2). The 4T1-CLL1 cell line exhibited similar growth rates when compared to 4T1 cells (Figure 2.2b). However, we did note an interesting shift in morphology within the 4T1-CLL1 cells, characterized by a tendency to spread into the empty spaces of the dish, rather than grow in compact colonies (Figure 2.2a).

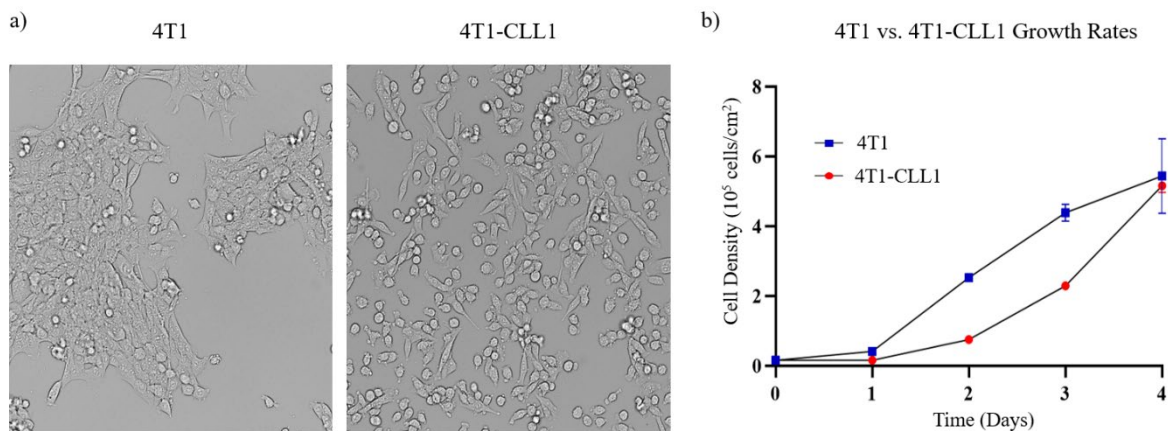


**Figure 2.2.** The 4T1-CLL1 line shows some phenotypic differences to 4T1 cells. a) Morphological comparison between the two cell lines at equivalent densities shows the 4T1-CLL1 cells appeared to transition from a clumped colony forming behavior to a migratory phenotype. b) To investigate possible changes in growth rate, 4T1 (P15) and 4T1-CLL1 cells were plated in triplicates, starting at 5,000 cells per well (96 well plate) and grown using Roswell Park Memorial Institute (RPMI) 1640 Medium (supplemented with 10% FBS). Cell density was recorded by hemocytometer and the mean of triplicates ( $\pm$ SEM) for each cell line was calculated every 24 hours.

The 4T1-CLL1 cell line was found to be extremely aggressive when delivered via the caudal artery to BALB/cJ mice (Figure 2.3). After only two weeks, leg bones received significant damage due to the osteolytic ability of the cells. We have previously shown the severe bone erosion this model produces via microCT scans [12]. 4T1-CLL1 cells ( $1 \times 10^4$ ) delivered by caudal artery produced extensive shaft and epiphysis damage. Bone metastases significantly reduced overall femur bone volumes and reduced trabecular bone in the epiphysis. While invasion into the bone marrow was frequent (Figure 2.3a,b,c), the majority of the tumor mass was concentrated in the epiphysis [12]. Bones were frequently so damaged and broken by tumor invasions that neither histology nor microCT were possible.

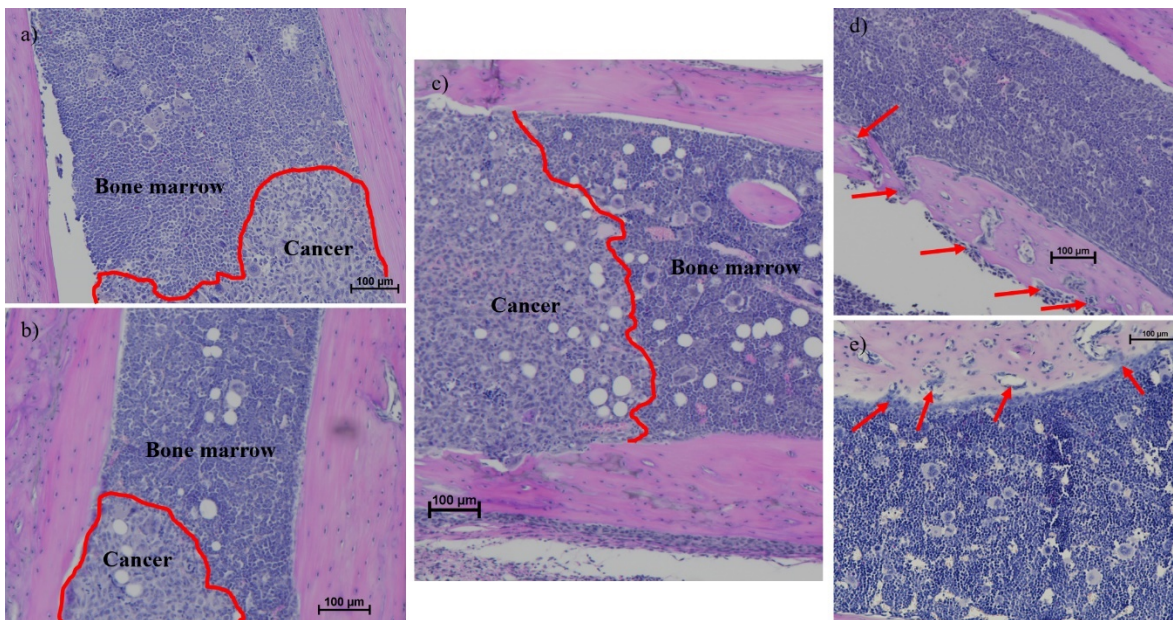


**Figure 2.3.** 4T1-CLL1 delivered via caudal artery produce invasive and destructive bone metastases. a), b), and c) show the invasion of cancer cells into the bone marrow of mouse femurs. The red line indicates the front of the tumor invasion. d) and e) show degradation of bone and simultaneous invasion of tumors cells (red arrows). Tumors developed after 10,000 to 20,000 4T1-CLL1 were delivered via caudal artery to BALB/cJ mice and allowed to grow for two weeks before being sacrificed for histological analysis.



### **2.3.2 Comparison of caudal artery injection route to other standard bone metastasis inducing cell delivery methods**

The standard routes of injecting cancer cells to produce bone metastasis (intravenous, intracardiac, subcutaneous mammary fat pad) were insufficient for our previous bone metastasis mouse studies, because they lacked speed, consistency, low mouse mortality (vital organ metastases), and high rates of bone metastasis. Mice injected with 4T1 by intravenous (IV) or intracardiac routes (IC), rapidly became unhealthy and died (Table 2.2). Bioluminescent imaging revealed large tumors in the lungs, intrapleural cavity, and/or heart for both IV and IC injection routes (Figure 2.4a). A high rate of mortality creates significant problems with consistency in a bone metastasis study, because animals die before bone metastasis or before bone metastasis growth can be sufficiently evaluated. Fat pad injections are used frequently for triple negative breast cancer and patient derived xenograft models and used to study cancer cell intravasation and dissemination. Subcutaneous mammary fat pad injections produced low rates of mortality, but had low rates of bone metastasis, took a long time to metastasize to bones, and/or were difficult to evaluate on a bioluminescent basis, due to the saturating signal produced by the large fat pad tumors (Figure 2.4a). The saturation of the primary tumors can be alleviated by surgical resection of the primary tumor, which can also result in even fewer vital organ metastases. However, tumor resections are invasive and can result in a significant increase in animal pain, which is avoided by use of the caudal artery route. The caudal artery injection route produced low rates of vital organ metastasis, high rates and of leg bone metastasis in only one to two weeks, and fat pad signal saturation was far less an issue (allowed identification of small bone metastases close to the fat pads) than was the case for a direct fat pad injection (Figure 2.4). Additionally, the ability to see the injection fluid traveling through the vessel after caudal artery injections, allows stringent judgement of precision compared to intracardiac injections, in which the



actual injection is not seen. A comparison of the four injection routes, shows similar rates of bone metastasis between intravenous, intracardiac, and caudal artery mice, but vital organ metastasis rates closer to those of the fat pad mice (Figure 2.4b). Significantly, for our study, leg bone metastasis rates were higher for caudal artery injection mice than any other route (Figure 2.4b). There were significant numbers of mice with tumors clearly localized in the lower inguinal fat pad regions for all models tested with 4T1 cell lines (Figure 2.4).

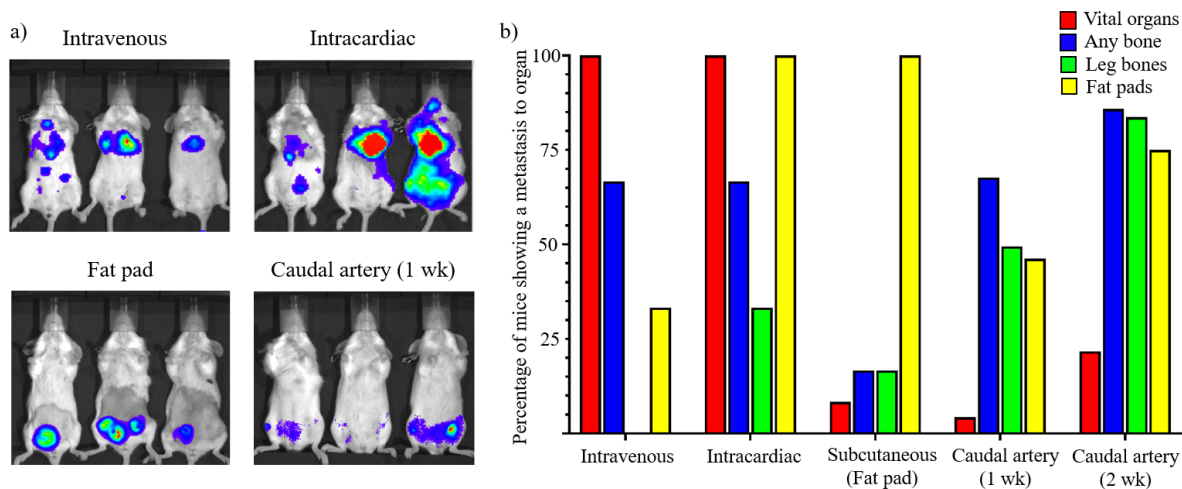


**Figure 2.4.** Graphical comparison of 4T1 breast cancer metastasis locations for different routes of cancer cell injection. a) Representative images of tumor growth for each route after one to two weeks post cell transplantation. b) Comparison of metastasis location for each Luc-RFP-4T1-CLL1 cell implantation route. The “Vital organs” were counted if a mouse had at least one clear tumor in the brain, lungs, heart, liver, and/or kidneys. The “Any bones” were counted as any signals that were determined to be in bones, including the femur and tibia/fibula leg bones, lower spine, pelvis, and ribs. The “Fat pads” included any tumors at the region of the abdominal mammary fat pads. The percentage of mice showing metastasis to organs was calculated by counting the number of animals showing bioluminescent signal in at least one of the organs in each group, divided by the total number of animals in the experiment and multiplying by 100. Cell quantities injected for each route, and the methods are described in more detail in Table 2.2.

### 2.3.3 Optimizing 4T1-CLL1 caudal artery injection for desired growth rates and consistency

Determining the appropriate cell number to inject is important, as it has a major impact on tumor growth rates [13,22,23]. Due to the high bone delivery rate of the caudal artery injection, and the aggression

of the 4T1 cell line, few cells are needed to generate detectable tumors, when compared to xenogeneic cell lines. The 4T1 cell line is so aggressive, that it causes mouse morbidity with off-target metastases (such as to the vital organs) in other injection routes. However, most of the growth from caudal artery delivered 4T1-CLL1 cells is localized in the bones (spine, leg bones, and pelvis) and/or the inguinal mammary fat pads (Table 2.2, Figure 2.4a, Figure 2.5). Injection of a lower number of cells (e.g., 1,000) can result in very specific bone metastasis, but the time it takes for the tumors to become detectable/trackable can vary (1 to 6 weeks). Since a few of the mice did not develop tumors within 6 weeks, the number of mice with bone metastases available for the experiment can be unclear. While the mice injected with 1,000 cells developed some of the cleanest bone metastases (minimal metastases outside leg bones), these metastases also appeared to be inconsistent in their growth rates, since some mice developed detectable tumors in much less time than others. This large baseline variation in growth can make comparison between treatment groups far more difficult. Depending on what the metastasis model is meant to evaluate, the growth rate can be controlled by injecting more cells (Figure 2.5). If many more cells are injected (e.g., 50,000), the rate of detectable bone tumor development becomes fast and consistent (5 to 6 days). However, the rapid growth of resulting tumors may require sacrificing the mice after only 2 weeks [24]. The ability to evaluate therapeutics may also be hindered by such a high rate of tumor growth, since even a high dose of standard chemotherapeutic drug (5-fluorouracil) was unable to sufficiently inhibit tumor growth (Supplemental Figure 2.4). Therefore, a reasonable balance between tumor growth rate and consistency seems to be 5,000 cells injected, but this will depend on the desired metastasis characteristics (ex. Consistency between animals, rate of tumor growth, and whether a leg bone specific tumor is required). A 5,000-cell caudal artery injection will produce a detectable tumor consistently within 2 weeks, if the injection itself is done correctly and the cells are healthy (Figure 2.5).

Interestingly, in an experiment where 32 mice received perfect injections (all cells delivered to caudal artery in first attempt) of 10,000 to 20,000 4T1-CLL1 cells, excluding one mouse which did not develop any detectable cancer, we achieved a 100% leg bone metastasis rate within 2 weeks (Table 2.2). Of these mice, only 13.33% developed metastases to vital organs within two weeks, most of which appeared to be in the lungs, liver, and kidneys (Table 2.2). The relatively low rate of vital organ metastasis limits morbidity in mice and allows a focus on bone tumors and their treatment. If the cells are not delivered perfectly, for example if some cells are delivered subcutaneously while attempting to insert the needle to the caudal artery, the rates of vital organ metastasis increase with each failed injection, most likely caused by the proximity of tail veins to the caudal artery (Supplemental Figure 2.1b) and the high motility of the 4T1-CLL1 cells (Figure 2.2).

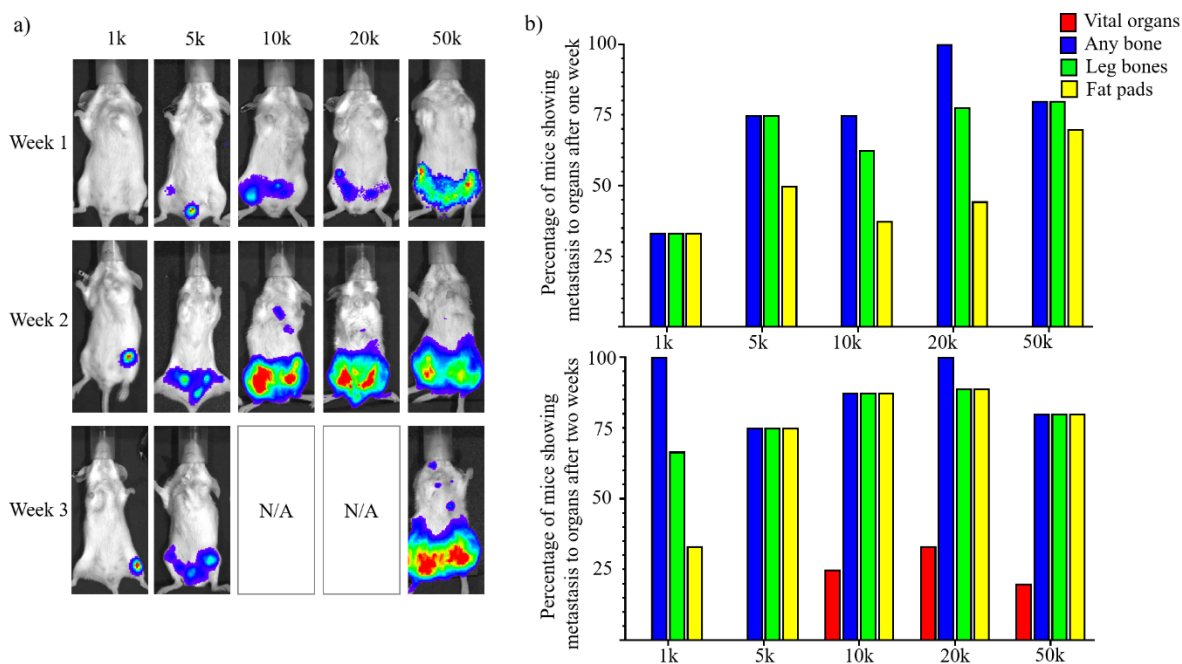


**Figure 2.5.** Quantity of cells injected alters pattern of 4T1-CLL1 metastasis. a) 4T1-CLL1 cells were injected via caudal artery and allowed to grow for three weeks (the 10k and 20k mouse groups were sacrificed, as part of an experiment, before a week three imaging could be performed). Bioluminescent imaging was performed biweekly to monitor tumor growth over time using automatic exposure and have automatic colorimetric scaling (non-quantitative). Images for each cell quantity group are representative of the overall progression of each group of mice over time. b) Comparison of metastasis locations for various cell quantities injected via caudal artery after one week (top) and two weeks (bottom) of growth. The “Vital organs” were counted if a mouse had at least one clear tumor in the brain, lungs, heart, liver, and/or kidneys. The “Any bone” were counted as any signals that were determined to be in bones, including the femur and tibia/fibula leg bones, lower spine, pelvis, and ribs. The “Fat pads” included any tumors at the region of the abdominal mammary fat pads. The percentage of mice showing metastasis to organs was calculated by counting the number of animals showing bioluminescent signal in at least one of the organs in each group, divided by the total number of animals in the experiment and multiplying by 100. Number of animals included: 1k n = 3, 5k n = 4, 10k n = 8, 20k n = 9, and 50k n = 10.

## 2.4 Discussion

Several factors significantly affect the success rate of injections. It is important to create detailed standard operating procedures for cell preparations, to minimize technique variations between different personnel, because these variations can cause different tumor growth rates. Mice should be sedated with a ketamine/xylazine solution, which has a greater effect on hemodynamics (including arterial pressure). Appropriate sedation is required so that injected cells can flow against arterial pressure until they reach the branching point of the iliac arteries and can flow toward the leg bones [25]. Adequate heating of the tail prior to injection (dilates caudal artery), and sufficient injection training of personnel is essential to getting perfect injections, thus minimizing vital organ metastases, while maximizing leg bone metastases.

One characteristic of the 4T1 cell line noticed in all experiments, was a tendency to form tumors at the mammary fat pad tissue beneath nipples #4 and #5 (Supplemental Figure 2.1a). While there were a high percentage of tumors in bones, many were also observed at these fat pads (Figure 2.4b). This is likely because the 4T1 cell line originates from mammary gland tissue, and that the caudal artery injection route delivers cells to vessels which feed the abdominal mammary glands [26]. Further rounds of *in vivo* selection might increase the propensity of the cells for bones over fat pads. Additionally, further studies should be done to characterize the 4T1-CLL1 cell line to determine what molecular alterations result in better osteotropism and to confirm maintenance of osteomimicry and osteotropism after *in vitro* passaging. It is important to minimize the number of *in vitro* passages for cell lines which have undergone *in vivo* selection, because they may lose some of their selected phenotype.

From the primary sites of tumor engraftment (usually bones and fat pads) the cells can further metastasize to any other location including vital organs but appeared to spread to neighboring organs more frequently than distant ones (Supplemental Figure 2.1c). The longer animals were kept alive, the more

vital organ metastases were detected. This is consistent with other routes of injection, except that other routes produced vital organ metastases much sooner after cells were injected. The preference for fat pad tumor growth makes this model similar to direct subcutaneous fat pad injection route, except that the resulting fat pad tumors in this model are relatively small and usually do not mask other sites of metastasis.

There are still several caveats to address with this bone metastasis model. The frequency of spine tumors produced high rates of lower body paralysis in mice with large tumors after two weeks, but this can also happen at high occurrence in other models of bone metastasis [27-29]. This can be mitigated by using a minimal cell injection numbers, that will slow overall tumor growth. As mentioned above, the precision of the injection and the quality of the cells are important to model consistency. In large experiments, where many mice require caudal artery injections within a short time period, the time constraints will increase the chance for mistakes and lower the ratio of “perfect injections”. Time constraints are an issue particularly because cells being used for animal injections should not be left sitting on ice for long, because it may reduce their health, viability, and cause cell clumping. While the percentage of “perfect injections” above may belie the ease of the technique, we defined a “perfect injection” strictly, such that repositioning of a needle after the first insertion (despite delivering cells directly to the caudal artery), was a disqualifier. In smaller experiments (under 20 mice), “perfect injections” can be completed in almost every mouse.

Another consideration is that while this model allows tracking tumor growth in live animals, determination of precise metastasis locations can be difficult, without sacrificing the animal and imaging the organs *ex vivo*. Unfortunately, in large animal studies, *ex vivo* imaging can be impractical because it requires time which might be used to preserve sensitive tissues for downstream assays (ex. FACS on bone marrow and spleen). The *in vivo* bioluminescent imaging method we mentioned above (Supplemental

Figure 2.5) uses two-dimensional images and requires us to estimate the actual position of a tumor in three-dimensional space and determining if a tumor is inside or outside of a bone can be difficult. To mitigate this issue, we performed *ex vivo* bioluminescence imaging in several studies to confirm our ability to determine if metastases were within the bone (Supplemental Figure 2.2). Additionally, we made use of multiple exposure times, which minimizes masking by saturating tumors in later stages of experiment, while also allowing detection of small tumors in early stages. Front and back images can be taken to show whether the signal is more ventral or dorsal and thus increase metastasis tracking accuracy. Some tumor positions can be better identified by the signal strength of front (ventral) images, relative to the back (dorsal). For example, if in the spine, the signal will be stronger on the back image than the front, but the position of the signal along the midline of the mouse will be consistent.

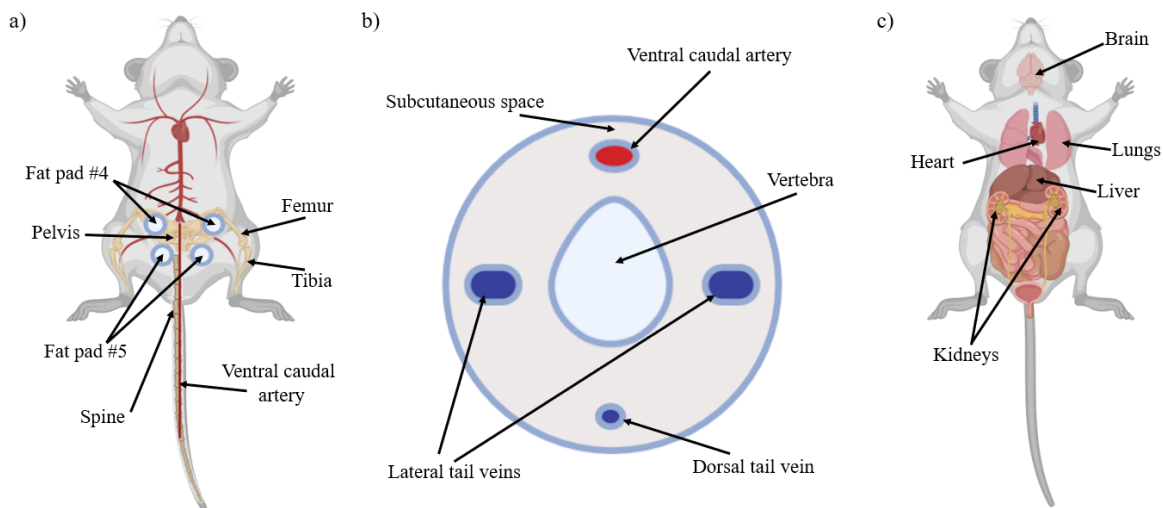
## **2.5 Materials and Methods**

*Note on animal studies: All experiments involving live animals should be performed under the guidance of an Institutional Animal Care and Use Committee and follow national and local regulations. Experiments in this study were performed at the University of California Irvine under IACUC protocol number AUP-18-134.*

### ***In Vivo* Bone Metastatic Cell Selection**

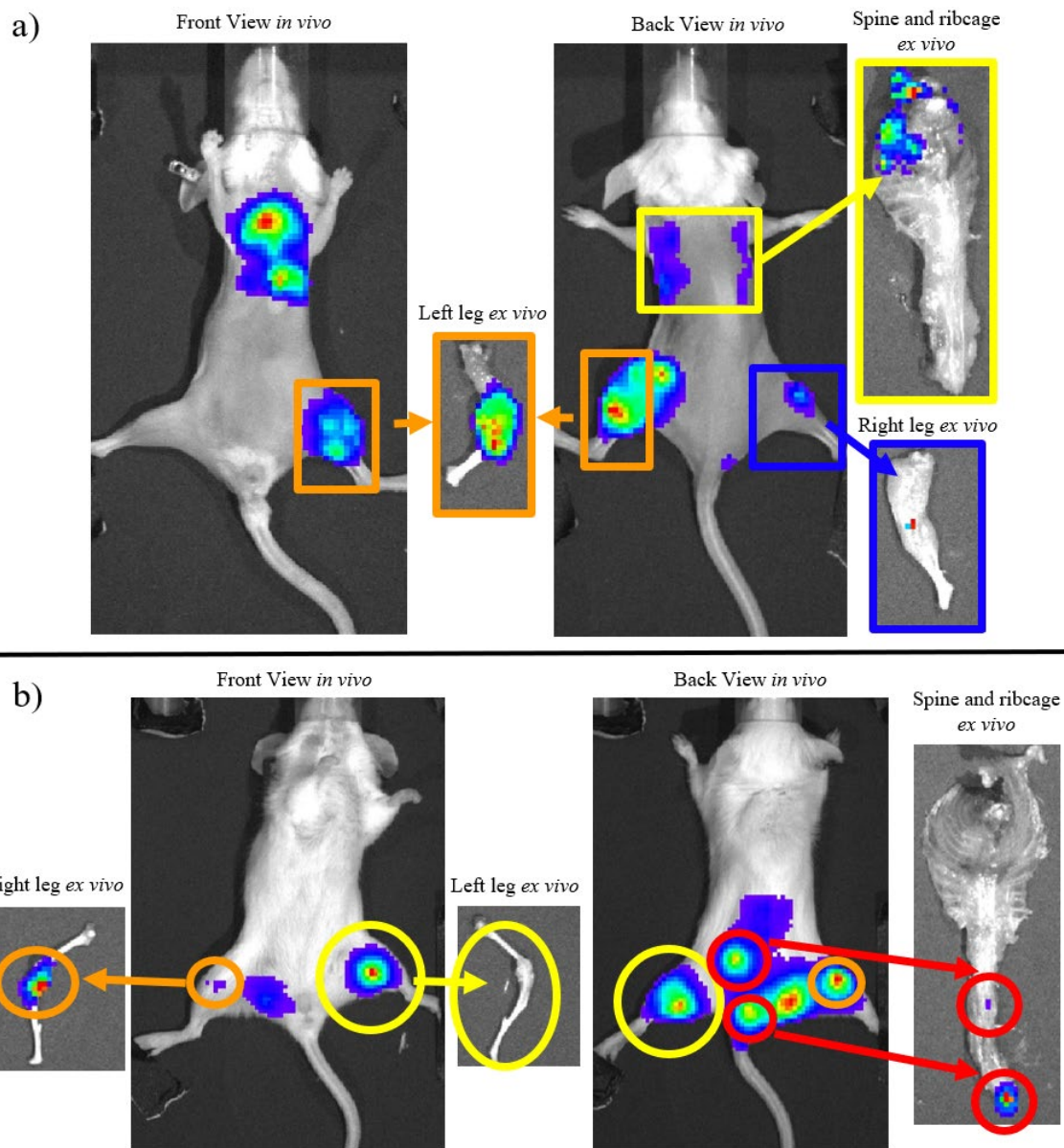
4T1 cells were transduced to express RFP and luciferase using a multiplicity of infection of 10 (see manufacturer protocol). Engineered 4T1 cells were then mixed with Matrigel™ at a concentration of 1 million cells/mL. 6-week-old female BALB/cJ mouse were fully sedated and their abdomens were shaved to expose mammary fat pads (Supplemental Figure 2.1a). The cell/Matrigel™ mixture was subcutaneously

injected to one or both lower inguinal mammary fat pads at 100,000 cells per mouse. Mice were monitored bi-weekly using *in vivo* bioluminescent imaging. After detecting leg bone metastasis in a mouse, the mouse was sacrificed, and the identified leg bone harvested. *Ex vivo* bioluminescent imaging was performed on the harvested leg to confirm that the metastasis is within the bone (Supplemental Figure 2.2). Leg bones were cleaned with 70% ethanol and ground to ~1 mm pieces using a mortar and pestle. Growth media (RPMI 1640, 10% FBS, 1% pen/strep) was used to rinse cells and collect them, before being run through a 70  $\mu$ m cell strainer into a clean 50 mL tube. The filtered cell solution was transferred to a T25 flask and allowed to grow in an incubator (37°C, 5% CO<sub>2</sub>) overnight. Growth media was changed the following day to selection media (RPMI 1640 containing 10% FBS, 1% pen/strep, and 3  $\mu$ g/mL puro) to remove dead cells and bone fragments and to begin selection for engineered cells. RFP fluorescence was confirmed using a Nikon Eclipse Ti fluorescent microscope. After the first passage, selective pressure was maintained with puromycin (RPMI 1640, 10% FBS, 1% pen/strep, and 1  $\mu$ g/mL puro). Cells were used below passage 6 to prevent phenotypic drift.



**Supplemental Figure 2.1.** Important landmarks in mice for a 4T1 caudal artery bone metastasis model. a) Important landmarks for primary metastases. b) Cross section view of mouse tail and blood vessels. c) Vital organ landmarks relating to 4T1 metastasis.





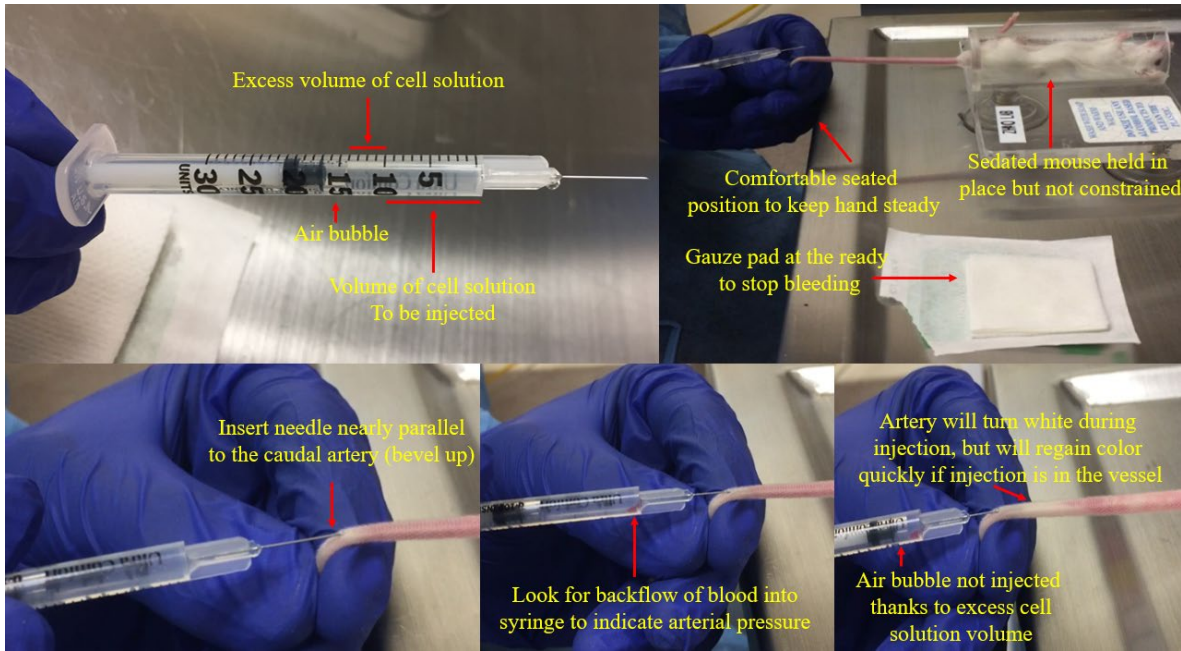
**Supplemental Figure 2.2.** Example *ex vivo* bioluminescent imaging to confirm bone presence of *in vivo* signals. a) Shows the *ex vivo* imaging of key bone metastases (orange boxes: Left leg, yellow boxes: Ribcage, blue boxes: Right leg). b) Shows another individual animal imaged *in vivo* then sacrificed and imaged *ex vivo*. Note that the right leg (orange circles) shows metastasis in the center of the leg bone *in vivo* and *ex vivo*, whereas the left leg (yellow circles) shows tumor growth off-center to the leg bone *in vivo*, and *ex vivo* imaging reveals no metastasis in the bone itself. The metastases to the spine (red circles) are clearly visible in the back view *in vivo* image and confirmed by *ex vivo* imaging. Note: a) and b) show two individual mice injected with 4T1-CLL1 cells ( $5 \times 10^3$ ) via the caudal artery and allowed to grow for two weeks before final *in vivo* imaging (shown above) and *ex vivo* imaging post-mortem.

## **4T1 Preparation for Caudal Artery Injection**

*In vivo* selected, luciferase-engineered 4T1 cells (4T1-CLL1) were grown to 70% confluence. Cells were trypsinized, washed, and spun down at 300 rcf for 5 minutes. Cells were then washed in 10 mL of ice-cold PBS, spun down at 300 rcf again, and resuspended in another 10 mL of ice-cold PBS before being gently passed through a 70  $\mu$ m cell strainer. Cells were counted and then diluted to 5,000 to 50,000 cells/100  $\mu$ l (depending on number needed to be injected per mouse). Cells were aliquoted into 1.5 mL microcentrifuge tubes and placed on ice before being injected to mice.

## **Caudal Artery Injection**

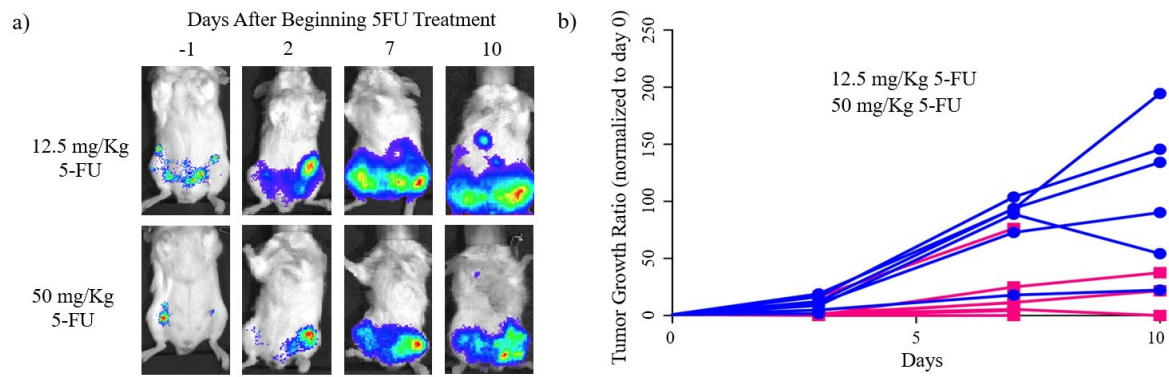
Six-week-old female BALB/cJ mice were fully sedated with a ketamine/xylazine solution (100 mg/Kg and 10 mg/Kg respectively). Mice were placed ventral side up in a cylindrical mouse restrainer and their tails were warmed with a heating lamp. An aliquot of 4T1-CLL1 cells was warmed up in hands and pipetted to mix before being loaded into a 29G $\frac{1}{2}$  300  $\mu$ L (3/10 cc) diabetes syringe, with a 30  $\mu$ L air pocket at the base of the plunger. The mouse tail was wiped with ethanol and the tip of the tail pulled straight before inserting the needle (bevel up) 2 cm to 3 cm from tail-tip to enter the caudal artery at a 0° to 10° angle, until a pulse of blood indicated correct position within artery (Supplemental Figure 2.3). The plunger was pressed carefully, making sure to feel for any resistance, until 100  $\mu$ L of cell solution was injected. After injection the needle was held in place for 5 seconds then rotated 90° before being slowly withdrawn from the artery. A sterile gauze pad was placed with pressure for 60 seconds to the needle insertion site, to stop bleeding. Mice were placed in a warmed cage and monitored closely prior to their awakening.



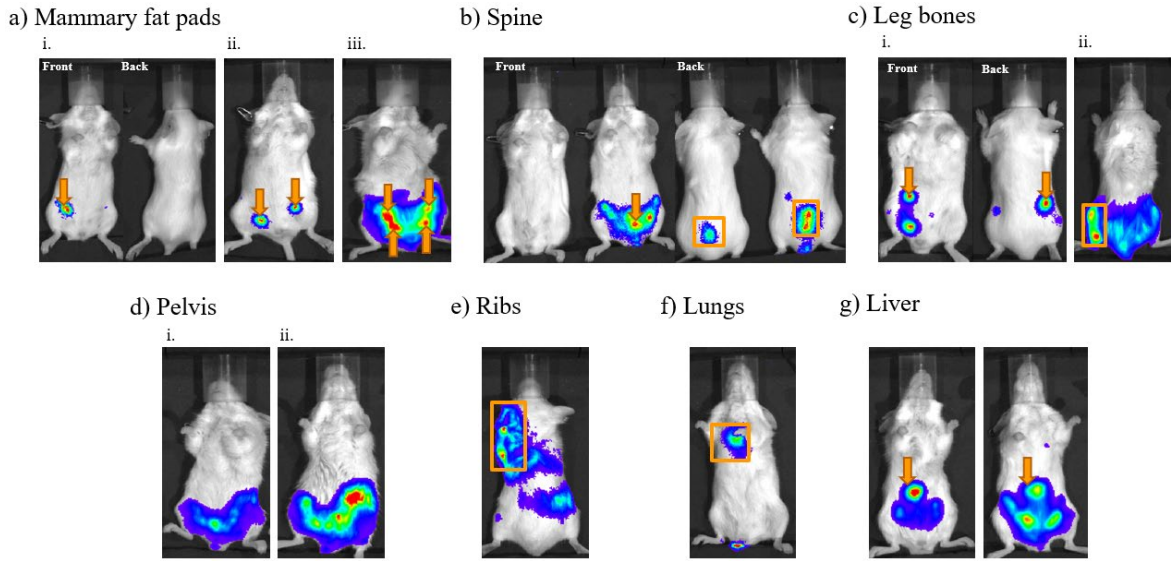
**Supplemental Figure 2.3.** Demonstration of caudal artery injection with comments.

### **Hematoxylin and Eosin Staining**

Bones were fixed in 10% formalin for 48 hours at 4°C before being decalcified in 14% EDTA, 0.4% PFA pH 7.4 in PBS while shaking at 4°C for 14 days. Decalcification solution was changed every two days. After decalcification, bones were paraffin embedded and sectioned to 7 µm slices before being mounted on Superfrost slides. Hematoxylin and eosin staining was performed using the standard procedure and slides were mounted in Permount. Slides were imaged using a Nikon Eclipse Ti microscope using a 10x objective.



**Supplemental Figure 2.4.** 4T1-CLL1 tumor growth over time is not sufficiently inhibited by 5-fluorouracil. a) Representative images showing the progression of tumors for two groups of mice receiving separate doses of 5-fluorouracil (5-FU) from one day prior to treatment, to 10 days after the first treatment injection. The 4T1-CLL1 cells were delivered via the caudal artery ( $5 \times 10^4$ ) 5 days prior to beginning of 5-FU treatment. The 5-FU Treatments were suspended in PBS and given via IP injection daily from day 0 until day 5. b) Tumor growth of each mouse treated by either 12.5 mg/Kg or 50 mg/Kg quantified by bioluminescent signal using the entire mouse as a ROI.



**Supplemental Figure 2.5.** Methodology for identifying metastasis location. a) i. Early mammary tissue (referred to as “fat pad”) metastases were identified using bioluminescent images of mice front side up. ii. Bioluminescent signals appeared circular and were positioned on abdominal mammary fat pads. iii. Distinct tumors in all four lower abdominal fat pads were identifiable even in later stages of tumor growth. b) Spine metastases were identified from imaging the back sides of mice. Signals from the spine appeared as elongated along the middle of the mouse (between the lower inguinal fat pads) and were exclusively found on the lower spine. c) i. Early signals indicating leg metastases were typically circular and seen on the lateral edge of the lower abdomen from both the front and back of the animal. ii. These signals began as circular foci around the ball of the femur before moving down the bone as the tumor developed. d) Pelvic metastases can be difficult to identify because the location is surrounded by sites of high metastasis, such as fat pads. The primary identifying mark of pelvic metastases were curved signals looping down and up towards the hip of the animal and may lack clear foci. e) Metastases to the ribs were rare and were strongest towards the edges of the chest. f) Metastases to the lungs are clearly visible on either side of the midline of the chest. These were characterized by a strong signal from the front of the mouse and little to no signal from the back of the animal. g) Signals which originated higher than the pelvis of the animal, but lower than the diaphragm, were considered to have metastasized to the liver. Liver signals were observed on the front of the abdomen as circular and slightly off-center towards the right side of the animal. Orange Arrow/Box: Indicates labeled signal. Images marked with “front” or “back” denote the same mouse, and images separated by a space indicate different mice.

## 2.6 Author Contributions

H.P.F., A.I.S. and W.Z. designed the research; H.P.F., A.I.S., J.L.C., Z.W.W., and L.L. performed the research; H.P.F., A.I.S, Z.W.W., and J.L.C. analyzed and interpreted the data; H.P.F., and Z.W.W. wrote the paper. All authors were involved in revising the manuscript. All authors have read and agreed to the published version of the manuscript.

## 2.7 Acknowledgments

This work was supported by the NIH (R21CA219225 to W.Z.), the DOD (W81XWH-17-1-0522 to W.Z.), and a contract with Baylx Inc. (BI-206512). H.P.F. was supported by the National Institute of Neurological Disorders and Stroke of the NIH (T32NS082174). A.I.S was supported by the Fondation ARC pour la recherche sur le cancer (SAE20150602901), and a contract with Amberstone Biosciences Inc., and L.L. was supported by Baylx Inc. (BI-206512). The project described was also supported by the National Center for Research Resources and the National Center for Advancing Translational Sciences, National Institutes of Health and National Cancer Institute of the National Institutes of Health under award number P30CA062203. The content of this paper is solely the responsibility of the authors and does not necessarily represent the official views of the National Institutes of Health. The funders above did not have any involvement in the study design, data collection, data analysis, interpretation, or manuscript writing.

## 2.8 References

1. Coleman RE, Rubens RD. The clinical course of bone metastases from breast cancer. *Br J Cancer*. 1987. doi:10.1038/bjc.1987.13
2. Chaffer CL, Weinberg RA. A perspective on cancer cell metastasis. *Science (80- )*. 2011. doi:10.1126/science.1203543
3. Roodman GD. Mechanisms of Bone Metastasis. *N Engl J Med*. 2004. doi:10.1056/NEJMra030831
4. Mundy GR. Metastasis to bone: Causes, consequences and therapeutic opportunities. *Nat Rev Cancer*. 2002. doi:10.1038/nrc867



5. Simmons JK, Hildreth BE, Supsavhad W, et al. Animal Models of Bone Metastasis. *Vet Pathol.* 2015. doi:10.1177/0300985815586223
6. Khanna C, Hunter K. Modeling metastasis in vivo. *Carcinogenesis.* 2005. doi:10.1093/carcin/bgh261
7. Werbeck JL, Thudi NK, Martin CK, et al. Tumor Microenvironment Regulates Metastasis and Metastasis Genes of Mouse MMTV-PyMT Mammary Cancer Cells In Vivo. *Vet Pathol.* 2014. doi:10.1177/0300985813505116
8. Jinnah AH, Zacks BC, Gwam CU, Kerr BA. Emerging and established models of bone metastasis. *Cancers (Basel).* 2018. doi:10.3390/cancers10060176
9. Wright LE, Ottewell PD, Rucci N, et al. Murine models of breast cancer bone metastasis. *Bonekey Rep.* 2016. doi:10.1038/bonekey.2016.31
10. Russell W, Burch R. The Principles of Humane Experimental Technique by W.M.S. Russell and R.L. Burch. John Hopkins Bloomberg School of Public Health.
11. Festing MFW, Altman DG. Guidelines for the Design and Statistical Analysis of Experiments Using Laboratory Animals. *ILAR J.* 2002. doi:10.1093/ilar.43.4.244
12. Segaliny AI, Cheng JL, Farhoodi HP, et al. Combinatorial targeting of cancer bone metastasis using mRNA engineered stem cells. *EBioMedicine.* 2019. doi:10.1016/j.ebiom.2019.06.047
13. Kuchimaru T, Kataoka N, Nakagawa K, et al. A reliable murine model of bone metastasis by injecting cancer cells through caudal arteries. *Nat Commun.* 2018. doi:10.1038/s41467-018-05366-3
14. Richmond A, Yingjun S. Mouse xenograft models vs GEM models for human cancer therapeutics. *DMM Dis Model Mech.* 2008. doi:10.1242/dmm.000976
15. Aslakson CJ, Miller FR. Selective Events in the Metastatic Process Defined by Analysis of the Sequential Dissemination of Subpopulations of a Mouse Mammary Tumor. *Cancer Res.* 1992.
16. Lelekakis M, Moseley JM, Martin TJ, et al. A novel orthotopic model of breast cancer metastasis to bone. *Clin Exp Metastasis.* 1999. doi:10.1023/A:1006689719505
17. Fidler IJ. Selection of successive tumour lines for metastasis. *Nat New Biol.* 1973. doi:10.1038/newbio242148a0
18. Clark EA, Golub TR, Lander ES, Hynes RO. Genomic analysis of metastasis reveals an essential role for RhoC. *Nature.* 2000. doi:10.1038/35020106
19. Rosol TJ, Tannehill-Gregg SH, LeRoy BE, Mandl S, Contag CH. Animal models of bone metastasis. *Cancer.* 2003. doi:10.1002/cncr.11150
20. Peyruchaud O, Winding B, Pécheur I, Serre CM, Delmas P, Clézardin P. Early detection of bone metastases in a murine model using fluorescent human breast cancer cells: Application to the use of the bisphosphonate zoledronic acid in the treatment of osteolytic lesions. *J Bone Miner Res.* 2001. doi:10.1359/jbmr.2001.16.11.2027
21. Bolin C, Sutherland C, Tawara K, Moselhy J, Jorcyk CL. Novel mouse mammary cell lines for in vivo bioluminescence imaging (BLI) of bone metastasis. *Biol Proced Online.* 2012. doi:10.1186/1480-9222-14-6
22. Gregório AC, Fonseca NA, Moura V, et al. Inoculated cell density as a determinant factor of the growth dynamics and metastatic efficiency of a breast cancer murine model. *PLoS One.* 2016. doi:10.1371/journal.pone.0165817
23. Kocatürk B, Versteeg HH. Orthotopic injection of breast cancer cells into the mammary fat pad of mice to study tumor growth. *J Vis Exp.* 2015. doi:10.3791/51967

24. Bailey-Downs LC, Thorpe JE, Disch BC, et al. Development and characterization of a preclinical model of breast cancer lung micrometastatic to macrometastatic progression. *PLoS One*. 2014. doi:10.1371/journal.pone.0098624
25. Janssen BJA, De Celle T, Debets JJM, Brouns AE, Callahan MF, Smith TL. Effects of anesthetics on systemic hemodynamics in mice. *Am J Physiol - Hear Circ Physiol*. 2004. doi:10.1152/ajpheart.01192.2003
26. Arguello F, Baggs RB, Frantz CN. A murine model of experimental metastasis to bone and bone marrow. *Cancer Res*. 1988.
27. Pulaski BA, Ostrand-Rosenberg S. Mouse 4T1 Breast Tumor Model. *Curr Protoc Immunol*. 2000. doi:10.1002/0471142735.im2002s39
28. Yoneda T, Sasaki A, Mundy GR. Osteolytic bone metastasis in breast cancer. *Breast Cancer Res Treat*. 1994. doi:10.1007/BF00666208
29. Nakai M, Mundy GR, Williams PJ, Yoneda T. A Synthetic Antagonist to Laminin Inhibits the Formation of Osteolytic Metastases by Human Melanoma Cells in Nude Mice. *Cancer Res*. 1992.



# CHAPTER 3

## Combinatorial targeting of cancer bone metastasis using mRNA engineered stem cells

**Authors:** Aude I. Segaliny<sup>1-6</sup>, Jason L. Cheng<sup>1-6</sup>, Henry P. Farhoodi<sup>1-6</sup>, Michael Toledano<sup>1-6</sup>, Chih Chun Yu<sup>1-6</sup>, Beatrice Tierra<sup>9</sup>, Leanne Hildebrand<sup>1-6</sup>, Linan Liu<sup>1-6</sup>, Michael J. Liao<sup>1-6</sup>, Jaedu Cho<sup>7</sup>, Dongxu Liu<sup>8</sup>, Lizhi Sun<sup>8</sup>, Gultekin Gulsen<sup>7</sup>, Min-Ying Su<sup>7</sup>, Robert L. Sah<sup>9</sup>, Weian Zhao<sup>1-6</sup>

<sup>1</sup> Sue and Bill Gross Stem Cell Research Center, University of California, Irvine, Irvine, CA 92697, USA

<sup>2</sup> Department of Pharmaceutical Sciences, University of California, Irvine, Irvine, CA 92697, USA

<sup>3</sup> Chao Family Comprehensive Cancer Center, University of California, Irvine, Irvine, CA 92697, USA

<sup>4</sup> Edwards Life Sciences Center for Advanced Cardiovascular Technology, University of California, Irvine, Irvine, CA 92697, USA

<sup>5</sup> Department of Biomedical Engineering, University of California, Irvine, Irvine, CA 92697, USA

<sup>6</sup> Department of Biological Chemistry, University of California, Irvine, Irvine, CA 92697, USA

<sup>7</sup> Department of Radiological Sciences, University of California, Irvine, Irvine, CA 92697, USA

<sup>8</sup> Department of Civil and Environmental Engineering, University of California, Irvine, Irvine, CA 92697, USA

<sup>9</sup> Department of Bioengineering, University of California, San Diego, San Diego, CA 92093, USA

### **3.1 Abstract**

Bone metastases are common and devastating to cancer patients. Existing treatments do not specifically target the disease sites and are therefore ineffective and systemically toxic. Here we present a new strategy to treat bone metastasis by targeting both the cancer cells (“the seed”), and their surrounding niche (“the soil”), using stem cells engineered to home to the bone metastatic niche and to maximize local delivery of multiple therapeutic factors. We used mesenchymal stem cells engineered using mRNA to simultaneously express P-selectin glycoprotein ligand-1 (PSGL-1)/Sialyl-Lewis X (SLEX) (homing factors), and modified versions of cytosine deaminase (CD) and osteoprotegerin (OPG) (therapeutic factors) to target and treat breast cancer bone metastases in two mouse models, a xenograft intratibial model and a syngeneic model of spontaneous bone metastasis. We first confirmed MSC engineered using mRNA produced functional proteins (PSGL-1/SLEX, CD and OPG) using various in vitro assays. We then demonstrated that mRNA-engineered MSC exhibit enhanced homing to the bone metastatic niche likely through interactions between PSGL-1/SLEX and P-selectin expressed on tumor vasculature. In both the xenograft intratibial model and syngeneic model of spontaneous bone metastasis, engineered MSC can effectively kill tumour cells and preserve bone integrity. The engineered MSC also exhibited minimal toxicity in vivo, compared to its non-targeted chemotherapy counterpart (5-fluorouracil).

### **Keywords**

Bone metastases, cell therapy, mesenchymal stem cell, mRNA engineering, combination therapy.

### **3.2 Introduction**

Bone metastasis is one of the most common complications in many cancers, and is present in over 350,000 people who die each year in the United States[1]. Bone metastases are incurable, largely untreatable, and have devastating effects on quality of life. They occur in up to 70 percent of patients with advanced breast cancer, and are associated with a median-survival of 19-25 months, along with severe morbidities including intractable pain, pathological fractures, spinal cord compression, and hypercalcemia[2]. Breast cancer cells alter the bone microenvironment and produce factors to promote osteoclastogenesis. In turn, bone resorption by osteoclasts releases growth factors, which stimulate tumor progression[3]. The reciprocal interaction between breast cancer cells and the bone microenvironment, called the “vicious cycle,” accelerates tumor growth and bone destruction. An effective therapy to treat bone metastasis, therefore, would require efficient targeting of both the cancer cells and their microenvironment. Such a treatment has been lacking. In fact, despite major progress in cancer therapies, the 5-year relative survival rate for metastatic breast cancer has barely improved over the past 20 years, remaining around 20%[2, 4]. Common treatments including surgery, chemotherapy, radiation therapy, and endocrine therapy are only palliative and are often associated with significant systemic toxicity[5]. Standard of care drugs targeting bone resorption, including bisphosphonates and Denosumab (antibody targeting the receptor activator of NF- $\kappa$ B ligand, RANKL), which act by inhibiting osteoclastogenesis through different mechanisms, are controversial in their anti-tumor mechanisms[6, 7]. Most importantly, these therapies, alone or in combination, are ineffective in targeting both tumor growth and osteolysis, often leading to relapse, new metastasis, drug resistance, and notably, high systemic toxicity[8]. In addition, targeted drug delivery systems for bone metastasis, especially those using nanoparticles, are still

in their infancy[9-13], and typically suffer from rapid clearance, poor targeting efficiency, and inability to penetrate to the center of large and poorly vascularized metastatic tumors[14].

Here we exploit a stem cell-based approach for targeted delivery of a combination of therapeutics, which interrogates both the cancer and its niche. Stem cells, including mesenchymal stem (or stromal) cells (MSC), act as potent, autonomous, and adaptive agents[15, 16], and have recently been tested as vehicles for drug delivery in cancer[17-22], including in clinical trials[23]. Specifically, using a facile mRNA-engineering approach, we programmed mesenchymal stem cells with machinery to enable a) specific and efficient bone metastases homing through engineered P-selectin glycoprotein ligand-1 (PSGL-1) and Sialyl-Lewis X (SLEX), which target highly expressed selectins in vessels surrounding the tumor[24-26], b) local cancer killing through the cytosine deaminase (CD)/pro-drug 5-Fluorocytosine (5-FC) system,[27] and c) osteolysis inhibition within the tumor niche through expression of modified osteoprotegerin (OPG)[28], a natural decoy receptor for RANKL, a key mediator in tumor-induced osteoclastogenesis (Figure 3.1). Previous studies targeting bone tumors through a cell-based therapy approach used genetically modified cells to only deliver a single therapeutic molecule[29-31]. Engineering cells with mRNA-based protein expression is advantageous for targeting bone metastasis due to its simplicity, safety (no genetic engineering), transient and rapid protein translation after transfection, and ability to express multiple factors simultaneously for combinatorial treatment[32-34]. In this report, using a xenograft intratibial model and a syngeneic model of spontaneous bone metastasis, we demonstrated that MSC engineered to simultaneously express PSGL-1/SLEX, CD, and OPG exhibit enhanced homing to the bone metastatic niche where they effectively kill tumor cells and preserve bone integrity with minimal toxicity.

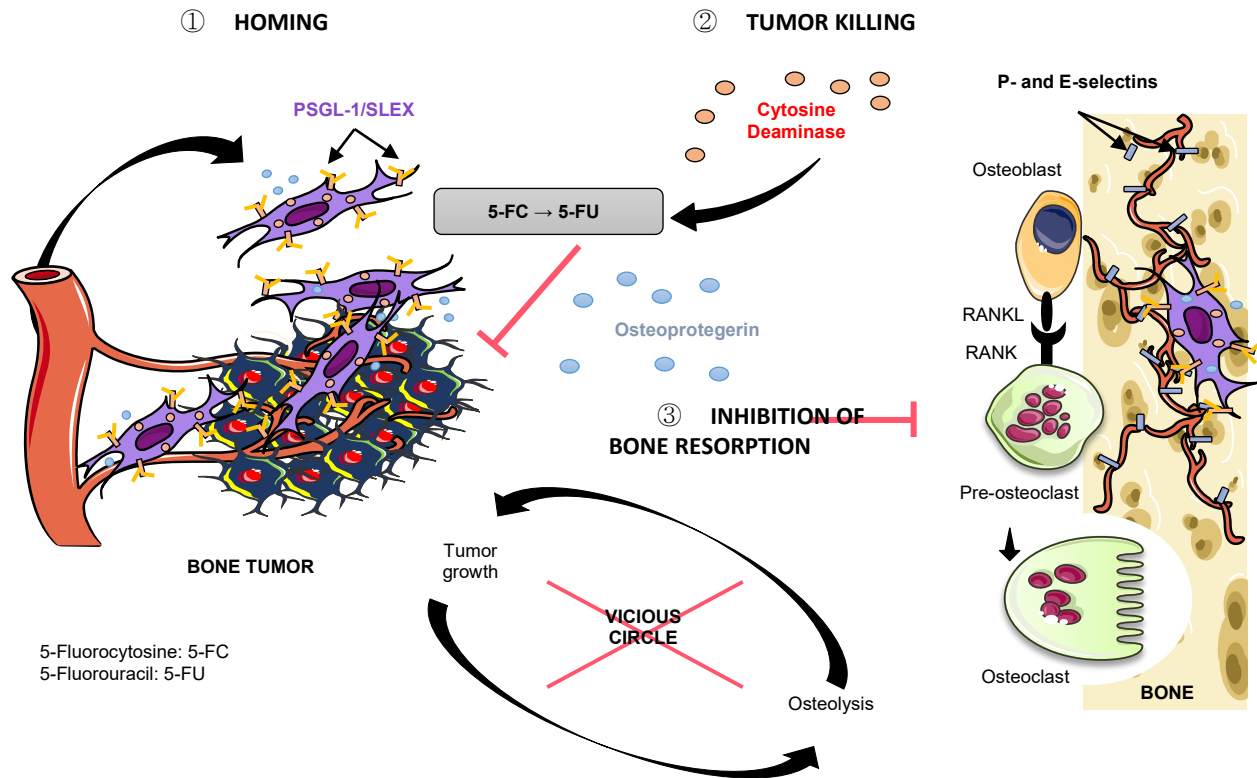


**Figure 3.1: Combinatorial targeting of cancer bone metastasis using mRNA engineered mesenchymal stem cells.** Proposed strategy for bone metastasis treatment by targeted delivery of multiple factors using mRNA-engineered mesenchymal stem cell (MSC) equipped with functions for a) specific and efficient bone metastases homing through P-selectin glycoprotein ligand-1 (PSGL-1) and Sialyl-Lewis X (SLEX), b) local cancer killing through cytosine deaminase (CD)/pro-drug 5-Fluorocytosine, and c) osteolysis inhibition within the tumor niche through a modified version of RANKL decoy receptor, osteoprotegerin (OPG).

### 3.3 Results

#### 3.3.1 MSC engineering using mRNA and *in vitro* functional validation

Modified mRNA encoding each target protein (PSGL-1, FUT-7 for post-translational SLEX modification, CD and OPG) were designed and synthesized following previous protocols[34]. We first transfected both PSGL-1 and FUT-7 mRNA into MSC, which resulted in a strong expression of fucosylated PSGL-1 at the membrane of MSC, with a typical transfection efficiency of 50-70%, as measured by flow cytometry (Supplementary Figure 3.4a, b). Interestingly, positive cells tend to express both transfected factors simultaneously with few cells transfected with only a single transcript[34]. The time-course showed that

expression of these markers was transient and persisted up to 6 days. Immunofluorescent staining was done 24 hours post-engineering and showed high PSGL-1 expression at the cell membrane, mainly localized in the pseudopodia (Supplementary Figure 3.4c), known to be important for leukocyte rolling[43]. The functional cell rolling enabled by these engineered homing ligands was then evaluated using a standard flow chamber assay, under shear forces mimicking *in vivo* circulatory conditions. When assayed on TNF- $\alpha$  activated endothelial cells under 1 to 10 dyn/cm<sup>2</sup>, Native MSC were not able to roll on the endothelium, while PSGL-1/SLEX MSC displayed a robust rolling profile comparable to that of a leukocyte model, HL-60, thus confirming the functionality of PSGL-1/SLEX modification (Figure 3.2a). In addition, cells engineered with the four factors (PSGL-1/SLEX/CD/OPG MSC) displayed a similar rolling profile from 1 to 5 dyn/cm<sup>2</sup> to that of PSGL-1/SLEX MSC, suggesting that engineering cells with multiple factors has minimal effect on the functionality of the others. We next assessed the expression and function of the first therapeutic factor, OPG, which should inhibit tumor-induced bone resorption by blocking RANKL. Note that our form of OPG is 1) truncated (no binding to glycosaminoglycans (GAGs)[44], 2) mutated (Y49R) to avoid binding to tumor necrosis factor-related apoptosis-inducing ligand (TRAIL), while preserving its binding to RANKL[29], and 3) fused to an Fc fragment of human IgG1 to increase its half-life[28] (Supplementary Table 3.2). As measured by ELISA, OPG accumulated over time in the culture medium of PSGL-1/SLEX/CD/OPG MSC and plateaued at approximately 70 ng/mL at day 6 (Supplementary Figure 3.5a). Native MSC also secreted OPG, but at a substantially lower concentration than engineered MSC, which is common upon confluence and subsequent differentiation *in vitro*, but is unlikely to occur *in vivo*[44]. In addition, only PSGL-1/SLEX/CD/OPG MSC secreted the truncated form of OPG fused to the human IgG1 Fc fragment, as both monomers and dimers were detected in lysates of engineered MSC, but not in lysates of

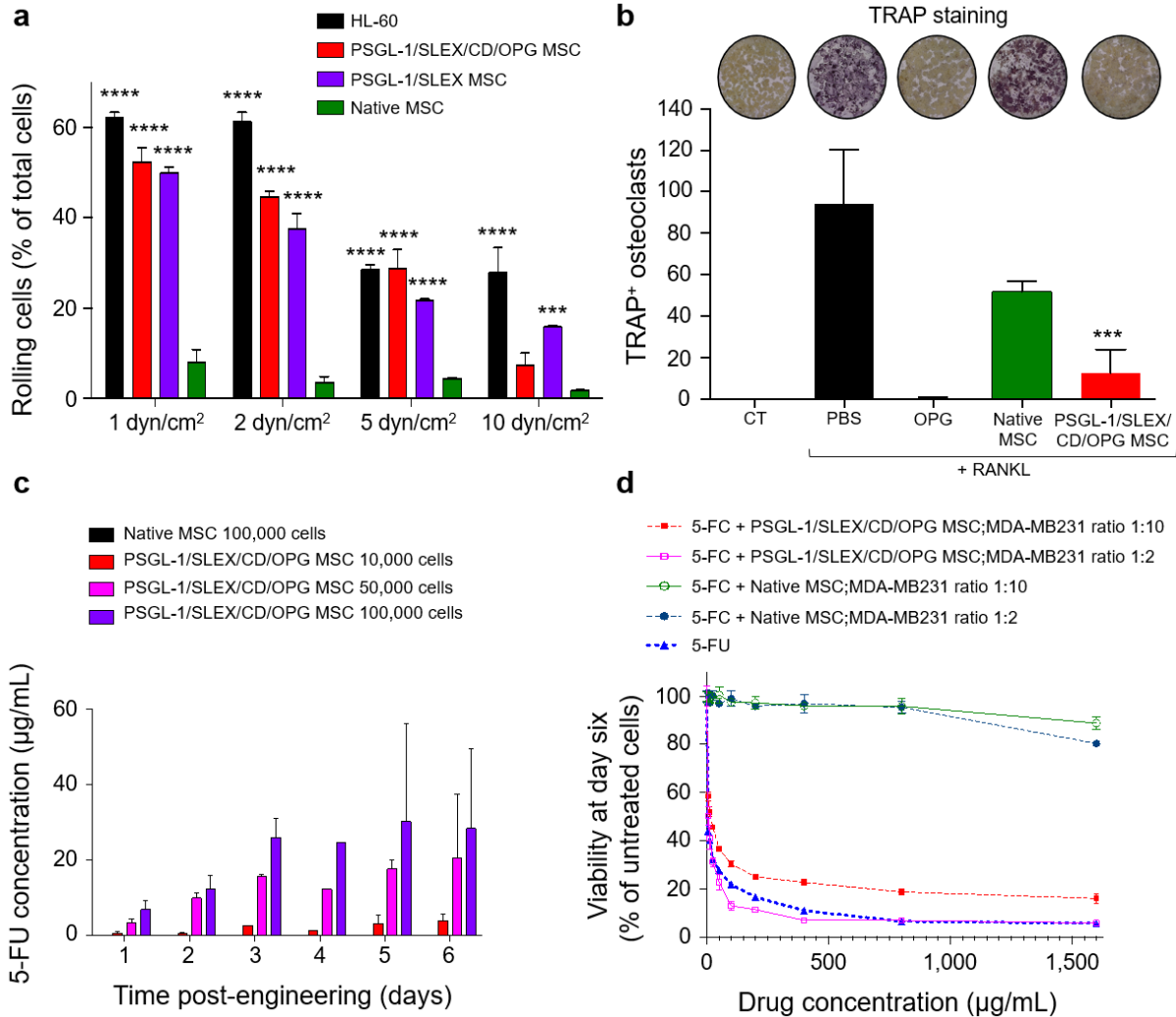


**Figure 3.2: MSC engineering using mRNA and *in vitro* functional validation.** (a) PSGL-1/SLEX/CD/OPG MSC display functional rolling on an endothelial layer under physiological shear flow. Native MSC, PSGL-1/SLEX MSC and PSGL-1/SLEX/CD/OPG MSC were flowed on a layer of endothelial cells at different physiological flow-rates 24 h post-MSCE engineering. HL-60 leukocytic cells were used as a positive control for rolling. Plot: mean + SD, statistical analysis: Two-way ANOVA test with Dunnett's multiple comparison test to compare each column to Native MSC, \*\*\*  $p \leq 0.001$ , \*\*\*\*  $p \leq 0.0001$ . (b) PSGL-1/SLEX/CD/OPG MSC inhibit osteoclastic differentiation *in vitro*. Murine osteoclast precursors (RAW264.7 cells) were plated for 6 days in media with the addition of nothing (CT), 100 ng/mL recombinant murine RANKL to induce osteoclastogenesis, and day 2 supernatant of MSC (Native and PSGL-1/SLEX/CD/OPG). 100ng/mL of recombinant human OPG was used as a positive control for osteoclastogenesis inhibition. Pictures show the TRAP stained culture at day 6 for each condition. Plot: mean + SD, statistical analysis: Kruskal-Wallis with Dunn's multiple comparison test, \*\*\*  $p \leq 0.001$  compared to PBS+RANKL condition. (c) PSGL-1/SLEX/CD/OPG MSC convert 5-FC into 5-FU *in vitro* in a cell concentration-dependent manner. 24 h post-engineering, MSC were plated at different concentrations in presence of 400 µg/mL 5-FC. LC-MS/MS was done on conditioned media collected at different days to measure the 5-FU converted from 5-FC. Plot shows mean + SD. (d) PSGL-1/SLEX/CD/OPG MSC kill MDA-MB231 cancer cells *in vitro*. Native MSC and PSGL-1/SLEX/CD/OPG MSC were plated at different ratios (1:2 and 1:10) on top of cancer cells in the presence of increasing doses of 5-FC, and the viability of the co-culture was determined at day 6. 5-FU was used as a positive control. Graph shows mean ± SD.

Native MSC when blotting for the Fc fragment (Supplementary Figure 3.5b). We showed that OPG secreted by PSGL-1/SLEX/CD/OPG MSC was significantly more efficient than that of Native MSC in inhibiting osteoclastic differentiation, as osteoclast numbers decreased by 89.1% compared to the PBS control (100 ng/mL RANKL alone) (Figure 3.2b). We further demonstrated that our engineered form of OPG did not block TRAIL-induced apoptosis of MDA-MB231, whereas the natural OPG protein did (Supplementary Figure 3.5c), therefore mitigating its risk in preventing cancer apoptosis when used as a treatment. Finally, we characterized the expression and activity of the second therapeutic factor, cytosine deaminase fused to the UPRT (CD)[27], used for direct tumor killing. The CD/5-FC system was chosen for this study among several options for pro-drug/cytotoxic combinations[45] for different reasons. First, it is widely used in the context of cell-based delivery. It was the first suicide gene therapy protocol in the clinic (NCT02015819 and NCT0117296), and it is currently being used in clinical trials by engineered neural stem cells for treatment of glioblastoma[46]. Besides, the product 5-Fluorouracil (5-FU) is one of the standard care chemotherapy drugs for breast cancer in the clinic[47]. Finally, compared to other pro-drug/cytotoxic systems, CD/5-FC demonstrated a potent anti-tumor efficacy *in vivo*[27]. We optimized a protocol using electrospray mass spectrometry, which allows discriminating between the chemically close 5-FC and 5-FU compounds to measure the pro-drug conversion by the CD (Supplementary Figure 3.3). Intracellular expression of CD was confirmed in PSGL-1/SLEX/CD/OPG MSC by both immunofluorescence and western blotting (Supplementary Figure 3.6a, a). Functionally, the CD convertase was able to hydrolyze 5-FC to 5-FU, which was detected in culture supernatants with LC-MS/MS, whereas 5-FU was not found in the supernatant of Native MSC (Figure 3.2c). The 5-FU concentration was dependent on the engineered cell numbers and reached up to 30  $\mu\text{g/mL}$ , from 100,000 PSGL-1/SLEX/CD/OPG



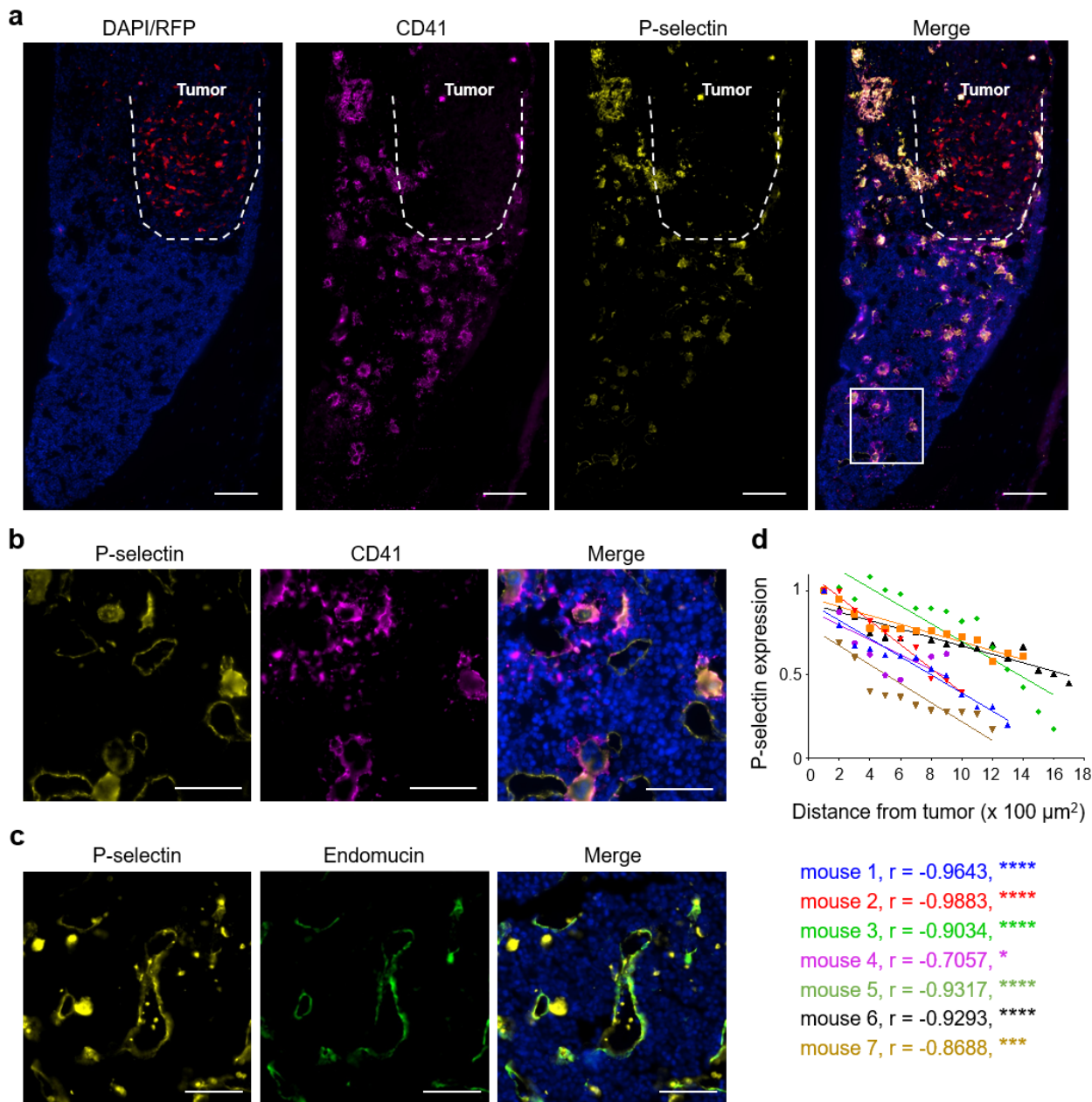


**Figure 3.3: P-selectin is highly expressed in the bone metastatic niche.** (a) Both high P-selectin expression and elevated megakaryocytes/platelets number are seen in the bone marrow surrounding the tumor. Red: RFP constitutively expressed by tumor cells. Yellow: P-selectin, magenta: CD41 and blue: nuclei (DAPI staining). Dashed line outlines the tumor. The area designated by a white rectangle is shown at higher magnification in panel B. Scale bar: 100  $\mu\text{m}$ . (b) Platelets and megakaryocytes express high level of P-selectin. Yellow: P-selectin, magenta: CD41 and blue: nuclei (DAPI staining). Scale bar: 50  $\mu\text{m}$ . (c) P-selectin is expressed at the bone marrow endothelium in the breast cancer bone metastatic environment. Yellow: P-selectin, green: endomucin (vascular endothelium) and blue: nuclei (DAPI staining). Scale bar: 50  $\mu\text{m}$ . (d) P-selectin expression is higher around the tumor area than in the rest of the bone marrow. P-selectin expression was quantified from bone marrow sections of 7 mice per area of 100  $\mu\text{m}^2$  from the tumor.  $r$  = Pearson correlation coefficient. \*  $p \leq 0.05$ , \*\*\*  $p \leq 0.001$ , \*\*\*\*  $p \leq 0.0001$ .

MSC, after 3 days of culture. Furthermore, the conversion of 5-FC into 5-FU by our mRNA-engineered MSC was shown to be as efficient as conversion by MSC constitutively expressing the CD-UPRT after lentiviral transduction[19]. When co-cultured with breast cancer cells in the presence of 5-FC, CD MSC were able to induce cell death, while Native MSC did not affect the cell viability for 6 days (Figure 3.2d). Remarkably, CD MSC plated at a 1:2 ratio with cancer cells turned out to be as potent as 5-FU at inducing cancer cell killing for equal concentrations of 5-FC and 5-FU. Pictures of the co-culture, at day 6, showed a confluent cell layer with healthy cancer cells expressing RFP in presence of Native MSC, whereas in the presence of CD MSC and 400  $\mu\text{g}/\text{mL}$  5-FC, there were only a few apoptotic cancer cells left (Supplementary Figure 3.6c).

### **3.3.2 Enhanced homing of engineered MSC to breast cancer bone metastases *in vivo***

Our engineered MSC's homing using PSGL-1/SLEX (not otherwise expressed on Native MSC), which targets bone niche selectins, recapitulates the bone homing cascade of hematopoietic stem cells (HSC)[43, 48] and circulating tumor cells[49]. We next assessed the homing ability of our engineered MSC to breast cancer bone metastases *in vivo*. For this experiment, to mimic the clinical setting of patients with established bone metastases, we first used an immunocompromised animal model, in which human breast tumors were grown locally within the marrow cavity of the left tibia. Intratibial injection of breast cancer cells, to establish bone metastases, is a widely-used model to evaluate therapeutic intervention[50]. This route of injection was initially chosen in our study because it allowed us to develop robust and relatively homogenous tumors in the bone so that we could efficiently investigate MSC homing and treatment efficacy. We first checked the selectin expression within the tumor niche and found high expression of P-selectin in the bone marrow of the tumor leg (Figure 3.3), but to a lesser extent in the healthy leg (Supplementary Figure 3.7). We observed an inverse correlation between P-selectin expression

and distance from the tumor site when we analyzed P-selectin expression in the tumor legs of seven different animals (Figure 3.3a,d). We observed large cells and smaller aggregates that highly express P-selectin, which we further identified to be megakaryocytes recruited to the tumor inflammatory site and their shed platelets, respectively, according to CD41 expression[25] (Figure 3.3b). P-selectin expression is also observed on blood vessel endothelium, as shown by endomucin expression, a vascular marker (Figure 3.3c).

A mock injection with PBS was performed in the healthy leg during the model induction. Once breast cancer bone metastases were established in all animals (typically 2 weeks post-implantation, around total bioluminescent signal  $10^7$ - $10^8$  p/s), and the inflammation caused by injection had been mostly resolved[51],  $7 \times 10^5$  Native or PSGL-1/SLEX/CD/OPG 24h post-engineered MSC, pre-labelled with lipophilic dye (DiD), were injected *i.v.* via the tail vein. Mice were euthanized at 6, 24, 48 and 72 hours post cell transplantation. Legs and several relevant organs (lungs, liver, spleen, kidneys and heart) were isolated to measure the fluorescence emitted by DiD-MSC, using IVIS fluorescence imaging, to determine cell bio-distribution (Figure 3.4, Supplementary Figure 3.8). PSGL-1/SLEX/CD/OPG MSC showed significantly increased migration to the tumor leg compared to Native MSC ( $p < 0.05$ , Kruskal-Wallis with Dunn's multiple comparison test) at 72 hours post-implantation (Figure 3.4a), although we did not observe any significant homing preferentially to the tumor leg versus healthy legs from the same animals. Over the combined time-points, PSGL-1/SLEX/CD/OPG MSC were significantly more localised in the mouse legs than Native MSC (Supplementary Figure 3.9a). We confirmed the cell integrity of the PSGL-1/SLEX/CD/OPG MSC that had homed to the bone marrow using fluorescent microscopy (Supplementary Figure 3.9b-c). These findings justify the use of PSGL-1/SLEX engineering, to maximize the number of MSC that reach the tumor site. Moreover, when analyzing the bone

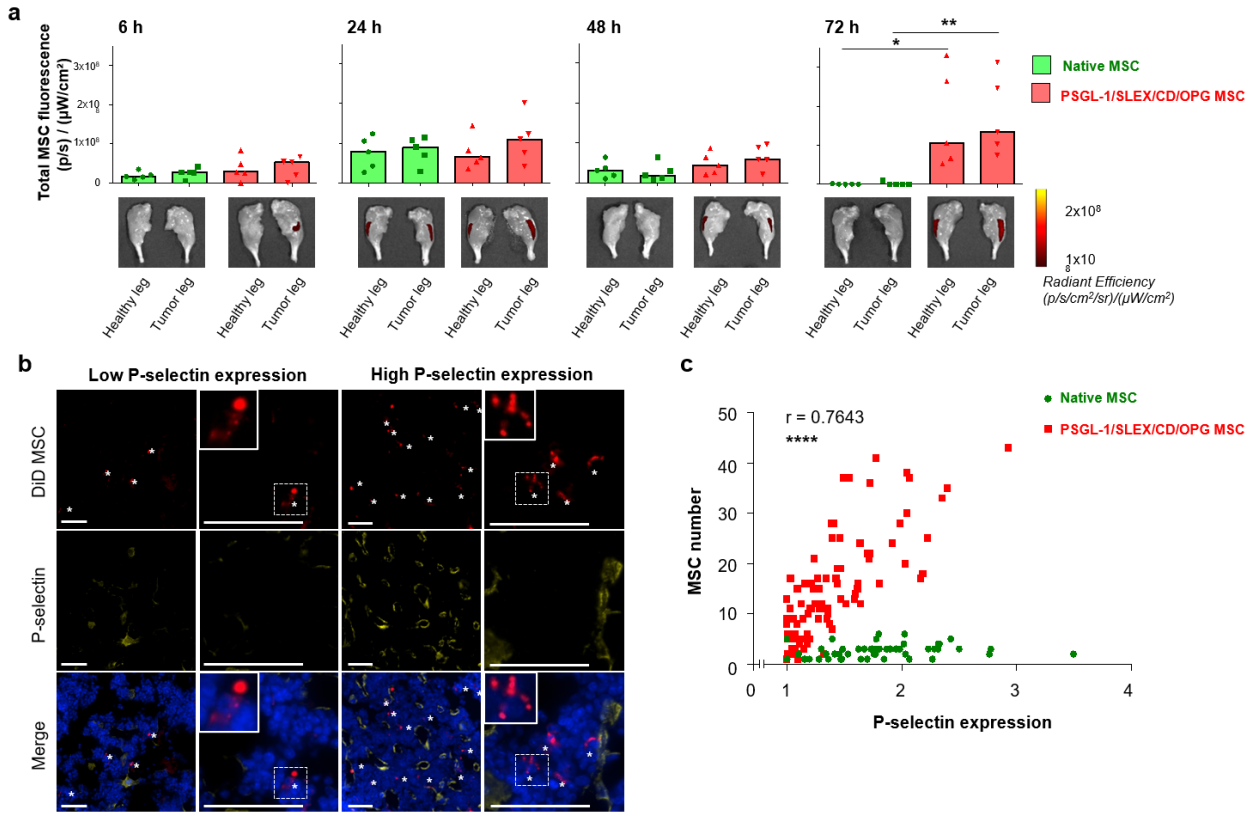


**Figure 3.4: Enhanced homing of engineered MSC to breast cancer bone metastases *in vivo* in the MDA-MB231 intratibial model.** (a) PSGL-1/SLEX/CD/OPG MSC display an increased homing to the tumor legs 72 hours post-transplantation. Native MSC or PSGL-1/SLEX/CD/OPG MSC labelled with DiD lipophilic dye were injected *i.v.*, then mice were euthanized at different time-points (6, 24, 48, and 72 hours). Homing to the legs was evaluated based on the fluorescence intensity of the DiD dye. Control animals that were not injected with MSC were used to subtract fluorescent background from true signal. Plot: median values, each point is an individual animal,  $n=5$  animals per group, statistical analysis: Kruskal-Wallis with Dunn's multiple comparison test \*  $p \leq 0.05$  between Native MSC (healthy leg) and PSGL-1/SLEX/CD/OPG MSC (healthy leg), \*\*  $p \leq 0.01$  between Native MSC (tumor leg) and PSGL-1/SLEX/CD/OPG MSC (tumor leg). (b) PSGL-1/SLEX/CD/OPG MSC accumulate in high P-selectin expression areas in the bone marrow section (48h post-transplantation time-point). Red: DiD stained MSC, yellow: P-selectin, blue: nuclei (DAPI staining). White stars designate MSC. Scale bars: 50  $\mu\text{m}$ . (c) PSGL-1/SLEX/CD/OPG MSC number within the bone marrow is positively correlated to P-selectin expression. 200  $\mu\text{m}$  by 200  $\mu\text{m}$  areas containing MSC were selected for quantification from the 72 h time-point post-MSD transplantation. Average P-selectin signal was measured by dividing total photon counts emitted in Cy5 per surface area and subtracting the background signal. 49 areas were evaluated for Native MSC, and 95 areas were assessed for PSGL-1/SLEX/CD/OPG MSC. Statistical analysis: Pearson correlation test, coefficient  $r=0.7643$ , \*\*\*\*  $p \leq 0.0001$  for PSGL-1/SLEX/CD/OPG MSC.

marrow for P-selectin expression and MSC content, we found that PSGL-1/SLEX/CD/OPG MSC tend to accumulate in areas with high vascular P-selectin expression (Figure 3.4b), which are usually found around the tumor site (Figure 3.3a-d). In fact, the number of PSGL-1/SLEX/CD/OPG MSC (but not Native MSC) that migrated to the bone marrow positively correlates with P-selectin expression (Pearson coefficient  $r=0.7643$ ,  $p<0.0001$ ) (Figure 3.4c), suggesting the active PSGL-1/SLEX and P-selectin axis drives the homing of PSGL-1/SLEX/CD/OPG MSC to the bone marrow. Moreover, we also characterized the bio-distribution of Native and PSGL-1/SLEX/CD/OPG MSC in other organs, and noticed that they initially accumulated in the lungs and liver within 24 hours post-transplantation, and were then rapidly cleared (Supplementary Figure 3.8), which is consistent with previous studies[52, 53].

Next, since the immune system could contribute to the clearance of transplanted MSC, we investigated the homing of PSGL-1/SLEX/CD/OPG MSC in a second, syngeneic, mouse model. This syngeneic model leads to spontaneous bone metastases, thus avoiding any potential inflammation created by needle insertion through the growth plate, such as during the intratibial model. We first identified a bone specific LucF/RFP 4T1 mouse breast cancer cell clone (CLL1) (see Methods). CLL1 (10,000 cells) were injected systemically, through the caudal artery, and within a week, small, but detectable bone metastases formed, preferential to the hind limbs and spine, as previously described[37]. The incidence of this model is excellent (>90% of animals developed bone metastases), but the model is very aggressive and mice usually have to be euthanized within 3 weeks. For this study, we aimed to further investigate engineered MSC homing to healthy legs versus tumor legs. As we were working with mouse tissue, we used Alu qPCR following an established approach[42] to detect human MSC in the leg. Despite the limited sensitivity of our protocol (see Methods), we were still able to detect PSGL-1/SLEX/CD/OPG MSC in 30% of the tumor legs, while none were detectable in the healthy legs. Up to 1,156 MSC were detected

per tumor leg 72 hours post transplantation, despite potential immune clearance in these immunocompetent animals (Supplementary Figure 3.9 d, e).

### **3.3.3 Engineered MSC with both CD and OPG exhibit therapeutic effects in treating bone metastases in MDA-MB231 xenograft intratibial model**

We then sought to determine the therapeutic efficacy of MSC further engineered with CD, OPG, or both factors to examine if 1) our therapy is efficient *in vivo*, in a breast cancer bone metastasis model, and 2) if such combinatorial delivery is more beneficial than either therapeutic alone. After verifying the presence of the tumor within the tibia of mice (typically 2 weeks post cancer induction), we injected  $1 \times 10^5$  MSC engineered with CD (PSGL-1/SLEX/CD MSC), OPG (PSGL-1/SLEX/OPG MSC), CD/OPG (PSGL-1/SLEX/CD/OPG MSC) or Mock-transfected MSC into the tumor-bearing tibia (curative model) (Figure 3.5a). PBS was injected in the control group (CT), as well as in the healthy legs (mock control for needle-induced inflammation and bone damages). We chose to use a local injection in this set of experiments, to allow for robust comparison between each treatment condition. The primary goal of this intratibial treatment injection was to test the efficacy of OPG and CD treatments, not to determine MSC homing (although the therapeutically engineered cells were also equipped with PSLG-1/SLEX, which replicates our final product, to be used in the systemic infusion in the following experiments). Mice were treated with 500 mg/kg of 5-FC pro-drug at 48 hours post-implantation, by which time MSC would have been cleared from filter organs if administered systemically as in our intended future clinical use.

A pilot experiment was first performed using  $n=4$  mice per group. Through this initial experiment, we established techniques to confirm tumor implantation within the tibia by



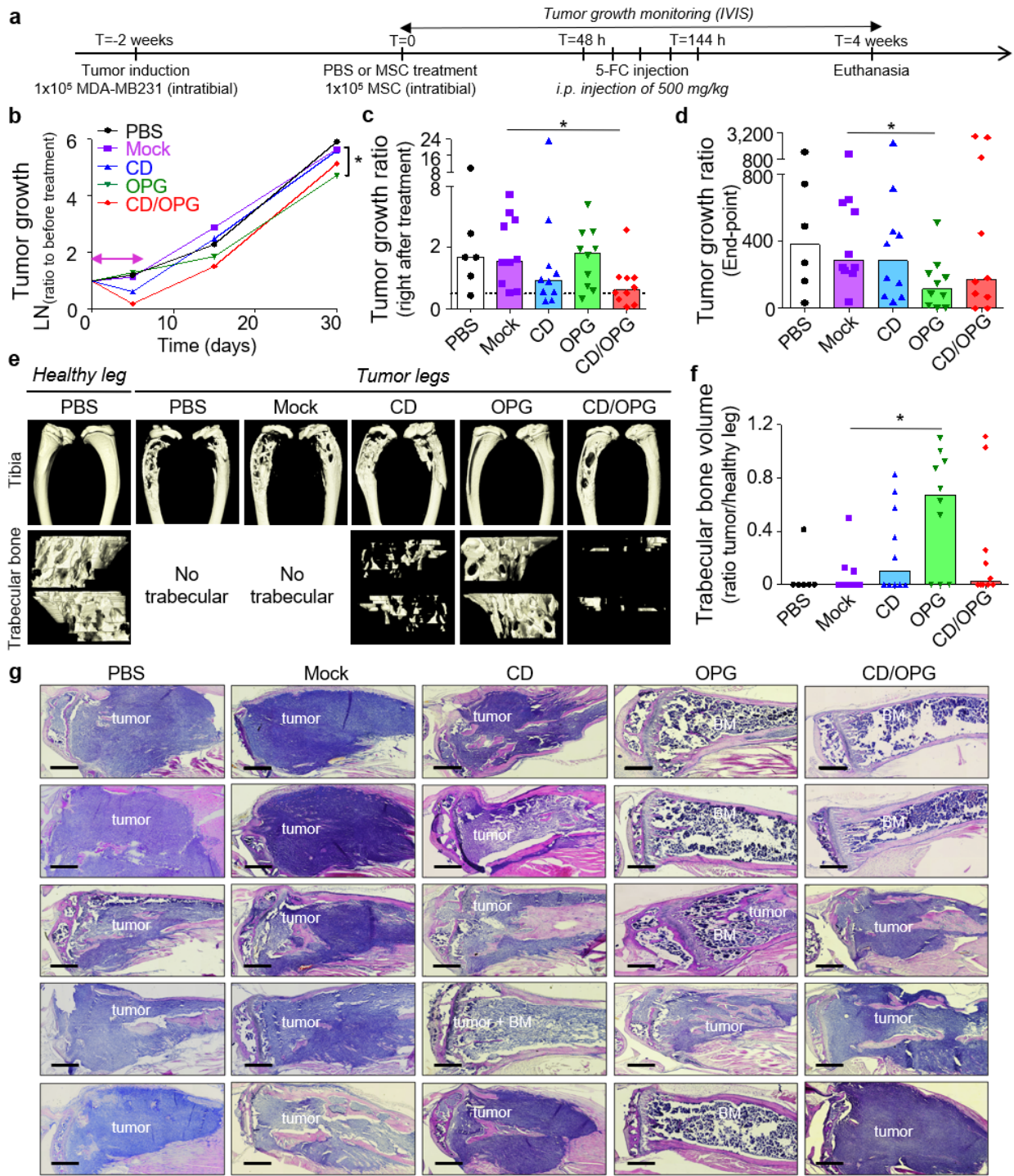


**Figure 3.5: Engineered MSC exhibit therapeutic effects in treating bone metastases *in vivo* in the MDA-MB231 intratibial model.** (a) Timeline of the therapeutic treatment validation. MSC were engineered as follows: Mock group (Mock transfected), CD group (PSGL-1/SLEX/CD), OPG group (PSGL-1/SLEX/OPG) and CD/OPG group (PSGL-1/SLEX/CD/OPG) and injected directly into the tibia, n=10 per group. PBS group only received PBS in the tibia instead of MSC, n=6. (b) The logarithm values of the tumor growth ratio (Total photon flux measured/Total photon flux on the day before

the treatment started) are plotted over time for each group. Median of each group is shown. Pink double-headed arrow shows treatment duration. Statistical analysis: Kruskal-Wallis with Dunn's multiple comparison *post hoc*, \*  $p \leq 0.05$  between Mock MSC and OPG MSC. (c) Bar graph shows the tumor growth ratio measured on the day after the treatment is done. Each point represents one animal, and the bars represent the median value of the group. Dashed line indicates a tumor growth ratio of 1 (animals below that line have tumor decrease). Statistical analysis: Kruskal-Wallis with Dunn's multiple comparison *post hoc*, \*  $p \leq 0.05$  between Mock MSC and CD/OPG MSC. (d) Bar graph shows the tumor growth ratio measured on the end-point day. Each point represents one animal, and the bars represent the median value of the group. Statistical analysis: Kruskal-Wallis with Dunn's multiple comparison *post hoc*, \*  $p \leq 0.05$  between Mock MSC and OPG MSC. (e) MicroCT imaging was done on mouse tibias after euthanasia. Representative 3D reconstructions matching the median of each group for bone analysis are shown. First row shows whole tibias without the fibula, while bottom row shows trabecular bone. (f) Bar graph shows the trabecular bone ratio measured by normalizing the trabecular bone volume of each tumor leg to the trabecular bone volume of healthy legs. Each point represents one animal, and the bars represent the median value of the group. Statistical analysis: Kruskal-Wallis with Dunn's multiple comparison *post hoc*, \*  $p \leq 0.05$  between Mock MSC and OPG MSC. (g) H&E staining of mouse tibias at end-point demonstrate treatment with OPG MSC and CD/OPG MSC can clear tumor cells and preserve the bone structure, while tumor invades the cortical bone in control animals (PBS and Mock MSC groups). 5 representative mouse tibias are shown for each group. BM=healthy bone marrow. Scale bar: 500  $\mu\text{m}$ .

overlaying bioluminescence and X-Ray (Supplementary Figure 3.10a) and to characterize the presence of tumor cells within the bone marrow of the tibia by using both immunofluorescence (RFP expressed by cancer cells) and H&E staining (Supplementary Figure 3.10b). From this experiment, we obtained a preliminary assessment on tumor killing and bone preservation among different treatment groups and determined the minimum number of mice per group required for statistical analysis using a power analysis (see Methods). We then repeated the experiment following the exact same treatment scheme (Figure 3.5a) with  $n=10$  mice per group. Tumor growth within the tibia was monitored using bioluminescence imaging. Animals were randomized in each group and showed comparable tumor signal across groups before treatment (Supplementary Figure 3.11). A tumor decrease was observed for animals treated with MSC engineered with both CD MSC groups, particularly CD/OPG MSC ( $p < 0.05$  from Kruskal-Wallis with Dunn's multiple comparison *post hoc*, compared to Mock MSC), immediately following the treatment (Figure 3.5b, c), but most of the tumors eventually grew back to a level comparable to control groups (PBS and Mock MSC). At the end-point, mice treated with CD/OPG MSC also exhibited smaller tumors compared to control groups (although the difference was not significant, due to high variability between



good and bad responders). However, OPG MSC slowed the tumor growth, leading to significantly smaller tumors than the Mock MSC group ( $p < 0.05$ , Kruskal-Wallis with Dunn's multiple comparison *post hoc*) in the longer-term (Figure 3.5b, d, Supplementary Figure 3.11). In addition, we analyzed the tumor growth data points from both pilot and larger-scale experiments using a linear mixed model (LMM), which takes inter-experiment variability into account (Supplementary Table 3.3. This LMM analysis showed CD/OPG MSC treatment is most effective among all engineered MSC groups in decreasing tumor growth both immediately after treatment ( $p = 0.0039$ ), and at the end-point ( $p = 0.0494$ ), compared to the PBS control as it was used in both studies.

We further investigated tumor-induced bone damage by analyzing bone structure of all tibias at the end-point, using microcomputed tomography (micro-CT). One representative animal from each group, which exhibited the closest values to the median of that group for the bone analysis, was presented in Figure 3.5e. The 3D reconstruction of the entire tibias clearly indicated extensive bone damage in the PBS and Mock MSC treated groups, while damage looked less severe in engineered MSC treated groups, in particular for animals treated with OPG MSC. As tumors grow inside the bone marrow cavity before invading the cortical bone, we also looked at the trabecular bone, which was mainly gone in most of the groups, except for the OPG MSC treated mice, which exhibited trabecular bone structure similar to the one found in healthy legs (Figure 3.5e). We further quantified the trabecular bone left in each tumor-bearing tibia, and illustrated the bone loss, by normalizing the obtained values to the trabecular bone volume of healthy legs (Figure 3.5f). Indeed, 70% of the mice from OPG MSC group had less than 50% trabecular bone loss, thus exhibiting significant protection against tumor-induced bone loss compared to Mock MSC group ( $p < 0.05$ , Kruskal-Wallis with Dunn's multiple comparison *post hoc*). We also performed histology on the tumor-bearing tibias from those animals (five representative animals from each

group as shown in Figure 3.5g). Control groups (PBS and Mock MSC) showed extensive tumor invasion through the cortical bone, with total loss of bone architecture in some cases. In contrast, bone structure was preserved for good responder animals treated with engineered MSC, in particular in the OPG MSC group, where the tibias look healthier than for the other groups. Moreover, the LMM analysis of trabecular bone, from both pilot and larger-scale experiments, showed that both OPG MSC and CD/OPG MSC displayed significantly less trabecular bone damage than the PBS control group, with the OPG MSC being the most effective in protecting against tumor-induced bone damage (Supplementary Table 3.4). Furthermore, we evaluated the impact of OPG MSC treatment in inhibiting tumor-induced osteoclastogenesis *in vivo* using tartrate-resistant acid phosphatase (TRAP) staining for osteoclasts in the growth plate of the tibias of mice (both healthy and tumor legs) (Supplementary Figure 3.12). Healthy legs of tumor mice treated with PBS were included as a control. Note that we could not include tumor legs, as the growth plates were gone, due to tumor invasion and high osteoclastic activity[3] (Figure 3.5g). We found that the number of TRAP<sup>+</sup> osteoclasts was significantly reduced in the tumor tibias from the mice treated with OPG MSC compared to the PBS control ( $p < 0.05$ , Kruskal-Wallis with Dunn's multiple comparison *post hoc*). Finally, in this experiment (Figure 3.5), we observed OPG MSC exerted a stronger therapeutic effect than CD/OPG MSC. This could be because CD/OPG MSC has lower expression levels of therapeutic proteins due to engineering with multiple factors compared to OPG MSC. Nevertheless, the data above suggest that both CD (in short term) and OPG (in long term) exhibit therapeutic effects *in vivo*, but their co-expression should be further investigated to maximize their combinatorial effect in inhibiting both tumor growth and preserving bone integrity. We reason that even if OPG MSC were able to slow down tumor growth, they could not clear the tumor as CD MSC do, justifying the potential benefit of combination therapy. After all, the LMM analysis suggested potential benefit of the CD/OPG MSC

combined therapy. Therefore, we decided to use the combination treatment PSGL-1/SLEX/CD/OPG MSC for the following intravenous (*i.v.*) administration studies. As our envisioned treatment in the clinic will be an off-the-shelf cell therapy administered via simple *i.v.* infusion, we next assessed efficacy, with a focus on survival, and systemic toxicity of our PSGL-1/SLEX/CD/OPG MSC following *i.v.* delivery. We compared their tumor-killing effect to a toxic dose of the chemotherapeutic drug 5-FU, a common treatment for breast cancer patients known for its side-effects[47]. As illustrated in Figure 3.6a, we intravenously injected our engineered MSC through the tail vein, followed by daily treatment with 500 mg/kg 5-FU intraperitoneally (*i.p.*), starting 48 hours post-transplantation over 5 days. The control group consisted of tumor bearing animals only injected with PBS. In another group, 200 mg/kg 5-FU was injected *i.p.* on the same schedule as the 5-FU group. This relatively high dose of 5-FU was used as a positive control for tumor killing and tissue toxicity, as previous studies we performed with lower doses (up to 50 mg/kg for five days during three consecutive weeks) neither induced toxicity nor killed MDA-MB231 xenografts in Nude animals[54]. We also included a triple MSC injection group to examine if multiple injections perform better than single injection; in this case, the treatment schedule was repeated for three consecutive weeks. 3 to 4 mice per group were sacrificed at the end of the treatment to evaluate tissue toxicity, while the rest of the mice were kept for long-term survival analysis. The overall survival of control animals or animals treated with Native MSC was very similar, with all the animals euthanized by 50 days (Figure

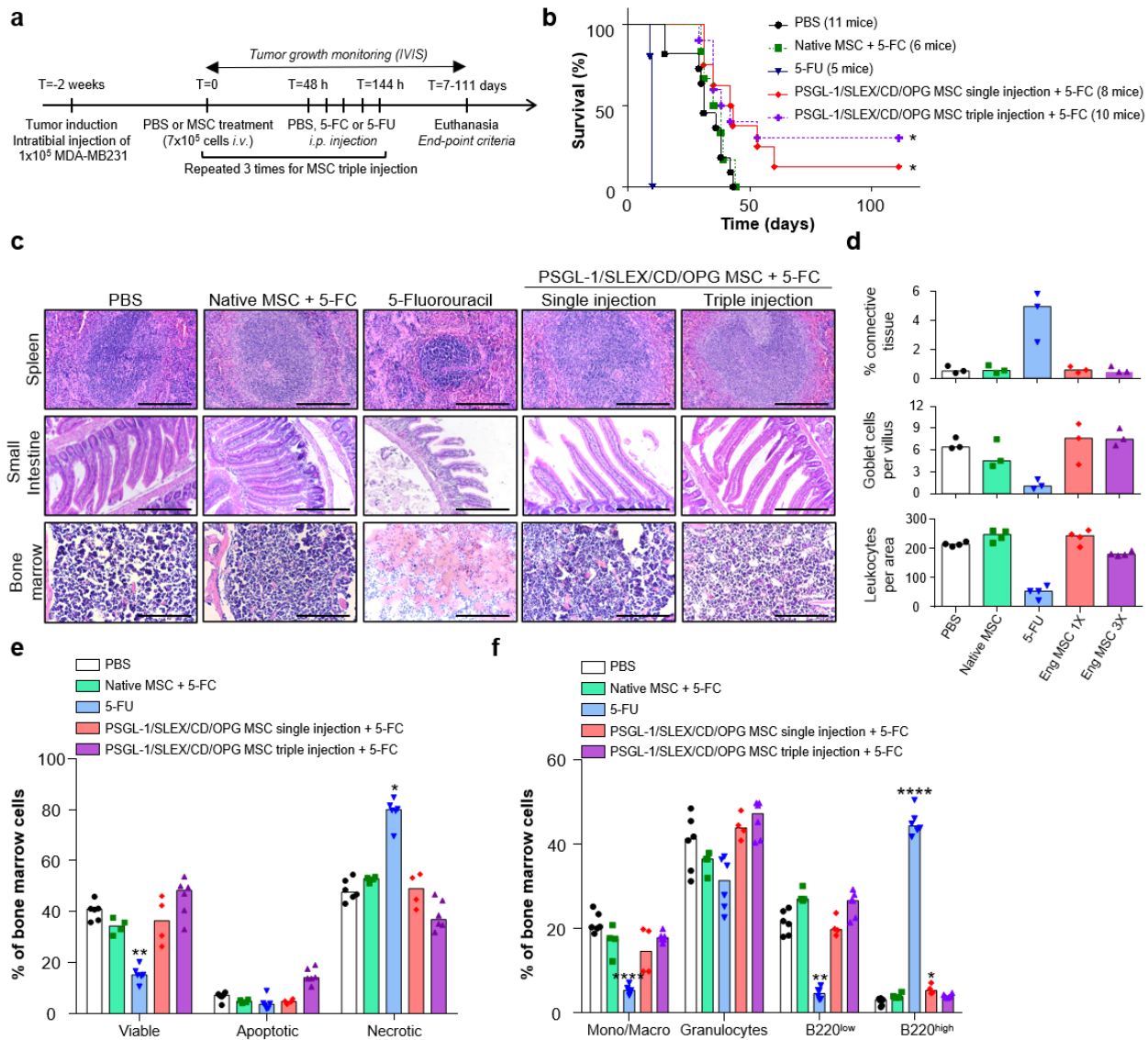


**Figure 3.6: Systemic infusion of PSGL-1/SLEX/CD/OPG MSC improves animal survival without inducing systemic toxicity in the MDA-MB231 intratibial model.**

(a) Timeline of the therapeutic treatments. PBS or  $7 \times 10^5$  MSC (Native or PSGL-1/SLEX/CD/OPG) were injected *i.v.* and 48 hours later 500 mg/kg 5-FC or 200 mg/kg 5-FU was injected *i.p.* once a day for 5 days. Mice were euthanized as defined by end-point criteria (total photon flux  $>10^{10}$  p/s, signs of pain or distress, *etc.*). (b) PSGL-1/SLEX/CD/OPG MSC treatment improves overall animal survival. The graph shows the percentage of survival of the animals in the different groups: CT (PBS control, 11 mice), Native MSC + 5-FC treatment (6 mice), 5-FU (5 mice), PSGL-1/SLEX/CD/OPG MSC single injection + 5-FC treatment (8 mice) and PSGL-1/SLEX/CD/OPG MSC triple injection + 5-FC treatment (10 mice). Statistical analysis: Log-rank (Mantel-Cox) test, \*  $p \leq 0.05$ . (c) PSGL-1/SLEX/CD/OPG MSC treatment group exhibits minimal systemic toxicity compared to 5-FU treatment. Tissue analysis was performed following H&E staining to evaluate toxicity-induced damage. Panel shows organs where the greatest damage was

observed: spleen, small intestine, and bone marrow. Scale bars: 500  $\mu\text{m}$  for spleen and bone marrow, 250  $\mu\text{m}$  for the small intestine. (d) Engineered MSC did not induce significant tissue damage. Quantifications were done on the H&E staining: percentage of connective tissue to assess of spleen fibrosis, number of goblet cells per villus to evaluate intestine damage, and number of leukocytes per bone marrow area to measure toxicity. Bar graph shows the median for each group, and each point represents one animal,  $n=4$  mice per group. Eng MSC = PSGL-1/SLEX/CD/OPG MSC. (e) Engineered MSC did not lead to significant cell death in the bone marrow. Flow cytometry was performed on bone marrow to analyze the percentages of viable, apoptotic and necrotic cells. 2 to 3 animals were used for each group, and both legs were analyzed. As no major differences were observed between the healthy and the tumor leg, data from both legs were pooled. Bar graph shows the median for each group, and each point represents one analyzed leg. Statistical analysis: Kruskal-Wallis followed by a Dunn's multiple comparison test among each group (viable, apoptotic and necrotic) to compare all conditions to the control; \*  $p \leq 0.05$ , \*\*  $p \leq 0.01$ . (f) Engineered MSC did not significantly alter cell composition of the bone marrow. Flow cytometry was performed on equal numbers of bone marrow cells to analyze the different populations: monocytes/macrophages (Mono/Macro), granulocytes and B lymphocytes (B220<sup>low</sup> and B220<sup>high</sup>). 2 to 3 animals were used for each group, and both legs were analyzed. As no major differences were observed between the healthy and the tumor leg, data from both legs were pooled. Bar graph shows the median for each group, and each point represents one analyzed leg. Statistical analysis: Kruskal-Wallis followed by a Dunn's multiple comparison test among each population to compare all conditions to the control; \*  $p \leq 0.05$ , \*\*\*\*  $p \leq 0.0001$ .

3.6b). The toxicity of 5-FU was so severe that all animals died or had to be euthanized by day 10. Notably, around day 7, the 5-FU treated mice stopped grooming, started having diarrhea and showed dramatic weight loss, indicating signs of toxicity. By contrast, mice treated with MSC did not show any sign of distress and gained weight during the experiment similar to the control mice. Importantly, their survival was significantly improved by the treatment, in particular for the triple injection group where 30% of the mice were still alive after 111 days, versus 12.5% for the single injection group (Figure 3.6b).

In addition, at the time of euthanasia, we observed a noticeable reduction (about 2/3) of the size of spleens in the 5-FU group compared to the control group, whereas MSC treatment did not seem to affect the spleen size and morphology (Supplementary Figure 3.13a). H&E analysis of spleen sections confirmed tissue damage induced by 5-FU, with a decrease of the size of germinal centers, replaced by fibrotic tissue (Figure 3.6c-d, Supplementary Figure 3.13b). In regard to toxicity to other organs, including lungs, liver,

kidney, bone marrow, and small/large intestines, we observed reduction of the size of villi in the small intestine and a decrease of the number of goblet cells per villus. Severe hemolysis happened in the bone marrow for the 5-FU group with a decrease of the number of leukocytes, while no significant difference in tissue structure was observed among groups for the other organs (Figure 3.6c-d, Supplementary Figure 3.14). In addition, we isolated the bone marrow to analyze the general cell viability and the different populations using flow cytometry. Consistent with our previous conclusions, PSGL-1/SLEX/CD/OPG MSC did not induce significant cell death within the healthy bone marrow, unlike the 5-FU treatment[55], which considerably increased the percentage of necrotic cells (1.68 fold increase), and decreased the percentage of viable cells (2.71 fold decrease) compared to the CT group (Figure 3.6e). Although the percentage of Annexin V<sup>+</sup> cells was not significantly different between each group, 5-FU induced stronger apoptosis with a median of fluorescence intensity (MFI) 4.8 times higher than that of the other groups for Annexin V FITC. The MFI for the 7-ADD<sup>+</sup> cells in the 5-FU group was also 16.7 times higher than the other groups, confirming an overall lower cell viability in the bone marrow of 5-FU treated animals (Supplementary Figure 3.13c). Regarding the populations affected, we only observed a slight increase of B cells B220<sup>high</sup> in the single injection group (5.24% versus 3%) (Figure 3.6f). However, these changes are minimal compared to those induced by high-doses of 5-FU, which, unsurprisingly, induced a 3.84-fold decrease of the myeloid component, a 4.7-fold decrease of B220<sup>low</sup> B cells and 14.8-fold increase of B220<sup>high</sup> B cells within the bone marrow, compared to the control group[55]. Taken together, these results showed that our engineered MSC based therapy was able to extend the animals' survival without inducing significant systemic toxicity compared to high-dose 5-FU treatment. Finally, we performed preliminary assessment of the bone integrity, which demonstrated PSGL-1/SLEX/CD/OPG MSC exhibited a promising protective effect on bone damage, compared to the Control (PBS) and Native MSC groups

(Supplementary Figure 3.15, Supplementary Table 3.5). With this encouraging preliminary study, we decided to extensively investigate our engineered MSC's therapeutic effects in killing tumor cells and protecting against bone loss, as well as its potential toxicity using a more clinically relevant animal model (immunocompetent, and of spontaneous bone metastasis, see below).

### **3.3.4 Engineered MSC with both CD and OPG exhibit superior therapeutic effects in a syngeneic model of spontaneous bone metastases**

We next tested our engineered MSC therapy in our second syngeneic mouse model, which takes into consideration the immune system component and leads to spontaneous bone metastases (Supplementary Figure 3.16a). We included PBS and Mock-transfected MSC, the combined therapy PSGL-1/SLEX/CD/OPG MSC (CD/OPG MSC), as well as the monotherapies PSGL-1/SLEX/CD MSC (CD MSC) and PSGL-1/SLEX/OPG (OPG MSC). We focused on two main outcomes for this study: efficacy and toxicity. A minimum number of 10 mice per group was determined by the power analysis; we included 10 animals for PBS, Mock-transfected MSC and 5-FU groups, while we used 13 animals in the CD MSC, OPG MSC and CD/OPG MSC groups. As soon as all animals had detectable bone metastases, we systemically injected engineered MSC groups, followed by 500 mg/kg 5-FU for 5 consecutive days, starting two days post MSC transplantation (Figure 3.7a). PBS injections were done as a control. For a treatment reference, we injected 5-FU *i.p.* with a clinically relevant dose of 12.5 mg/kg[38] (see Methods for dose optimization), following the same schedule as for 5-FU injections. We first evaluated the efficacy by measuring the tumor growth ratio over time (total photon flux divided by the total photon flux measured before treatment for each animal). PBS was used as a control since MSC transplantation

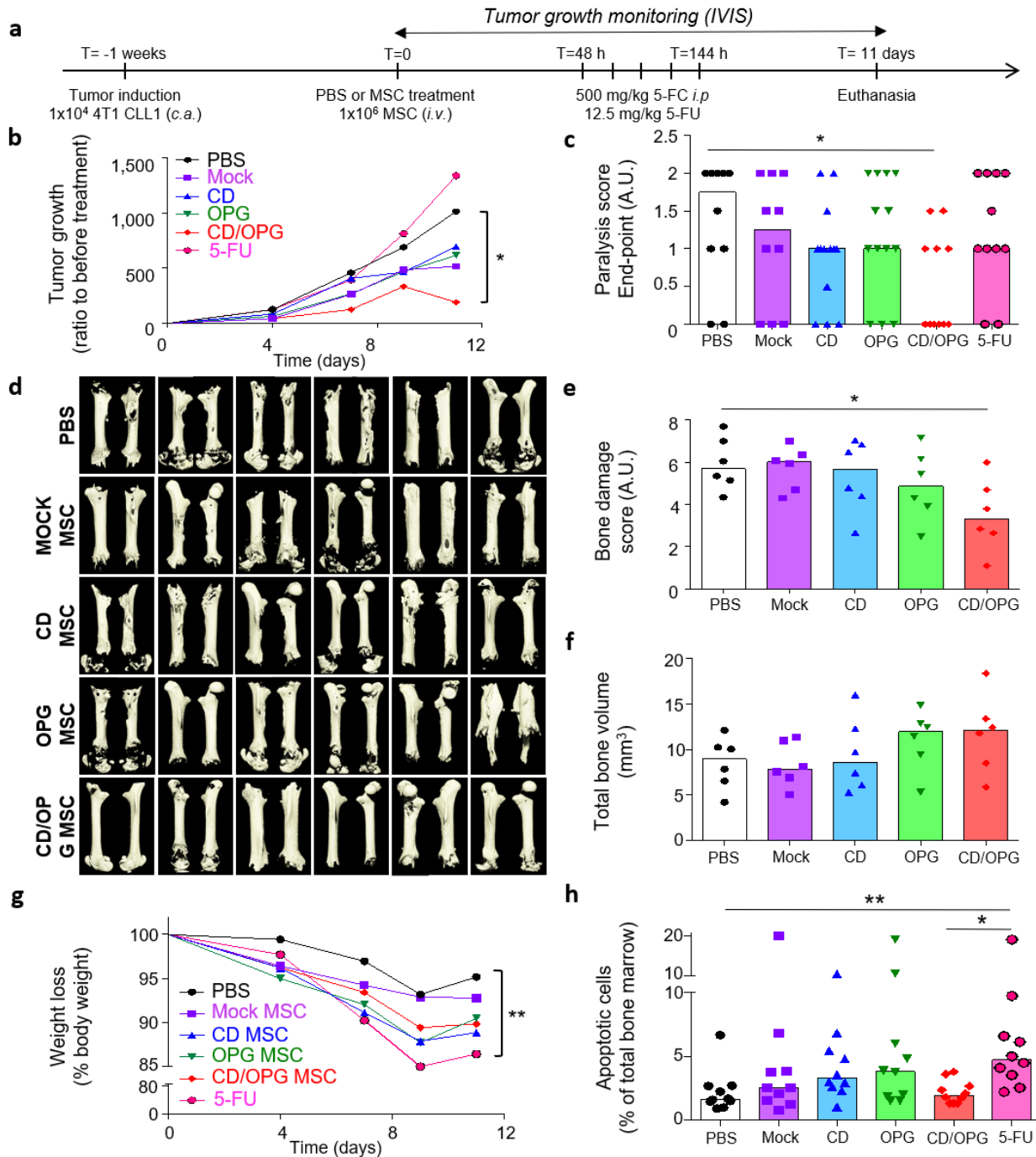


**Figure 3.7: CD/OPG MSC exhibit therapeutic effects and minimal toxicity in a syngeneic mouse model of spontaneous bone metastases.** (a) Timeline of the therapeutic treatment. Spontaneous bone metastases were induced by caudal artery injection of a 4T1 bone metastatic clone (CLL1) to BALB/cJ mice. Once bone metastases were detected, engineered MSC or PBS were systemically administered to animals via *i.v.* injection, and 5-FC was injected *i.p.* for 5 consecutive days 48 h post transplantation. 12.5 mg/kg 5-FU was used as a reference group for treatment. MSC were engineered as follows: Mock group



(Mock transfected), CD group (PSGL-1/SLEX/CD), OPG group (PSGL-1/SLEX/OPG) and CD/OPG group (PSGL-1/SLEX/CD/OPG). PBS, Mock and 5-FU groups: n=10 animals per group. CD, OPG and CD/OPG groups: n=13 per group. (b) CD/OPG MSC inhibits tumor growth compared to PBS control group. Bioluminescence imaging was performed over time and signal was quantified in the lower body to measure bone metastases development in legs and spine. The median of the tumor growth ratio (total photon flux over time normalized to total photon flux before treatment) was plotted for each group. Statistical analysis done at the end-point: Kruskal-Wallis with Dunn's multiple comparison post hoc, \*  $p \leq 0.05$  between PBS and CD/OPG MSC. (c) CD/OPG treatment improved mouse mobility. Paralysis of the animals was scored at the end-point (see Methods). Bar graph shows the median score for each group, and each point represents one animal. Statistical analysis: Kruskal-Wallis with Dunn's multiple comparison post hoc, \*  $p \leq 0.05$  between PBS and CD/OPG MSC. (d) Femurs bearing bone metastases are less damaged in CD/OPG MSC treated group. Micro-CT analysis was done on mouse femurs exhibiting clear leg metastases (usually around the hip area) before treatment from 6 mice per group. 3D reconstructions were made from the whole femurs. (e) Bone damage was blindly scored by a panel of 20 unbiased persons (shaft damage from 0-3 and epiphysis damage from 0-5 based on importance of damage). The average scoring was shown for each animal. Bar graph represents the median score for each group, and each point represents one animal. Statistical analysis: Kruskal-Wallis with Dunn's multiple comparison post hoc, \*  $p \leq 0.05$  between PBS and CD/OPG MSC. (f) CD/OPG MSC and OPG MSC treatments seem to protect against bone loss. The total bone volume was quantified for each femur. Bar graph shows the median bone volume for each group, and each point represents one animal. Statistical analysis: Kruskal-Wallis with Dunn's multiple comparison post hoc. (g) 5-FU treatment, but not MSC groups, induces significant body weight loss. Graph shows the median body weight loss for each group over time. Statistical analysis done at the end-point: Kruskal-Wallis with Dunn's multiple comparison post hoc, \*\*  $p \leq 0.01$  between PBS and 5-FU. (h) Only 5-FU treatment induces additional apoptosis in the bone marrow. At the end-point, the bone marrow of the healthier leg was isolated and cell apoptosis was analyzed using flow-cytometry (AnnexinV+/7-AAD-) for n=10 animals per group. Bar graph shows the median percent of apoptosis for each group, and each point represents one animal. Statistical analysis: Kruskal-Wallis with Dunn's multiple comparison post hoc, \*  $p \leq 0.05$  between 5-FU and CD/OPG MSC, and \*\*  $p \leq 0.01$  between PBS and 5-FU.

could induce an immune response in this model, thus not being an appropriate control. Although initially very small, tumors developed extremely rapidly (Supplementary Figure 3.16). Among the groups tested, only the CD/OPG MSC treatment was able to induce a significant tumor decrease, as determined by a non-parametric ANOVA at the end-point ( $p < 0.05$  between PBS and CD/OPG groups) (Figure 3.7b). We further investigated the differences between the combined therapies and the monotherapies and plotted the tumor growth ratio at the end-point, for each animal, for CD and CD/OPG groups as well as for OPG and CD/OPG groups (Supplementary Figure 3.16b and c). We noticed several populations based on response

to treatment, with a clear good responder group for the mice treated by CD/OPG MSC, which was absent in groups treated by CD MSC or OPG MSC. The combined therapy was more efficient in preventing tumor growth than CD MSC monotherapy ( $p < 0.05$ , Kruskal-Wallis with Dunn's multiple comparison *post hoc*), and also tends to be more efficient than OPG MSC therapy ( $p = 0.0638$ , Kruskal-Wallis with Dunn's multiple comparison *post hoc*). Moreover, mice treated by CD/OPG MSC seemed healthier than other groups overall, with less moribund mice, better grooming and ability to move around, at the end-point. Due to the aggressiveness of this model, mouse condition deteriorated extremely rapidly (paraplegia and diarrhea due to spine metastasis, weight loss, and tumors breaking through the cortical bone). We decided to score the paralysis to quantify this effect, and confirmed that CD/OPG MSC treated mice were less paralyzed than mice in PBS control group ( $p < 0.05$ , Kruskal-Wallis with Dunn's multiple comparison *post hoc*), with the majority of mice being free of movement, while the majority of animals in other groups were dragging their hind limbs (Figure 3.7c). We then examined treatment effects on tumor-induced bone damage for those animals, and randomly picked 6 animals per groups, which possessed clear bone metastatic signal coming from the leg before the treatment. As a majority of bone metastases found in the hind limbs were located in the hip and femur area, we decided to focus on the femurs, instead of the tibias, for this model (Figure 3.7D). For each sample, we asked twenty people (75% of them not being familiar with this study or not doing research) to blindly score the shaft damage and the epiphysis damage. The scoring matched the 3D reconstructions, with significantly less bone damage in the group treated with CD/OPG MSC ( $p < 0.05$  analyzed by Kruskal-Wallis with Dunn's multiple comparison *post hoc* test, between PBS and CD/OPG groups, Figure 3.7e). In addition, we quantified the total bone volume and the remaining trabecular bone in the epiphysis. CD/OPG MSC and OPG MSC tend to have more total bone volume than the PBS control (although the results were not significant) (Figure 3.7f). Similarly, animals

treated with CD/OPG MSC tended to have more remaining trabecular bone than the PBS control group ( $p=0.0748$  analyzed by Kruskal-Wallis with Dunn's multiple comparison *post hoc* test, Supplementary Figure 3.16d).

Our second goal was to evaluate potential toxicity of our engineered MSC. This time, we compared the toxicity of each treatment to our 5-FU reference. First, we measured the body weight of the animals during the whole experiment, and although all animals did lose weight because of the aggressive bone metastases, our engineered MSC therapies did not induce significant weight loss compared to the PBS group, while 5-FU did (Figure 3.7g). Then, we performed H&E staining on peripheral organs, including spleen, intestines, and bone marrow, which did not exhibit any major toxicity among all treatment groups (Supplementary Figure 3.16e). We also analyzed the bone marrow of the mouse femur for 10 animals per group at the end-point, both for cell viability (Figure 3.7h, Supplementary Figure 3.16f), and myeloid cell population (Supplementary Figure 3.16g). MSC groups had minimal effect on these measures, while 5-FU reference treatment exhibited significant toxicity. Taken together, these findings suggest that 1) our combined CD/OPG MSC therapy exhibited therapeutic efficacy in a syngeneic mouse model of bone metastasis, while monotherapies and 5-FU did not, and 2) our targeted approach is significantly less toxic than its non-targeted chemotherapy counterpart *in vivo*.

### **3.4 Discussion**

Bone metastases are common, incurable, and associated with debilitating complications. Existing monotherapies and drug delivery systems are ineffective and often present severe side effects[2, 8]. Efficient treatment of metastatic bone diseases requires simultaneous addressing of tumor growth and bone resorption. Although previous studies showed synergistic effects for breast cancer bone metastases

treatment when combining bisphosphonates and chemotherapeutic agents[56, 57], drug delivery and associated systemic toxicity remain a challenge. Here, we introduce a new paradigm of bone metastasis treatment by embracing a combination therapy that targets both the cancer cells and their niche through a stem-cell-based vehicle that homes to the bone tumor sites. We reasoned that such a combinatorial treatment targeting multiple cancer mechanisms would be of paramount importance to efficiently treat bone metastases along with preventing drug resistance, relapse, and development of new metastases compared to monotherapies, with limited side-effects. Indeed, by co-delivering both an anti-tumor agent (CD/5-FC pro-drug)[20] and an anti-osteolytic agent (OPG)[58], our engineered stem cell system displayed great potential in both killing tumor cells and preserving bone integrity. Given the current challenges in co-delivery of biologics in a controlled fashion, our mRNA-based cell engineering presents a simple and powerful way to target multiple mechanisms (tumor-selectin expression, tumor growth and bone resorption) simultaneously in a rapid and transient way following treatment, therefore avoiding potential long-term safety issues observed in traditional viral engineering approaches[59, 60]. Previous studies targeting bone tumors through a cell-based therapy used genetically modified cells, which usually only delivered a single therapeutic molecule[29-31]. We showed that not only does mRNA engineering allow concurrent expression of multiple factors, but that it also leads to therapeutic efficacy similar to that of genetic engineering[19]. Moreover, safety concerns are limited regarding MSC persistence following transplantation as MSC are killed along with the surrounding cancer cells within days after converting 5-FC to 5-FU[19].

MSC represent ideal trophic vehicles for drug delivery to bone metastases as systemically delivered MSC have been shown to preferentially localize to, and subsequently integrate with the bone marrow[61], showing promising potential for bone tumor treatment[62]. Our system also takes advantage of the

engineered homing of MSC to specifically and efficiently deliver ‘cargo’ to the target tumor site. This ‘active’ targeting circumvents many hurdles associated with conventional delivery systems (*i.e.*, by direct administration or nanoparticles), which cannot efficiently reach and penetrate metastatic sites[14]. By recapitulating the bone-homing cascade of HSC and metastatic cancer cells, we are able to maximize MSC delivery to bones, through interactions between PSGL-1/SLEX and selectins on activated bone vasculature[9], and on megakaryocytes and platelets[63], in the tumor area. Indeed, P- and E- selectins are overexpressed in many patients’ tumors[64]. It is also interesting to note that PSGL-1/SLEX-engineered MSC could interact with circulating platelets, as observed in the leukocyte and tumor cell trafficking cascades[63, 65, 66], en-route to the bone metastatic niche, which could further facilitate MSC delivery, and will be investigated in the future. This targeted approach would significantly minimize undesirable toxicity, as observed in treatment with chemotherapeutics, including 5-FU, in the clinic. Our results clearly showed that engineered MSC home more to the bone metastatic sites than Native MSC. Interestingly, we did not observe a significant difference in the homing of engineered MSC to tumor-bearing legs and to healthy legs overall, (whole leg imaging) in our first MDA-MB231 intratibial model. This could be due to the basal expression of selectins and/or activated selectin expression following needle-induced inflammation in the tibia, or tumor-induced systemic inflammation in the bone marrow vasculature of healthy legs[25, 26]. In fact, we also noticed P-selectin expression within the bone marrow of the healthy leg of tumor-bearing mice, corroborating this hypothesis. We observed that MSC were sparse in the healthy leg, but in the tumor leg they were concentrated around the tumor area[67] and positively correlated with P-selectin expression. Moreover, although limited by animal number, we detected more engineered MSC in the tumor bearing legs than in the healthy legs in our second syngeneic model of spontaneous bone metastases. Nevertheless, future studies can further improve target specificity by exploiting irradiation of

tumor sites, which is a current clinical practice for bone metastasis and known to upregulate selectins[34, 64, 68], other homing ligands, and chemokines. Engineering MSC with additional homing receptors (*e.g.*, HCELL[69] or CXCR4, as CXCL-12 is highly produced within the bone marrow environment[3, 70, 71]) could further improve their bone metastasis homing ability.

In summary, we have presented a platform technology that enables targeted delivery of biologics to disease sites, targeting multiple disease pathways in a combinatorial fashion. The modularity of RNA engineering allows us to mitigate the intrinsic heterogeneity of stem cells, and to fine-tune treatments by introducing new functions to stem cells, based on patient characteristics, tumor type, and tumor stage, in a personalized way. Importantly, as MSC have been proven safe for transplantation in humans in many clinical trials, and approved for use in children with Graft-versus-Host disease (GvHD)[72], we anticipate that application of our system as a therapeutic could occur relatively rapidly. We will further investigate the added effect of co-delivering OPG with CD, in preserving bone integrity *in vivo*, at different stages of tumor induced bone damage. In particular, we will dissect therapeutic effects of combined versus monotherapies in the first intratibial model to further understand why CD/OPG MSC did not perform as potently as OPG MSC. Through our study, it became clear to us that, due to the different mechanisms of action between CD and OPG, the optimal, sustained therapeutic benefits from combinatorial treatment will likely be dependent on tumor size and bone damage levels at study entry as well as treatment schedules, which will be exploited in the future. In particular, we will assess *in vitro* and *in vivo* expression of the therapeutic factors over time for cell engineered with one or multiple factors to make sure they have comparable expression, and that there are no competition for protein translation in the case of engineering with multiple mRNA. In addition, we will further characterize the impact of monotherapies versus combined therapy on the bone metastatic niche, by testing sequential injection of CD MSC and OPG MSC

versus injection of CD/OPG MSC. In particular, we would like to assess the CD's bystander effect on OPG's therapeutic function *in vivo* when killing cancer, MSC and niche cells. We remain convinced that CD and OPG co-delivered by MSC would exhibit different and complementary mechanisms in blocking the vicious circle between tumors and their niche, and therefore is advantageous in effectively managing bone metastases. Indeed, our data from the second syngeneic model, which is extremely aggressive, confirmed that combination therapy with both CD and OPG is more beneficial in treating bone metastases than monotherapies. In addition, we will characterize the amount of 5-FU converted *in vivo* by our engineered MSC and compare their tumor killing properties and associated toxicity, compared to therapeutically relevant doses of 5-FU. When moving to clinical studies, future work should systematically study the dosage, number, frequency, and schedules of treatments[73, 74]. Clinical studies should also look at patient stratification based on disease stages (*e.g.* tumor sizes and bone damage levels) at study entry, in order to obtain optimal therapeutic outcome especially in the long-term. Given the profound anti-tumor effect we observed in treatments with OPG, it will be particularly interesting to investigate if our approach, of both targeting cancer cells and normalizing the niche, can eradicate the metastases or at least control their growth, even with a single, transient MSC transplantation. In any case, scaling up the manufacturing process, potentially using an automated system that standardizes batch-to-batch variation, and implements quality control (QC) and release assays for efficacy and toxicity, will be needed for future clinical applications[75]. Furthermore, potential immunity-mediated side effects resulting from ectopically engineered MSC should be investigated in detail.

We demonstrate a new strategy using mRNA-engineered stem cells for combinatorial targeting and delivery of multiple factors to interrogate both cancer cells and the metastatic niche in treating bone metastases. Our technology for combinatorial targeting could be extended to other types of systemic bone

metastases and skeletal disorders including prostate cancer bone metastasis, multiple myeloma, and osteoporosis. As a platform technology, our system can be used to deliver other pro-drug systems[16, 45], or combinations of pro-drug systems shown to be synergistic[20]. As a facile RNA delivery tool, we also envisage that our technology can be used for simultaneous delivery of next-generation genome editing components (e.g., Cas9 mRNA and guide RNAs in CRISPR)[76, 77] in molecular biology and gene therapy.

### **3.5 Materials and Methods**

#### *Ethics statement*

All studies were done in accordance with National Institutes of Health guidelines for care and use of animals under approval of the Institutional Animal Care and Use Committees of the University of California, Irvine (IACUC protocol #AUP-18-134).

#### *Reagents*

Minimum Essential Medium  $\alpha$ , Roswell Park Memorial Institute (RPMI) 1640 Medium, Dulbecco's Modified Eagle Medium, Leibowitz' L-15 Medium, EGM-2 Endothelial Cell Growth Medium, M-199 Medium, Endothelial Cell Growth Suspension (ECGS), Penicillin/streptomycin solution, 2% gelatin solution, Opti-MEM Reduced Serum Medium, RNAiMAX Lipofectamine, 10x Tris-buffered saline (TBS), Scott's Bluing Solution, Fisherfinest Histoplast paraffin, MX35 Ultra low-profile cryotome blades, polylysine slides, HPLC grade ethyl acetate, acetonitrile, ACS grade glacial acetic acid, 2-propanol, recombinant human TNF-  $\alpha$ , recombinant human OPG, recombinant murine RANKL, Vybrant™ DiD lipophilic dye, CellTrace™ Calcein Green dye and 7-AAD viability assay dye were purchased from Fisher Scientific. 4% paraformaldehyde (PFA) solution was purchased from Santa Cruz Biotechnology.



Recombinant human TRAIL was obtained from Peprotech. Fetal bovine serum (FBS), sterile phosphate-buffered saline (PBS), ACK lysis Buffer, Tissue-Tek Optimal Cutting Temperature (OCT) embedding medium and Superfrost Plus slides were purchased from VWR. Puromycin powder, crystalline bovine serum albumin (BSA), Tween 20, Triton X-100, as well as donkey and goat normal sera, Harris' Hematoxylin, Eosin Y, 2-methylbutane, 10% Formalin solution, sucrose, EDTA, 5-Fluorouracil (5-FU), and 5-Fluorocytosine (5-FC) were purchased from MilliporeSigma. Isoflurane was purchased from Piramal Healthcare. Ketamine, xylazine, and buprenorphine were purchased from Western Medical Supply. D-luciferase was purchased from Perkin Elmer. Histo-Clear II was used as a xylene substitute for dehydration of tissue samples and was purchased from National Diagnostics. Water was purified using the Millipore Milli-Q system.

### *Cell culture*

MDA-MB-231 human ductal adenocarcinoma cells, 4T1 murine breast cancer, RAW264.7 macrophages, and HL-60 promyeloblasts were purchased from American Type Culture Collection, Inc. (ATCC) and respectively cultured in Leibovitz' L-15 medium, RPMI medium, Dulbecco's Modified Eagle Medium and RPMI medium supplemented with 10% FBS. MDA-MB-231 and 4T1 cells were transduced to express both firefly luciferase enzyme and RFP (LucF/RFP) using CMV-Luc3-2A-RFP (Puro) lentiviral particles (GenTarget, San Diego, CA, USA) per the manufacturer's protocol. Briefly,  $1 \times 10^4$  cells were seeded in a 24-well plate and infected with a multiplicity of infection of 10 particles/cell. 72 hours post-transduction, media was replaced with fresh media containing  $20 \mu\text{g/mL}$  puromycin for selection.  $5 \mu\text{g/mL}$  puromycin was used for routine culture to maintain transduction. LucF/RFP 4T1 CLL1 cells were *in vivo* selected from a mouse femur metastasis, which arose from a mammary fat pad injection of LucF/RFP 4T1 cells. 4T1 CLL1 were cultured similarly to parental 4T1 cells. Human mesenchymal stem cells (MSC),

obtained under principles of informed consent from the bone marrow of a healthy donor (#8011L), were purchased from Texas A&M Institute for Regenerative Medicine (Bryan, TX, USA), a NIH-funded non-profit organization for MSC isolation, characterization and distribution. These cells were fully characterized per established guidelines[35, 36]: MSC were tested for presence of viruses (HIV, hepatitis, *etc.*), characterized by their ability to differentiate into bone and fat, and by their negative expression for CD45, CD19, CD34, CD11b, CD79a, HLA-II:DR DQ DP, CD14 and positive expression for CD90, CD105, CD73a. MSC were cultured in Minimum Essential Medium- $\alpha$  enriched with 15% FBS, 2% L-glutamine, and 1% penicillin-streptomycin solution. To further characterize if engineering affects MSC function, we performed additional osteogenic and adipogenic differentiations of our engineered MSC (Supplementary Figure 3.1). Specifically, PSGL-1/SLEX/CD/OPG MSC were seeded onto 24-well tissue culture plates at a density of  $6 \times 10^4$  cells/well and cultured for 2-3 weeks. The media was made from Osteogenesis or Adipogenesis Differentiation Kits (EMD Millipore) and changed according to the manufacturer's instructions. At the end-point, cells were fixed and stained with Alizarin Red-S or Oil-Red-O, according to the manufacturer's instructions. Human umbilical vein endothelial cells (HUVEC) were kindly provided by Dr. Hughes (Department of Cellular and Molecular Biosciences, University of California, Irvine) and cultured in M-199 medium supplemented with 10% FBS, 2% L-glutamine, 1% penicillin-streptomycin solution, and 50 $\mu$ g/mL ECGS. MDA-MB231 LucF/RFP were cultured without CO<sub>2</sub>.

#### *mRNA synthesis and cell engineering*

mRNA were synthesized by TriLink BioTechnologies (San Diego, CA, USA) as previously described using *in vitro* transcription (32, 34). mRNA were capped and modified with a polyadenylated tail along with pseudouridine and 5-methylcytidine bases to decrease immunogenicity, enhance

translation, and enhance stability. DNA coding sequences used for the mRNA synthesis are specified in Supplementary Table 3.1. P2 MSC were transfected with Lipofectamine RNAiMAX in Opti-MEM reduced serum medium at 80% confluency using 1 µg mRNA per 10 cm<sup>2</sup> of surface area.

### *Flow Cytometry*

A minimum of 150,000 cells was used for all membrane staining. Cells were washed and stained in 1% BSA in PBS on ice. 7-AAD was used as a viability dye at a concentration of 5 µg/mL and antibodies were used at 4 µg/mL (Supplementary Table 3.1). For apoptosis staining, 5 µL of Annexin V-FITC was added to 100 µL of cells re-suspended at 1x10<sup>6</sup> cells/mL in binding buffer, following the manufacturer's recommendations. A minimum of 10,000 events was collected in the gates of interest. Unstained and single stained cells were used to generate the compensation matrix. An example of the gating strategy used for the analysis is shown in Supplementary Figure 3.2. Flow cytometry was performed on an Accuri C6 flow cytometer and an LSR II flow cytometer (BD Biosciences, San Jose, CA, USA). Data were analyzed using FlowJo version 10.1 software.

### *Immunofluorescence*

For immunohistochemistry and immunofluorescence, 8 µm sections were rehydrated using TBS. When necessary, tissue was permeabilized for 15 minutes with Tween 20 or Triton X-100. Blocking was done for 30 minutes using 5% normal serum from the appropriate species, diluted in a 1% BSA TBS solution. Primary antibodies were added at designated dilutions in blocking buffer (Supplementary Table 3.1) and incubated at 4°C overnight. Primary antibody binding was detected using appropriate secondary antibodies incubated at room temperature for 60 minutes, and mounting was done using Fluoromount G containing DAPI (Southern Biotech) and 0.17 mm glass coverslips.

For the quantification of P-selectin expression, we selected 200µm by 200µm areas within the tibia containing MSC, and the average P-selectin signal was measured by dividing total photon counts emitted in Cy5 channel per surface area and subtracting the background signal. To evaluate how P-selectin expression varied depending on the distance from the tumor, we randomly selected large longitudinal leg sections containing both tumor and at least 900 µm of marrow. We used NIS-Elements AR Analysis 4.50.00 64-bit grid utility (Nikon) to automatically generate a grid with 100 µm by 100 µm squares (ROIs) covering the whole marrow section. All ROIs not covering marrow vasculature were excluded. Automated measurement calculated the mean fluorescent signal for each ROI, and background was subtracted for each. The ROIs were assigned a distance from the tumor per 100µm by 100µm area, and P-selectin signal, and average signal was calculated per distance area from the tumor.

#### *Western Blotting*

Cell lysates were prepared using an SDS-based buffer, and subsequent protein concentration was determined using a standard bicinchoninic acid (BCA) assay. 40µg of proteins were separated using SDS-PAGE and transferred to Immun-Blot PVDF Membrane (Biorad, Hercules, CA, USA). After blocking in a 5% milk TBS-Tween solution, the membrane was blotted overnight at 4°C with primary antibodies directed against cytosine deaminase, Fc specific human IgG, and GAPDH before being probed with secondary antibodies conjugated to horseradish peroxidase for 1 hour at RT (Supplementary Table 3.1). After incubation with ECL substrate (Fisher Scientific), luminescence was detected using a ChemiDoc XRS+ (Bio-rad) and quantified using Image Lab 3.0.1 Beta 2 (Bio-rad).

#### *ELISA*

OPG concentration was measured in culture supernatants of MSC using a human osteoprotegerin/TNFRSF11B DuoSet ELISA (R&D Systems) according to the manufacturer's

recommendations. Each supernatant was assessed undiluted, diluted 1:10, and diluted 1:50 to be quantified in the linear range, and dosed in duplicates. As a control, 1ng/mL of recombinant human OPG was included in the assays.

#### *Flow chamber assay*

$5 \times 10^5$  P-2 HUVEC were seeded onto 35x10mm petri dishes (Corning) coated with 1% gelatin (Sigma) and incubated for one day to reach confluence. HUVEC were stimulated using 50ng/mL human TNF- $\alpha$  six hours prior to the assay to induce selectin expression. A flow chamber assay was performed using a PicoPlus syringe pump (Harvard Apparatus, Holliston, MA, USA) set at four different flow rates (4.42  $\mu$ L/min to create 1 dyn/cm<sup>2</sup> shear force, 8.84  $\mu$ L/min for 2 dyn/cm<sup>2</sup>, 17.68  $\mu$ L/min for 5 dyn/cm<sup>2</sup>, and 35.36  $\mu$ L/min for 10 dyn/cm<sup>2</sup>), and a vacuum pump (Welch, Mt. Prospect, IL, USA) collecting post-chamber efflux. Briefly,  $1 \times 10^6$  cells/mL of each cell type to be assayed were stained with 2.5 $\mu$ M CellTrace™ Calcein Green dye for better quantification using fluorescence, suspended in fresh EGM-2, and loaded in a 1mL syringe attached to the syringe pump. A flow chamber gasket (GlycoTech, Gaithersburg, MD, USA) was attached to the top of the HUVEC-seeded petri dish, a Silastic™ (GlycoTech) fluid line was fixed to the tip of the syringe and connected to the inflow port of the flow chamber gasket, and a drain line was run from the outflow port of the gasket to the waste chamber of the vacuum pump. 300 $\mu$ L of cell suspension was injected across the HUVEC layer for each run.

#### *MDA-MB-231/MSC Co-killing Assays*

On day 0, MSC were engineered using mRNA transfection. On day 1, MDA-MB231 LucF/RFP cells were respectively plated in a 96-well plate at  $1.5 \times 10^4$  cells per well and in a 24-well plate at  $1 \times 10^5$  cells per well, to reach 90% confluency on day 2. On day 3, depending on the assay conditions, 5-FC or 5-FU was added, and different ratios of MSC were plated on top of cancer cells in MSC culture media. On

day 9, the 24-well plate was imaged using brightfield and fluorescence to visualize the co-culture and MDA-MB-231 expressing RFP. The 96-well plate was incubated with AlamarBlue™ (Fisher Scientific) at a 1:10 dilution in 100µL fresh culture medium to measure the viability of the co-culture. After 5 to 6 hours, the absorbance was measured at a wavelength of 570nm (the peak absorbance for the reduced form) and 600nm (peak absorbance for the oxidized form) using a plate reader (Synergy HT, Biotek, Winooski, VT, USA). Briefly, the metabolic growth (and thereby the viability) of the cells was determined by subtracting the absorbance of the oxidized form from that of the reduced form. Data were normalized to the control (untreated cells).

#### *TRAIL-OPG Assay*

Concentrated media enriched for osteoprotegerin was generated by centrifuging 15 mL of conditioned media from MSC (day 3 post-engineering) using a 30 kDa Amicon Ultra-15 centrifugal filter unit (EMD Millipore, Temecula, CA, U.S.A.) at 4,000g for 15 minutes. MDA-MB-231 cells were plated in a 96-well plate at a density of  $1.5 \times 10^4$  cells/well and treated with recombinant human TRAIL in addition to rhOPG or concentrated MSC supernatant containing an equivalent concentration of OPG (as determined by ELISA).

#### *Osteoclastic differentiation*

Murine macrophages RAW264.7 cells were seeded at  $1 \times 10^3$  cells per well in a 96-well plate and treated with 100ng/mL murine RANKL in addition to human OPG or concentrated supernatant of MSC (from day 3 post-engineering). Medium was changed every other day. Each condition was performed in triplicate for each independent experiment. At day 6, cells were washed and fixed with 4% PFA and then TRAP stained using the Acid Phosphatase, Leukocyte (TRAP) Kit (MilliporeSigma) per manufacturer's instructions, with a 1:100 Harris' hematoxylin dilution in water for counterstaining. The entire wells were

imaged under a light microscope and multinucleated TRAP-positive osteoclasts with more than 3 nuclei were counted.

#### *Generation of conditioned media*

MSC were seeded to a 24-well plate at  $0.1 \times 10^5$ ,  $0.5 \times 10^5$  and  $1.0 \times 10^5$  cells per well in the presence of  $400 \mu\text{g/mL}$  5-FC. At different time-points (1 to 6 days), media was collected, centrifuged to remove floating cells and debris, and frozen at  $-80 \text{ }^\circ\text{C}$  until chemical extraction.

#### *Compound extraction*

To determine the extraction yield, culture medium was spiked with known concentrations of 5-FU ( $50$  and  $100 \mu\text{g/mL}$ ).  $250 \mu\text{L}$  of conditioned media sample was processed using  $1.75 \text{ mL}$  extraction buffer (1:1 ethyl acetate/2-propanol). After incubation and agitation, tubes were centrifuged at  $3,000g$  for 10 minutes, and the organic layers were collected. Remaining proteins were precipitated from the organic layers by adding  $100 \mu\text{L}$  saturated ammonium sulphate solution. After centrifugation, the organic phases were transferred to new centrifuge tubes and the solvent was evaporated in a Savant DNA120 SpeedVac Concentrator (ThermoScientific, Waltham, MA, USA). Extracted compounds were then resuspended for LC-MS/MS in analysis buffer (Milli-Q water containing 2% acetonitrile and 0.2% acetic acid, similar to the mobile phase A used for the UPLC).

#### *LC-MS/MS analysis*

$10 \mu\text{L}$  of extract was injected into an Acquity UPLC system (Waters Corporation, Milford, MA, USA) and separated with an Acquity UPLC-BEH C18  $1.7 \text{ mm } 2.1 \times 50 \text{ mm}$  analytical column (Waters). The auto-injector temperature was maintained at  $5^\circ\text{C}$  and the column temperature at  $25^\circ\text{C}$ . A gradient mobile phase elution was used, starting with 98% of solvent A (98% Milli-Q water, 2% acetonitrile and 0.2% acetic acid), and progressing in 3 minutes to 95% of solvent B (99.8% acetonitrile and 0.2% acetic acid).

acid) before holding in B for 60 seconds to elute the samples. The samples were then injected into a triple quad mass spectrometer (Waters Micromass Quattro Premier XE™ Tandem Quadrupole Mass Spectrometer, Waters) for mass analysis. Electrospray ionization was done using the negative ion mode (ESI<sup>-</sup>), which generates a precursor to product ion transition of  $m/z$  128>85 for 5-FC and 129>42 for 5-FU, thus allowed discrimination of the two compounds for analysis. Cone voltage and collision cell energy were optimized using training samples: 20V (CV) and 10V (CE) for 5-FC, 20V (CV) and 30V (CE) for 5-FU. MassLynx version 4.1 software was used for data acquisition, and QuantLynx software for downstream analysis. A 7-point 5-FU standard curve was prepared in serial dilution (1/3 dilution factor) starting from 60µg/mL down to 0µg/mL (analysis buffer alone) in order to determine the 5-FU concentration inside the samples ( $r^2 > 0.98$ , quadratic fit). An example of mass spectrometry data obtained for 5-FC and 5-FU is shown in Supplementary Figure 3.3.

#### *Animal experiments*

Animal subjects were first sedated in a chamber, then kept under a nosecone for the procedures, using either 2% isoflurane mixed with 2 L/min O<sub>2</sub>, or by intraperitoneal (*i.p.*) injection of a 100mg/kg ketamine and 10mg/kg xylazine mixture. For all intratibial injections, animals were injected *i.p.* with 0.1mg/kg buprenorphine for pre- and post-procedure analgesia.

To mimic established breast cancer bone metastases,  $1 \times 10^5$  MDA-MB-231 LucF/RFP cells in 10µL of sterile PBS were injected into the marrow cavity of the left tibia of 4- to 5-week-old female nude mice (strain code #194, CAnN.Cg-Foxn1<sup>nu</sup>/CrJ), purchased from Charles River Laboratories (Wilmington, MA, USA), using a 28Gx1/2", 1/2cc insulin syringe (ADW Diabetes). Note that for all studies (homing and efficacy studies) we also performed a mock PBS injection in the healthy tibia in the same animal to eliminate potential bias resulted from inflammation due to injection.



To establish a robust and spontaneous bone metastasis model[37],  $1 \times 10^4$  of our bone metastatic clone 4T1 CLL1 LucF/RFP were injected, via the caudal artery (c.a), into 5-week-old female BALB/cJ mice (JAX#000651, The Jackson Laboratory, Bar Harbor, ME, USA) using 29Gx1/2” 3/10cc insulin syringes (ADW Diabetes). This model had a 90% incidence for bone metastases, and the majority of bone metastases were located in legs (femur/hip area) and spine, but we also found some metastases in the rib cage, the scapula and the mammary fad pad. For therapeutic treatment, MSC were injected either intratibially ( $1 \times 10^5$  cells in 10 $\mu$ L sterile PBS) or intravenously ( $7 \times 10^5$  –  $1 \times 10^6$  cells in 200 $\mu$ L sterile PBS) into the lateral tail veins. 5-FC (500mg/kg) and 5-FU (12.5mg/kg for syngeneic model, 200mg/kg for immunocompromised model) were injected *i.p.* in PBS. For our syngeneic model, we chose a 5-FU dose that was not overly toxic to animals but sufficient to induce anti-tumor effect based on the literature, and clinically relevant: several clinical dose recommendations for breast cancer include 375mg/m<sup>2</sup> *i.v.* daily for five days every 3 weeks, which is equivalent to 12.84 mg/kg for an average American[38]. We performed a pilot study using 12.5 and 50 mg/kg of 5-FU and determined that 50 mg/kg was too toxic to animals, therefore deciding to use 12.5 mg/kg for the final study. Animals were closely monitored on an individual basis (visual examination, weight measurements).

Tumor growth inside the tibia was measured using bioluminescence. Mice were injected *i.p.* with 150mg/kg sterile D-luciferase substrate (Perkin Elmer). After a 15min hold time (peak of enzyme kinetics), tumor bioluminescence data were collected after 1second and 1minute integration times using a Xenogen IVIS Lumina II multispectral imager (Caliper LifeSciences, Waltham, MA, USA). Bioluminescence data were analyzed using Living Image version 4.3.1 software (Perkin Elmer, Waltham, MA, USA).

For homing experiments, DiD-labelled MSC were imaged *in vivo* and *ex vivo* using the Cy5.5 filter sets (615-665 nm excitation, 695-770 nm emission) of the Xenogen IVIS Lumina II. Animals not

transplanted with DiD-labelled MSC were used as a control to subtract tissue auto-fluorescence and obtain true signal from labelled MSC.

For survival experiments, animals were euthanized following well-defined end-point criteria: any evidence of pain or suffering (prostration, isolation, absence of grooming, lethargy, anorexia, dehydration, *etc.*) or, in our particular model, 1) when the tumor invaded the cortical bone, which was typically equivalent to a total photon flux  $\geq 1 \times 10^{10}$  photons/sec and was frequently accompanied by a visible limb deformity, 2) when the animal began to show signs of paraplegia, or 3) when the animal showed persistent cachexia and/or a greater than 10% loss of body weight that was uncorrectable by supplemental nutrition and fluids.

The progression of paralysis in mice was assessed on a three-point scale. A score of zero indicated free mouse movement with no obvious signs of paralysis. A score of one indicated the presence of retracted limbs, hunched posture, and visible trouble moving around. A score of one and a half indicated greatly restricted movement of hind limbs, which neared paralysis. A score of two indicated total paralysis of the hind limbs.

#### *Bone marrow isolation*

Mouse femurs and tibias were harvested immediately after sacrifice, and bones were thoroughly cleaned of all muscle tissue. Epiphyses were cut to expose the bone marrow cavity and bones were centrifuged in a perforated tube at 12,000g for 30s to isolate the bone marrow in a collection tube. Extracted marrow was washed in PBS then incubated in ACK lysis buffer at 37°C for 3min to lyse erythrocytes. After quenching with PBS, the bone marrow suspension was resuspended in PBS-BSA 1% at the desired concentration for subsequent flow-cytometry analysis.

#### *Alu qPCR analysis for MSC homing*

Whole legs were harvested after euthanasia, stripped down to a thin layer of muscle surrounding the bones (muscle prevents loss of fragilized bones fragments), and flash frozen in slurry of 70% ethanol and dry ice. Surgical tools were cleaned in between each leg to prevent cross contaminations. Tissues were thawed and immediately homogenized with mechanical force using metal bead agitation at 4°C (Next Advance Bullet Blender® Storm with Navy 5 mL Lysis Kit). DNA extraction was performed on 25mg of homogenized tissues (1/28<sup>th</sup> of the initial lysate) using chemical lysis and silica spin column purification (Qiagen DNeasy® Blood and Tissue Kit).

To quantify human MSC numbers in each mouse leg, an Alu qPCR assay was performed on 50ng of extracted DNA using PowerUp™ SYBR™ Green Master Mix (Applied Biosystems, Dun Laoghaire, Ireland), optimized primer sets for the human Alu transposable element (FWD: CACCTGTAATCCCAGCACTTT and REV: CCCAGGCTGGAGTGCAGT)[39], and the mouse GAPDH gene as an endogenous control (FWD: TGGCCTTCCGTGTTCTAC and REV: GAGTTGCTGTTGAAGTCGCA)[40]. A QuantStudio™ 6 Flex Real-Time PCR System was used to run the qPCR, and data were analyzed using QuantStudio™ 6 and 7 Flex Real-Time PCR System Software (Applied Biosystems, Dun Laoghaire, Ireland). A comparative CT value ( $\Delta$ CT) for human MSC in each tissue was derived by subtracting the mean of triplicate mGAPDH CT values from the mean of triplicate hAlu CT values[41].

A standard curve was established by injecting known quantities of MSC into the tibias of BALB/cJ mice following 6 fold serial dilutions of the cell suspension (100, 600, 3600, 21600 and 130000 MSC), followed by tissue homogenization/DNA extraction/qPCR (as described above). The logarithm of the number of MSC injected was plotted versus the  $\Delta$ CT, and a linear regression was done to generate a standard curve slope equation. Cell numbers in each sample leg were calculated by the standard curve

equation from the obtained  $\Delta CT$  value. The limit of detection was determined by subtracting 2 from the negative control (PBS injection only in the mouse tibia)  $\Delta CT$  value[42].

#### *Bone micro-computed analysis and bone damage scoring*

Mouse tibias were fixed in 4% PFA for 48h immediately after dissection. After tissue fixation, samples were transferred to a radiotransparent container in sterile PBS. For our initial study, 3D X-Ray imaging was performed using VersaXRM™ 410 (Xradia, Pleasanton, CA, USA) with 14 $\mu$ m voxel size. 3D volumes for whole tibias and trabecular bone were reconstructed into DICOM files for segmentation using ScanIP software (Ver. 7.0, Simpleware Ltd). ROIs were defined as the following: 1) epiphysis of the tibia down to the fibula insertion point for the whole tibia reconstruction, and 2) 100 slices (1.4mm total) starting below the growth plate down to the diaphysis where trabeculae disappear for the trabecular bone reconstruction. Bone was segmented from the background using grayscale values, and a mask was generated from that thresholding to reconstruct the whole tibia via a built-in rendering function, followed by whole tibia smoothing using a “Recursive Gaussian” filter with cubic values of 2.0 cm. For trabecular reconstructions, a second ROI was generated on 2D slices after thresholding to outline the trabecular cavity and exclude the cortical bone. The morphological “Close” function was then used to fill the space in between outlines, thus generating a first mask, filling the cavity of the tibia. A “Multilevel Otsu segmentation” was applied to generate a second mask which encompassed only the background, excluding the trabecular bone. To generate a 3D trabecular bone model, a built-in rendering function was applied to a final mask resulting from the subtraction of the second mask from the first mask.

For our final studies, femur or tibia samples were imaged on a micro-Computed Tomography scanner, Skyscan 1076 (Bruker, Kontich, Belgium) at (9 $\mu$ m)<sup>3</sup> voxel size, 50kVp, 200uA and using a 0.5mm aluminium filter. Image reconstruction was performed with NRecon software (Bruker, Kontich, Belgium)

using a beam-hardening correction algorithm, at a setting of 40% and a ring artefact reduction size of 8. Samples were aligned vertically with Dataviewer software (Bruker, Kontich, Belgium). As reference points, the tips of the proximal tibial growth plate and distal femoral growth plate were noted. Then, using a custom method, an overview of each sample was visualized as 15 transverse 2D sections spaced every  $\sim 140\mu\text{m}$ . In addition, CTvox software (Bruker, Kontich, Belgium) used with a global threshold value that selected the majority of cortical bone outline and trabecular bone to make 3D renders. Total bone volume and trabecular bone volume were analyzed across  $900\mu\text{m}$  (100 slices), starting  $180\text{-}360\mu\text{m}$  from the reference point of the selected growth plate. The total bone was selected by manual contouring with elliptical cross-sections, encompassing the periosteal tissue and the marrow cavity. A global threshold was used to identify total bone and an erosion of 1-2 pixel was performed to eliminate partial volume effects. The trabecular region, inward  $\sim 100\mu\text{m}$  from the cortex, was selected by an automated contouring routine or else by manual tracing every  $\sim 20$  slices with automated interpolation. An adaptive threshold (using the mean maximum and minimum pixel intensity values of the surrounding ten pixels) was used to identify trabecular bone. The bone volume (BV) was determined using CTan (Bruker, Kontich, Belgium). For the femurs, analysis of the total BV was performed for the entirety of the femur bones.

For femur scoring, we asked 20 individuals, including 70% being unfamiliar with the research study, to blindly score each femur from the 3D reconstructions (videos and pictures). Scoring took into account the shaft damage (0: no visible damage, 1: less than 10% of bone missing, 2: 10-30% of bone missing and 3: extensive damage with  $>30\%$  of the shaft missing) and the epiphysis damage (0: presence of both epiphysis with no damage, 1: presence of both epiphysis with little damage, 2: extensive damage/loss of one epiphysis and little to no damage on the other epiphysis, 3: extensive damage on both epiphysis, 4: loss of one epiphysis and extensive damage on the other one and 5: loss of both epiphysis).

### *Tissue processing*

Mouse organs and limbs were respectively fixed for 24 or 48h in 4% PFA at 4°C. Mouse legs were then incubated in a decalcification solution (14% EDTA, 0.4% PFA (pH 7.4), in PBS) at 4°C, on a shaker, for 14 days. Decalcification solution was changed every other day, to gently decalcify the bones. All tissues to be flash-frozen were treated in a sucrose gradient (6% then 30%) for 48h, followed by a 6h incubation in a 1:1 mixture of OCT and 30% sucrose solution, prior to being embedded in OCT using liquid-nitrogen-cooled isopentane. Sectioning of frozen tissue was performed on a CM1950 Ag Protect cryostat (Leica Biosystems, Wetzlar, GER) on polylysine slides using MX35 Ultra low-profile microtome blades.

Tissues destined for paraffin embedding were fixed in 10% formalin for 48h, prior to an ethanol gradient dehydration and paraffin embedding cycle. 7µm tissue sectioning was performed using an RM2255 microtome (Leica) with Superfrost slides.

### *H&E staining and TRAP staining*

Hematoxylin and Eosin (H&E) staining was performed following the standard procedure, and slides were mount using Permount (Fisher Scientific) and 0.17mm glass coverslips. Quantifications from H&E staining were done as the following. The entire spleen sections were scanned using a 10X objective, and connective tissue was outlined and measured using NIS Elements AR Analysis area function. In order to derive percentages, the total spleen area divided the sum of all connective tissue measurements. Three independent images of each animal's intestine (550 µm by 750 µm) were imaged using a 10X objective. Goblet cells were identified by absence of staining in secretory region and counted using NIS Elements AR Analysis count function per villus (only intact villi counted). Bone marrow sections were imaged using a 20X objective, and four images were randomly selected per animal. Leukocytes were analyzed on the red channel of RGB images using NIS Elements AR Analysis Spot Finder, on Dark Spot mode, "dark,

clustered” profile, with a 3.5  $\mu\text{m}$  expected diameter and 7.5 contrast ratio selected to differentiate between cells and morphological features. “Remove bright” was set to 90 to reject erythrocytes. Counting methodology was validated using a manual count on a small region and was found to be >99% accurate using the above settings. Total leukocyte count was divided by total enumerated region to yield a measurement of leukocytes per unit area.

TRAP staining was performed per manufacturer’s protocol using the using the Acid Phosphatase, Leukocyte (TRAP) Kit. Briefly, slides were deparaffinized using histoclear and tissue rehydrated through an ethanol gradient. Tissue was then incubated in TRAP staining solution at 37°C for 60min, then counterstained with a 1:4 dilution of Harris’ Hematoxylin in Milli-Q-water. The nuclear membranes were blued using Scott’s Bluing Reagent. Slides were mounted using Aquamount medium (Fisher Scientific) under 0.17mm cover slips. For analysis, images were cropped to select the growth plate of the tibia. A 12mm by 12 =mm ROI was positioned to be horizontally centered relative to the growth plate, with the top edge of the ROI aligning with the highest point of the border between the proliferative and hypertrophic zones of the bone. This ROI was then duplicated to the immediate right and left of the initial counting ROI, creating a total of three counting ROI’s. Osteoclasts were counted on the basis of TRAP<sup>+</sup> staining coloration, cell morphology and presence of multiple nuclei using the Cell Counter ImageJ plugin (NIH).

### *Microscopy*

Imaging was performed using an Eclipse Ti epifluorescent microscope (Nikon, Tokyo, JPN). For brightfield imaging, the Nikon DS-Ri2 color camera was used. For fluorescent imaging, a Lumencor Spectra X light engine was utilized to power LED light sources for excitation. Emission filters for DAPI, FITC, TRITC, Cy5, and Li-Cor 740 dyes were used, and fluorescent emissions were detected using an Andor Zyla 5.5 sCMOS camera. Confocal microscopy was performed using an Olympus FV3000RS laser-

scanning confocal microscope, utilizing OBIS LS/LX laser modules (Coherent, Santa Clara, CA, USA) and FV3000 Spectral Detector and High-sensitivity Spectral Detector units (Olympus, Center Valley, PA, USA). Final image processing was performed using NIS Elements Advanced Research package (Nikon) and ImageJ software (NIH).

### *Statistical analysis*

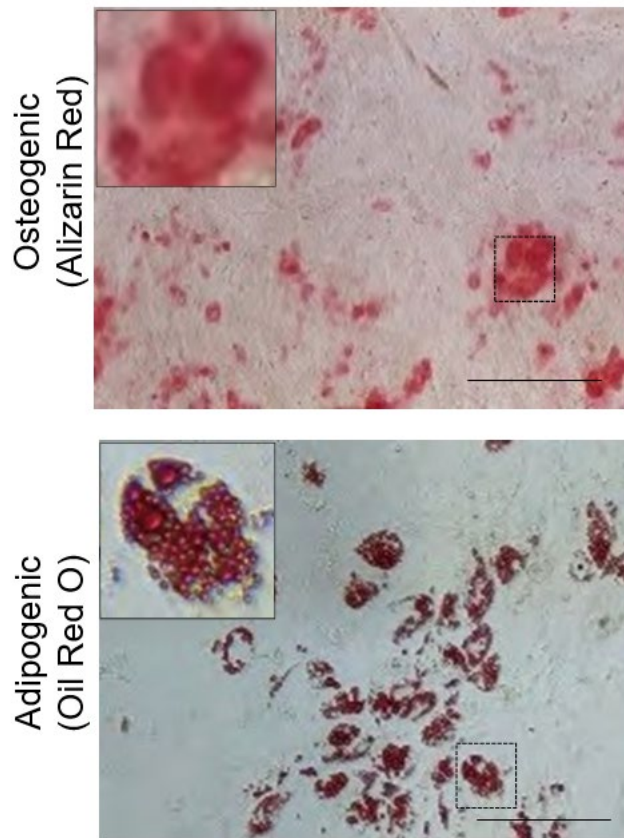
All experiments were performed independently at least twice, and each condition within an experiment was done in duplicates or triplicates. When sample size was  $< 30$ , or normal distribution and variance equality were not confirmed, non-parametric tests were used. To compare two groups, a Mann-Whitney test was performed (non-parametric  $t$  test), and when comparing more than two groups a Kruskal-Wallis test was applied (non-parametric variance analysis). Both tests were followed by a multiple comparison test (adjusted  $p$  values for multiple comparison). For the flow-chamber assay, a two-way ANOVA test and Dunnett's multiple comparisons test was done, and each column was compared to native MSC. For the survival analysis, a log-rank (Mantel-Cox) test was performed to compare treated groups to the control group.  $*p<0.05$ ,  $**p<0.01$ ,  $***p<0.001$  and  $****p<0.0001$ . For animal experiments, the value for each animal and the median of the group were plotted. A power analysis was done from the first animal studies performed in order to determine the minimum animal number to be used for following studies. The first study's goal was to evaluate the effect of three mRNA engineered MSC therapies (CD, OPG and CD/OPG BM-MSC) compared to PBS and Mock MSC. In our pilot data, the mean and standard deviation of the log-transferred before and after tumor growth ratio was 1.71 (1.03) in PBS group and -0.91 (1.90) in CD/OPG group respectively. For the ex-vivo bone analysis, the mean (SD) of bone loss was 0.18 (0.23) for PBS group and 0.94 (0.30) for the CD/OPG group. The primary comparisons were the three-treatment groups versus PBS. Based on the above summary information, a sample size of 10 mice per group can



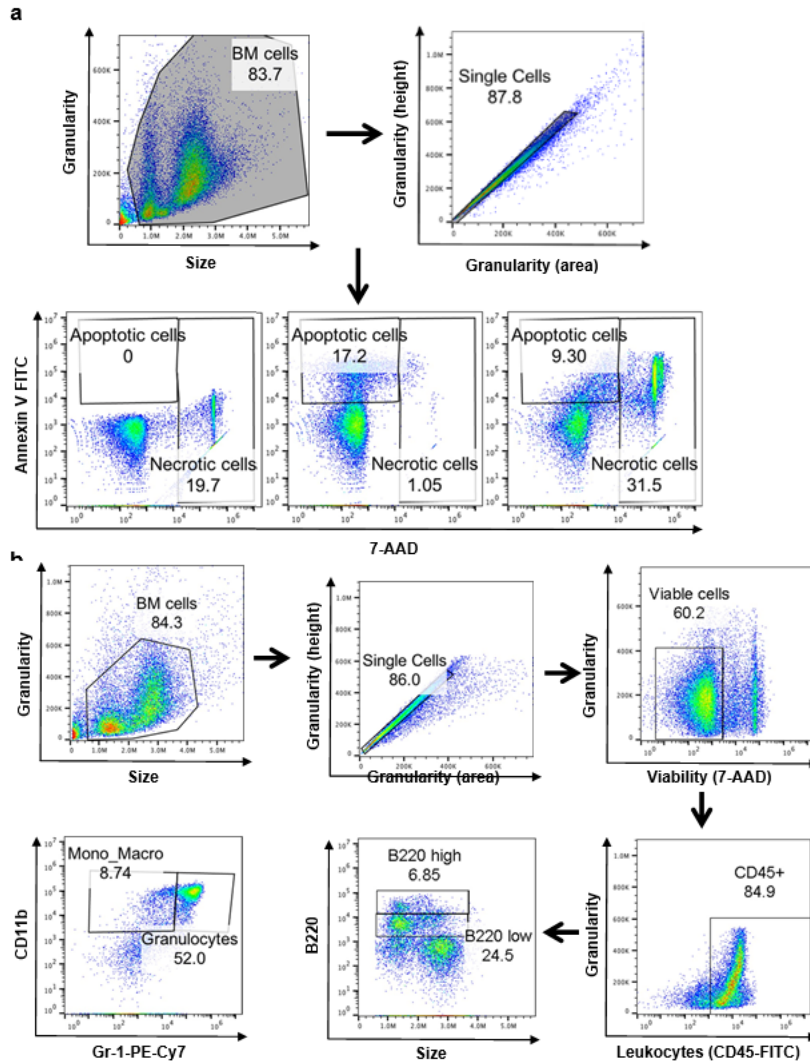
achieve 81.6% power to detect the observed difference of tumor growth with an adjusted significance level at 0.0167 ( $= 0.05/3$ ), and a 99% power for the observed difference in bone loss. The sample size was calculated based on a two-sample two-sided t-test. To evaluate the efficacy of our therapies in a second animal model, we decided to compare tumor growth. The primary comparison would be the three-treatment therapies (CD, OPG and CD/OPG MSC) *v.s.* PBS group. We assumed that the effect size would be similar for this proposed study. Therefore, a sample size of 10 mice per group can achieve 84.9% power to detect the assumed difference of tumor growth with an adjusted significance level at 0.0167 ( $= 0.05/3$ ). A two-sample t-test was used in the sample size calculation. Bonferroni correction was applied to adjust for the three primary comparisons. For the toxicity study, the percentage of viable and necrotic cells are the two primary outcomes that reflect toxicity level and our main comparison was the three-treatment therapies (CD, OPG and CD/OPG) *v.s.* 5-FU group. In a similar study performed in immunocompromised animals, the mean difference between 5FU and CD/OPG BM-MSc triple injection was 30.3% (with SD = 16.8%) for viable cells and 40.7% (with SD = 21.9%) for necrotic cells. The proposed 10 mice per group can achieve a 90.5% power to detect the observed difference in viable cells between 5FU and CD/OPG, and 92.2% power for necrotic cells, both at significance level = 0.0167 ( $=0.05/3$ ). In order to analyze our pilot study and the repeated experiment for the local injection of engineered MSC into the intratibial MDA-MB231 tumors, a linear mixed model compared the tumor growth and the bone volume among different treatment groups, with a random effect, to adjust for the potential mouse correlation within each experiment. A method of false discovery rate (FDR) was used to correct for multiple comparisons.

All graphs and statistical analysis were done using GraphPad Prism version 6.0h for Macintosh (GraphPad Software, La Jolla, CA, USA; [www.graphpad.com](http://www.graphpad.com)).

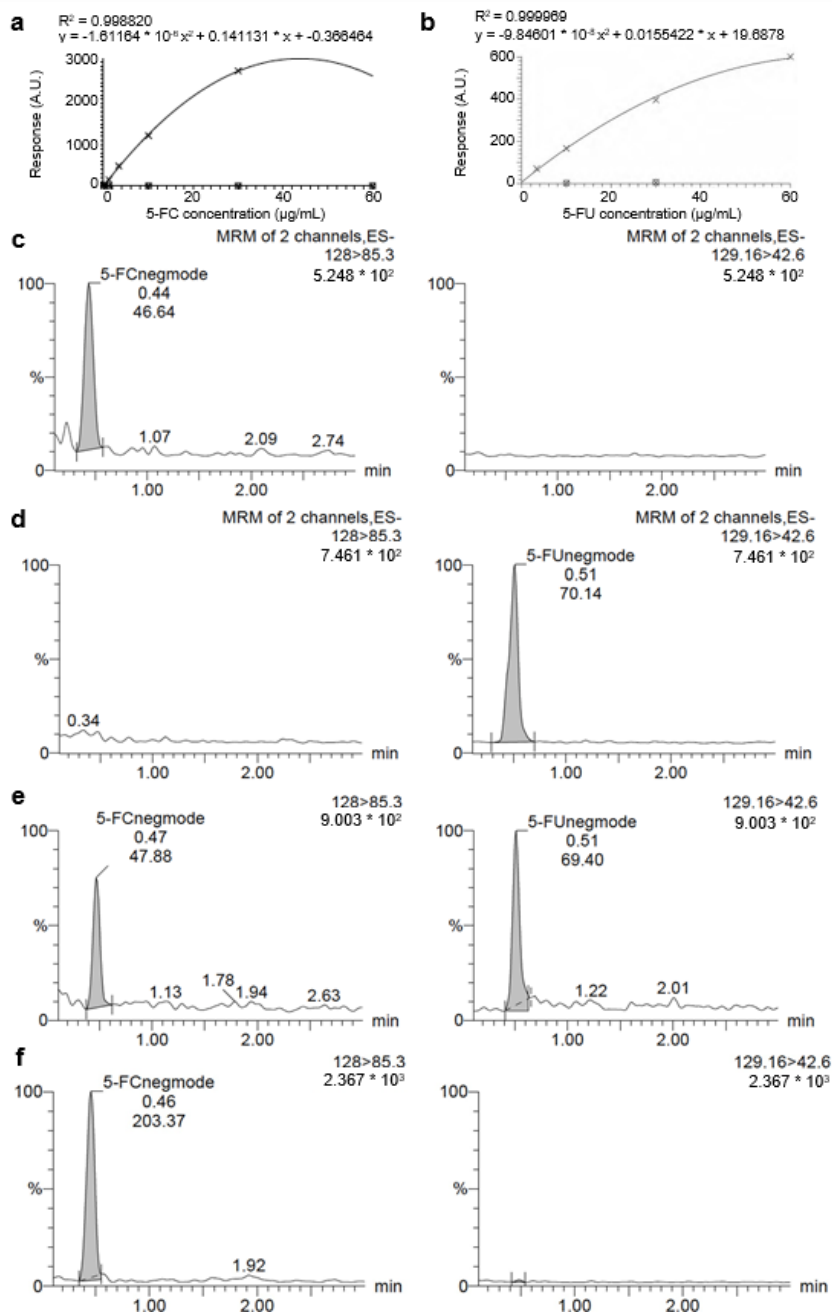
### 3.6 Supplemental Materials



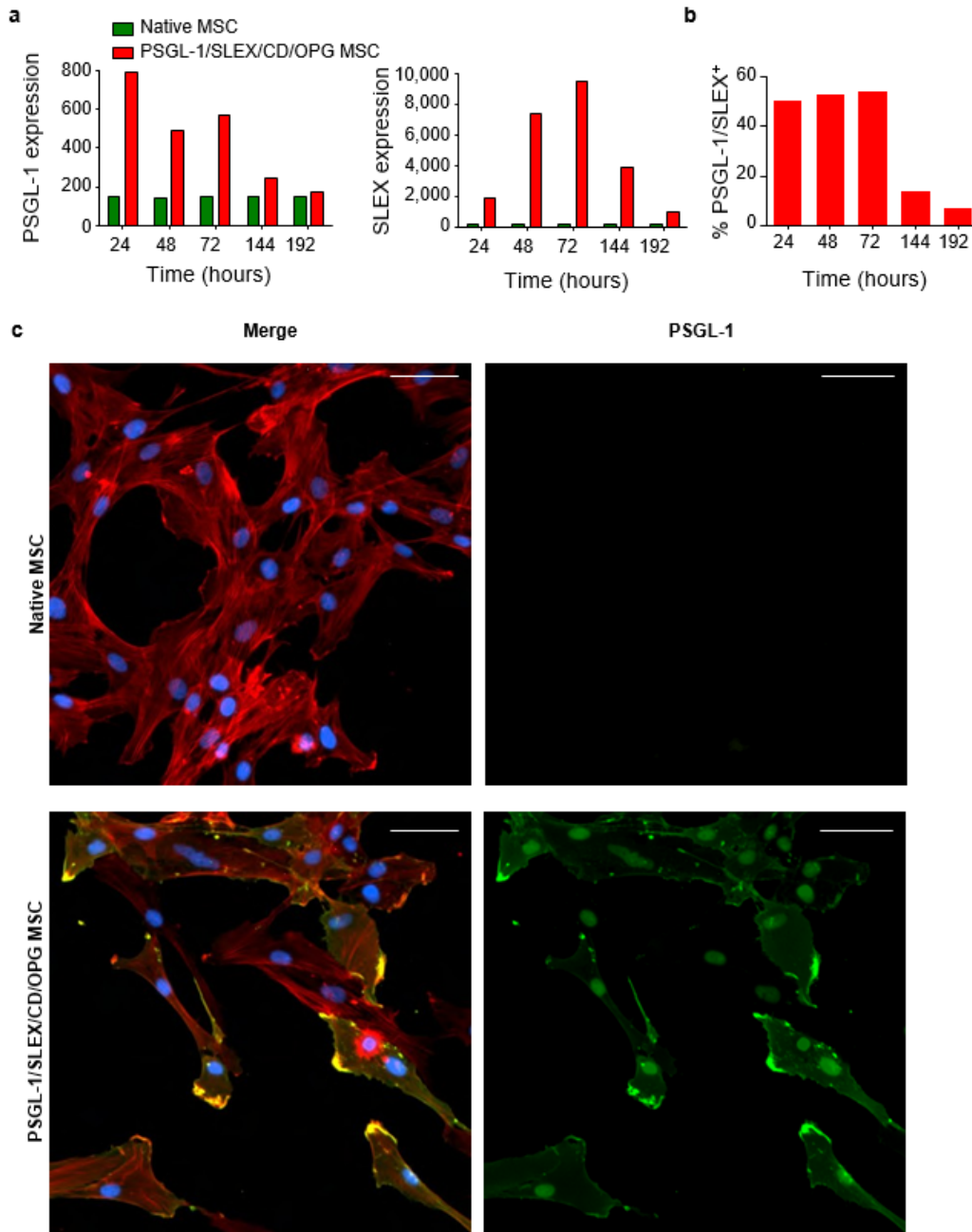
**Supplementary Figure 3.1: PSGL-1/SLEX/CD/OPG MSC conserve their differentiation abilities after mRNA engineering.** 24 h post mRNA engineering, PSGL-1/SLEX/CD/OPG MSC were plated to confluence and treated for osteogenic and adipogenic differentiation for 2-3 weeks. Image in the upper left corner shows a higher magnification of the area selected by the dashed line square in the larger image. Alizarin Red: calcium staining, Oil Red O: lipids staining. Scale bar: 250  $\mu$ m.



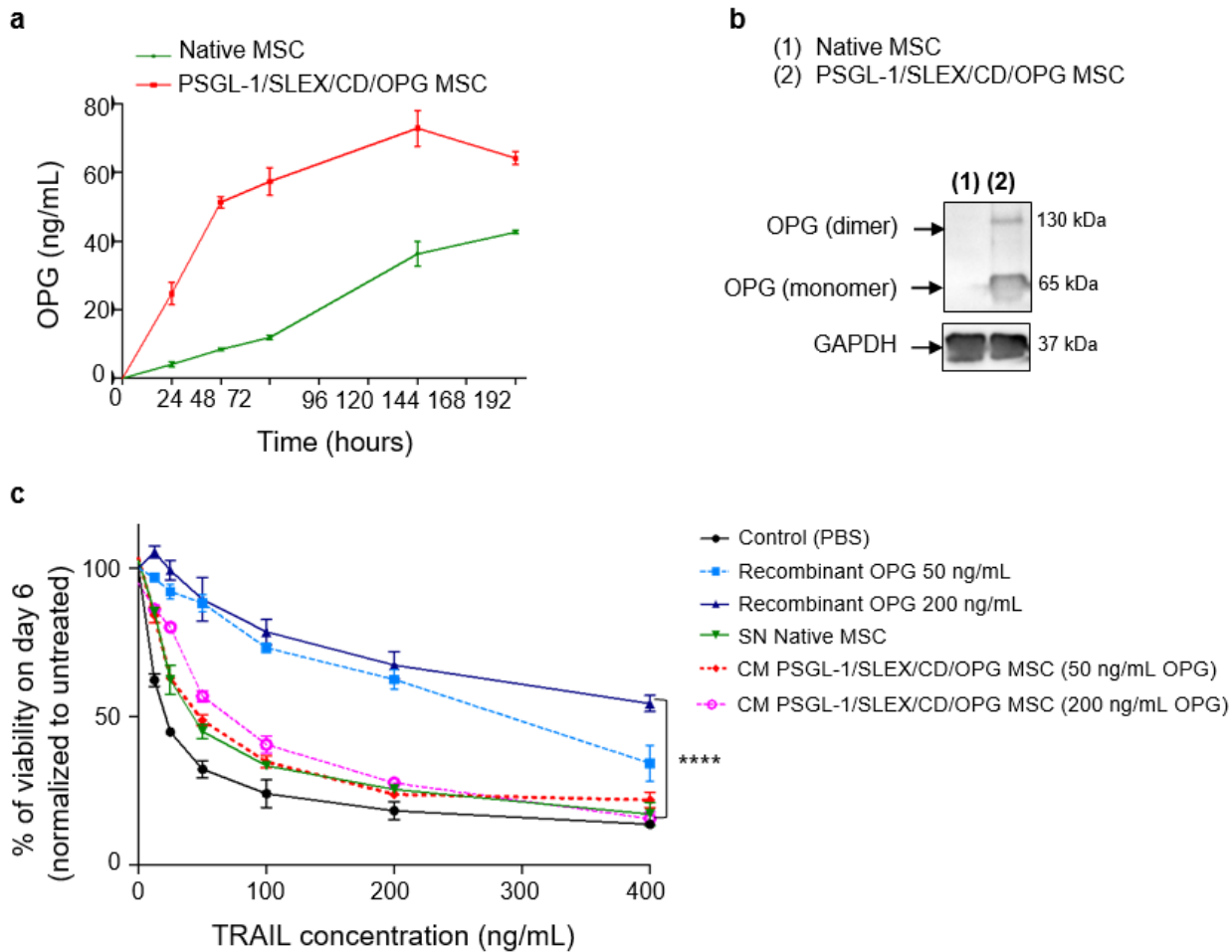
**Supplementary Figure 3.2: Example of gating strategies used to analyze bone marrow cells.** (a) Apoptotic cells and necrotic cells were analyzed using 7-AAD and Annexin V FITC. After gating bone marrow cells based on size and granularity, single cells were selected, then apoptotic gate (Annexin V<sup>+</sup>/7-AAD<sup>-</sup>) and necrotic gate (Annexin V<sup>+</sup>/7-AAD<sup>+</sup>) were drawn from single stains. (b) Different cell populations were analyzed in the bone marrow. First, bone marrow cells were selected based on their size and granularity, then single cells were selected. Within the viable cells (7-AAD<sup>-</sup>), leukocytes (CD45<sup>+</sup>) were selected to remove erythrocytes which did not get lysed. Finally, B cells (B220<sup>low</sup> or <sup>high</sup>), monocytes/macrophages (CD11b<sup>+</sup>/Gr-1<sup>neg</sup> or <sup>low</sup>), and granulocytes (CD11b<sup>+</sup>/Gr-1<sup>high</sup>) were quantified.



**Supplementary Figure 3.3: The conversion of 5-Fluorocytosine (5-FC) pro-drug into 5-Fluorouracil (5-FU) by PSGL-1/SLEX/CD/OPG MSC were measured by mass spectrometry.** (a) A standard curve was determined from serial dilutions of 5-FC in water using negative ion mode (ES-). (b) A standard curve was determined from serial dilutions of 5-FU in analysis buffer using negative ion mode (ES-). (c) 370 ng/mL of 5-FC was easily detectable using m/z 128>85 specific transition for 5-FC, while nothing was detected using m/z 129>42 specific transition for 5-FU. (d) 3,300 ng/mL of 5-FU was easily detectable using m/z 129>42 specific transition for 5-FU while nothing was detected using m/z 128>85 specific transition for 5-FC. (e) 5-FC and 5-FU compounds were detected in conditioned medium of 100,000 PSGL-1/SLEX/CD/OPG MSC plated in presence of 400 µg/mL 5-FC after 1 day of culture. (f) 5-FC but no 5-FU compound was detected in conditioned medium of 100,000 Mock MSC plated in presence of 400 µg/mL 5-FC after 1 day of culture.

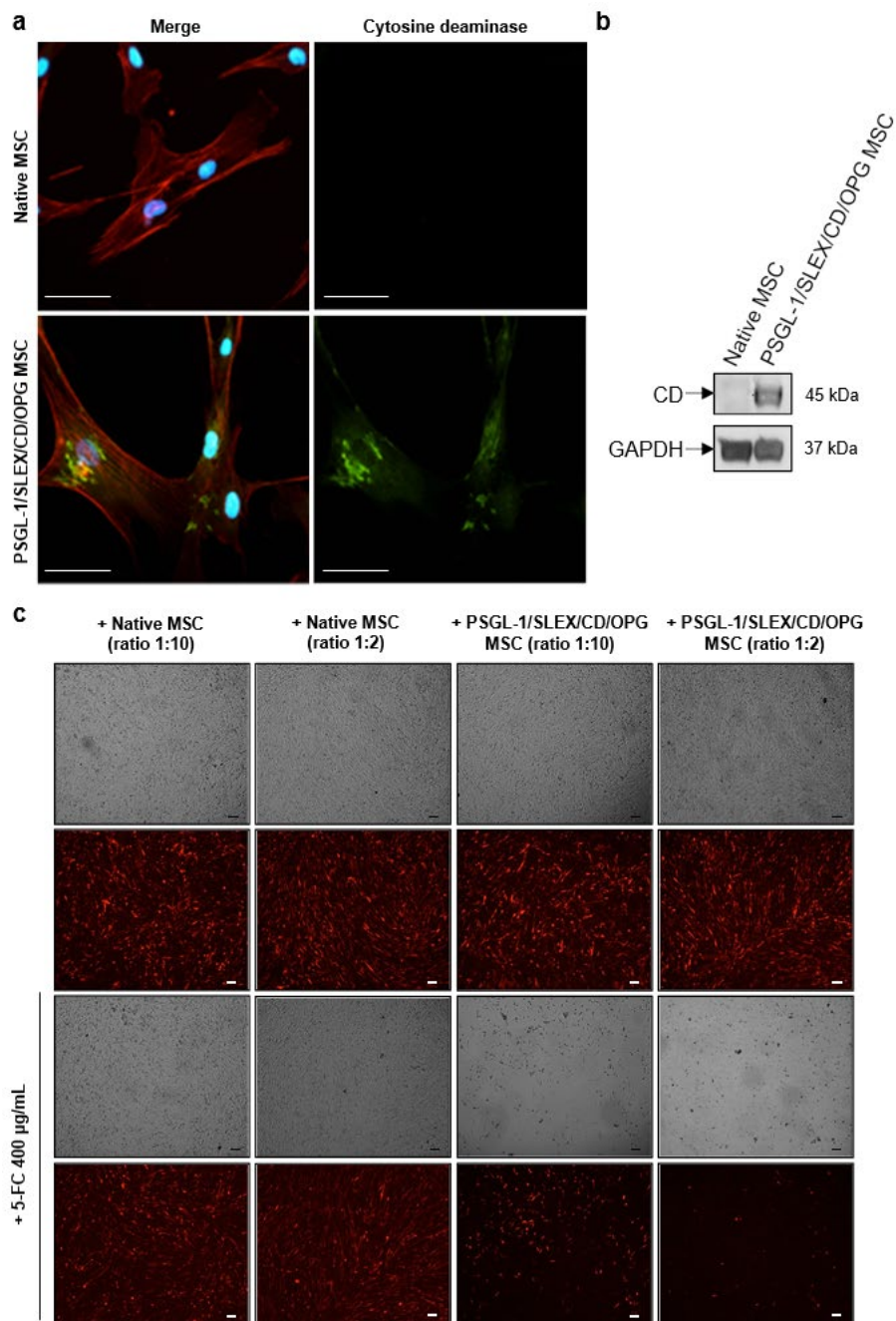


**Supplementary Figure 3.4: *In vitro* functional validation of PSGL-1/SLEX expression by engineered MSC.** (a) PSGL-1/SLEX/CD/OPG MSC expressed PSGL-1 and SLEX up to 6 days at the cell membrane. Flow cytometry was done on Native MSC and PSGL-1/SLEX/CD/OPG MSC at days 1, 2, 3, 6, and 8 to measure PSGL-1 and SLEX expression at the cell surface. Histograms show the median of fluorescence (MFI) for SLEX expression (FL-1) and PSGL-1 expression (FL-2). (b) Approximately 50% of engineered MSC expressed both PSGL-1 and SLEX over 3 days post-transfection. Percent of double positive cells for PSGL-1 and SLEX was analyzed by flow cytometry. Histogram shows percentages of double positive MSC for PSGL-1 and SLEX. (c) PSGL-1 was localized at the pseudopodia of PSGL-1/SLEX/CD/OPG MSC. Immunofluorescence staining was done against PSGL-1 on Native MSC and PSGL-1/SLEX/CD/OPG MSC 24 h post-engineering. Green: PSGL-1, red: F-Actin (Phalloidin 594 nm) and blue: nuclei (DAPI staining). Scale bar: 100  $\mu$ m.

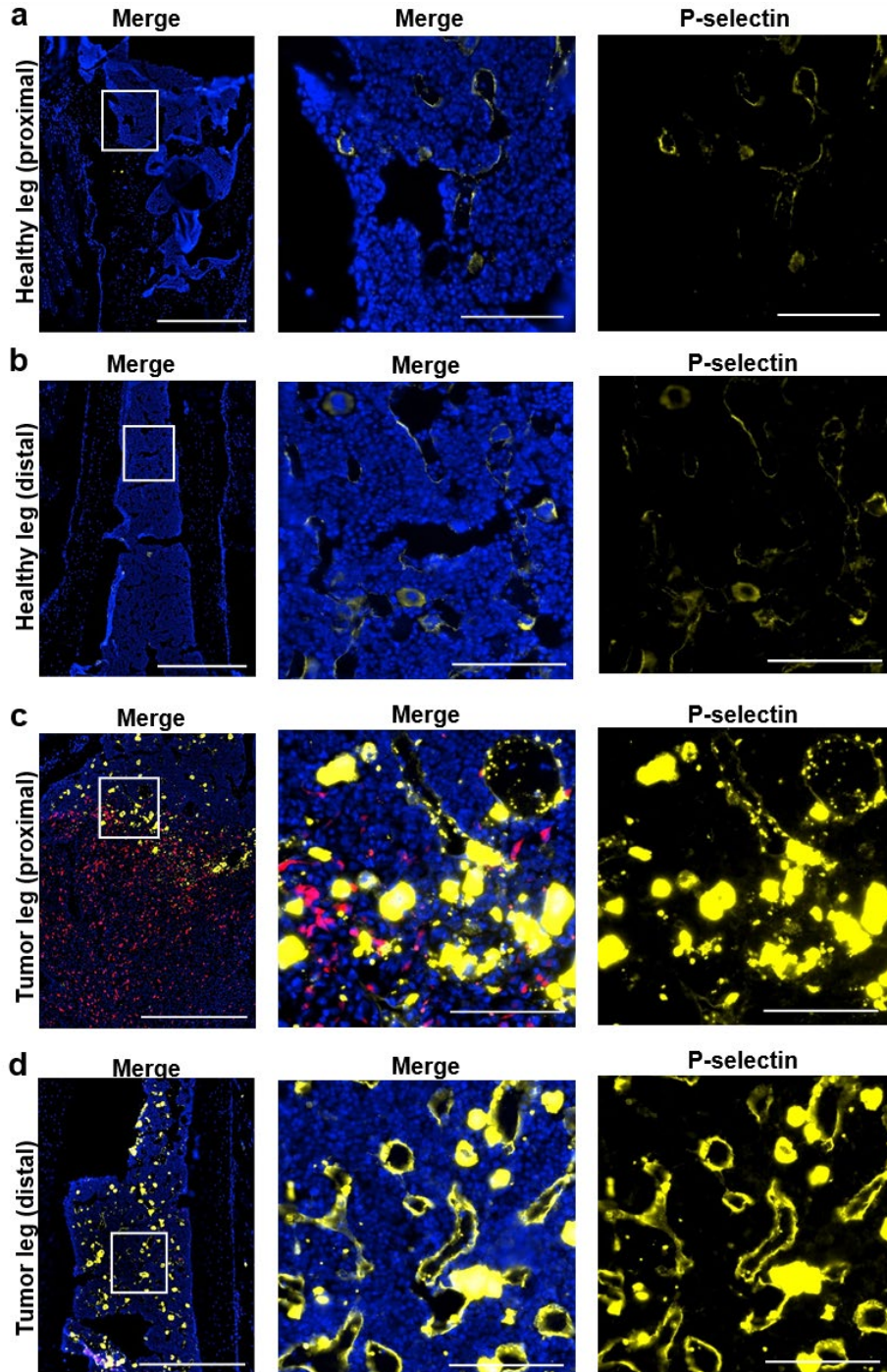


**Supplementary Figure 3.5: *In vitro* functional validation of OPG secreted by engineered MSC.** (a) PSGL-1/SLEX/CD/OPG MSC secrete soluble form of human OPG. ELISA was performed on conditioned media from Native MSC and PSGL-1/SLEX/CD/OPG MSC cultured for 8 days to measure secreted OPG (Native and engineered forms). Graph shows mean  $\pm$  SD. (b) PSGL-1/SLEX/CD/OPG MSC express truncated OPG fused to Fc fragment from human IgG1. Western blot was performed on cell lysates at 24 h post-engineering against human Fc fragment. GAPDH was used as a loading control. (c) Recombinant human osteoprotegerin inhibits TRAIL apoptotic activity whereas the engineered form of OPG secreted by PSGL-1/SLEX/CD/OPG MSC does not. Viability of MDA-MB231 cells was determined in presence of increasing concentrations of TRAIL and recombinant human osteoprotegerin or concentrated conditioned media of Native and PSGL-1/SLEX/CD/OPG MSC (10  $\mu$ L of PSGL-1/SLEX/CD/OPG MSC concentrated supernatant is equivalent to 50 ng/mL and 40  $\mu$ L is equivalent to 200 ng/mL as previously determined by ELISA). Viability assay was performed 24 h after treatment using Alamar blue assay. Graph shows mean  $\pm$  SD. \*\*\*\* $p \leq 0.0001$  between recombinant OPG 200 ng/mL and CM PSGL-1/SLEX/CD/OPG MSC (200 ng/mL OPG) using unpaired *t* test.



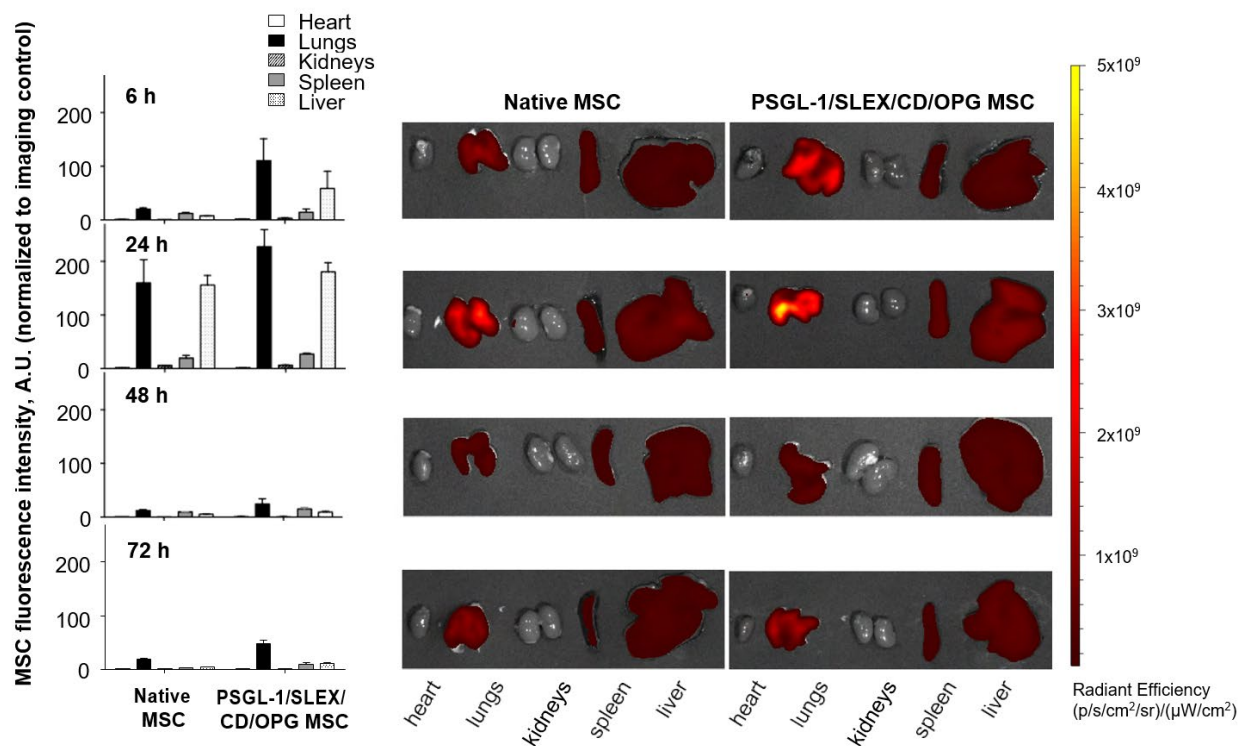


**Supplementary Figure 3.6: *In vitro* functional validation of CD expression by engineered MSC.** (a) PSGL-1/SLEX/CD/OPG MSC showed intracellular expression of CD. Immunofluorescence was done on Native and PSGL-1/SLEX/CD/OPG MSC at 24 h post-engineering. Green: CD, red: phalloidin, and blue: nuclei (DAPI staining). Scale bar: 100  $\mu$ m. (b) The molecular weight of the CD expressed by PSGL-1/SLEX/CD/OPG MSC matched the molecular weight of the original protein (CD fused to uracil phosphoribosyltransferase). Western blot against CD was performed on cell lysates at 24 h post-engineering. GAPDH was used as a loading control. (c) PSGL-1/SLEX/CD/OPG MSC killed cancer cells when co-cultured in presence of 5-Fluorocytosine. Pictures show the co-cultures at day six; brightfield shows both cell types in direct co-culture, whereas fluorescent images only show MDA- MB231 expressing RFP (red). Scale bar: 100  $\mu$ m.

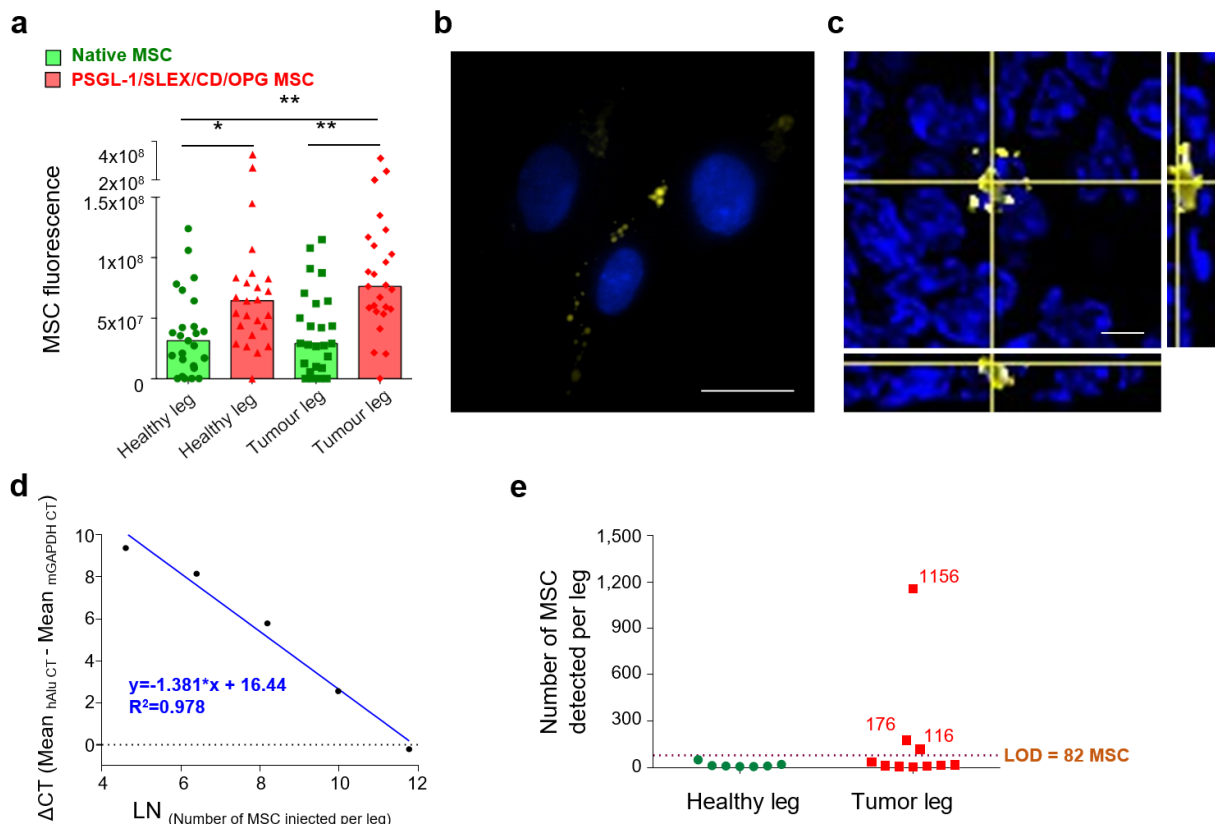


**Supplementary Figure 3.7: P-selectin expression within the bone marrow was increased around the tumor area.** Panels a to d show bone marrow sections from the healthy tibia and tumor bearing tibia from the same mouse sectioned, stained, and imaged side by side. The two images on the right are higher magnifications of the area delimited by a white rectangle on the left image. Red: RFP constitutively expressed by tumor cells, yellow: P- selectin, blue: nuclei (DAPI staining). Scale bar is 5,000  $\mu\text{m}$  for the left merge image, and 100  $\mu\text{m}$  for the two higher magnification images on the right. (a) Proximal extremity of the tibia section of the healthy leg. (b) Distal extremity of the tibia section of the healthy leg. (c) Proximal extremity of the tibia section of the tumor leg. (d) Distal extremity of the tibia section of the tumor leg.

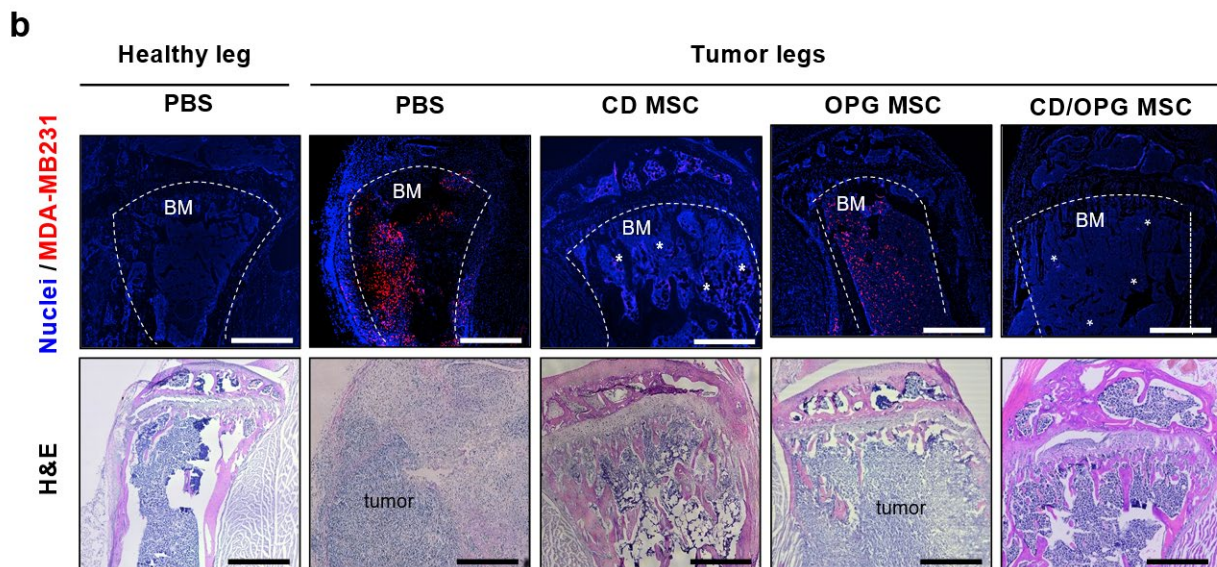
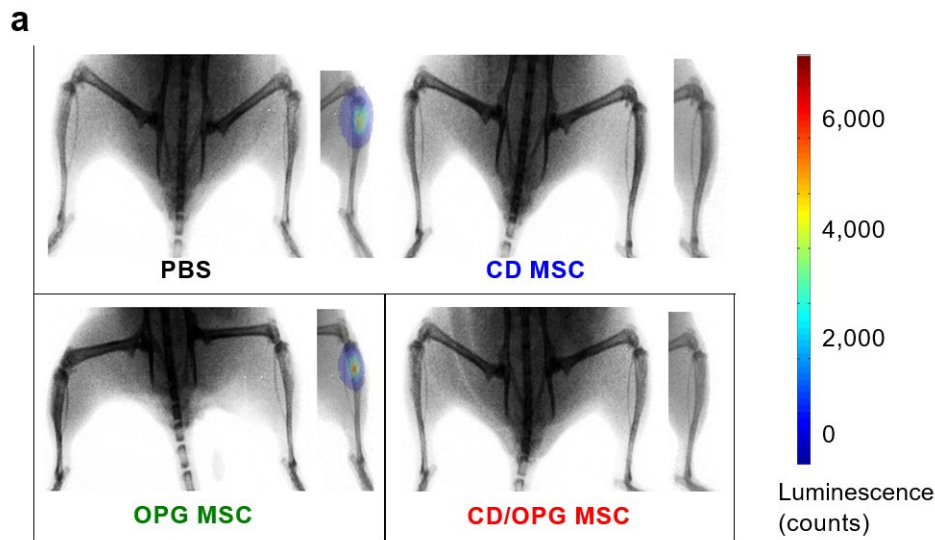




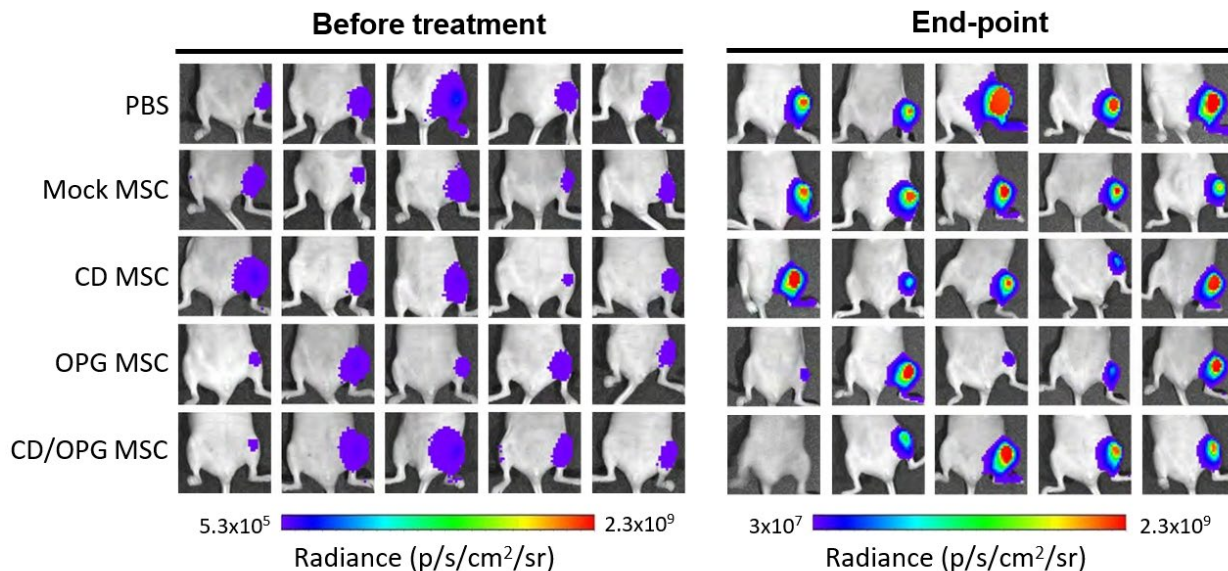
**Supplementary Figure 3.8: MSC entrapped into the lungs following *i.v.* injection, in the MDA-MB231 intratibial model, and were mostly cleared out by 48 hours post-transplantation.** Native or PSGL-1/SLEX/CD/OPG MSC labelled with DiD lipophilic dye were injected *i.v.* and mice were euthanized at different time-points (6, 24, 48, and 72 h) to harvest the different organs. MSC signal in the heart, lungs, kidneys, spleen, and liver was measured using fluorescence intensity. Control mice without MSC injection were used to normalize the data and discriminate fluorescent background from true signal.



**Supplementary Figure 3.9: PSGL-1/SLEX/CD/OPG MSC display more effective homing than Native MSC to the bone marrow, in particular to bone metastatic tumors, in the immunocompromised intratibial model (a-c) and in the syngeneic model of spontaneous bone metastasis (d,e).** (a) Native MSC or PSGL-1/SLEX/CD/OPG MSC labelled with DiD lipophilic dye were injected *i.v.*, then mice were euthanized at different time-points (6, 24, 48, and 72 hours, and 1 week). Homing to the legs was evaluated based on the fluorescence intensity of the DiD dye. All time-points were combined together to compare overall homing to the healthy and to the tumor legs for Native MSC or PSGL-1/SLEX/CD/OPG MSC. Bar graph shows median values, and each point represents one animal at a specific time post-MSC transplantation. Statistical test: ANOVA with Turkey's multiple comparisons test, \*  $p \leq 0.05$  and \*\*  $p \leq 0.01$ . (b) Remaining PSGL-1/SLEX/CD/OPG MSC were put back in culture after cell transplantation to animals, and MSC were imaged 72 hours later, which shows DiD lipophilic dye persists several days post MSC labelling. Scale bar: 25  $\mu$ m. (c) DiD stained PSGL-1/SLEX/CD/OPG MSC are seen in the bone marrow of transplanted animals 72 hours post-transplantation. Scale bar: 20  $\mu$ m. (d) Human MSC can be detected in mouse legs of BALB/cJ using *Alu* qPCR (see Methods). (e) PSGL-1/SLEX/CD/OPG MSC are detected in tumor legs in a syngeneic model of bone metastasis, but not in healthy legs. Five healthy BALB/cJ and 10 animals bearing bone metastasis in the legs (4T1 CLL1 model) were injected *i.v.* with PSGL-1/SLEX/CD/OPG MSC, and euthanized 72 hours post-transplantation to collect the legs. Healthy legs (n=7; six from healthy animals and one from a tumor animal) and tumor legs (n=10) were analyzed. Graph shows MSC number detected for each animal, as well as the limit of detection (LOD) of our assay, as determined from the  $\Delta CT$  value for the negative control minus 2 CT.

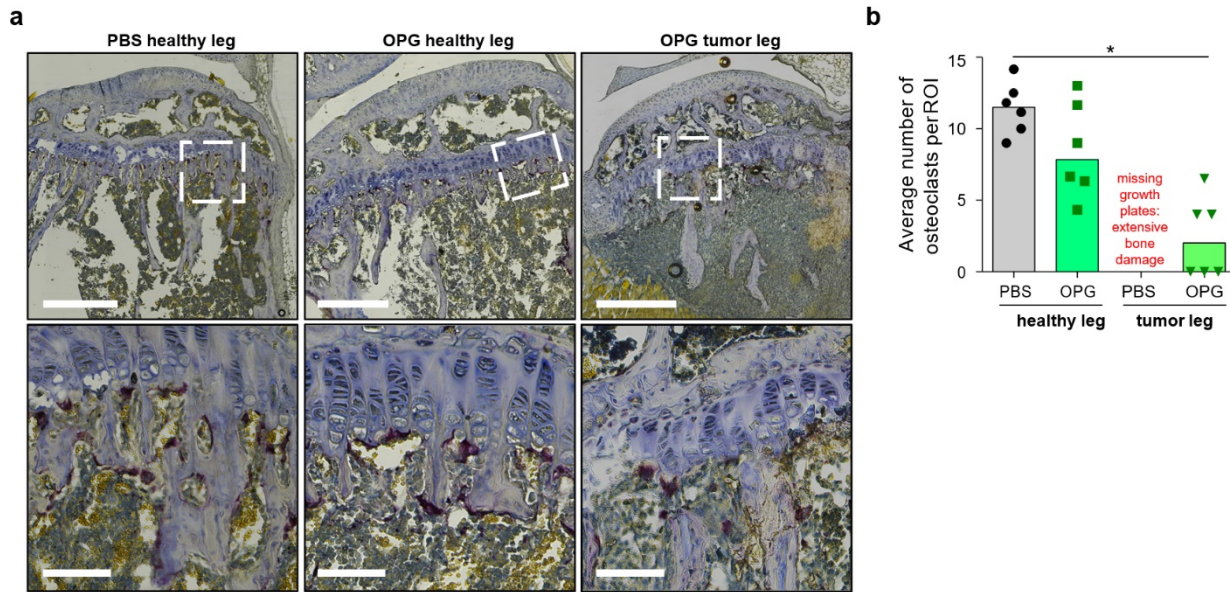


**Supplementary Figure 3.10: Representative techniques to monitor and characterize engineered MSC's tumor killing efficacy in the MDA-MB231 intratibial model.** (a) Representative combined *in vivo* X-ray imaging and bioluminescence imaging were used to confirm that breast tumors were growing within the bone marrow cavity of the tibias and to quickly assess tumor-induced bone damage. (b) Representative *ex vivo* analysis shows CD and CD/OPG MSC treatments injected directly into the tibia prevented tumor invasion within the bone marrow and cortical bone damages. Top panel shows DAPI staining (nuclei in blue) on representative tibia sections for each group. MDA-MB231 were localized using their RFP expression (red). BM: bone marrow cavity. \*: residual RFP positive tumor cells not detected using IVIS imaging. Bottom panel shows corresponding H&E staining for each tibia sections (serial cuts). Scale bar: 500  $\mu$ m.

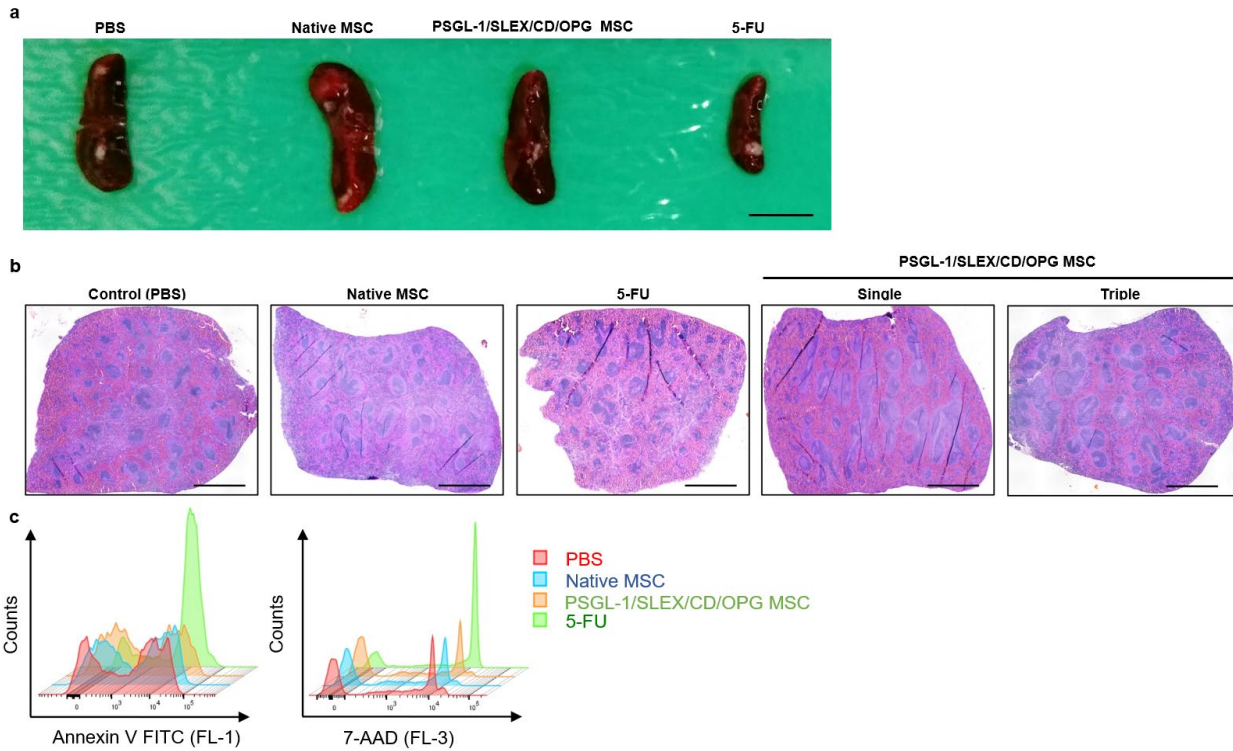


**Supplementary Figure 3.11: Representative *in vivo* imaging data demonstrate the inhibition by engineered MSC treatment on MDA-MB231 tumor growth in the tibias of Nude mice in the MDA-MB231 intratibial immunocompromised model.** Tumor growth within the tibia was monitored using bioluminescence imaging following transplantation of mock transfected MSC (Mock MSC group), PSGL-1/SLEX/CD MSC (CD MSC group), PSGL-1/SLEX/OPG MSC (OPG MSC group) or PSGL-1/SLEX/CD/OPG MSC (CD/OPG MSC group), all administered via an intratibial injection. Figure shows tumor signal before the treatment and at the end-point for five representative animals. Quantification of this study is presented in Figure 5.



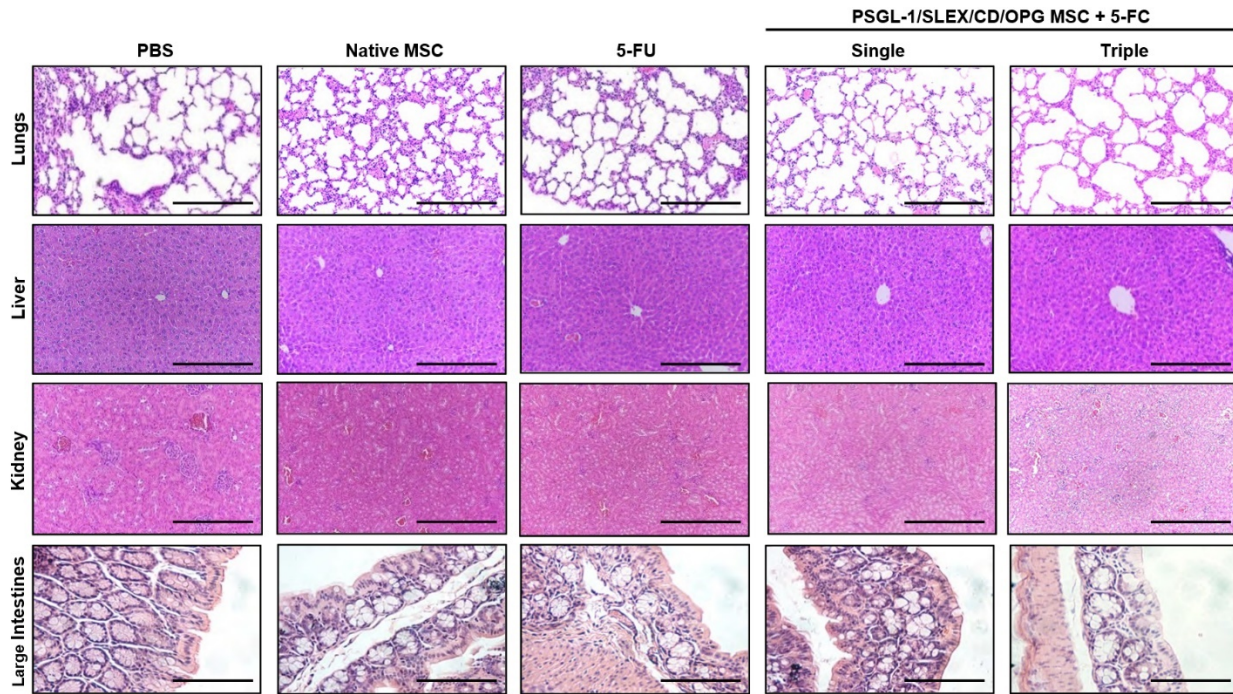


**Supplementary Figure 3.12: PSGL-1/SLEX/OPG MSC inhibit tumor-induced osteoclast activity in the MDA-MB231 intratibial model, thus preventing bone loss.** (a) OPG MSC treatment via intratibial injection reduced the density of TRAP<sup>+</sup> activated osteoclasts seen at the tibia epiphysis. TRAP staining followed by Hematoxylin counterstain was performed on several tibia sections from the healthy legs of control animals (PBS group), and the healthy legs and tumor legs of animals treated with PSGL-1/SLEX/OPG MSC (OPG group) injected directly into the tibia. Second row shows higher magnification of the selected ROI (white dashed line) from the images presented on the top panel. Scale bars: 500  $\mu$ m for upper panel and 100  $\mu$ m for lower panel. (b) The number of TRAP<sup>+</sup> activated osteoclasts were significantly lower in the tumor legs of mice treated with PSGL-1/SLEX/OPG MSC injected directly into the tibia. The average number of TRAP<sup>+</sup> osteoclasts was counted in a minimum of three ROIs per leg, distributed across the tibia growth plate, for each animal. Bar graph shows the average number of osteoclasts per ROI for each animal, n=6 per group. Each point represents one animal, and the bars represent the median value of the group. No analysis could be done on tumor legs of mice from the PBS group as the growth plate was destroyed by the tumor, indicating a strong osteoclast activity. PBS: PBS treated group, OPG group: PSGL-1/SLEX/OPG MSC treated group. Statistical analysis: Kruskal-Wallis with Dunn's multiple comparison *post hoc*, \*  $p \leq 0.05$  between PBS healthy legs and OPG MSC tumor legs.

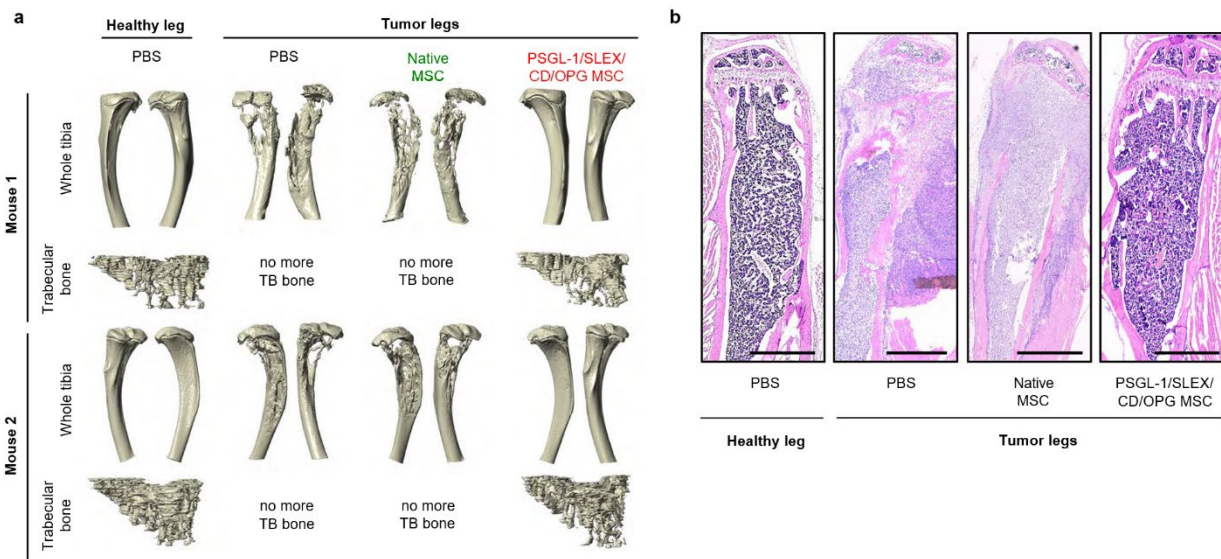


**Supplementary Figure 3.13: MDA-MB231 intratibial model mice infused with PSGL-1/SLEX/CD/OPG MSC via *i.v.* injection exhibited minimal toxicity.** (a) 5-Fluorouracil treatment caused spleen reduction. Whole spleens were taken in pictures right after mice euthanasia. Scale bar: 1 mm. (b) 5-Fluorouracil induced toxicity led to death of germinal centers and tissue fibrosis in the mouse spleen. Images show H&E staining on spleen longitudinal sections. Scale bar: 1,000  $\mu$ m. (c) 5-Fluorouracil treatment induced cell apoptosis and necrosis within the bone marrow. For each group [Control (PBS), Native, PSGL-1/SLEX/CD/OPG MSC + 5-FC and 5-FU], 10,000 cells were analyzed. Histograms show Annexin V FITC binding to the cell membrane (FL-1) and 7-AAD staining (FL-3). For Annexin V FITC, the medians of fluorescence of each group were 2,797, 2,204, 1,028, and 9,677, respectively. Whereas for 7-AAD, the medians of fluorescence of each group were: 713, 836, 361, and 10,640, respectively.

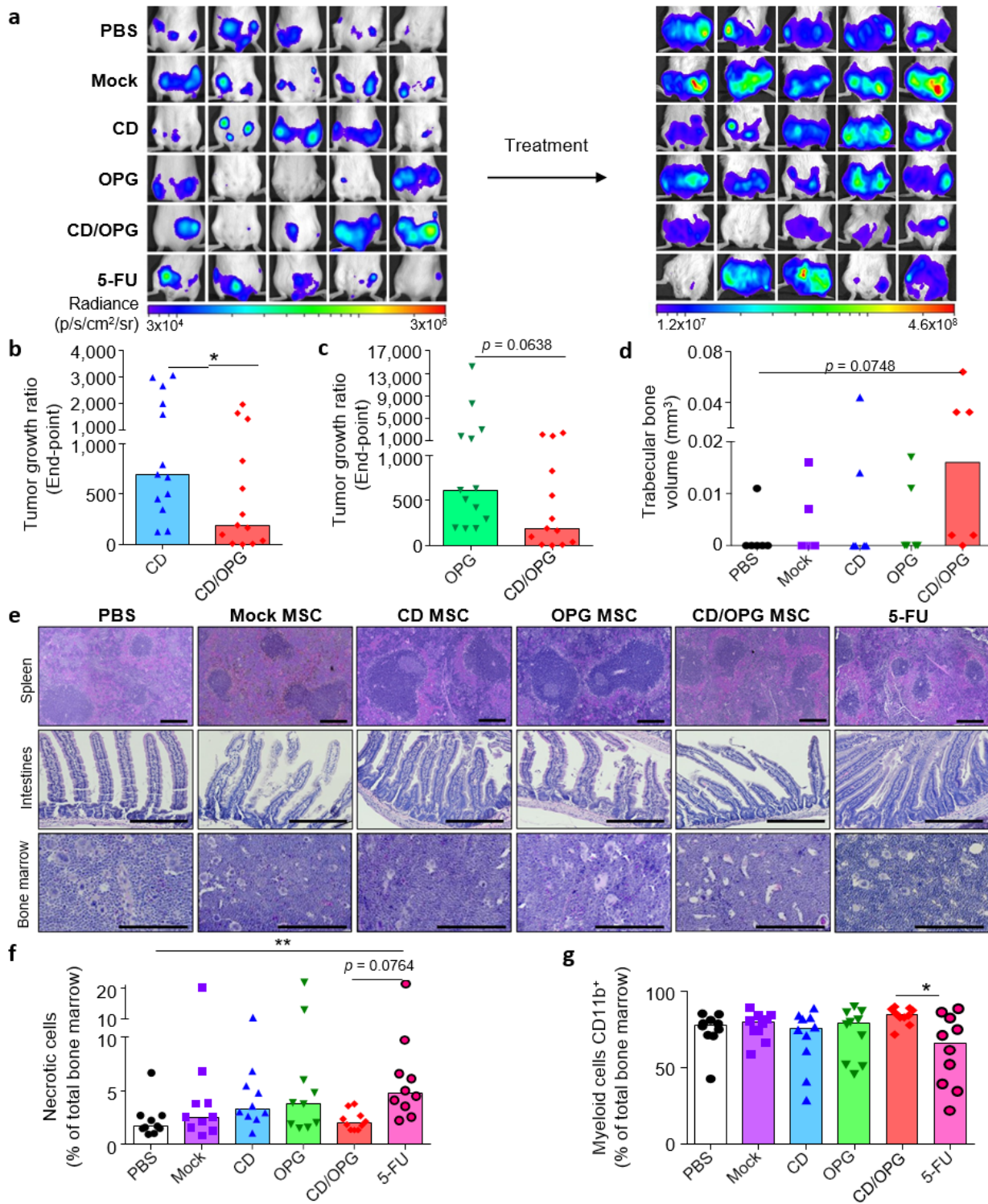




**Supplementary Figure 3.14: MDA-MB231 intratibial model mice infused with PSGL-1/SLEX/CD/OPG MSC via *i.v.* injection exhibited minimal toxicity.** Tissue analysis was performed following H&E staining to evaluate toxicity-induced damages. Scale bar: 500  $\mu\text{m}$  for lungs, liver, and kidney, and 250  $\mu\text{m}$  for large intestines.



**Supplementary Figure 3.15: Illustrative bone integrity analyses following systemic *i.v.* infusion of PSGL-1/SLEX/CD/OPG MSC in MDA-MB231 intratibial model mice.** (a) Representative bone analysis using nanoCT imaging. At the end-point of treatment, mouse tibias were harvested, fixed for 48 h, and tibias of two mice per group [Control (PBS), Native MSC and PSGL-1/SLEX/CD/OPG MSC] were analyzed. Top panel shows 3D reconstructions of whole tibias (without the fibula) and bottom panel shows 3D reconstruction of trabecular bone. (b) H&E staining was performed on representative tibia sections for each group to assess tumor invasion within the bone marrow and bone integrity. A healthy tibia section is also shown as a reference. Scale bar: 1,000  $\mu\text{m}$ .



**Supplementary Figure 3.16: PSGL-1/SLEX/CD/OPG MSC exhibit therapeutic effects and minimal toxicity in a syngeneic mouse model of spontaneous bone metastasis.** (a) Bioluminescence imaging was done to monitor bone metastasis



development. Panel shows tumor signal before and after treatment for five representative mice per group. MSC were engineered as follows: Mock group (Mock transfected), CD group (PSGL-1/SLEX/CD), OPG group (PSGL-1/SLEX/OPG), and CD/OPG group (PSGL-1/SLEX/CD/OPG). (b) CD/OPG MSC treatment is more effective than CD MSC in inhibiting tumor growth. All MSC infusions were via *i.v.* injection. Bar graph shows the median tumor growth ratio at the end-point for each group; each point represents one animal.  $n=13$ . Statistical analysis: Mann–Whitney, \*  $p \leq 0.05$ . (c) CD/OPG MSC treatment tends to be more effective than OPG MSC in inhibiting tumor growth. Bar graph shows the median tumor growth ratio at the end-point for each group; each point represents one animal.  $n=13$ . Statistical analysis: Mann–Whitney, \*  $p=0.0638$ . (d) CD/OPG MSC treatment tends to prevent bone loss in metastatic femurs. Micro-CT was done on  $n=6$  tumor-bearing femurs per group, and remaining trabecular bone volume was quantified. Bar graph shows the median trabecular bone volume for each group; each point represents one animal. Statistical analysis: Kruskal-Wallis with Dunn’s multiple comparison *post hoc*,  $p=0.0748$  between PBS and CD/OPG MSC. (e) No obvious signs of toxicity were detected in peripheral organs. Spleen, intestines, and bone marrow were analyzed for each group using H&E staining. Representative images are shown here. Scale bar = 250  $\mu\text{m}$ . (f) 5-FU treatment, but not MSC groups, induces more necrosis in the bone marrow. At the end-point, the bone marrow of the healthier leg was isolated and cell necrosis was analyzed using flow cytometry (7-AAD+) for  $n=10$  animals per group. Bar graph shows the median percent of necrosis for each group, and each point represents one animal. Statistical analysis: Kruskal-Wallis with Dunn’s multiple comparison *post hoc*, \*\*  $p \leq 0.01$  between 5-FU and PBS, and  $p=0.0764$  between CD/OPG and 5-FU. (g) Engineered MSC are less toxic than 5-FU and induces less reduction of myeloid cells (CD11b+) in the bone marrow. At the end-point, the bone marrow of the healthier leg was isolated, and phenotyping was done on living cells (7-AAD-) using flow cytometry for  $n=10$  animals per group. Bar graph shows the median percent of CD11b+ cells for each group, and each point represents one animal. Statistical analysis: Kruskal-Wallis with Dunn’s multiple comparison *post hoc*,\*  $p \leq 0.05$  between CD/OPG and 5-FU.

### **3.7 Acknowledgements**

This work was supported by the NIH (1DP2CA195763-01 and R21CA219225 to W.Z.), the DOD (W81XWH-17-1-0522 to W.Z.), the contract with Baylx Inc (BI-206512), the Fondation ARC pour la recherche sur le cancer (SAE20150602901 to A.I.S.), and the California Institute of Regenerative Medicine (EDUC2-08383 to M.T.). H.P.F. was supported by NINDS/NIH (NS082174). L.L. was supported by Baylx Inc: BI-206512. D.L. and L.S. were supported by the National Science Foundation (NSF) under Grant CMMI-1229405. The project described was also supported by the National Center for Research Resources and the National Center for Advancing Translational Sciences, National Institutes of Health and National Cancer Institute of the National Institutes of Health under award number P30CA062203 (The content is solely the responsibility of the authors and does not necessarily represent the official views of the National Institutes of Health). The funders above did not have any involvement in the study design, data collection, data analysis, interpretation, and manuscript writing.

### **3.8 Author Contributions**

A.I.S. and W.Z. designed the research; A.I.S., J.L.C., H.P.F., M.T., C.C.Y., L.H. and L.L. performed the research; M.J.L. contributed to the *in vivo* homing study and helped with animal experiments. J.C., G.G. and M.Y.S performed the X-Ray coupled with bioluminescence imaging. D.L. and L.S. did the NanoCT imaging for the pilot study. B.T. performed the MicroCT of the main experiments on the two models. A.I.S., J.L.C., H.P.F., M.T., C.C.Y., L.H., B.T. and R.L.S. analyzed and interpreted the data; A.I.S and W.Z. wrote the paper.

### **3.9 References**

1. Mundy GR. Metastasis to bone: causes, consequences and therapeutic opportunities. *Nat Rev Cancer*. 2002;2(8):584-593.
2. Coleman RE. Skeletal complications of malignancy. *Cancer*. 1997;80(8 Suppl):1588-1594.
3. Kan C, Vargas G, Pape FL, Clezardin P. Cancer Cell Colonisation in the Bone Microenvironment. *Int J Mol Sci*. 2016;17(10).
4. Siegel RL, Miller KD, Jemal A. Cancer Statistics, 2017. *CA Cancer J Clin*. 2017;67(1):7-30.
5. Coleman RE. Management of bone metastases. *Oncologist*. 2000;5(6):463-470.
6. Coleman R, Gnant M, Morgan G, Clezardin P. Effects of bone-targeted agents on cancer progression and mortality. *J Natl Cancer Inst*. 2012;104(14):1059-1067.
7. Petrut B, Trinkaus M, Simmons C, Clemons M. A primer of bone metastases management in breast cancer patients. *Curr Oncol*. 2008;15(Suppl 1):S50-57.
8. Weilbaecher KN, Guise TA, McCauley LK. Cancer to bone: a fatal attraction. *Nat Rev Cancer*. 2011;11(6):411-425.
9. Mai J, Huang Y, Mu C, Zhang G, Xu R, Guo X, et al. Bone marrow endothelium-targeted therapeutics for metastatic breast cancer. *J Control Release*. 2014;187:22-29.
10. Saracino R, Luciano R, Battafarano G, Perrotta A, Muraca M, Del Fattore A. Nanoparticles-Based Treatment for Bone Metastasis. *Curr Drug Targets*. 2016;17(3):303-310.
11. Schroeder A, Heller DA, Winslow MM, Dahlman JE, Pratt GW, Langer R, et al. Treating metastatic cancer with nanotechnology. *Nat Rev Cancer*. 2011;12(1):39-50.
12. Swami A, Reagan MR, Basto P, Mishima Y, Kamaly N, Glavey S, et al. Engineered nanomedicine for myeloma and bone microenvironment targeting. *Proc Natl Acad Sci U S A*. 2014;111(28):10287-10292.
13. Zhao YP, Ye WL, Liu DZ, Cui H, Cheng Y, Liu M, et al. Redox and pH dual sensitive bone targeting nanoparticles to treat breast cancer bone metastases and inhibit bone resorption. *Nanoscale*. 2017;9(19):6264-6277.
14. Wilhelm S, Tavares AJ, Dai Q, Ohta S, Audet J, Dvorak HF, et al. Analysis of nanoparticle delivery to tumours. *Nat Rev Mater*. 2016;1(5).
15. Droujinine IA, Eckert MA, Zhao W. To grab the stroma by the horns: from biology to cancer therapy with mesenchymal stem cells. *Oncotarget*. 2013;4(5):651-664.
16. Shah K. Mesenchymal stem cells engineered for cancer therapy. *Adv Drug Deliv Rev*. 2012;64(8):739-748.
17. Du WL, Seah I, Bougazzoul O, Choi GH, Meeth K, Bosenberg MW, et al. Stem cell-released oncolytic herpes simplex virus has therapeutic efficacy in brain metastatic melanomas. *P Natl Acad Sci USA*. 2017;114(30):E6157-E6165.
18. Grisendi G, Bussolari R, Cafarelli L, Petak I, Rasini V, Veronesi E, et al. Adipose-Derived Mesenchymal Stem Cells as Stable Source of Tumor Necrosis Factor-Related Apoptosis-Inducing Ligand Delivery for Cancer Therapy. *Cancer Res*. 2010;70(9):3718-3729.
19. Liu LN, Zhang SX, Liao WB, Farhoodi HP, Wong CW, Chen CC, et al. Mechanoresponsive stem cells to target cancer metastases through biophysical cues. *Sci Transl Med*. 2017;9(400).
20. Matuskova M, Kozovska Z, Toro L, Durinikova E, Tyciakova S, Cierna Z, et al. Combined enzyme/prodrug treatment by genetically engineered AT-MSC exerts synergy and inhibits growth of MDA-MB-231 induced lung metastases. *J Exp Clin Canc Res*. 2015;34.

21. Studeny M, Marini FC, Champlin RE, Zompetta C, Fidler IJ, Andreeff M. Bone marrow-derived mesenchymal stem cells as vehicles for interferon-beta delivery into tumors. *Cancer Res.* 2002;62(13):3603-3608.
22. Yi BR, Hwang KA, Aboody KS, Jeung EB, Kim SU, Choi KC. Selective antitumor effect of neural stem cells expressing cytosine deaminase and interferon-beta against ductal breast cancer cells in cellular and xenograft models. *Stem Cell Res.* 2014;12(1):36-48.
23. Niess H, von Einem JC, Thomas MN, Michl M, Angele MK, Huss R, et al. Treatment of advanced gastrointestinal tumors with genetically modified autologous mesenchymal stromal cells (TREAT-ME1): study protocol of a phase I/II clinical trial. *BMC Cancer.* 2015;15:237.
24. Schweitzer KM, Drager AM, van der Valk P, Thijsen SF, Zevenbergen A, Theijssmeijer AP, et al. Constitutive expression of E-selectin and vascular cell adhesion molecule-1 on endothelial cells of hematopoietic tissues. *Am J Pathol.* 1996;148(1):165-175.
25. Sipkins DA, Wei X, Wu JW, Runnels JM, Cote D, Means TK, et al. In vivo imaging of specialized bone marrow endothelial microdomains for tumour engraftment. *Nature.* 2005;435(7044):969-973.
26. Xia L, McDaniel JM, Yago T, Doeden A, McEver RP. Surface fucosylation of human cord blood cells augments binding to P-selectin and E-selectin and enhances engraftment in bone marrow. *Blood.* 2004;104(10):3091-3096.
27. Nouri FS, Wang X, Hatefi A. Genetically engineered theranostic mesenchymal stem cells for the evaluation of the anticancer efficacy of enzyme/prodrug systems. *J Control Release.* 2015;200:179-187.
28. Body JJ, Greipp P, Coleman RE, Facon T, Geurs F, Ferman JP, et al. A phase I study of AMGN-0007, a recombinant osteoprotegerin construct, in patients with multiple myeloma or breast carcinoma related bone metastases. *Cancer.* 2003;97(3 Suppl):887-892.
29. Higgs JT, Jarboe JS, Lee JH, Chanda D, Lee CM, Deivanayagam C, et al. Variants of Osteoprotegerin Lacking TRAIL Binding for Therapeutic Bone Remodeling in Osteolytic Malignancies. *Mol Cancer Res.* 2015;13(5):819-827.
30. NguyenThai QA, Sharma N, Luong do H, Sodhi SS, Kim JH, Kim N, et al. Targeted inhibition of osteosarcoma tumor growth by bone marrow-derived mesenchymal stem cells expressing cytosine deaminase/5-fluorocytosine in tumor-bearing mice. *J Gene Med.* 2015;17(3-5):87-99.
31. Qiao B, Shui W, Cai L, Guo SQ, Jiang DM. Human mesenchymal stem cells as delivery of osteoprotegerin gene: homing and therapeutic effect for osteosarcoma. *Drug Des Dev Ther.* 2015;9:969-976.
32. Kariko K, Muramatsu H, Welsh FA, Ludwig J, Kato H, Akira S, et al. Incorporation of Pseudouridine Into mRNA Yields Superior Nonimmunogenic Vector With Increased Translational Capacity and Biological Stability. *Mol Ther.* 2008;16(11):1833-1840.
33. Lee J, Dykstra B, Spencer JA, Kenney LL, Greiner DL, Shultz LD, et al. mRNA-mediated glycoengineering ameliorates deficient homing of human stem cell-derived hematopoietic progenitors. *J Clin Invest.* 2017;127(6):2433-2437.
34. Levy O, Zhao WA, Mortensen LJ, LeBlanc S, Tsang K, Fu MY, et al. mRNA-engineered mesenchymal stem cells for targeted delivery of interleukin-10 to sites of inflammation. *Blood.* 2013;122(14):E23-E32.
35. Sekiya I, Larson BL, Smith JR, Pochampally R, Cui JG, Prockop DJ. Expansion of human adult stem cells from bone marrow stroma: Conditions that maximize the yields of early progenitors and evaluate their quality. *Stem Cells.* 2002;20(6):530-541.

36. Dominici M, Le Blanc K, Mueller I, Slaper-Cortenbach I, Marini FC, Krause DS, et al. Minimal criteria for defining multipotent mesenchymal stromal cells. The International Society for Cellular Therapy position statement. *Cytotherapy*. 2006;8(4):315-317.
37. Kuchimaru T, Kataoka N, Nakagawa K, Isozaki T, Miyabara H, Minegishi M, et al. A reliable murine model of bone metastasis by injecting cancer cells through caudal arteries. *Nat Commun*. 2018;9.
38. Swain SM, Lippman ME, Egan EF, Drake JC, Steinberg SM, Allegra CJ. Fluorouracil and High-Dose Leucovorin in Previously Treated Patients with Metastatic Breast-Cancer. *Journal of Clinical Oncology*. 1989;7(7):890-899.
39. Schneider T, Osl F, Friess T, Stockinger H, Scheuer WV. Quantification of human Alu sequences by real-time PCR--an improved method to measure therapeutic efficacy of anti-metastatic drugs in human xenotransplants. *Clin Exp Metastasis*. 2002;19(7):571-582.
40. Yasuma T, Yano Y, D'Alessandro-Gabazza CN, Toda M, Gil-Bernabe P, Kobayashi T, et al. Erratum. Amelioration of Diabetes by Protein S. *Diabetes* 2016;65:1940-1951. *Diabetes*. 2016;65(12):3812.
41. McBride C, Gaupp D, Phinney DG. Quantifying levels of transplanted murine and human mesenchymal stem cells in vivo by real-time PCR. *Cytotherapy*. 2003;5(1):7-18.
42. Funakoshi K, Bagheri M, Zhou M, Suzuki R, Abe H, Akashi H. Highly sensitive and specific Alu-based quantification of human cells among rodent cells. *Sci Rep-Uk*. 2017;7.
43. Ley K, Laudanna C, Cybulsky MI, Nourshargh S. Getting to the site of inflammation: the leukocyte adhesion cascade updated. *Nat Rev Immunol*. 2007;7(9):678-689.
44. Baud'huin M, Duplomb L, Teletchea S, Lamoureux F, Ruiz-Velasco C, Maillason M, et al. Osteoprotegerin: multiple partners for multiple functions. *Cytokine Growth Factor Rev*. 2013;24(5):401-409.
45. Kucerova L, Durinikova E, Toro L, Cihova M, Miklikova S, Poturnajova M, et al. Targeted antitumor therapy mediated by prodrug-activating mesenchymal stromal cells. *Cancer Letters*. 2017;408:1-9.
46. Aboody KS, Najbauer J, Schmidt NO, Yang W, Wu JK, Zhuge Y, et al. Targeting of melanoma brain metastases using engineered neural stem/progenitor cells. *Neuro-Oncology*. 2006;8(2):119-126.
47. Cameron DA, Gabra H, Leonard RC. Continuous 5-fluorouracil in the treatment of breast cancer. *Br J Cancer*. 1994;70(1):120-124.
48. Winkler IG, Barbier V, Nowlan B, Jacobsen RN, Forristal CE, Patton JT, et al. Vascular niche E-selectin regulates hematopoietic stem cell dormancy, self renewal and chemoresistance. *Nat Med*. 2012;18(11):1651-1657.
49. Stubke K, Wicklein D, Herich L, Schumacher U, Nehmann N. Selectin-deficiency reduces the number of spontaneous metastases in a xenograft model of human breast cancer. *Cancer Lett*. 2012;321(1):89-99.
50. Wright LE, Ottewell PD, Rucci N, Peyruchaud O, Pagnotti GM, Chiechi A, et al. Murine models of breast cancer bone metastasis. *Bonekey Rep*. 2016;5.
51. Andersen C, Bagi CM, Adams SW. Intra-tibial injection of human prostate cancer cell line CWR22 elicits osteoblastic response in immunodeficient rats. *J Musculoskelet Neuronal Interact*. 2003;3(2):148-155.
52. Karp JM, Teol GSL. Mesenchymal Stem Cell Homing: The Devil Is in the Details. *Cell Stem Cell*. 2009;4(3):206-216.
53. Wang H, Cao F, De A, Cao Y, Contag C, Gambhir SS, et al. Trafficking mesenchymal stem cell engraftment and differentiation in tumor-bearing mice by bioluminescence imaging. *Stem Cells*. 2009;27(7):1548-1558.

54. Direcks WGE, van Gelder M, Lammertsma AA, Molthoff CFM. A new rat model of human breast cancer for evaluating efficacy of new anti-cancer agents in vivo. *Cancer Biol Ther.* 2008;7(4):532-537.
55. Shaikh A, Bhartiya D, Kapoor S, Nimkar H. Delineating the effects of 5-fluorouracil and follicle-stimulating hormone on mouse bone marrow stem/progenitor cells. *Stem Cell Res Ther.* 2016;7(1):59.
56. Hiraga T, Ueda A, Tamura D, Hata K, Ikeda F, Williams PJ, et al. Effects of oral UFT combined with or without zoledronic acid on bone metastasis in the 4T1/luc mouse breast cancer. *Int J Cancer.* 2003;106(6):973-979.
57. Michailidou M, Holen I. Combinations of bisphosphonates and classical anticancer drugs: a preclinical perspective. *Recent Results Cancer Res.* 2012;192:145-169.
58. Ottewell PD, Wang N, Brown HK, Fowles CA, Croucher PI, Eaton CL, et al. OPG-Fc inhibits ovariectomy-induced growth of disseminated breast cancer cells in bone. *Int J Cancer.* 2015;137(4):968-977.
59. Nowakowski A, Andrzejewska A, Janowski M, Walczak P, Lukomska B. Genetic engineering of stem cells for enhanced therapy. *Acta Neurobiol Exp.* 2013;73(1):1-18.
60. Thomas CE, Ehrhardt A, Kay MA. Progress and problems with the use of viral vectors for gene therapy. *Nat Rev Genet.* 2003;4(5):346-358.
61. Devine SM, Bartholomew AM, Mahmud N, Nelson M, Patil S, Hardy W, et al. Mesenchymal stem cells are capable of homing to the bone marrow of non-human primates following systemic infusion. *Exp Hematol.* 2001;29(2):244-255.
62. Kidd S, Spaeth E, Dembinski JL, Dietrich M, Watson K, Klopp A, et al. Direct Evidence of Mesenchymal Stem Cell Tropism for Tumor and Wounding Microenvironments Using In Vivo Bioluminescent Imaging. *Stem Cells.* 2009;27(10):2614-2623.
63. Jackson W, Sosnoski DM, Ohanessian SE, Chandler P, Mobley A, Meisel KD, et al. Role of Megakaryocytes in Breast Cancer Metastasis to Bone. *Cancer Res.* 2017;77(8):1942-1954.
64. Shamay Y, Elkabets M, Li HY, Shah J, Brook S, Wang F, et al. P-selectin is a nanotherapeutic delivery target in the tumor microenvironment. *Sci Transl Med.* 2016;8(345).
65. Suva LJ, Washam C, Nicholas RW, Griffin RJ. Bone metastasis: mechanisms and therapeutic opportunities. *Nat Rev Endocrinol.* 2011;7(4):208-218.
66. Zhao WA, Loh W, Droujinine IA, Teo WS, Kumar N, Schafer S, et al. Mimicking the inflammatory cell adhesion cascade by nucleic acid aptamer programmed cell-cell interactions. *Faseb J.* 2011;25(9):3045-3056.
67. Lorincz T, Timar J, Szendroi M. Alterations of microvascular density in bone metastases of adenocarcinomas. *Pathol Oncol Res.* 2004;10(3):149-153.
68. Klopp AH, Spaeth EL, Dembinski JL, Woodward WA, Munshi A, Meyn RE, et al. Tumor irradiation increases the recruitment of circulating mesenchymal stem cells into the tumor microenvironment. *Cancer Res.* 2007;67(24):11687-11695.
69. Sackstein R, Merzaban JS, Cain DW, Dagia NM, Spencer JA, Lin CP, et al. Ex vivo glycan engineering of CD44 programs human multipotent mesenchymal stromal cell trafficking to bone. *Nature Medicine.* 2008;14(2):181-187.
70. Bobis-Wozowicz S, Miekus K, Wybieralska E, Jarocho D, Zawisz A, Madeja Z, et al. Genetically modified adipose tissue-derived mesenchymal stem cells overexpressing CXCR4 display increased motility, invasiveness, and homing to bone marrow of NOD/SCID mice. *Exp Hematol.* 2011;39(6):686-696 e684.

71. Wynn RF, Hart CA, Corradi-Perini C, O'Neill L, Evans CA, Wraith JE, et al. A small proportion of mesenchymal stem cells strongly expresses functionally active CXCR4 receptor capable of promoting migration to bone marrow. *Blood*. 2004;104(9):2643-2645.
72. LeBlanc K, Frassoni F, Ball L, Locatelli F, Roelofs H, Lewis I, et al. Mesenchymal stem cells for treatment of steroid-resistant, severe, acute graft-versus-host disease: a phase II study. *Lancet*. 2008;371(9624):1579-1586.
73. Jarocho D, Milczarek O, Wedrychowicz A, Kwiatkowski S, Majka M. Continuous Improvement After Multiple Mesenchymal Stem Cell Transplantations in a Patient With Complete Spinal Cord Injury. *Cell Transplant*. 2015;24(4):661-672.
74. Kucerova L, Skolekova S, Demkova L, Bohovic R, Matuskova M. Long-term efficiency of mesenchymal stromal cell-mediated CD-MSC/5FC therapy in human melanoma xenograft model. *Gene Ther*. 2014;21(10):874-887.
75. Special issue on Cell Therapy Manufacturing and Scale-Up Introduction: TA Brieva, Celgene, Co-Chair, Scale-up and Manufacturing of Cell-based Therapies IV. *Biochem Eng J*. 2016;108:1-2.
76. Bak RO, Hendel A, Clark JT, Kennedy AB, Ryan DE, Roy S, et al. Chemically modified guide RNAs enhance CRISPR/Cas genome editing in human primary cells. *Hum Gene Ther*. 2015;26(10):A11-A12.
77. Chen ZH, Yu YP, Zuo ZH, Nelson JB, Michalopoulos GK, Monga S, et al. Targeting genomic rearrangements in tumor cells through Cas9-mediated insertion of a suicide gene. *Nat Biotechnol*. 2017;35(6):543-+.

# CHAPTER 4

## Pre-Clinical Evaluation of BX-U001 Human Umbilical Cord MSC to Treat Inflammatory Bowel Disease

**Authors:** Henry P. Farhoodi<sup>1-3</sup>, Linan Liu<sup>8</sup>, Menglu Han<sup>1-3</sup>, Brenda Nguyen<sup>1-3</sup>, Artin Ziary<sup>1-3</sup>, Lily Nguyen<sup>1-3</sup>, Wenbin Liao<sup>8</sup>, Weian Zhao<sup>1-6</sup>

<sup>1</sup> Sue and Bill Gross Stem Cell Research Center, University of California, Irvine, Irvine, CA 92697, USA;

<sup>2</sup> Department of Pharmaceutical Sciences, University of California, Irvine, Irvine, CA 92697, USA;

<sup>3</sup> Chao Family Comprehensive Cancer Center, University of California, Irvine, Irvine, CA 92697, USA;

<sup>4</sup> Edwards Life Sciences Center for Advanced Cardiovascular Technology, University of California, Irvine, Irvine, CA 92697, USA;

<sup>5</sup> Department of Biomedical Engineering, University of California, Irvine, Irvine, CA 92697, USA;

<sup>6</sup> Department of Biological Chemistry, University of California, Irvine, Irvine, CA 92697, USA;

<sup>7</sup> Department of Surgery, University of California, Irvine, Orange, CA 92868, USA;

<sup>8</sup> Baylx, Inc., Irvine, CA 92618, USA.

#### 4.1 Abstract

**Objective:** To evaluate the efficacy of a single tail vein infusion of BX-U001 hUC-MSc to treat an inflammatory bowel disease (IBD) animal model in BALB/c mice in support of an FDA IND application.

**Method:** To evaluate the therapeutic efficacy, 18 BALB/c mice (males, 7 weeks old, and body weight 21-26 g) were randomly assigned to four groups: test group (T Group, n = 5), vehicle control group (V Group, n = 4), ethanol control group (E Group, n = 5) and healthy control group (H Group, n = 4). Trinitrobenzene sulfonic acid (TNBS) was used to induce IBD in animals from T and V groups via enema. Animals from T Group were intravenously (i.v.) infused with  $2 \times 10^6$  hUC-MSc/mouse via tail vein, about 12 hours (D0) after TNBS induction. Animals from V Group were infused with the same volume of cell-free injection solution (vehicle) via enema. Animals from E Group were induced with ethanol only (solvent used to dissolve TNBS) via enema and i.v. infused with cell-free suspension solution. Animals from H groups received no induction or treatment. Animal monitoring and assessment (i.e., body weight (BW), rectal bleeding score (RBS) and diarrhea score (DS)) was performed daily for 3 days (D(-3) to D(-1)) and then twice per day for 9 days (D0 to D8). Day 8 after disease model induction (D8) was the endpoint. Dissections of all animals were conducted after a period of animal monitoring. In addition to the efficacy study, a survival study was done using 19 mice in a similar manner.

**Result:** After administration of hUC-MSc, animal survival was significantly improved in the T Group, compared to the V Group (85.7% in T Group vs 14.3% in V Group,  $p < 0.01$ ). The body weight change (BWC) of T Group mice were significantly reduced by endpoint (D8) ( $-9.21\% \pm 2.44\%$  in T Group vs  $-22.53\% \pm 4.11\%$  in V Group,  $p < 0.05$ , starting from 2 days after administration (D2)) compared to V Group. Disease activity index (DAI) of T Group was significantly attenuated after treatment ( $2.80 \pm 1.36$  in T Group vs  $7.50 \pm 0.29$  in V Group on D8,  $p < 0.05$ ), when compared to V Group. Mice were sacrificed and colons were harvested and weighed on endpoint (D8). Colon weights (g) of T Group were significantly reduced after treatment ( $1.00 \pm 0.34$  g in T Group vs  $2.82 \pm 0.65$  g in V Group,  $p < 0.05$ ), when compared to V Group. Colons were also pictured for macroscopic scoring, then colons were processed, sectioned, and H&E stained. The macroscopic scores of T Group colons were significantly reduced



compared to V Group ( $2.90 \pm 1.68$  in T Group vs  $9.00 \pm 0.58$  in V Group,  $p < 0.05$ ). For assessment of H&E stained colons, images were taken of all samples and compared. The H&E staining of T Group suggested less severe IBD symptoms, when compared to the V Group. Mice were observed twice daily for the full 8 days after the administration. No abnormalities (unrelated to IBD) were observed on murine hair and skin, behavior, and water intake. No abnormal condition was observed at infusion location.

**Conclusion:** A single infusion of hUC-MSC infusate ( $2 \times 10^6$  cells/mouse), administered via tail vein, to TNBS-induced male BALB/c mice, resulted in significant alleviation of IBD symptoms and significant improvement of survival rate.

## 4.2 Introduction

Autoimmune diseases are a class of diseases in which one's own immune system responds to normal cells, proteins, or tissues as if they are pathogens, and attacks them<sup>1</sup>. These diseases affect over 50 million Americans, costing over \$100 billion dollars per year in the US alone<sup>2</sup>. Inflammatory bowel diseases (IBDs) are autoimmune diseases affecting over 1.6 million Americans, with symptoms ranging from mild to life threatening<sup>3</sup>. IBD is not a not uniform illness and has two forms; Ulcerative Colitis and Crohn's Disease, which display distinct symptoms and pathologies, and require different treatment plans to manage<sup>4</sup>.

There are several different disease models which can be employed when studying intestinal inflammation in mice. While none of these models can completely recapitulate the onset and progression of IBD symptoms, the most widely accepted practice for generating these models has been through the use of chemicals inducers, of which 2,4,6-trinitrobenzene sulfonic acid (TNBS), oxazolone, and sodium sulfate (DSS) are the most commonly utilized. While there are some commonalities among the physiological responses each of these drugs elicit, including epithelial wall break down and immune cell recruitment, there are significant differences one should consider when deciding which drug to utilize. Primarily, these drugs have been shown to engage different populations of T effector cells. TNBS and oxazolone have been found to engage elements of the adaptive immune system, more commonly

associated with the development of Crohn's disease, with TNBS involving a Th1 cell response and oxazolone initiating a Th2 response. Meanwhile, DSS initiates the recruitment of innate immune cells which play a major role in the initiation and exacerbation of ulcerative colitis. Additionally, the timeline of the project is an important variable when deciding which of the two drugs to use. TNBS induces disease symptoms more rapidly, at around 3 days, compared to DSS which takes around a week to induce only acute symptoms with chronic onset requiring between weeks to months to fully develop.

IBDs have limited treatment options culminating in partial or complete removal of the affected digestive tract organs, which sometimes does not resolve the massive inflammation<sup>5</sup>. It is difficult to treat these diseases because part of the immune system cannot be shut down without increasing the risk of infection by pathogens<sup>1</sup>. Despite this, many standard treatments for autoimmune diseases work by suppressing immunity<sup>6</sup>. As a result, these treatments increase the risk of viral/bacterial infection and aid cancer development<sup>7</sup>. Another problem with the standard treatments for autoimmune diseases is that they are limited to a particular pathway (*e.g.*, TNF- $\alpha$  blockers, only decrease one pro-inflammatory cytokine), but autoimmune diseases are complex and involve activation of many inflammatory pathways and patients vary in how their immune system is activating<sup>8,9</sup>. For example, in rheumatoid arthritis alone, there are over 100 unique single nucleotide polymorphisms that can produce similar diseases, so treatments have variable results<sup>10,11</sup>. Standard treatments for autoimmune diseases are also transient, so that they must be kept up for the rest of a patient's life<sup>12</sup>. As a result, there is a need for a more flexible, long term treatment that works as a "reset switch" on an overactive immune system, rather than just shutting down part of it<sup>13</sup>.

Cell therapies have the potential to act on many pathways simultaneously due to the higher complexity of a cell compared to a small molecule drug or peptide-based treatment<sup>14</sup>. These cell-based therapeutics can activate beneficial alternative pathways and promote healing and regeneration in ways traditional therapeutics cannot<sup>15</sup>. Additionally, cells have their own directional motility, allowing them to home to sites of disease, rather than the passive movement that simpler therapeutics are limited by<sup>16,17</sup>. Once at their target sites engineered cell therapies can promote angiogenesis - allowing for improved efficacy of the innate tissue regeneration mechanisms<sup>18</sup>. Finally,

the complexity and modularity of cells allows them to be engineered or modified to become more effective at their intended therapeutic functions<sup>19</sup>. One type of cell therapy that is becoming increasingly popular is Mesenchymal Stem Cell transplants. Mesenchymal Stem Cells (also known as Mesenchymal Stromal Cells or MSC) are multipotent cells that can differentiate into several types of tissues (bone, cartilage, fat, muscle, neural tissue) depending on the signals they receive from their surroundings<sup>20,21,22</sup>. MSC are also known to promote angiogenesis, decrease scarring, maintain stem cell niches, and prevent tissue death<sup>23,24,25</sup>. MSC secrete several molecules that influence immune cell differentiation and fate including transforming growth factor  $\beta$  (TGF- $\beta$ ), prostaglandin-E2 (PGE2), Indolamine 2,3-dioxygenase (IDO), interleukin 4 (IL-4), and nitric oxide (NO)<sup>26,27</sup>. MSC can be given as allogeneic transplants (from one person to another) with very limited immune reaction, minimizing graft vs host disease (GvHD, immune rejection of transplanted donor cells by recipient)<sup>27</sup>.

There are several sources of MSC including bone marrow, adipose tissue, umbilical cord blood, and umbilical cord tissue<sup>28</sup>. The source has a noticeable impact on the MSC's ability to perform specific functions and thus one source may be best for a therapeutic purpose<sup>29</sup>. For example, MSC derived from bone marrow (BM-MS) are larger in size and their proliferative potential has been seen as lower compared to those found in adipose or umbilical cord tissues<sup>30</sup>; however, BM-MS have been demonstrated as effective localizers and have successfully treated pain relating to the joint and spine<sup>31</sup>. BM-MS are the most commonly studied type of MSC treatment, but other sources of MSC have therapeutic advantages. For example, MSC derived from umbilical cords (UC-MS) can be obtained through non-invasive procedures, they can produce a larger concentration of stem cells in the tissue, and they are more epigenetically similar to embryonic expression profiles, than bone marrow, adipose derived, or other adult sources of MSC, which can correlate to higher plasticity and potency<sup>32</sup>. Cells of the same origin can also have heterogeneous properties/therapeutic abilities, depending on the donor<sup>33</sup>. Compounding these sources of MSC variability is that the production of each batch of MSC is not consistent between one study to the next<sup>33</sup>. In total there are a broad range of cell treatments that are all being called "MSC", which may have very different therapeutic potentials, depending on the specific phenotype of the disease they are being applied to, and many of these clinical

trials have failed<sup>34</sup>. Umbilical cord MSC partially ameliorate this issue because their high proliferative capacity allows one cell line derived from a single cord to be given to more patients after thorough evaluation of potency, giving more consistent therapeutic effect.

Recently, MSC have been investigated for their beneficial therapeutic effects in multiple diseases, including myocardial infarction, connective tissue, autoimmune, inflammatory, lung, and kidney diseases. MSC have also been investigated in animal studies and human clinical trials of autoimmune diseases, including Inflammatory Bowel Diseases (IBD, both Ulcerative Colitis and Crohn's Disease)<sup>35</sup>. The capacity of MSC for immunomodulation and tissue repair make them excellent potential therapeutics for diseases involving localized inflammation and tissue damage, such as IBD<sup>36</sup>. Therefore, the prevalence, severity, and limitations of current treatments for IBD make it an excellent target for a human umbilical cord MSC (hUC-MSC) based cell therapy. Here we determined the efficacy of a new hUC-MSC product (BX-U001) to treat IBD symptoms in a mouse model of IBD, in support of an FDA IND application, and upcoming clinical trials in humans.

### **4.3 Results**

Human umbilical cord mesenchymal stem cells (hUC-MSC) were cultivated by a tissue explant method and assayed for mesenchymal phenotype per ISCT guidelines<sup>39</sup>. The hUC-MSC used in these experiments were shown to adhere to plastic, differentiate into both osteocytes and adipocytes, were positive for CD73, CD90, CD105, and negative for CD45, CD34, and HLA-DR (Figure 4.1a-d). The hUC-MSC also showed anti-inflammatory functional capacity *in vitro*, by suppressing production of inflammatory cytokines in PBMCs (Figure 4.1e).

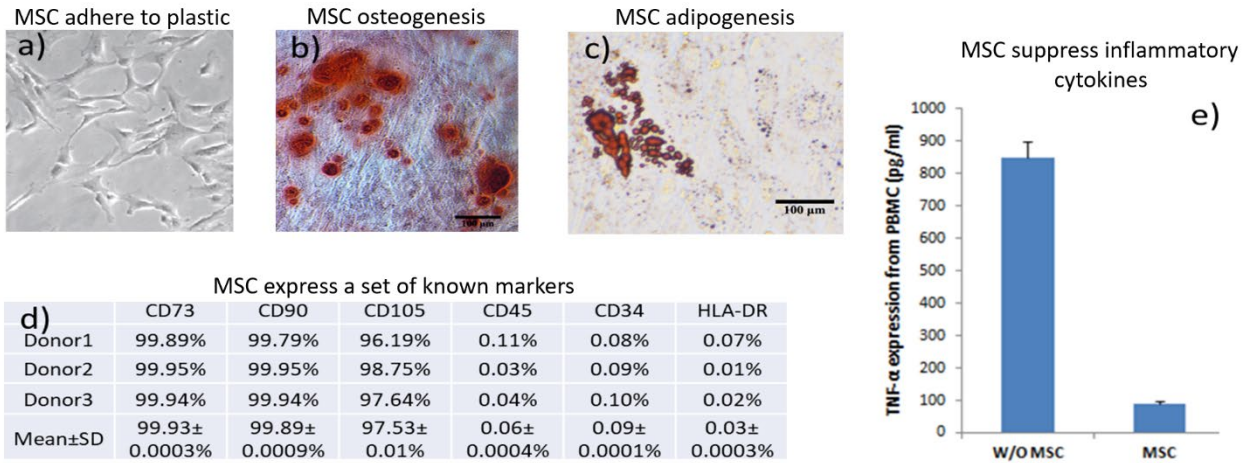


**Figure 4.1. hUC-MSC are characterized by standard MSC phenotypes established by the International Society for Cellular Therapy (ISCT).**

A mouse model of inflammatory bowel disease was established in male BALB/cJ mice, by intrarectal administration of 70  $\mu$ L of TNBS dissolved in 50% ethanol<sup>38</sup>. Mice treated with TNBS showed standard inflammatory bowel disease symptoms such as rapid weight loss, macroscopic and microscopic damage to their colons, and they began having diarrhea and rectal bleeding by 24 hours post-TNBS administration.

To determine the biodistribution of hUC-MSC in TNBS model mice, firefly luciferase (Fluc) expression was engineered into hUC-MSC, which were intravenously infused to IBD mice, the day of TNBS administration, and healthy control mice. The engineered hUC-MSC showed an increase in Fluc expression in the lower abdomen between 6 hours and 24 hours, particularly for the IBD mice, indicating hUC-MSC have some homing to sites of inflammation (Figure 4.2). The signal in the lower abdomen rapidly reduced by 48 hours post injection, indicating hUC-MSC localization to inflamed areas is transient.

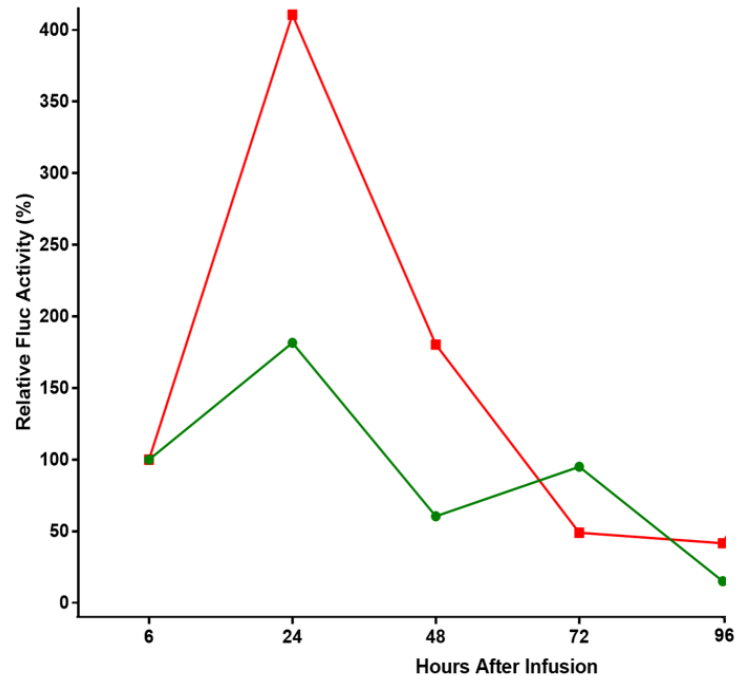


**Figure 4.2. Relative Fluc signal in colons of healthy mice (Green line, n=3) and IBD mice (Red, n=3) after infusion with 1 million Luc-MS. Normalized to 6hr fluorescent signal.**

To determine the therapeutic effects the hUC-MS. might have on IBD pathology, a TNBS IBD mouse model was established in BALB/cJ mice. Four groups were created by randomly separating mice of equivalent overall body weights. Two groups were given IBD by rectal infusion of 2 mg TNBS dissolved in 50% ethanol solution. One IBD group received 2 million intravenous hUC-MS. on the day of disease induction to test general treatment (T Group), and one IBD group received only cell suspension solution (V Group). One group was kept as a healthy control (H Group), and one group was only given ethanol via rectal infusion (E Group), to demonstrate the difference between tissue damage caused by ethanol and inflammation caused by IBD symptoms.

Mice were measured daily to monitor IBD induced weight loss (Figure 4.4). Fasting from Day -1 to Day 0 produced rapid weight loss in all groups prior to IBD induction (Figure 4.4 and Table 4.1). Mice from the H Group recovered by Day 1, but mice in the E, T, and V groups recovered more slowly and did not recover to the levels of H Group mice within the time limit of the experiment. T Group mice recovered weight at the same rate as the E Group, and significantly more than the V Group.

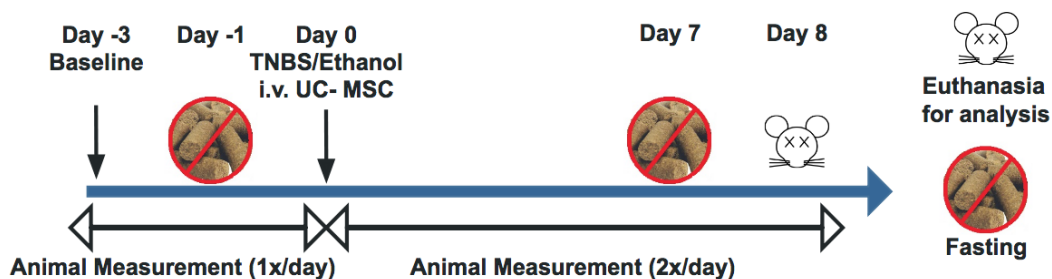


Figure 4.3. Experimental timetable for establishing TNBS animal model and treatment with hUC-MSC.

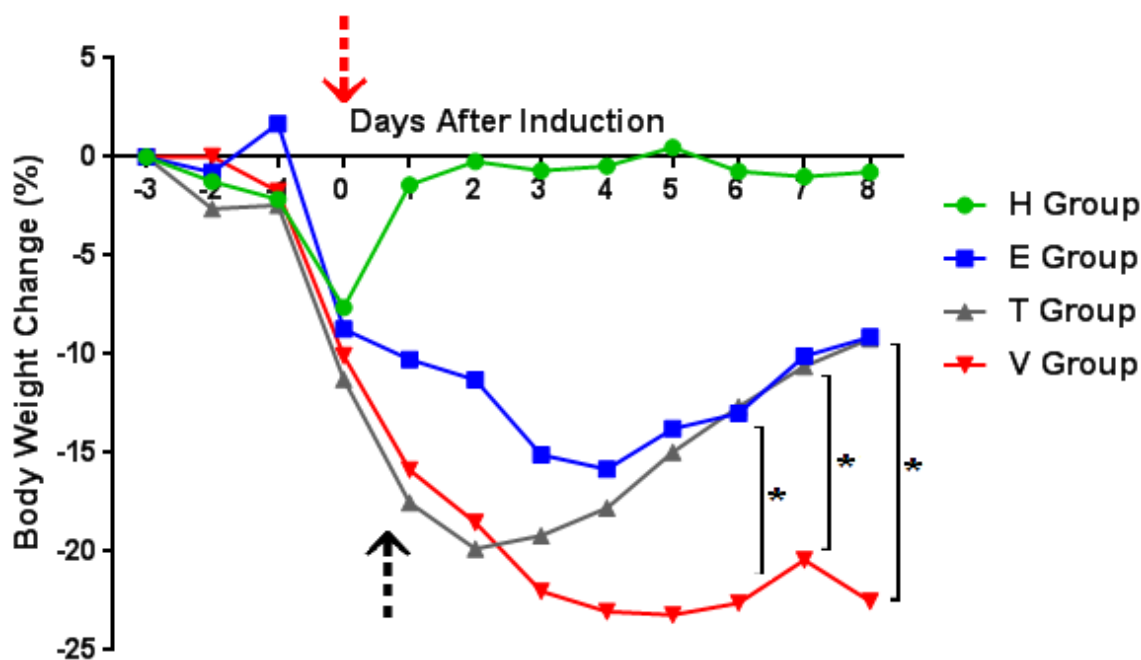


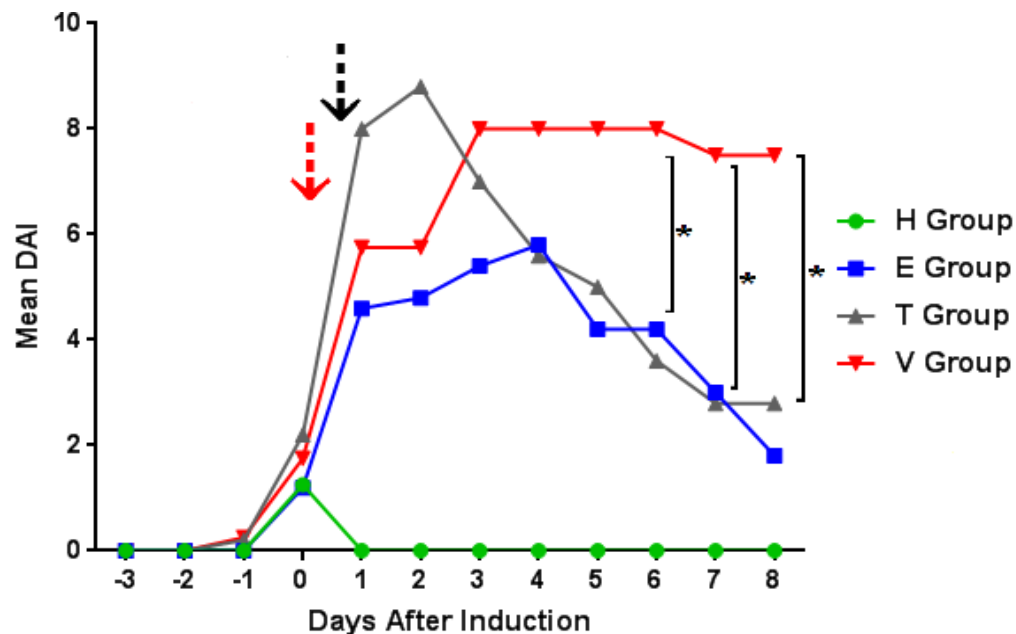
Figure 4.4. hUC-MSC treatment significantly reduced the body weight change of TNBS-induced mice (T vs V:  $*p < 0.05$ ). T Group:  $n = 5$ , V Group:  $n = 4$ , E Group:  $n = 5$  and H Group:  $n = 4$ . Both TNBS induction and treatment was given on D0. The red arrow indicates TNBS/ethanol induction, the black arrow indicates UC-MSC infusion (infusion was given 12hrs post induction).

Table 4.1. Body Weight Change Percentage (BWC%, Mean  $\pm$  SEM)

| Time point | T Group (n = 5)   | V Group (n = 4)   | H Group (n = 4)  | E Group (n = 5)  |
|------------|-------------------|-------------------|------------------|------------------|
| Day -3     | 0 $\pm$ 0         | 0 $\pm$ 0         | 0 $\pm$ 0        | 0 $\pm$ 0        |
| Day -2     | -2.62 $\pm$ 0.75  | 0.03 $\pm$ 1.84   | -1.23 $\pm$ 0.88 | -0.78 $\pm$ 0.60 |
| Day -1     | -2.45 $\pm$ 1.67  | -1.75 $\pm$ 2.67  | -2.14 $\pm$ 0.89 | 1.70 $\pm$ 2.63  |
| Day 0      | -11.28 $\pm$ 0.86 | -10.08 $\pm$ 1.97 | -7.63 $\pm$ 1.02 | -8.72 $\pm$ 0.40 |

|       |               |               |              |               |
|-------|---------------|---------------|--------------|---------------|
| Day 1 | -17.52 ± 1.24 | -15.86 ± 2.07 | -1.40 ± 0.88 | -10.26 ± 1.33 |
| Day 2 | -19.86 ± 0.98 | -18.52 ± 2.60 | -0.22 ± 0.85 | -11.29 ± 2.79 |
| Day 3 | -19.20 ± 2.59 | -22.01 ± 3.19 | -0.69 ± 1.42 | -15.09 ± 4.37 |
| Day 4 | -17.80 ± 3.68 | -23.04 ± 3.25 | -0.45 ± 1.51 | -15.83 ± 4.78 |
| Day 5 | -14.96 ± 3.78 | -23.22 ± 3.36 | 0.49 ± 1.26  | -13.78 ± 4.93 |
| Day 6 | -12.67 ± 3.29 | -22.60 ± 2.93 | -0.73 ± 1.19 | -12.99 ± 4.50 |
| Day 7 | -10.60 ± 3.02 | -20.42 ± 2.74 | -0.99 ± 0.98 | -10.09 ± 3.77 |
| Day 8 | -9.21 ± 2.44  | -22.53 ± 4.11 | -0.76 ± 0.81 | -9.12 ± 3.03  |

Disease activity index (DAI) is a measure of IBD severity, which combines quantitative parameters (weight loss), and qualitative parameters (diarrhea and rectal bleeding) and was calculated daily for all groups. Weight loss caused a small spike in DAI for all groups after fasting, but H Group mice rapidly recovered within one day (Figure 4.5 and Table 4.2). Similar to weight loss measurements, the DAI of T Group matched that of E Group, with values close to those of H Group and was significantly improved compared to the untreated V Group.



**Figure 4.5. hUC-MSc treatment reduces mean DAI of T Group (T vs V:  $*p < 0.05$ ).** All induced groups get higher DAI (indicating worse DAI symptoms) until D2, when T Group improved to the level of E group, but V



group did not improve. T Group: n = 5, V Group: n = 4, E Group: n = 5, H Group: n = 4. Red arrow indicates TNBS/ethanol induction, and black arrow indicates hUC-MSC infusion (infusion was given 12hrs post induction).

**Table 4.2. Disease Activity Index (DAI, Mean  $\pm$  SEM)**

| Time point | T Group (n = 5) | V Group (n = 4) | H Group (n = 4) | E Group (n = 5) |
|------------|-----------------|-----------------|-----------------|-----------------|
| Day -3     | 0 $\pm$ 0       | 0 $\pm$ 0       | 0 $\pm$ 0       | 0 $\pm$ 0       |
| Day -2     | 0 $\pm$ 0       | 0 $\pm$ 0       | 0 $\pm$ 0       | 0 $\pm$ 0       |
| Day -1     | 0.20 $\pm$ 0.20 | 0.25 $\pm$ 0.25 | 0 $\pm$ 0       | 0 $\pm$ 0       |
| Day 0      | 2.20 $\pm$ 0.20 | 1.75 $\pm$ 0.48 | 1.25 $\pm$ 0.25 | 1.20 $\pm$ 0.20 |
| Day 1      | 8.00 $\pm$ 1.14 | 5.75 $\pm$ 1.03 | 0 $\pm$ 0       | 4.60 $\pm$ 1.12 |
| Day 2      | 8.80 $\pm$ 0.86 | 5.75 $\pm$ 0.85 | 0 $\pm$ 0       | 4.80 $\pm$ 1.46 |
| Day 3      | 7.00 $\pm$ 1.30 | 8.00 $\pm$ 0    | 0 $\pm$ 0       | 5.40 $\pm$ 1.66 |
| Day 4      | 5.60 $\pm$ 1.50 | 8.00 $\pm$ 0    | 0 $\pm$ 0       | 5.80 $\pm$ 1.85 |
| Day 5      | 5.00 $\pm$ 1.38 | 8.00 $\pm$ 0    | 0 $\pm$ 0       | 4.20 $\pm$ 1.80 |
| Day 6      | 3.60 $\pm$ 1.36 | 8.00 $\pm$ 0    | 0 $\pm$ 0       | 4.20 $\pm$ 1.74 |
| Day 7      | 2.80 $\pm$ 1.39 | 7.50 $\pm$ 0.29 | 0 $\pm$ 0       | 3.00 $\pm$ 1.38 |
| Day 8      | 2.80 $\pm$ 1.36 | 7.50 $\pm$ 0.29 | 0 $\pm$ 0       | 1.80 $\pm$ 0.73 |

At endpoint, mouse colons were harvested and imaged, so that they could be evaluated for macroscopic indicators of inflammation via the Wallace scoring system<sup>40</sup>. All scoring was done completely blinded to sample identity. Colons from H group showed no inflammation or bleeding and were generally longer and thinner (Figure 4.8). Group E colons showed very mild inflammation, in some cases, but were generally healthy (Figure 4.8). Group T colons were generally less inflamed and had less blockage than those of V Group ( $p < 0.05$ ) (Figures 4.7 and 4.8, Table 4.3).



**Figure 4.7. Representative pictures of colons.** These pictures are examples of images used to determine the macroscopic scores of mouse colons.

**Table 4.3. Macroscopic scores (Mean  $\pm$  SEM)**

| H Group (n = 4) | E Group (n = 5) | T Group (n = 5) | V Group (n = 3) |
|-----------------|-----------------|-----------------|-----------------|
| 0 $\pm$ 0       | 1.70 $\pm$ 0.37 | 2.90 $\pm$ 1.68 | 9.00 $\pm$ 0.52 |

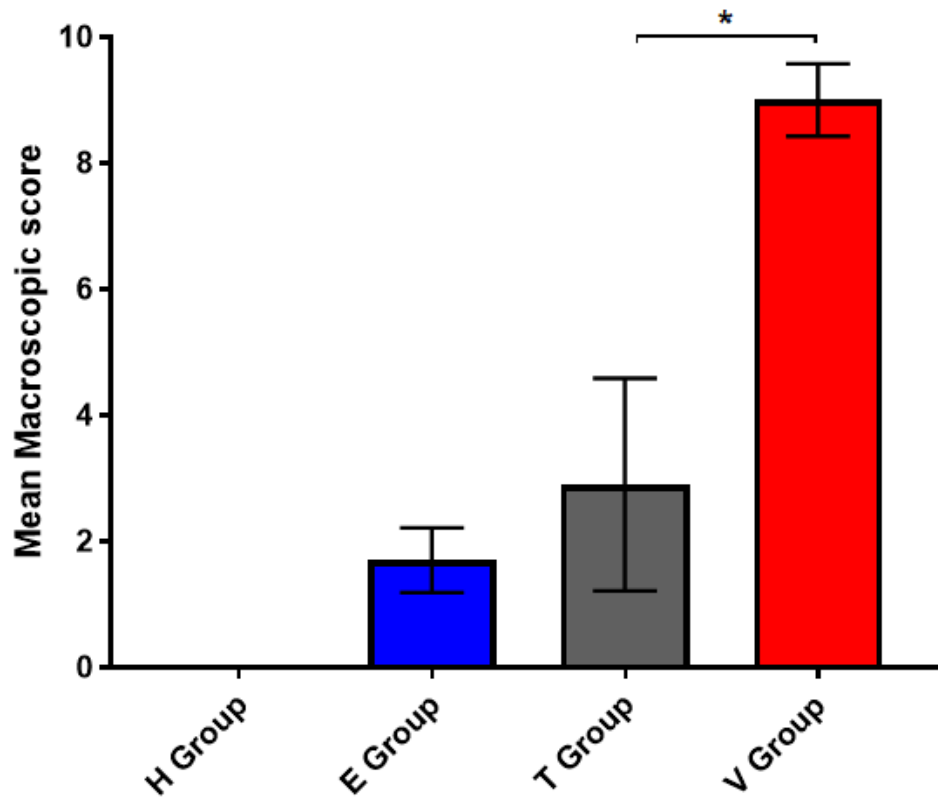


**Figure 4.8. hUC-MSC treatment reduced macroscopic damage to IBD mouse colons.** T Group showed significant improvement of macroscopic scores compared to V group ( $*p < 0.05$ ). Wallace score method was used (scale 0 to 10). T Group:  $n = 5$ , V Group:  $n = 3$ , E Group:  $n = 5$ , H Group:  $n = 4$ . Macroscopic scores given as Mean  $\pm$  SEM.

Additionally, to quantify IBD severity, freshly harvested colons were weighed after endpoint (D8), because the inflammation and fecal build up were more severe in sicker mice. The Group H, E, and T mice showed much lighter colons than Group V mice (Figure 4.9). In addition to a macroscopic evaluation, colons were given microscopic assessments via Hematoxylin and Eosin staining. After fixation and tissue processing, colons were cut so that the same 2 cm region of colon from each animal was embedded in paraffin and cross-sections cut at 5  $\mu$ m slices. Colons from Group T appeared to have less infiltration of immune cells and less structural damage to goblet cells and crypts than those of V Group (Figure 4.10).

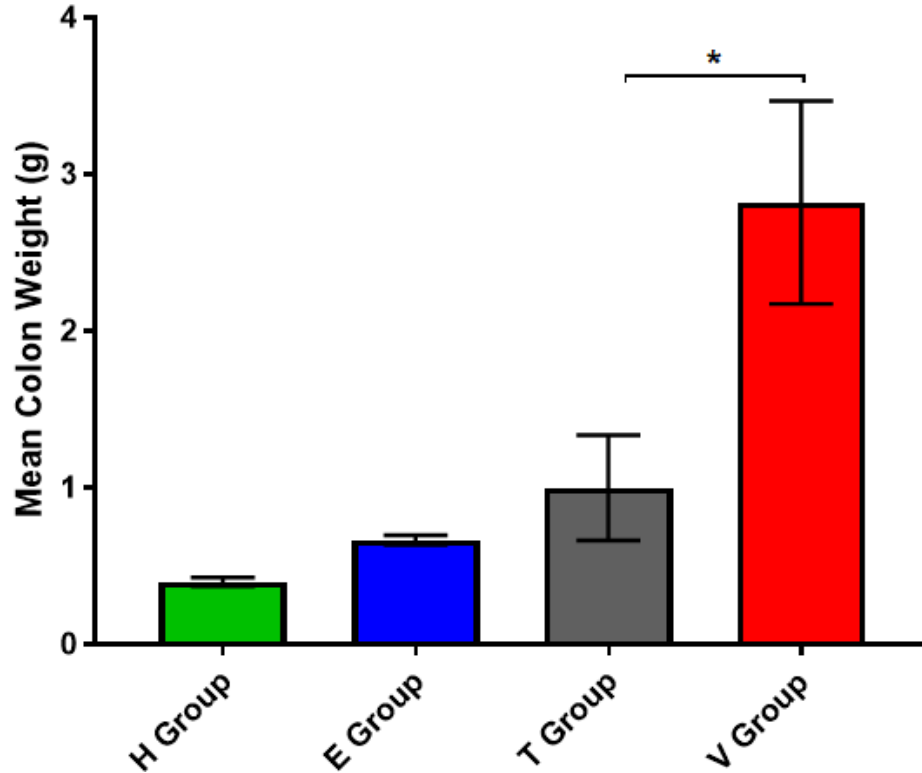


**Figure 4.9. hUC-MSC infusion significantly reduced colon weight gain from TNBS model.** T Group colon weights are close to E group and are much lower than those of V group (\* $p < 0.05$ ). T Group:  $n = 5$ , V Group:  $n = 3$ , E Group:  $n = 5$ , H Group:  $n = 4$ . Mean  $\pm$  SEM.

In order to understand mechanisms of any potential therapeutic effects the hUC-MSC have, the most important cytokines relevant to the IBD inflammatory cascade were identified from the literature (Table 4.4). IFN- $\gamma$ , TNF- $\alpha$ , IL-1B, IL-6, and IL-12 were identified as being the strongest mediators of IBD. A multiplex ELISA cytokine assay was performed on serum from mice in each group to determine the effect of hUC-MSC on these important IBD cytokines. Group T mice showed a significant decrease in \*\*\* cytokines, compared to Group V mice (Figure 4.12).

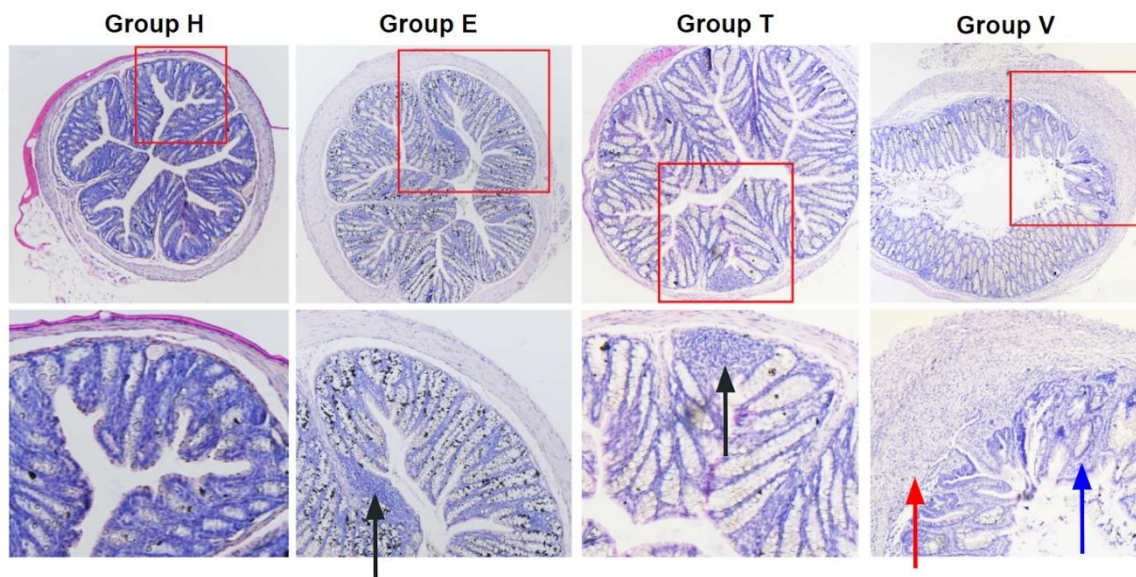


**Figure 4.10. Representative pictures of histological exam.** Full colon sections (upper images) and zoomed in regions highlighted by red boxes (lower images) Black arrows indicate mild lymphocyte infiltration, red arrow indicates thickening of colon walls, blue arrow indicates goblet cell loss and crypt damage, The histology of T Group appears improved when compared to the histology of V Group.

**Table 4.4. Important cytokines relating to IBD and MSC treatment.**

| Essential cytokines (Inflammatory)          | Important (Inflammatory)     | Possibly important cytokines related to IBD                        | Important relating to MSC treatment (anti-inflammatory)                        |
|---|------------------------------|--|--|
| IFN $\gamma$ <sup>2,7</sup>                 | IL18 <sup>2</sup>            | TL1A <sup>7</sup>  | IL10 <sup>6</sup>  |
| TNF $\alpha$ <sup>1,3,8,11</sup> (Th1 - CD) | IL17F <sup>4</sup>           | Colonic leptin <sup>8</sup>  | IL6 <sup>13</sup> (heavily secreted by MSCs and necessary for induced healing) |
| IL-1B <sup>1,8,10,11</sup>                  | IL13 <sup>7</sup> (Th2 - UC) | ENA-78 <sup>9</sup>  | IDO <sup>14</sup>  |
| IL12 <sup>5,12,7</sup> (Th1 activator)      | IL8 <sup>9,10</sup>          | MCP-1 <sup>9</sup>   | PGE2 <sup>14</sup>   |
| IL6 <sup>1,6,8,10,11</sup> (Th17 activator) | IL2 <sup>9</sup>             | RANTES <sup>9</sup>  | TGFB <sup>14</sup>   |
|   | IL17 <sup>12</sup>           | IL-4 <sup>9</sup> (Th1->Th2, decrease in TNBS but increase in DSS) | Nitric Oxide <sup>14</sup>   |
|   | IL22 <sup>7</sup>            | Gro <sup>10</sup> (UC)   | TSG-6 <sup>14</sup>  |
|   |                              | IL5 <sup>7</sup> (UC)  | FAS ligand <sup>15</sup>   |

LPMC's are responsible for the majority of cytokine production

Since patient survival is the most important goal of IBD treatment, and untreated mice had high mortality, we performed an additional study with more animals to quantify survival rates for each group. The survival rate of

T Group mice was 86% compared to 15% for mice in V Group ( $p < 0.01$ ) (Figure 4.11).

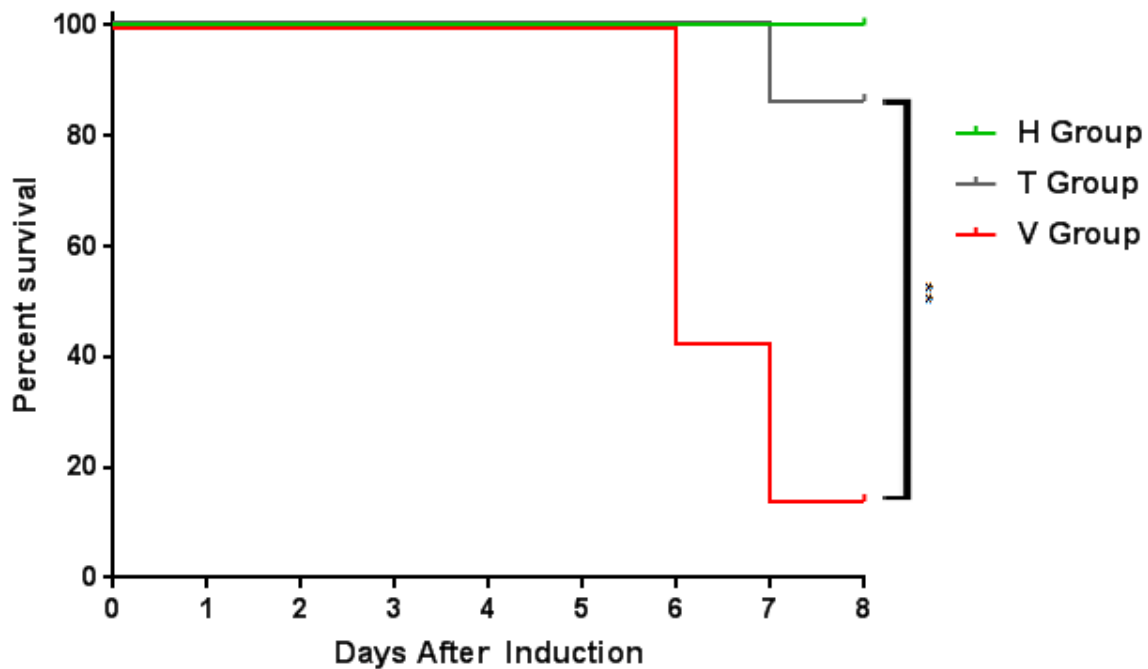


**Figure 4.11. hUC-MSC infusion significantly improved survival from TNBS Model over 8 days ( $p < 0.01$ ).** T Group:  $n = 7$ , V Group:  $n = 7$ , H Group:  $n = 5$ .

#### 4.4 Discussion

After many years of anticipation from patients and doctors, stem cell therapies are making progress from the lab bench to the bedside. In particular, some IBD patients are refractory to standard IBD treatments, and are desperate for alternative treatments, such cell-based immunomodulation<sup>41</sup>. Previous preclinical and clinical trials have seen strong immunomodulatory effects from intravenous infusion of mesenchymal stem cells, and showed positive efficacy and tolerability warranting further investigation into the clinical benefits of MSC as a treatment for autoimmune diseases, including IBD<sup>42</sup>. Human umbilical cord derived Mesenchymal Stem Cells (hUC-MSC), are a type of adult stem cell and the main components of BX-U001, a new hUC-MSC based treatment for IBD. This preclinical study evaluates the efficacy from a single infusion of BX-U001 hUC-MSC to treat IBD in a TNBS murine model via tail vein, and supports an IND application with the FDA, and clinical trials.

After the administration of hUC-MSC, the clinical parameters of T Group, including BWC and DAI, were

all significantly reduced. This benefit was evident from 6 days after hUC-MSC administration onward, compared to V Group. In addition, macroscopic scores ( $p < 0.05$ ), colon weights ( $p < 0.05$ ) and survival ( $p < 0.01$ ) were also significantly improved after treatment of this test agent, compared to the vehicle group (V group). No abnormalities were observed in murine hair and skin, behavior, or water intake that were unrelated to the TNBS model. No abnormal conditions were observed at infusion sites. Previous clinical studies of MSC to treat IBD have had mixed results (Table 4.5). Most clinical trials have used MSC derived from bone marrow (BM) or adipose (A). There are four large scale, phase 3 trials; two of which used (BM) MSC and the other two used (A) MSC. The (BM) MSC trials were conducted in the U.S. and ended in February 2019 and in July 2020 but have yet to disclose their findings. The two (A) MSC trials were conducted in Europe; one of which concluded in May 2017 and found that 53 of 107 patients experienced combined remission compared to the 36 of 103 patients in the placebo group. The other (A) MSC trial is expected to conclude in October 2021.

MSC are understood to function as immunomodulatory agents by interfacing with cells of the innate and adaptive immune system through membrane-bound receptors and paracrine signaling<sup>43</sup>. This immunoregulatory capacity is strongly influenced by which cytokines are present in the surrounding microenvironment which direct MSC functionality to properly coordinate inflammation resolution and tissue repair<sup>43</sup>. In the context of Crohn's disease, globally high concentrations of pro-inflammatory cytokines, mainly TNF $\alpha$  and IFN $\gamma$ , in animals and humans elicit strong activation of MSC anti-inflammatory pathways (Figure 9A). The initiation of transient T-cell apoptosis via the Fas ligand (FasL)-dependent Fas pathway in inflammatory tissue is a critical component of this anti-inflammatory response, as supported by a knockout study in mice, which found that FASL $^{-/-}$  generated bone marrow MSC were unable to induce T-cell apoptosis in recipient mice<sup>44</sup>. MSC also respond through the release of a wide variety of soluble factors including IL-4, IDO, TSG-6, TGF- $\beta$ , and PGE2 which collectively serve to disrupt the rampant inflammatory milieu observed in Crohn's disease\*. One key mechanism is to recruit and influence the differentiation of native CD4 $^{+}$  T cells away from inflammatory Th1 and Th17 states and towards the development of anti-inflammatory and tolerogenic CD4 $^{+}$ CD25 $^{+}$ Foxp3 $^{+}$  regulatory T cells (Treg) and Th2 phenotypes (A14 -

Th1/Th17, A15 -CD4+CD25+Foxp3+, Th2 citation needed ). Additionally, it's likely that this process of effector T cell polarization could also be indirectly mediated by MSC through the generation of intermediate phagocytes which regulate these processes through the release of anti-inflammatory molecules such as IL-10 and IDO (Figure 4.9B). Collectively, both mechanisms enable MSC to establish anti-inflammatory and tolerogenic outcomes through the subsequent induction of Treg and DCreg populations.

While these pathways likely work together to achieve this result, it is interesting to consider how the involvement of each mechanism could shift in regard to the route of administration used and how this could alter the effectiveness of treatment. MSC transplantation for the treatment of IBD is typically performed using systemic, intraperitoneal, or more recently, *in-situ* administration directly into sites of inflammation (Table 4.5). It's possible that MSC have experienced increased efficacy/recent success using *in-situ* administration, such is the case in recent trials looking at fistula healing, because they are able to take advantage of both these mechanisms of action to enable healing and immunomodulation more efficiently and at a greater quantity (Table 4.5). Meanwhile, when MSC are administered systemically it's likely that their therapeutic capacity is mediated primarily through the indirect generation of anti-inflammatory immune cell intermediates which translocate to sites of inflammation following MSC clearance<sup>45</sup>. This is supported by the common observation that MSC, when administered systemically, become entrapped within the microvasculature of filter organs such as the lungs, liver, and spleen - coined as the "first-pass" effect<sup>46</sup>. While most cells never reach the targeted inflammatory site, MSC administration continues to produce beneficial results, which is further supported by our study.

Understanding how these routes of administration lead to differences in MSC functionality could be very useful for the future development of patient stratification strategies. These administration routes could be strategically applied to fully address different aspects of an individual's IBD condition and its progression. For example, it could be that severe cases would benefit most from the administration of MSC directly at the sites of damage to address the immediate need for MSC immunosuppression and epithelial wall reconstruction. Meanwhile, systemic administration could be a better option for treating patients with less developed symptoms or those that



have associated secondary disease conditions associated with IBD by generating large pools of anti-inflammatory immune intermediates which can be redistributed through the bloodstream to ameliorate the prevalence of systemic inflammation. These routes could theoretically also be used in combination in severe cases to ensure that both local and systemic inflammation are being addressed.

The MSC instigated *in vivo* generation of M2 anti-inflammatory macrophages - which are major contributors to ECM remodeling, apoptotic cell clearance, and tissue repair - is performed through the secretion of local factors such as anti-inflammatory cytokines<sup>47</sup> and various growth factors<sup>48</sup>. These M2 macrophages have previously been shown to decrease inflammation of the inner lining of the colon in mouse colitis models and reduce tissue death<sup>49</sup>. One possible mechanism for how the M2 macrophages promote tissue repair in ulcerative colitis models might be the activation of the canonical Wnt pathway in epithelial cells of the intestine<sup>50</sup>. This signaling pathway has been implicated to promote stem cell growth, self-renewal, and tissue repair<sup>50</sup>. Another key factor in inhibiting the progression of ulcerative colitis is the M1/M2 macrophage balance. The proliferation of M2 macrophages is able to reduce the differentiation into M1 macrophages - thereby reducing their pro-inflammatory secretions and the subsequent damage done by the M1 phenotype<sup>51</sup>. Overall, the M2 anti-inflammatory macrophage could also help to explain how immune cell intermediates could additionally help in resolving the complications associated with Crohn's disease and other IBD related ailments such as the breakdown of the epithelial wall resulting in immune exposure and sensitization to intestinal bacteria.

Ultimately, we propose a combination of direct and indirect interactions between transplanted hUC-MSC and the recipient's immune system, is likely responsible for the therapeutic effects observed in this study (Figure 4.12). The direct interaction of MSC with T cells can reduce Th1 and Th17 T cell activity and increase the number of FoxP3+ T regulatory cells, reducing inflammation (Figure 4.12a). We expect the indirect effects of hUC-MSC are more relevant to intravenous injections, because most of the MSC are entrapped in the lungs, and relatively few reach the inflamed colon (Figure 4.12b). The M2 macrophages induced by direct interactions with the MSC in the lungs and immune tissues (lymph nodes, spleen, Peyer's patches) execute the global immunomodulation seen in this

and other studies of MSC treatment of inflammatory diseases, such as a large increase in the circulation of T regulatory cells.

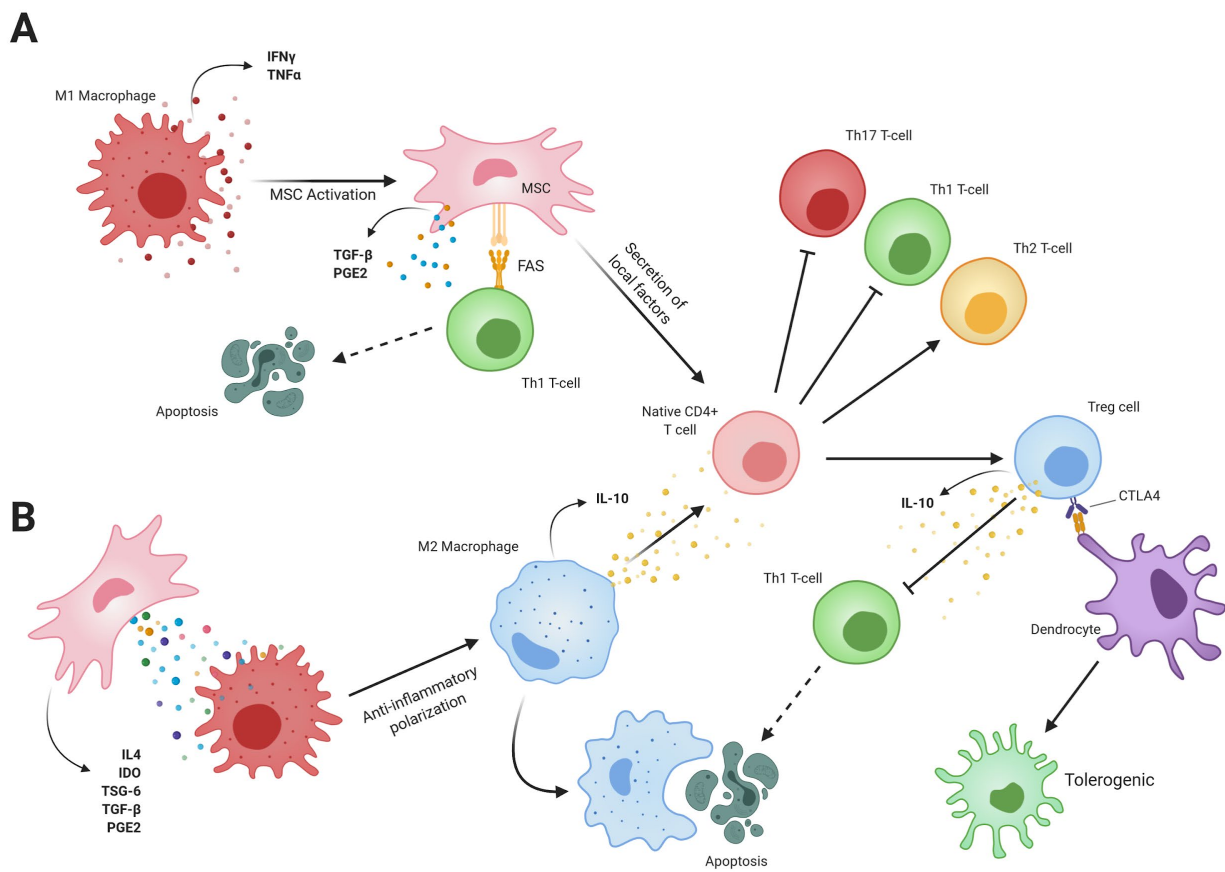


**Figure 4.12. Proposed mechanism of action for hUC-MSC in IBD.** MSC confer their therapeutic function by downregulating the presence of Th1 cells in diseased tissue while inducing the proliferation CD4+CD25+Foxp3+ regulatory T cells (Tregs) and the generation of tolerogenic phagocytes. This can be accomplished by A) direct immunosuppression, in response to stimulatory cytokines (e.g. IFN $\gamma$  and TNF $\alpha$ ) released by inflammatory phagocytes present in diseased regions, or B) indirectly through the generation of immune cell intermediates by polarizing tissue-resident and circulating macrophage populations from pro-inflammatory (M1) to resolving (M2) phenotypes through paracrine signaling.

**Table 4.5. Previous and ongoing clinical trials using MSC to treat IBD.**

| Phase | Date                              | Location  | Treatment  | # patients | Parameters   | Results |
|-------|-----------------------------------|---|--|------------|--|---------|
| 1/2   | 06/05/2017 - 01/2020              | Cell Therapy Center Amman, Jordan, 11942                    | 120 million cells of Wharton Jelly MSC in 10 mL injected intravenously every 2 weeks | 20         | safety, endoscopy, disease remission                               | N/A     |
| 1/2   | 01/15/2018 - estimated 12/31/2021 | CHU de Liège Liège, Belgium                                 | suspension of MSC for intra-fistula injection  | 60         | MRI, safety, Crohn's disease activity index, Lamann Index, surveys | N/A     |
| 1/2   | 07/01/2018 - estimated 02/01/2021 | Liaocheng city people's hospital Liaocheng, Shandong, China | 5 mil AMSC injected in colonic submucosa once a week for 2 weeks                     | 50         | UCEIS, CDAI, surveys, Riley index                                  | N/A     |

|     |                   |   |   |    |   |  |
|-----|-------------------|---|---|----|---|--|
| N/A | 08/2013 - 03/2020 | Beneficencia Portuguesa Sao Jose do Rio Preto, SP, Brazil                           | Autologous HSCT + Cyclophosphamide (200 mg/kg total dose for four days), rabbit antithymocyte globulin (6.5 mg/kg total dose for four days) and methylprednisolone (500 mg/day) | 50 | safety, CDAI, Rutgeerts endoscopic score, HBI, surveys for 2 years                              | N/A  |
| 1/2 | 04/2015 - 12/2016 | Affiliated Hospital to Academy of Military Medical Sciences Beijing, Beijing, China | 1 mil UC-MSK 6 times within 8 weeks   | 30 | PASI, DLQI, body temperature and pressure   | N/A  |
| 2/3 | 01/2017 - 12/2019 | Sun Yat-sen University, China   | 3 or 6 mil/kg MSC via Perianal injection  | 3  | Fistula healing (>2cm) and C-reactive protein and CDAI  | N/A  |
| 3   | 01/2016 - 12/2018 | Sun Yat-sen University, China   | 3 or 6 mil MSC/kg + Drugs (6MP, AZA, infliximab and thalidomide) via IV injection   | 3  | 100   | Reduced CDAI score from 250-450 to below 100   |
| 2   | 01/2010 - 06/2015 | Royal Perth Hospital, Australia   | 2mil (BM?) MSC/kg each wk for 4 wks via IV  | 21 | CDAI score reduction of >100 after 6 weeks. Toxicity and endoscopic/qual of life improvement    | 12/15 had positive response (avg CDAI from 370 to 203), 8/15 had remission, 7/15 endoscopic improvement, 1 developed dysplasia associated lesion or mass (DALM), which is a carcinoma polyp.                           |
| 2   | 03/2012 - 02/2016 | University of Liege, Belgium  | 1.5-2 mil (BM) MSC/kg via IV twice 4 weeks apart  | 20 | CDAI, CRP, fecal calprotectin levels, toxicity and survival                                     | N/A  |
| 2   | 06/2012 - 06/2015 | Fuzhou General Hospital, China  | (UC) MSC via IV + hormone drug therapy  | 82 | CDAI, Harvey-Bradshaw index, corticosteroid dosage over 12mo                                    | N/A  |
| 2   | 10/2013 - 03/2018 | Beneficencia Portuguesa, Brazil   | HSCT via IV + Cyclophosphamide, Globulin anti thymocytes (rabbit), and methylprednisolone   | 20 | CDAI, Harvey-Bradshaw index, endoscopy, patient surveys for 2 yrs                               | N/A  |
| 2   | 06/2010 - 09/2014 | Leiden University Medical Center, Netherlands                                       | 10, 30, 90 mil (BM) MSC via Perianal injection  | 21 | Fistula analysis (endoscopy, cytokine assay of biopsy, leakage), MRI, CRP, CDAI, survey, safety | Perianal fistula healing observed in 10, 30mil groups, no adverse side effects. Interestingly, 90mil had negligible improvement  |
| 2   | 02/2006 - 09/2008 | Osiris Ltd. (Prochymal), USA  | 2 or 8 mil (BM) MSC with plasmalyte and DMSO via IV twice (one week apart)  | 10 | CDAI, survey, endoscopy after 4 weeks   | Average CDAI reduction of 105, 3/9 drug resistant saw improvement, and all had improvement by 28 days. Safety: 1 anemia (unrelated), 5 mild to moderate non-serious reactions. Again lower dose may have better effect |
| 1/2 | 05/2015 - 12/2017 | Ivy Institute of Stem Cells Ltd., China   | (C) MSC via IV three times  | 30 | CDAI, endoscopy, CRP after 6mo  | N/A  |
| 2   | 08/2014 - 10/2018 | Kang Stem Biotech Co. Ltd.  | 50 or 100 mil (UCB) MSC via IV  | 24 | safety, CDAI, CRP, endoscopy, MRI, fecal calprotectin, surveys                                  | N/A  |
| 2   | 12/2014 - 12/2018 | Papa Giovanni XXIII Hospital, Italy   | (A)MSC via perianal injection   | 10 |   | N/A  |
| 3   | 06/2006 - 03/2017 | European Group for Blood and  | HSC mobilization then immunoablation then HSC   | 45 | Disease remission, safety, surveys over 2   | Terminated due to safety concerns  |

|   |                   |   |   |     |   |  |
|---|-------------------|---|---|-----|---|--|
|   |                   | Marrow Transplantation, Europe          | transplant via bone marrow  |     | years   |  |
| 3 | 05/2007 - 07/2020 | Mesoblast Ltd. (Prochymal), USA         | 0.6 to 1.2 bil (BM)MSC via IV in 4 treatments over 2 weeks  | 330 | CDAI <150, surveys, draining fistulas   | N/A  |
| 3 | 09/2010 - 02/2019 | Mesoblast Ltd. (Prochymal), USA         | 200mil (BM)MSC via IV every 40 days four times total  | 120 | CDAI, Disease remission, surveys, safety over 6mo   | N/A  |
| 3 | 10/2007 - 07/2009 | Osiris Ltd. (Prochymal), USA            | 0.6 to 1.2 bil (BM)MSC via IV in 4 treatments over 2 weeks  | 98  | CDAI <150, surveys, draining fistulas   | Terminated due to study design failure   |
| 3 | 07/2012 - 05/2017 | Cellerix (TiGenix S.A.U), Europe        | 120mil (A)MSC via intralesional injection   | 278 | Clinical remission, time response, surveys, CDAI up to 2 years  | 53/107 achieved combined remission vs 36/105 for placebo. 18/103 experienced adverse effects (abscess and proctalgia) vs 30/1-3 in placebo |
| 3 | 12/2008 - 02/2010 | Cellerix (TiGenix S.A.U), Europe        | 20mil (A)MSC then 40mil (A)MSC after 12 weeks via translesional injection                         | 56  | Perianal fistula closure, CDAI, surveys, MRI, safety over 24 weeks  | Terminated due to study design failure   |
| 3 | 09/2017 - 10/2021 | Cellerix (TiGenix S.A.U), Europe        | (Cx601) 120mil A-MSC via intralesional injection (5mil cells/ml) or placebo                       | 326 | Perianal fistula remission by Wk24 and Wk52 (closure of 50% or 100%), Adverse effects at 24wks and 52 wks | N/A  |
| 2 | 07/2017 - 01/2020 | Icahn School of Medicine at Mount Sinai | 50mil HSC via IV combo with Vendolizumab, Cyclophosphamide, Thymoglobulin, and Methylprednisolone | 50  | CDAI <150 after 1 yr, 50% reduction in endoscopic score, surveys  | N/A  |

Note: Information collected from the U.S National Library of Medicine (clinicaltrials.gov).

#### 4.5 Materials and Methods

**Isolation and culture of hUC-MSC:** Umbilical cords were obtained from the UCI medical center (Orange, CA). The hUC-MSC used in this study were isolated and cultured from umbilical cord tissue by a standard tissue explant method<sup>37</sup>. Briefly, umbilical cords were minced into 1-2 mm pieces and then digested with 0.075% collagenase type II for 30 minutes and followed by 0.125% trypsin digestion for 30 minutes under gentle agitation at 37C. The digested tissue was passed through a 100 µm filter and plated at 1 x 10<sup>6</sup> cells per cm<sup>2</sup> in T-75 flasks. Cells were cultured in DMEM F12 with 10% FBS and 1% Pen/Strep and grown at 37C in 5% CO<sub>2</sub>. Cells were used in experiments at passage 5 or 6 from tissue harvest.

**Animal studies:** For all experiments 6-week-old male BALB/cJ mice were used. For the efficacy study 24 mice were grouped randomly into a healthy control group (H Group), an ethanol control group (E Group), a test group,

which received hUC-MSC (T Group), and a vehicle group, which received only cell injection solution (V Group) (Table 4.6). For the survival studies, 39 mice were grouped randomly into the same groups used for the efficacy studies (Table 4.7). All animal experiments and procedures were performed under permission from the UCI Institution of Animal Care and Use Committee (IACUC protocol number AUP-19-082) and conducted per the Animal Welfare Assurance (#A3416.01).

**Table 4.6. Animal grouping for efficacy studies**

| Group | TNBS         | IV injection given           | Dosage (cells)         | Volume of infusion | n |
|-------|--------------|------------------------------|------------------------|--------------------|---|
| V     | 2 mg/mouse   | Cell-free injection solution | -                      | 200 µL/mouse       | 4 |
| E     | Ethanol only | Cell-free injection solution | -                      | 200 µL/mouse       | 5 |
| T     | 2 mg/mouse   | hUC-MSC infusate             | $2 \times 10^6$ /mouse | 200 µL/mouse       | 5 |
| H     | -            | -                            | -                      | -                  | 4 |

**Table 4.7. Animal grouping for survival study**


| Group | TNBS       | IV injection given           | Dosage (cells)         | Volume of infusion | n |
|-------|------------|------------------------------|------------------------|--------------------|---|
| V     | 2 mg/mouse | Cell-free injection solution | -                      | 200 µL/mouse       | 7 |
| T     | 2 mg/mouse | hUC-MSC infusate             | $2 \times 10^6$ /mouse | 200 µL/mouse       | 7 |
| H     | -          | -                            | -                      | -                  | 5 |

**TNBS Model Induction:** BALB/c mice were injected with TNBS with 70 µL of a 50% ethanol solution containing 2 mg of TNBS via a rectal enema. Briefly, after mice were anesthetized, sterile surgical lubricant was applied to anus and polyethylene tube attached via Luer stub to a 1 mL syringe containing the TNBS solution. The tubing was gently inserted 4 cm proximal to the anus and TNBS was injected at a rate of about 2 µL per second until 70 µL of TNBS solution was delivered. The tubing was withdrawn slowly and the mice were inverted for 90 seconds to prevent solution leaking from anus. Mice were monitored for 2 hours for signs of abnormality.

**Animal evaluation:** The mice were monitored and assessed every day, in a randomized and double-blind fashion, based on body weight, diarrhea and rectal bleeding. Mice were assessed once daily before the day of induction (D(-3) to D(-1)) and thereafter twice daily (D0 to D8, 8-12 hours apart). The average of the two measurements was used to calculate the body weight change (BWC) and disease activity index (DAI). Diarrhea was defined as the presence or absence of mucus/fecal material adherent to anal fur. For diarrhea assessment, a score of 0 was given for no visible diarrhea, a score of 2 if some diarrhea presented, and a score of 4 if lots of diarrhea presented (smear tail

to stomach fur) (Supplemental Table 4.1). Rectal bleeding was defined as the presence or absence of blood in mucus or frank rectal bleeding in diarrhea. For rectal bleeding assessment, a score of 0 was given if no visible blood and feces failed a Hemocult test, a score of 2 was given for a low amount of blood (not visible, but caused Hemocult reaction), and a score of 4 was given if definitive blood (clearly visible). A DAI was calculated based on the above three parameters (*i.e.*, BWC, DS and RBS), and was considered as a measure of IBD symptoms in the mice.

**Supplemental Table 4.1. TNBS model mice exhibiting diarrhea and/or rectal bleeding with corresponding scores.**

|                  |  |   |   |   |   |   |
|------------------|--|---|---|---|---|---|
| Diarrhea         | 0  | 2 | 4 | 2 | 2 | 4 |
| Rectal Bleeding  | 0  | 0 | 0 | 2 | 4 | 4 |
| Example Pictures |  |   |   |   |   |   |

**MSC Administration:** At Day 0 approximately 12 hours after primary induction of CIA (after disease onset), a single infusion of 200  $\mu$ L MEI (Multiple electrolytes injection) solution or 2 million MSC suspended in 200  $\mu$ L MEI solution ( $1 \times 10^7$  cells/mL) was intravenously infused via tail vein to each mouse from MSC treatment groups. The intravenous infusion via tail vein was used to mimic the clinical administrative route and was done with 1 mL sterile syringes with 30 G  $\times$   $\frac{1}{2}$  disposable needles and an infusion speed of 8-20  $\mu$ L/second. After drug administration, animals were closely monitored for 2 hours. If any abnormality was observed (*e.g.*, any profound paralysis that inhibits animals' ability to eat or drink, any signs of pain including piloerected/unkept fur, squinted eyes, ataxia, hunched posture, or labored breathing, that is not relieved with analgesia), symptoms and their starting time, severity, duration, *etc.* were recorded in detail. Thereafter monitoring was also conducted twice a day with notes taken accordingly.

**Tissue harvest and processing:** All animals were sacrificed 8 days after primary induction (D8, endpoint) with CO<sub>2</sub>

overdose and cervical dislocation. Mice were opened by cutting through dermal layers from 1 cm proximal to the anus up to the throat. Notes were taken and a histopathological exam was conducted if any abnormality in the volume, color, texture, *etc.* of organs was observed. Colons were harvested, weighed, and pictured prior to further processing. The feces were gently pushed out of the colon. The colon was then separated into 4 parts: the secum was discarded, the middle third was quickly washed in PBS and placed in 10% formalin at 4°C overnight, and the upper and lower third were flash frozen in a slurry of 70% ethanol and dry ice, and then stored at -80°C. The following day, the middle third of colons were moved into separate cassettes and placed in 70% ethanol. Colons remained in ethanol for roughly 3 hours before being processed in a 12-hour protocol using paraffin, HistoClear, and various concentrations of ethanol. Colons were cut into smaller pieces, embedded in paraffin and stored at room temperature. Then 5 µm paraffin sections were stained using hematoxylin and eosin to assess the difference in tissue morphology between T Group, V Group, E Group and H Group. All animal experiments and procedures were performed after approval from the University of California-Irvine (UCI) Institution of Animal Care and Use Committee (IACUC protocol number 2016-3212) and conducted per the Animal Welfare Assurance (#A3416.01).

**Macroscopic colon assessment:** At endpoint mice colons were harvested and pictured for macroscopic scoring. Images were graded by two independent blinded researchers. A scoring method based on Wallace *et al.* was used to determine the health of colons. The scoring goes from 0 (most healthy) to 10 (most diseased). For example, a score of 0: Healthy appearance; 1: Focal hyperemia, slight thickening, no ulcers; 2: Hyperemia, prominent thickening, no ulcers; 3: Ulceration with inflammation at one site; 4: Ulceration with inflammation at two or more sites; 5: Major sites of damage extending > 1 cm; 6-10: When damaged area extends > 2 cm, the score is increased by each additional centimeter of tissue involvement. The animal macroscopic scores per sample were checked for outliers, and outlier scores were not included in analysis. The average of the two macroscopic scores per sample was used for data analysis. Due to some mice dying before endpoint, some colons were not harvestable and are not represented in scoring.

**Luminex serological assay:** Murine blood was collected by tail-tip clip into EDTA-coated collection tubes at

baseline (2-3 days before primary induction), before treatment (D(-3)), and at experimental endpoint (D8) (Figure 4.3). Then the sera were harvested from blood samples after centrifugation. The pro-inflammatory cytokine levels (including IL-1 $\beta$ , TNF- $\alpha$ , IFN- $\gamma$  and IL-6) were determined by Luminex assay following the manufacturer's protocol.

**Histological assessment:** Representative images of H&E stained colons from all three groups were independently scored by two blinded investigators on a scale from 0–4, where 0 = no cell infiltration, villi damage, and 4 = severe immune cell infiltration and destruction of colonic tissue.

**Data Analysis and Statistics:** Data were analyzed by Student's t test. Outliers were removed if data cannot pass Grubbs' test ( $p < 0.05$ ). Log-rank (Mantel-Cox) test was performed for animal survival data analysis. Data were expressed as the mean  $\pm$  SEM, and differences were considered significant at  $p < 0.05$ .

#### 4.6 Acknowledgements

This work was supported by the NIH (R21CA219225 to W.Z.), the DOD (W81XWH-17-1-0522 to W.Z.), and a contract with Baylx Inc. (BI-206512). H.P.F. was supported by the National Institute of Neurological Disorders and Stroke of the NIH (T32NS082174). The content of this paper is solely the responsibility of the authors and does not necessarily represent the official views of the National Institutes of Health.

#### 4.7 References

- 1) Smith DA, Germolec DR. Introduction to Immunology and Autoimmunity. *Environmental Health Perspectives*. 1999;107:5.
- 2) Walsh SJ, Rau LM. Autoimmune Diseases: A Leading Cause of Death Among Young and Middle-Aged Women in the United States. 2000;90(9):4.
- 3) Loftus EV, Jr., Shivashankar R, Tremaine WJ, Harmsen WS, Zinsmeister AR. Updated Incidence and Prevalence of Crohn's Disease and Ulcerative Colitis in Olmsted County, Minnesota (1970-2011). ACG 2014 Annual Scientific Meeting. October 2014.
- 4) Lennard-Jones JE. Classification of Inflammatory Bowel Disease. *Scandinavian Journal of Gastroenterology*. 1989;24(sup170):2-6. doi:10.3109/00365528909091339.
- 5) Sachar DB. The problem of post-operative recurrence of Crohn's disease. *Med Clin North Am*. 1990;74:183-188.
- 6) Rosenblum MD, Gratz IK, Paw JS, Abbas AK. Treating Human Autoimmunity: Current Practice and Future Prospects. *Science Translational Medicine*. 2012;4(125):125sr1-125sr1. doi:10.1126/scitranslmed.3003504.



- 7) Orlicka K, Barnes E, Culver EL. Prevention of infection caused by immunosuppressive drugs in gastroenterology. *Therapeutic Advances in Chronic Disease*. 2013;4(4):167-185. doi:10.1177/2040622313485275.
- 8) Faustman D, Davis M. TNF receptor 2 pathway: drug target for autoimmune diseases. *Nat Rev Drug Discov*. 2010;9(6):482-493. doi:10.1038/nrd3030.
- 9) Theofilopoulos AN, Kono DH, Baccala R. The multiple pathways to autoimmunity. *Nat Immunol*. 2017;18(7):716-724. doi:10.1038/ni.3731.
- 10) Raychaudhuri S. Recent advances in the genetics of rheumatoid arthritis. Published online 2011:18.
- 11) Kozuch PL, Hanauer SB. Treatment of inflammatory bowel disease. A review of medical therapy. *World J Gastroenterol*. 2008;14(3):354-377.
- 12) Rosenblum MD, Gratz IK, Paw JS, Abbas AK. Treating human autoimmunity: current practice and future prospects. *Sci Transl Med*. 2012;4(125):125sr1.
- 13) Gharagozloo M, Majewski S, Foldvari M. Therapeutic applications of nanomedicine in autoimmune diseases: From immunosuppression to tolerance induction. *Nanomedicine: Nanotechnology, Biology and Medicine*. 2015;11(4):1003-1018. doi:10.1016/j.nano.2014.12.003.
- 14) Fan, C. G., Zhang, Q. J. & Zhou, J. R. Therapeutic potentials of mesenchymal stem cells derived from human umbilical cord. *Stem cell reviews* 7, 195-207, doi:10.1007/s12015-010-9168-8 (2011).
- 15) Marbán E. A mechanistic roadmap for the clinical application of cardiac cell therapies. *Nat Biomed Eng*. 2018;2(6):353-361. doi:10.1038/s41551-018-0216-z.
- 16) Liew, A., O'Brien, T. & Egan, L. Mesenchymal stromal cell therapy for Crohn's disease. *Digestive diseases* 32 Suppl 1, 50-60, doi:10.1159/000367826 (2014).
- 17) Ghannam, S., Bouffi, C., Djouad, F., Jorgensen, C. & Noel, D. Immunosuppression by mesenchymal stem cells: mechanisms and clinical applications. *Stem cell research & therapy* 1, 2, doi:10.1186/scrt2 (2010).
- 18) Alessandri G, Emanuelli C, Madeddu P. Genetically Engineered Stem Cell Therapy for Tissue Regeneration. *Annals of the New York Academy of Sciences*. 2004;1015(1):271-284. doi:10.1196/annals.1302.023.
- 19) Esensten JH, Bluestone JA, Lim WA. Engineering Therapeutic T Cells: From Synthetic Biology to Clinical Trials. *Annu Rev Pathol Mech Dis*. 2017;12(1):305-330. doi:10.1146/annurev-pathol-052016-100304.
- 20) Han Y, Li X, Zhang Y, Han Y, Chang F, Ding J. Mesenchymal Stem Cells for Regenerative Medicine. *Cells*. 2019;8(8):886. doi:10.3390/cells8080886.
- 21) Krampera M, Franchini M, Pizzolo G, Aprili G. Mesenchymal stem cells: from biology to clinical use. *Blood Transfusion*. Published online 2007. doi:10.2450/2007.0029-07.
- 22) Erices A., Conget P., Minguell J.J. Mesenchymal progenitor cells in human umbilical cord blood. *Br. J. Haematol*. 2000;109:235-242. doi: 10.1046/j.1365-2141.2000.01986.x
- 23) Jiang D, Scharffetter-Kochanek K. Mesenchymal Stem Cells Adaptively Respond to Environmental Cues Thereby Improving Granulation Tissue Formation and Wound Healing. *Front Cell Dev Biol*. 2020;8:697. doi:10.3389/fcell.2020.00697.
- 24) Pittenger MF, Discher DE, Péault BM, Phinney DG, Hare JM, Caplan AI. Mesenchymal stem cell perspective: cell biology to clinical progress. *npj Regen Med*. 2019;4(1):22. doi:10.1038/s41536-019-0083-6.
- 25) Méndez-Ferrer S, Michurina TV, Ferraro F, et al. Mesenchymal and haematopoietic stem cells form a unique bone marrow niche. *Nature*. 2010;466:829-34.
- 26) Noronha N de C, Mizukami A, Caliári-Oliveira C, et al. Priming approaches to improve the efficacy of mesenchymal stromal cell-based therapies. *Stem Cell Res Ther*. 2019;10(1):131. doi:10.1186/s13287-019-1224-y.
- 27) Wang M, Yuan Q, Xie L. Mesenchymal Stem Cell-Based Immunomodulation: Properties and Clinical Application. *Stem Cells International*. 2018;2018:1-12. doi:10.1155/2018/3057624.

- 28) Secunda R, Vennila R, Mohanashankar AM, Rajasundari M, Jeswanth S, Surendran R. Isolation, expansion and characterisation of mesenchymal stem cells from human bone marrow, adipose tissue, umbilical cord blood and matrix: a comparative study. *Cytotechnology*. 2015;67(5):793-807. doi:10.1007/s10616-014-9718-z.
- 29) Parekkadan B, Milwid JM. Mesenchymal Stem Cells as Therapeutics. *Annu Rev Biomed Eng*. 2010;12(1):87-117. doi:10.1146/annurev-bioeng-070909-105309.
- 30) Wagner W, Wein F, Seckinger A, et al. Comparative characteristics of mesenchymal stem cells from human bone marrow, adipose tissue, and umbilical cord blood. *Experimental Hematology*. 2005;33(11):1402-1416. doi:10.1016/j.exphem.2005.07.003.
- 31) Richardson SM, Kalamegam G, Pushparaj PN, et al. Mesenchymal stem cells in regenerative medicine: Focus on articular cartilage and intervertebral disc regeneration. *Methods*. 2016;99:69-80. doi:10.1016/j.ymeth.2015.09.015.
- 32) Atluri S, Manchikanti L, Hirsch JA. Expanded Umbilical Cord Mesenchymal Stem Cells (UC-MSCs) as a Therapeutic Strategy In Managing Critically Ill COVID-19 Patients: The Case for Compassionate Use. *Pain Physician*.:14.
- 33) McKay Orthopaedic Research Laboratory, University of Pennsylvania, 424 Stemmler Hall, 36th Street and Hamilton Walk, Philadelphia, PA 19104, USA, McLeod C, Mauck R. On the origin and impact of mesenchymal stem cell heterogeneity: new insights and emerging tools for single cell analysis. *eCM*. 2017;34:217-231. doi:10.22203/eCM.v034a14.
- 34) Childs PG, Reid S, Salmeron-Sanchez M, Dalby MJ. Hurdles to uptake of mesenchymal stem cells and their progenitors in therapeutic products. *Biochemical Journal*. 2020;477(17):3349-3366. doi:10.1042/BCJ20190382.
- 35) Tsuchiya A. Clinical trials using mesenchymal stem cells in liver diseases and inflammatory bowel diseases. Published online 2017:15.
- 36) Kode JA, Mukherjee S, Joglekar MV, Hardikar AA. Mesenchymal stem cells: immunobiology and role in immunomodulation and tissue regeneration. *Cytotherapy*. 2009;11(4):377-391.
- 37) Lu LL, Liu YJ, Yang SG, Zhao QJ, Wang X, Gong W, Han ZB, Xu ZS, Lu YX, Liu D, Chen ZZ, Han ZC: Isolation and characterization of human umbilical cord mesenchymal stem cells with hematopoiesis-supportive function and other potentials. *Haematologica*. 2006, 91: 1017-1026.
- 38) Randhawa PK, Singh K, Singh N, Jaggi AS. A review on chemical-induced inflammatory bowel disease models in rodents. *Korean J Physiol Pharmacol*. 2014;18(4):279-288. doi:10.4196/kjpp.2014.18.4.279.
- 39) Marbán E. A mechanistic roadmap for the clinical application of cardiac cell therapies. *Nat Biomed Eng*. 2018; 2:353-361. doi: 10.1038/s41551-018-0216-z
- 40) Morris GP, Beck PL, Herridge MS, De-pew WT, Szewczuk MR, Wallace JL. 1989. Hapten-induced model of colonic inflammation and ulceration in the rat colon. *Gastroenterology* 96:795-803.
- 41) Dave M, Mehta K, Luther J, Baruah A, Dietz AB, Faubion WA. Mesenchymal Stem Cell Therapy for Inflammatory Bowel Disease: A Systematic Review and Meta-analysis. *Inflammatory Bowel Diseases*. 2015;21(11):2696-2707. doi:10.1097/MIB.0000000000000543.
- 42) Ben-Ami E, Berrih-Aknin S, Miller A. Mesenchymal stem cells as an immunomodulatory therapeutic strategy for autoimmune diseases. *Autoimmunity Reviews*. 2011;10(7):410-415. doi:10.1016/j.autrev.2011.01.005.
- 43) Zhou Y, Yamamoto Y, Xiao Z, Ochiya T. The Immunomodulatory Functions of Mesenchymal Stromal/Stem Cells Mediated via Paracrine Activity. *JCM*. 2019;8(7):1025. doi:10.3390/jcm8071025.
- 44) Akiyama K, Chen C, Wang D, et al. Mesenchymal-Stem-Cell-Induced Immunoregulation Involves FAS-Ligand-/FAS-Mediated T Cell Apoptosis. *Cell Stem Cell*. 2012;10(5):544-555. doi:10.1016/j.stem.2012.03.007.

- 45) de Witte SFH, Luk F, Sierra Parraga JM, et al. Immunomodulation By Therapeutic Mesenchymal Stromal Cells (MSC) Is Triggered Through Phagocytosis of MSC By Monocytic Cells: The Fate of MSC Post Infusion. *Stem Cells*. 2018;36(4):602-615. doi:10.1002/stem.2779.
- 46) Fischer UM, Harting MT, Jimenez F, et al. Pulmonary Passage is a Major Obstacle for Intravenous Stem Cell Delivery: The Pulmonary First-Pass Effect. *Stem Cells and Development*. 2009;18(5):683-692. doi:10.1089/scd.2008.0253.
- 47) Fu X-L. Interleukin 6 induces M2 macrophage differentiation by STAT3 activation that correlates with gastric cancer progression. *Cancer Immunol Immunother*. Published online 2017:12.
- 48) Choi W, Lee J, Lee J, Lee SH, Kim S. Hepatocyte Growth Factor Regulates Macrophage Transition to the M2 Phenotype and Promotes Murine Skeletal Muscle Regeneration. *Frontiers in Physiology*. 2019;10:11.
- 49) Hunter MM, Wang A, Parhar KS, et al. In Vitro-Derived Alternatively Activated Macrophages Reduce Colonic Inflammation in Mice. *Gastroenterology*. 2010;138(4):1395-1405. doi:10.1053/j.gastro.2009.12.041
- 50) Goessling W, North TE, Loewer S, et al. Genetic Interaction of PGE2 and Wnt Signaling Regulates Developmental Specification of Stem Cells and Regeneration. *Cell*. 2009;136(6):1136-1147. doi:10.1016/j.cell.2009.01.015
- 51) Zhu W, Yu J, Nie Y, Shi X, Liu Y, Li F, Zhang XL. Disequilibrium of M1 and M2 macrophages correlates with the development of experimental inflammatory bowel diseases. *Immunol Invest* 2014;43:638–652.

# CHAPTER 5

## Meta-analysis of Preclinical Studies of Mesenchymal Stromal Cells to Treat Rheumatoid Arthritis

**Authors:** Linan Liu<sup>1,2,3,4,\*,#</sup>, Chi W. Wong<sup>1,2,3,4,\*</sup>, Menglu Han<sup>1,2,3,4</sup>, **Henry P. Farhoodi**<sup>1,2,3,4</sup>, Guangyang Liu<sup>1,5</sup>, Yongjun Liu<sup>1,2,3,4</sup>, Wenbin Liao<sup>6,†</sup>, Weian Zhao<sup>1,2,3,4,7,†</sup>

<sup>1</sup>Sue and Bill Gross Stem Cell Research Center, 845 Health Sciences Road, University of California-Irvine, Irvine, CA 92697, USA.

<sup>2</sup>Department of Pharmaceutical Sciences, University of California-Irvine, Irvine, CA 92697, USA.

<sup>3</sup>Chao Family Comprehensive Cancer Center, University of California-Irvine, Irvine, CA 92697, USA.

<sup>4</sup>Edwards Life Sciences Center for Advanced Cardiovascular Technology, University of California-Irvine, Irvine, CA 92697, USA.

<sup>5</sup>Department of Surgery, University of California-Irvine, Irvine, CA 92697, USA.

<sup>6</sup>Bayl, Inc., 1 Technology Dr., C511, Irvine, CA 92618, USA.

<sup>7</sup>Departments of Biomedical Engineering and Biological Chemistry, University of California-Irvine, Irvine, CA 92697, USA.

## 5.1 Abstract

**Background:** This study aims to evaluate the quality of preclinical data, determine the effect sizes, and identify experimental measures that inform efficacy using mesenchymal stromal (or stem) cells (MSC) therapy in animal models of rheumatoid arthritis (RA).

**Methods:** Literature searches were performed on MSC preclinical studies to treat RA. MSC treatment effect sizes were determined by the most commonly used outcome measures, including paw thickness, clinical score, and histological score.

**Findings:** A total of 48 studies and 94 treatment arms were included, among which 42 studies and 79 treatment arms reported that MSC improved outcomes. The effect sizes of RA treatments using MSC, when compared to the controls, were: paw thickness was ameliorated by 53.6% (95% confidence interval (CI): 26.7% - 80.4%), histological score was decreased by 44.9% (95% CI: 33.3% - 56.6%), and clinical score was decreased by 29.9% (95% CI: 16.7% - 43.0%). Specifically, our results indicated that human umbilical cord derived MSC led to large improvements of the clinical score (-42.1%) and histological score (-51.4%).

**Interpretation:** To the best of our knowledge, this meta-analysis is to quantitatively answer whether MSC represent a robust RA treatment in animal models. It suggests that in preclinical studies, MSC have consistently exhibited therapeutic benefits. The findings demonstrate a need for considering variations in different animal models and treatment protocols in future studies using MSC to treat RA in humans to maximise the therapeutic gains in the era of precision medicine.

**Keywords:** Mesenchymal stromal (or stem) cells; MSC; Rheumatoid arthritis; Pre-clinical study; Clinical trials; Meta-analysis.

## 5.2 Introduction

Rheumatoid arthritis (RA) is a chronic autoimmune disease and systemic disorder that primarily affects the joints(1). In RA, the immune system attacks the synovial membrane, causing chronic inflammation, disintegration of bone and cartilage, and potential damage to other organs(2, 3). In the United States, it is estimated that about 1.5 million adults are affected by RA(4). The conventional treatment regimen is a progression through corticosteroids, non-steroidal anti-inflammatory drugs (NSAIDs), non-biologic disease-modifying anti-rheumatic drugs (DMARDs), and biologic DMARDs (*e.g.*, anti-tumour necrosis factor (anti-TNF)(5, 6). Unfortunately, 15-40% of RA patients become resistant to long-term treatments and can become non-responsive to all existing clinical therapies(7, 8). Therefore, there is an exigent need for novel RA therapies(9, 10).

Stem cell therapies are emerging as potential medical treatments for RA. In particular, mesenchymal stem or stromal cells (MSC) are a type of multipotent adult stem cells, which are currently used in many clinical trials. Cells meeting the MSC minimal criteria (per International Society for Cell Therapy guidelines)(11) have been isolated from bone marrow (BM)(12, 13), adipose tissues (AD)(14-16), umbilical cord (UC)(17-19) and gingival tissue (G)(20, 21). They can be quickly expanded *in vitro* and used as an “off-the-shelf” allogeneic cell therapy due to their immune-evasive properties(22). From animal models to clinical trials, MSC have shown promise in the treatment of many diseases including tissue injuries and immune disorders(22-26). In particular, MSC have been widely investigated for their beneficial therapeutic effects in rheumatic diseases(27, 28) including RA, in both preclinical studies (29) and clinical studies (30-33). Possible mechanisms of MSC combating RA include MSC-immune cell contact, induced death of effector lymphocytes and/or induction of regulatory T (Treg) cells, and production of soluble mediators, including anti-inflammatory cytokines such as Transforming growth factors (TGFs) and Indoleamine 2, 3-Dioxygenase (IDO)(34-36). Preliminary insight of mechanism of action (MOA) based on the use of MSC derived from human umbilical cords (hUC-MSC) in RA treatment in human clinical trials revealed

increased levels of CD4<sup>+</sup> CD25<sup>+</sup> Foxp3<sup>+</sup> Treg cells and decreased levels of pro-inflammatory factors including IL-6 and TNF-alpha in circulation(30, 33).

The purpose of this meta-analysis is to review and analyse preclinical studies of MSC in the treatment of RA. Several variables were compared, including donor species, tissues of origin, routes of administration, transplant types (*i.e.*, autologous, allogeneic and xenogeneic). This meta-analysis also aims to identify optimal treatment variables and conditions by meta-regression and subgroup analysis, which can inform future experimental and trial designs. This analysis began by reviewing each study's quality using an Risk of bias (RoB) tool for animal intervention studies, presented by the SYstematic Review Centre for Laboratory Animal Experimentation (SYRCLE): SYRCLE's RoB tool(37). Next, the effect size of MSC treatment was determined for the clinical score, paw thickness and histological scores. Finally, the MSC efficacy was examined across several variables of interest including dosage, number of injections, tissue source of MSC, MSC donor species, and other parameters listed in Table 5.1 and 5.2.

### 5.3 Materials and methods

**Effect size estimation.** The effect sizes of MSC therapy were analysed based on the three different indicators most frequently used in preclinical MSC in RA animal studies: (1) clinical score (a semi-quantitatively summative macroscopic measure of animal anatomical conditions), (2) histological score (a pathological microscopic measure of joint conditions), and (3) paw thickness (a measurement of paw swelling to determine arthritis severity)(38). Due to methodical variations in histology scoring, we separated histological data into a "general" score if the paper combined several scoring parameters into an overall score. In papers that listed individual histology assessment parameters (bone erosion, cartilage damage, and inflammation) we reported them individually. We averaged (presented as mean) both general and individual histological scores of each treatment arm. The changes in mean clinical scores and paw thickness were evaluated with the measurements before and after

MSC treatments. If the changes in clinical score and paw thickness were not provided directly from the included literature, these indicators were calculated by subtracting the mean endpoint measurement by the baseline (standard deviations were estimated by assuming all the measurements were independent). All treatment arms included in the quantitative meta-analysis used PBS as the control group, which is the most commonly used control, although some high-quality studies included multiple control groups (e.g. fibroblast and methotrexate). All study design differences were normalised before comparing the PBS treated RA group and MSC treatment RA group. Normalisation of data and effect sizes were determined by the method outlined in Vesterinen, *et al.* 2013. In brief, the effect sizes were normalised to the sham control group (*i.e.* healthy animals)(39). If there was no difference between the MSC treated RA group and the sham control group, it was scored 0. The directionality was positive if indicating more pathological conditions, therefore a higher score means worse disease conditions. Thus, positive efficacy from MSC treated RA group shows a negative normalised value. The effect sizes were estimated by subtracting the normalised values of the MSC treated RA group by the PBS treated RA group. All the effect sizes are unitless due to normalisation (Eq. 1). Some studies included multiple treatment arms, so to avoid overestimating treatment effects and unit-of-analysis error, we split the PBS treated RA group so that it could be compared to each treatment arm separately, without being counted more than once. If there were not enough PBS-treated RA mice to split, the MSC treated groups were combined. Standardised mean difference (SMD) using exact Hedge’s G effect sizes was also performed as sensitivity analysis.

$$ES_i = 100\% \times \frac{(\bar{x}_c - \bar{x}_{sham}) - (\bar{x}_{rx} - \bar{x}_{sham})}{(\bar{x}_c - \bar{x}_{sham})} \times direction \quad (Eq.1)$$

**Statistical analysis, subgroup analysis and meta-regression.** The random-effects model method in the *R* package “*meta*” was used to calculate the mean effect size, 95% CIs, forest plots, and significance. Heterogeneity was calculated/analysed in the restricted maximum-likelihood estimator (REML) with the  $I^2$  and  $\tau^2$  values, which are the ratio of true heterogeneity to total observed variation and the variance between studies respectively. A subgroup analysis was conducted using routes of administration, donor



species, transplant types, or tissue of origin of MSC as categorical variables assuming there is a common  $\tau^2$  among the groups. A mixed-effects model of regression was performed in the “*metafor*” package in *R* to address heterogeneity. Variations in MSC tissues of origin, MSC donor species, routes of administration, dosage of administration, number of injections and transplant types were tested as covariate separately. After fitting moderators, residual heterogeneity was assessed by the “adjusted  $R^2$  value”, which can be used to test variation in the effect size. Potential interactions between the moderators were also tested. An omnibus test, as well as all pairwise comparisons between the factor levels, were used for the statistical test of the moderator, and a likelihood ratio test (LRT) was used to test the interaction. The confidence intervals were adjusted with the Knapp-Hartung method. The  $p$ -value threshold was set to 0.1 for heterogeneity, to increase the power of the test, and 0.05 for other tests. Funnel plots were drawn with the *meta* package to assess the publication bias, if there were at least nine included studies in that indicator. Trim and fill correction were done where there was significant asymmetry of the plot.

## **5.4 Results**

### **5.4.1 Study characteristics**

The article selection process is summarised in Supplementary Figure 5.1 (See Supplementary Materials). Literature searches retrieved 4745 articles from PubMed and the Institute for Scientific Information Web of Science, in which 661 were duplicates. A total of 3912 articles were excluded by title alone. Overall, articles were screened by title and abstract, however, a further 111 did not meet the inclusion criteria. The remaining 61 full text articles were assessed for eligibility resulting in 48 articles meeting the criteria to be included in the meta-analysis review (Table 5.1).

A total of 48 studies and 94 treatment arms were identified (Table 5.1), which were further categorised based on experimental variables of interest listed in Table 5.2. In this meta-analysis,

**Table 5.1: Pre-clinical studies using MSC to treat RA included in this study**

| Author (year)                               | Arm | P b 0.05 | MSC favor? | Origin      | Donor  | Control   | Transplant type | Treatment protocol              | Rept  | Age    | n    |
|---|-----|----------|------------|-------------|--------|-----------|-----------------|---------------------------------|-------|--------|------|
| Zhou et al. (2011) <sup>51</sup>            | 1   | Y        | Y          | AD          | Human  | PBS/Other | Xenogenic       | CIA, no booster, IV, Multiple   | Mouse | 8w     | 10   |
| #Garimella, et al. (2015) <sup>52</sup>     | 1   | Y        | Y          | AD          | Murine | PBS       | Autologous      | CIA, with booster, IP, Single   | Mouse | 8-10w  | 6-7  |
| Chen et al. (2013) <sup>53</sup>            | 1   | Y        | Y          | Other (G)   | Human  | Nil       | Xenogenic       | CIA, IV, Single                 | Mouse | 8-10w  | 6    |
|   | 2   | Y        | Y          | Other (G)   | Human  | Nil       | Xenogenic       | CIA, IV, Single                 | Mouse | 8-10w  | 6    |
|   | 3   | Y        | Y          | Other (G)   | Human  | Nil       | Xenogenic       | CIA, IV, Single                 | Mouse | 8-10w  | 6    |
| Lee et al. (2015) <sup>54</sup>             | 1   | Y        | Y          | BM          | Other  | PBS       | Xenogenic       | CIA, with booster, IP, Multiple | Mouse | 7-9w   | 5    |
|   | 2   | Y        | Y          | Other (SF)  | Other  | PBS       | Xenogenic       | CIA, with booster, IP, Multiple | Mouse | 7-9w   | 5    |
| Augello et al. (2007) <sup>55</sup>         | 1   | N        | Y          | BM          | Murine | PBS       | Allogeneic      | CIA, with booster, IP, Multiple | Mouse | 6w     | 6    |
| #Chen et al. (2009) <sup>56</sup>           | 1   | Y        | N          | BM          | Murine | Nil       | Autologous      | CIA, with booster, IV, Single   | Mouse | 8-10w  | N/A  |
| Lopez-Santalla, et al. (2015) <sup>57</sup> | 1   | Y        | Y          | AD          | Human  | Other     | Xenogenic       | CIA, with booster, IV, Single   | Mouse | 8w     | 64   |
| #Greish et al. (2012) <sup>58</sup>         | 1   | Y        | Y          | UC          | Human  | PBS/Other | Xenogenic       | AIA, no booster, IA, Single     | Rat   | N/A    | 8    |
| Gonzalo-Gil, et al. (2016) <sup>59</sup>    | 1   | Y        | Y          | Other (ESC) | Human  | PBS       | Xenogenic       | CIA, IP, Single                 | Mouse | 10w    | 7    |
|   | 2   | Y        | Y          | Other (ESC) | Human  | PBS       | Xenogenic       | CIA, IP, Multiple               | Mouse | 10w    | 4    |
|   | 3   | Y        | Y          | Other (ESC) | Human  | PBS       | Xenogenic       | CIA, IP, Multiple               | Mouse | 10w    | 20   |
| Mao et al. (2010) <sup>510</sup>            | 1   | Y        | Y          | N/A         | Rat    | PBS       | Xenogenic       | CIA, with booster, IV, Multiple | Mouse | 8w     | 6    |
| #Swart et al. (2016) <sup>511</sup>         | 1   | Y        | Y          | BM          | Murine | PBS       | Autologous      | hPG, IP, Multiple               | Mouse | N/A    | 10   |
|   | 2   | Y        | Y          | BM          | Murine | PBS       | Autologous      | hPG, IA, Multiple               | Mouse | N/A    | 10   |
| #Papado-poulou et al. (2012) <sup>512</sup> | 1   | N        | N          | BM          | Rat    | PBS/Other | Allogeneic      | AIA, IV, Single                 | Rat   | 7w     | 4-5  |
|   | 2   | N        | N          | BM          | Rat    | PBS/Other | Allogeneic      | AIA, IV, Multiple               | Rat   | 7w     | 4-5  |
|   | 3   | N        | N          | BM          | Rat    | PBS/Other | Allogeneic      | AIA, IP, Multiple               | Rat   | 7w     | 4-5  |
|   | 4   | N        | N          | BM          | Rat    | PBS/Other | Allogeneic      | AIA, IBM, Multiple              | Rat   | 7w     | 4-5  |
|   | 5   | N        | N          | BM          | Rat    | PBS/Other | Allogeneic      | AIA, IS, Multiple               | Rat   | 7w     | 4-5  |
|   | 6   | Y        | Y          | BM          | Murine | PBS/Other | Allogeneic      | STA, IP, Multiple               | Mouse | 7w     | 4-5  |
| Rui et al. (2016) <sup>513</sup>            | 1   | Y        | Y          | BM          | Murine | PBS       | Allogeneic      | CIA, with booster, IV, Multiple | Mouse | 8-10w  | 6    |
|   | 2   | Y        | Y          | Other (OE)  | Murine | PBS       | Allogeneic      | CIA, with booster, IV, Multiple | Mouse | 8-10w  | 6    |
| #Djouad et al. (2005) <sup>514</sup>        | 1   | N        | Y          | N/A         | Murine | N/A       | Allogeneic      | CIA, with booster, IV, Single   | Mouse | 8-10w  | 5-11 |
|   | 2   | N        | N          | N/A         | Murine | N/A       | Allogeneic      | CIA, with booster, IV, Single   | Mouse | 8-10w  | 5-11 |
|   | 3   | N        | Y          | N/A         | Murine | N/A       | Allogeneic      | CIA, with booster, IP, Single   | Mouse | 8-10w  | 5-11 |
|   | 4   | N        | Y          | N/A         | Murine | N/A       | Allogeneic      | CIA, with booster, IM, Single   | Mouse | 8-10w  | 5-11 |
|   | 5   | N        | Y          | N/A         | Murine | N/A       | Allogeneic      | CIA, with booster, IA, Single   | Mouse | 8-10w  | 5-11 |
| Santos et al. (2013) <sup>515</sup>         | 1   | N        | Y          | UC          | Human  | PBS       | Xenogenic       | AIA, no booster, IA, Multiple   | Rat   | 16w    | 8    |
|   | 2   | N        | Y          | UC          | Human  | PBS       | Xenogenic       | AIA, no booster, IA, Multiple   | Rat   | 16w    | 8    |
|   | 3   | Y        | Y          | UC          | Human  | PBS       | Xenogenic       | AIA, no booster, IP, Multiple   | Rat   | 16w    | 8    |
| Wu et al. (2012) <sup>516</sup>             | 1   | N        | Y          | UC          | Human  | PBS       | Xenogenic       | CIA, with booster, IA, Single   | Mouse | 7-8w   | 6    |
| Kim et al. (2014) <sup>517</sup>            | 1   | N        | Y          | AD          | Human  | PBS       | Xenogenic       | Curdian, IP, Multiple           | Mouse | 10-12w | 6    |
| Liu et al. (2010) <sup>518</sup>            | 1   | Y        | Y          | UC          | Human  | PBS/Other | Xenogenic       | CIA, with booster, IP, Multiple | Mouse | 6-8w   | 10   |
| Shu et al. (2015) <sup>519</sup>            | 1   | Y        | Y          | Other (AM)  | Human  | Nil/PBS   | Xenogenic       | CIA, with booster, IP, Single   | Rat   | N/A    | 6    |
| Park et al. (2016) <sup>520</sup>           | 1   | Y        | Y          | UC          | Human  | Other     | Xenogenic       | CIA, with booster, IV, Multiple | Mouse | 8w     | 5    |
|   | 2   | Y        | Y          | BM          | Human  | Other     | Xenogenic       | CIA, with booster, IV, Multiple | Mouse | 8w     | 5    |
|   | 3   | Y        | Y          | AD          | Human  | Other     | Xenogenic       | CIA, with booster, IV, Multiple | Mouse | 8w     | 5    |
|   | 4   | Y        | Y          | UC          | Human  | Other     | Xenogenic       | CIA, with booster, IV, Multiple | Mouse | 8w     | 5    |
|   | 5   | Y        | Y          | BM          | Human  | Other     | Xenogenic       | CIA, with booster, IV, Multiple | Mouse | 8w     | 5    |
|   | 6   | Y        | Y          | AD          | Human  | Other     | Xenogenic       | CIA, with booster, IV, Multiple | Mouse | 8w     | 5    |
|   | 7   | Y        | Y          | BM          | Human  | Other     | Xenogenic       | CIA, with booster, IV, Multiple | Mouse | 8w     | 5    |
|   | 8   | Y        | Y          | BM          | Human  | Other     | Xenogenic       | CIA, with booster, IV, Multiple | Mouse | 8w     | 5    |
|   | 9   | Y        | Y          | BM          | Human  | Other     | Xenogenic       | CIA, with booster, IV, Multiple | Mouse | 8w     | 5    |
| #Gonzalez et al. (2009) <sup>521</sup>      | 1   | Y        | Y          | AD          | Human  | PBS/Other | Xenogenic       | CIA, with booster, IP, Multiple | Mouse | 7-10w  | 8-11 |
|   | 2   | Y        | Y          | AD          | Murine | PBS/Other | Allogeneic      | CIA, with booster, IP, Multiple | Mouse | 7-10w  | 8-10 |
|   | 3   | Y        | Y          | AD          | Murine | PBS/Other | Autologous      | CIA, with booster, IP, Multiple | Mouse | 7-10w  | 8-10 |
|   | 4   | Y        | Y          | AD          | Human  | PBS/Other | Xenogenic       | CIA, with booster, IA, Single   | Mouse | 7-10w  | 8-11 |
| #Zhao et al. (2015) <sup>522</sup>          | 1   | Y        | Y          | UC          | Human  | PBS/Other | Xenogenic       | CIA, with booster, IV, Single   | Rat   | 8w     | N/A  |
| #Bouffi et al. (2010) <sup>523</sup>        | 1   | Y        | Y          | BM          | Murine | N/A       | Autologous      | CIA, with booster, IV, Multiple | Mouse | 9-10w  | N/A  |
|   | 2   | Y        | Y          | BM          | Murine | N/A       | Allogeneic      | CIA, with booster, IV, Multiple | Mouse | 9-10w  | N/A  |
|   | 3   | Y        | Y          | BM          | Murine | N/A       | Autologous      | CIA, with booster, IV, Multiple | Mouse | 9-10w  | N/A  |
|   | 4   | Y        | Y          | BM          | Murine | N/A       | Autologous      | CIA, with booster, IV, Multiple | Mouse | 9-10w  | N/A  |
|   | 5   | Y        | Y          | BM          | Murine | N/A       | Autologous      | CIA, with booster, IV, Multiple | Mouse | 9-10w  | N/A  |
|   | 6   | Y        | Y          | BM          | Murine | N/A       | Autologous      | CIA, with booster, IV, Multiple | Mouse | 9-10w  | N/A  |
|   | 7   | Y        | Y          | BM          | Murine | N/A       | Autologous      | CIA, with booster, IV, Multiple | Mouse | 9-10w  | N/A  |
| Sullivan et al. (2012) <sup>524</sup>       | 1   | Y        | N          | BM          | Murine | PBS       | Autologous      | CIA, with booster, IV, Single   | Mouse | 7-9w   | 12   |
|   | 2   | Y        | N          | BM          | Murine | PBS       | Allogeneic      | CIA, with booster, IV, Single   | Mouse | 7-9w   | 12   |
|   | 3   | Y        | N          | BM          | Murine | PBS       | Allogeneic      | CIA, with booster, IV, Single   | Mouse | 7-9w   | 12   |
| Schurgers et al. (2010) <sup>525</sup>      | 1   | N        | N          | BM          | Murine | PBS       | Autologous      | CIA, no booster, IV, Single     | Mouse | 8-12w  | 9    |
| Liu et al. (2015) <sup>526</sup>            | 1   | Y        | Y          | UC          | Human  | PBS       | Xenogenic       | CIA, with booster, IV, Single   | Mouse | 6-8w   | 5    |
| Choi et al. (2008) <sup>527</sup>           | 1   | N        | N          | BM          | Murine | PBS       | Autologous      | CIA, with booster, IV, Multiple | Mouse | 8-12w  | 10   |
| Park et al. (2011) <sup>528</sup>           | 1   | N        | N          | BM          | Murine | PBS       | Autologous      | CIA, with booster, IP, Single   | Mouse | N/A    | 6    |
| Parolini et al. (2014) <sup>529</sup>       | 1   | Y        | Y          | Other (AM)  | Human  | PBS       | Xenogenic       | CIA, with booster, IP, Multiple | Mouse | 8w     | 8-10 |
|   | #2  | Y        | Y          | Other (AM)  | Murine | PBS       | Allogeneic      | CIA, with booster, IP, Multiple | Mouse | 8w     | 8-10 |

**Table 5.1 cont.**

| Author (year)                               | Arm | P b 0.05 | MSC favor? | Origin      | Donor  | Control   | Transplant type | Treatment protocol              | Rept  | Age   | n   |
|---|-----|----------|------------|-------------|--------|-----------|-----------------|---------------------------------|-------|-------|-----|
| Sullivan et al. (2013) <sup>530</sup>       | 1   | N        | N          | BM          | Murine | PBS       | Allogeneic      | CIA, with booster, IV, Single   | Mouse | 7-9w  | 10  |
| El-Denshary, et al. (2013) <sup>531</sup>   | 1   | Y        | Y          | BM          | Murine | PBS       | Allogeneic      | CIA, with booster, IV, Single   | Mouse | 6w    | 10  |
| Choi et al. (2016) <sup>532</sup>           | 1   | Y        | Y          | AD          | Human  | PBS       | Xenogenic       | CIA, with booster, IV, Multiple | Mouse | 8w    | 12  |
| #Luz-Crawford, et al. (2015) <sup>533</sup> | 1   | Y        | Y          | BM          | Murine | PBS/Other | Allogeneic      | CIA, with booster, IV, Multiple | Mouse | 9-10w | 16  |
| Kehoe et al. (2014) <sup>534</sup>          | 1   | Y        | Y          | BM          | Murine | PBS       | Autologous      | AIA, IA, Single                 | Mouse | 7-8w  | 6   |
| Gu et al. (2016) <sup>535</sup>             | 1   | Y        | Y          | Other (G)   | Murine | PBS       | Allogeneic      | CIA, with booster, IV, Single   | Mouse | 6-8w  | 6   |
| Luo et al. (2019) <sup>536</sup>            | 1   | Y        | Y          | Other (G)   | Human  | Nil       | Xenogenic       | CIA, IV, Single                 | Mouse | 8-10w | 6   |
|   | 2   | Y        | Y          | Other (G)   | Human  | Nil       | Xenogenic       | CIA, IV, Single                 | Mouse | 8-10w | 4   |
| Nam et al. (2018) <sup>537</sup>            | 1   | Y        | Y          | BM          | Human  | Nil       | Xenogenic       | CAIA, IP, Multiple              | Mouse | 6w    | 10  |
| Park et al. (2017) <sup>538</sup>           | 1   | Y        | Y          | BM          | Human  | Nil       | Xenogenic       | CIA, IP, Multiple               | Mouse | 6w    | 5   |
| Shin et al. (2016) <sup>539</sup>           | 1   | Y        | Y          | Other (UCB) | Human  | Nil       | Xenogenic       | CIA, with booster, IP, Multiple | Mouse | 6-8w  | 5   |
|   | 2   | Y        | Y          | Other (UCB) | Human  | Nil       | Xenogenic       | CIA, with booster, IV, Single   | Mouse | 6-8w  | 7   |
| Feng et al. (2018) <sup>540</sup>           | 1   | Y        | Y          | UC          | Human  | PBS       | Xenogenic       | CIA, with booster, IV, Single   | Mouse | N/A   | 5   |
| Zhang et al. (2019) <sup>541</sup>          | 1   | Y        | Y          | BM          | Human  | PBS       | Xenogenic       | CIA, with booster, IV, Single   | Mouse | 8w    | 6   |
|   | 2   | Y        | Y          | UC          | Human  | PBS       | Xenogenic       | CIA, with booster, IV, Single   | Mouse | 8w    | 6   |
|   | 3   | Y        | Y          | Other (ED)  | Human  | PBS       | Xenogenic       | CIA, with booster, IV, Single   | Mouse | 8w    | 6   |
| #Tian et al. (2019) <sup>542</sup>          | 1   | Y        | Y          | BM          | Rat    | PBS       | Autologous      | CIA, with booster, IV, Single   | Rat   | 3-4w  | N/A |
| Abd-Elhalem et al. (2018) <sup>543</sup>    | 1   | Y        | Y          | BM          | Rat    | Nil       | Autologous      | AIA, with booster, Transplant   | Rat   | 6w    | 6   |
| Mancheño-Corvo et al. (2017) <sup>544</sup> | 1   | Y        | Y          | AD          | Human  | Ringer    | Xenogenic       | CIA, with booster, IL, Multiple | Mouse | 8w    | 34  |
|   | 2   | Y        | Y          | AD          | Human  | Ringer    | Xenogenic       | CIA, with booster, IL, Multiple | Mouse | 8w    | 34  |
|   | 3   | N        | N          | AD          | Human  | Ringer    | Xenogenic       | CIA, with booster, IV, Multiple | Mouse | 8w    | 40  |
| Li et al. (2017) <sup>545</sup>             | 1   | Y        | Y          | BM          | Murine | Nil       | Autologous      | CIA, with booster, IV, Multiple | Mouse | 7w    | 5   |
| Yan et al. (2017) <sup>546</sup>            | 1   | Y        | Y          | SM          | Human  | PBS       | Xenogenic       | CIA, with booster, IA, Multiple | Mouse | 7-9w  | 8   |
| Sun et al. (2017) <sup>547</sup>            | 1   | N        | Y          | UC          | Human  | PBS       | Xenogenic       | CIA, with booster, IP, Single   | Mouse | 6-8w  | 5   |
| Yu et al. (2018) <sup>548</sup>             | 1   | Y        | Y          | Other (UCB) | Human  | PBS       | Xenogenic       | CIA, with booster, IV, Multiple | Mouse | 6w    | 5   |
|   | 2   | Y        | Y          | Other (UCB) | Human  | PBS       | Xenogenic       | CIA, with booster, IV, Multiple | Mouse | 6w    | 5   |
|   | 3   | Y        | Y          | Other (UCB) | Human  | PBS       | Xenogenic       | CIA, with booster, IV, Multiple | Mouse | 6w    | 5   |

*Abbreviations: Age: age of induction; AA: adjuvant-induced arthritis; AD: adipose tissue; AIA: adjuvant-induced arthritis; AM: amniotic membrane; BM: bone marrow; CAIA: collagen antibody-induced arthritis; CarrIA: carrageenan-induced arthritis; CIA: collagen-induced arthritis; ED: Exfoliated deciduous teeth; ESC: Embryonic stem cells; GI: gingival tissue; hPG: proteoglycan-induced arthritis; IA: intra-articular injection; IBM: intra-bone marrow injection; IL: intralymphatic injection; IM: intramuscular injection; IP: intraperitoneal injection; IS: intrasplenic injection; IV: intravenous injection; Multiple: multiple injections; n: sample size; N/A: not reported; OE: Olfactory ecto; OIA: ovalbumin-induced arthritis; Origin: tissue of origin; PBS: phosphate-buffered saline; Rept: recipient specie; Ringer: Ringer's Lactate; SC: subcutaneous injection; SF: Synovial fluid; Single: single injection; SM: Synovial Membrane; STA: K/BxN serum-transfer arthritis; UC: umbilical cord tissue; UCB: umbilical cord blood; w: weeks.*

*#: studies that have been excluded from the parametric meta-analysis due to missing values or high risk of biases.*

86.2% of the treatment arms used mouse models, and 13.8% of the treatment arms used rat models. The RA models included mainly collagen-induced arthritis (CIA) induction (83.0%) and adjuvant-induced arthritis (AIA) induction (11.7%). Among 94 treatment arms, 72.3% used an immunisation booster for model induction. Human derived MSC were used in 52.1% of the 94 treatment arms, 37.2% used murine MSC, and 8.5% used rat derived MSC. The tissue of origin of MSC varied by study, such that 13.8% of 94 treatment arms used umbilical cord, 42.6% bone marrow, and 14.9% adipose. Other MSC tissue of

origin including gingiva was used in 28.7% of the treatment arms. Transplant types were also compared, such that 55.3% of the 94 treatment arms were xenogeneic, 24.5% allogeneic, and 20.2% autologous. The routes of administration were intravenous (IV) injection in 57.4% of 94 treatment arms, 26.6% intraperitoneal (IP) injection and 9.6% intra-articular (IA) injection (Table 5.1 and 5.2).

#### **5.4.2 Quality of included studies**

The quality of studies was assessed (Supplemental Figure 5.2, Supplementary Materials). Most studies avoided selection/reporting bias, and all reported the baseline characteristics (Q2). Selective outcome (Q9) and other sources of bias (Q10) appeared to be low in these reports. Nonetheless, few studies attempted to report the strategies to mitigate potential performance bias, detection bias and attrition bias. Therefore, there was uncertainty regarding the actual risk of bias. Notably, some of the studies included blindness on evaluation protocol (Q7: 35.42% of “yes”) in their study.

#### **5.4.3 Effect size**

Three indicators were used to study effect sizes in this meta-analysis review: (1) clinical score, (2) histological score, and (3) paw thickness. Qualitative analysis was done to show the effect size of MSC administration in preclinical studies of RA (Table 2). MSC improved outcomes (*i.e.*, at least one indicator was improved) in 87.5% of the 48 studies and in 84.0% of the 94 treatment arms (Tables 5.1 and 5.2). Clinical score difference was used to illustrate effect size for MSC administration in 73.4% of the 94 treatment arms, 38.3% included histological scoring and 39.4% included paw thickness difference. In terms of clinical score, 87.0% of 69 treatment arms favoured MSC treatment, while 13.0% favoured the PBS control treatment. Histological scoring showed 91.7% of the 36 total treatment arms favoured MSC treatment, vs 8.3% for PBS control. Finally, paw thickness measurements showed 94.6% of the 37 treatment arms favoured MSC treatment, vs 5.4% for PBS control. Interestingly, 60.0% of the treatment arms that favoured PBS control treatment used MSC derived from mice; however, 98.0% of human derived MSC improved RA pathophysiology (Table 5.2).

Quantitatively, clinical scores of the MSC treated RA groups were reduced by an average of 29.9% compared to the PBS treated RA groups (Figure 5.1). While this reduction was statistically significant

**Table 5.2. Study arms categorized by experimental variables of interest and their qualitative effect size.**

| Experimental variables  | Total no. of arms | Favor MSC | Favor control |
|-------------------------|-------------------|-----------|---------------|
|                         | 94                | 79        | 15            |
| Donor species           |                   |           |               |
| Human                   | 49                | 48        | 1             |
| Mouse                   | 35                | 26        | 9             |
| Rat                     | 8                 | 3         | 5             |
| Others                  | 2                 | 2         | 0             |
| Recipient species       |                   |           |               |
| Mouse                   | 81                | 71        | 10            |
| Rat                     | 13                | 8         | 5             |
| MSC transplant types    |                   |           |               |
| Autologous              | 19                | 14        | 5             |
| Allogeneic              | 23                | 14        | 9             |
| Xenogenic               | 52                | 51        | 1             |
| MSC tissue of origin    |                   |           |               |
| Umbilical cord          | 13                | 13        | 0             |
| Bone marrow             | 40                | 27        | 13            |
| Adipocyte               | 14                | 13        | 1             |
| Others/Unknown          | 27                | 26        | 1             |
| Route of administration |                   |           |               |
| IV                      | 54                | 43        | 11            |
| IP                      | 25                | 23        | 2             |
| IA                      | 9                 | 9         | 0             |
| Others                  | 6                 | 4         | 2             |
| RA model                |                   |           |               |
| CIA                     | 78                | 68        | 10            |
| AIA                     | 11                | 6         | 5             |
| Others                  | 5                 | 5         | 0             |

( $p$ -value < 0.0001), it contained both total and sampling variabilities. The estimated total heterogeneity ( $\tau^2$ ) was 0.1524, and  $I^2$ , which is defined as a ratio of total heterogeneity to total variability, was 96% ( $p$ -value < 0.0001)(39). Second, there was a 44.9% decrease in histological scores ( $p$ -value < 0.0001) in MSC treated groups compared to PBS groups in 8 studies (with 9 treatment arms) which used a general histological score obtained by summarising

the pathological condition of the joint tissues (Figure 5.2a). Despite the heterogeneity of this indicator being statistically significant ( $p$ -value  $< 0.0001$ ), it is much lower than the clinical score heterogeneity. Some of the studies grouped histology measurements into categories, such as

### Normalised Mean Differences of Clinical Score Increments (General)

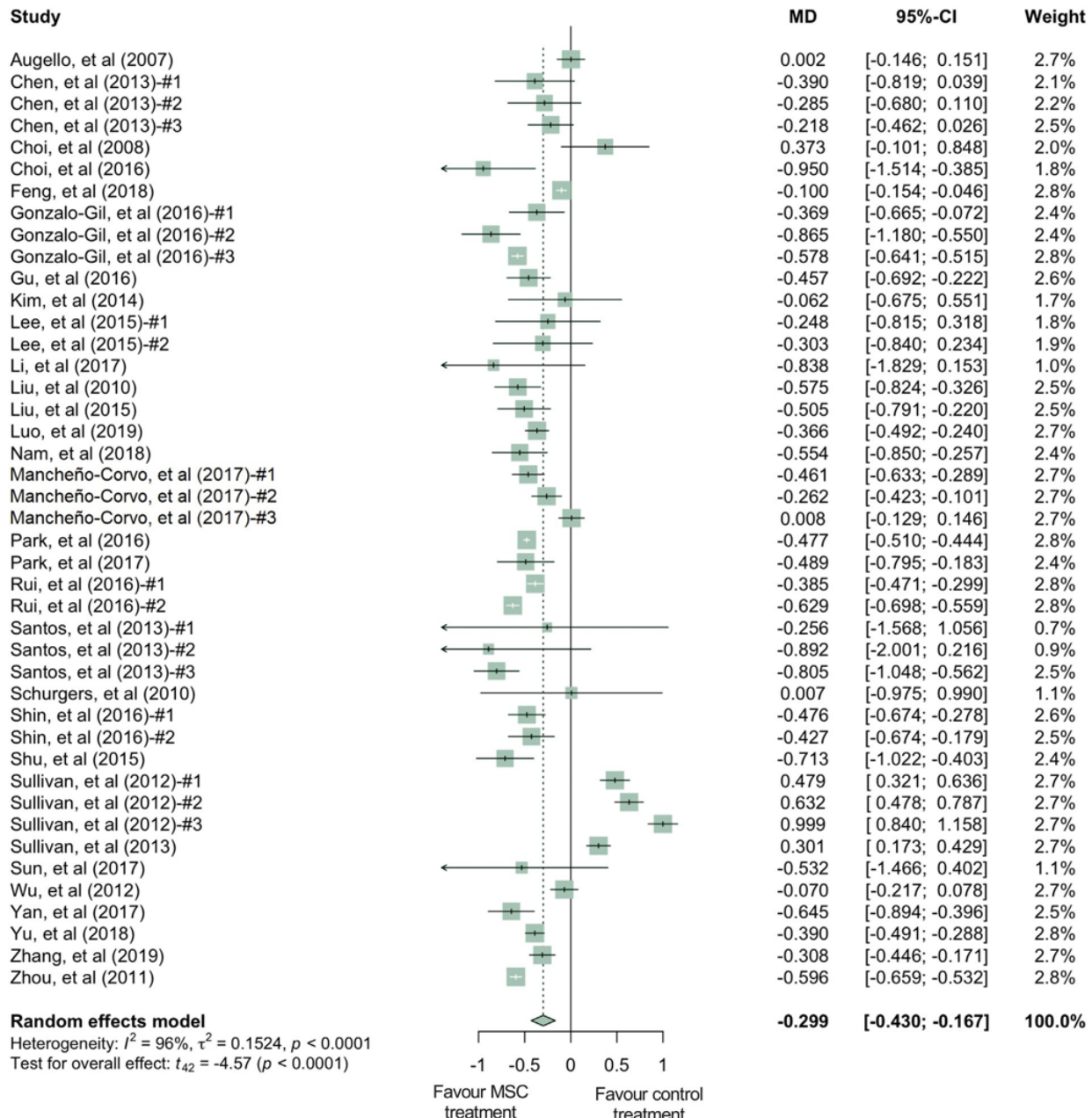
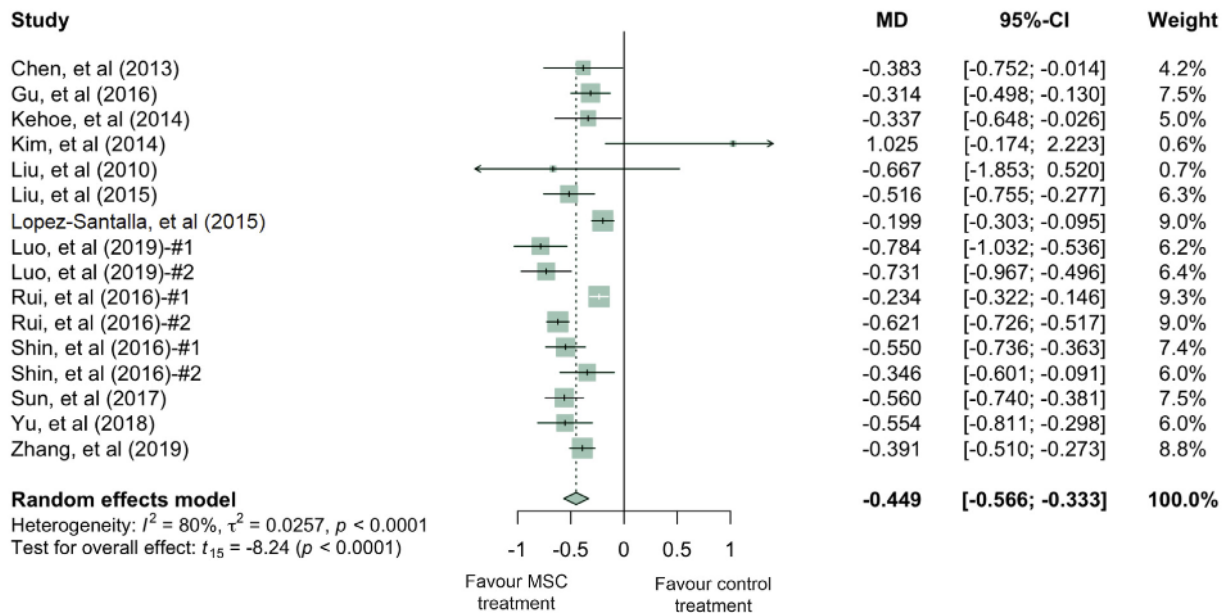


Figure 5.1. Forest plots showing the normalized mean difference (MD) and 95% CI of the clinical score for each study

**included in the meta-analysis.** The graph was generated using the meta package in R. All results have been normalized with sham control group as described in the methods. For all the plots, the vertical line indicates no effect, left hand side indicates favoring MSC treatment while right side indicates favoring PBS control treatment. The size of the box indicates the weighting of each study, and the thin horizontal whisker indicates the 95% CI. Random-effects model was used to summarize the effect sizes. Heterogeneity is denoted by the I2 and  $\tau^2$ .

**a**

**Normalised Mean Differences of Histological Score (General)**



**b**

**Normalised Mean Differences of Paw Thickness Increments (General)**

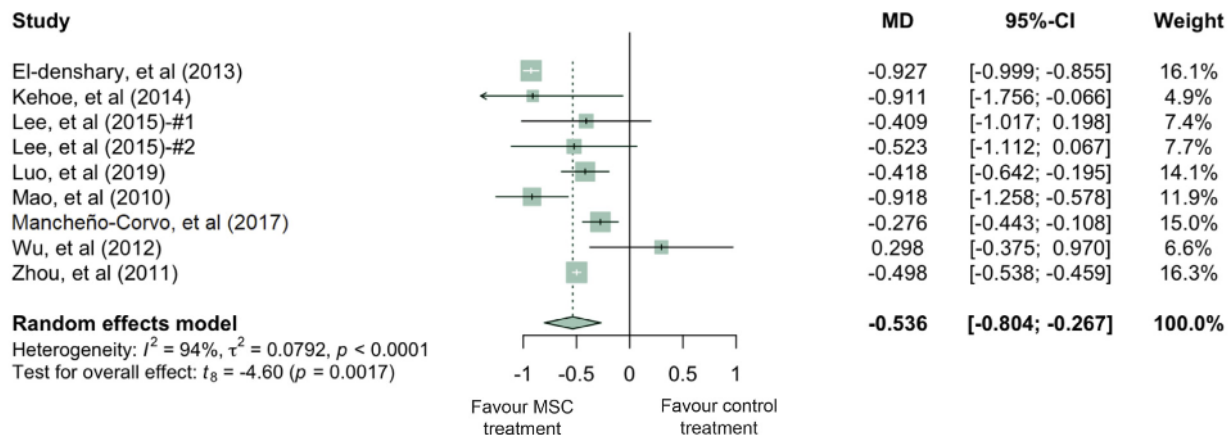


**Figure 5.2. Forest plots showing the normalized mean difference (MD) and 95% CI of (a) histological score, (b) paw thickness for each study included in the meta-analysis.** The graphs were generated using the meta package in R. All results have been normalized with sham control group as described in the methods. For all the plots, the vertical line indicates no effect, left hand side indicates favoring MSC treatment while right side indicates favoring PBS control treatment. The size of the box indicates the weighting of each study, and the thin horizontal whisker indicates the 95% CI. Random-effects model was used to summarize the effect sizes. Heterogeneity is denoted by the I2 and  $\tau^2$ .



bone erosion, cartilage damage and inflammation. For example, 4 studies (5 treatment arms) reported the histological score for bone erosion, and the normalised mean difference was -0.538 ( $p$ -value = 0.0210) when comparing the MSC treated groups to the PBS control groups (Supplemental Figure 5.3a, Supplementary Materials). MSC treatment significantly decreased cartilage damage by 51.6% and reduced inflammation by 42.3% (Supplemental Figure 5.3b and 5.3c, respectively, Supplementary Materials). Third, paw thickness in MSC treatment groups was significantly reduced, on average, by 53.6% ( $p$ -value = 0.0017). Variations between these studies, using paw thickness as an indicator, were relatively small ( $\tau^2$  = 0.0792) (Figure 5.2b). As a sensitivity analysis, similar conclusions can be drawn for clinical score and histological score when using the standardised mean difference (SMD) method (Supplemental Figure 5.4a and 5.4b, Supplementary Materials). Notably, 88.9% of the 9 included treatment arms showed results favouring MSC treatment in terms of paw thickness. The wide confidence interval of the SMD estimate of paw thickness could be due to the high inter-study variability (Supplemental Figure 5.4c, Supplementary Materials).

More than one method was used in our study to estimate effect sizes. Systematic results showed that MSC produced a significantly beneficial treatment effect in 42 of the 48 studies and 79 of the 94 treatment arms, based on the three indicators (paw thickness, clinical score and histological score). Notably, majority of the meta-analysis results remain robust in the sensitivity analysis. Over all studies combined (by SMD), there was a drop (1.383,  $p$ -value = 0.0008) in clinical score, a decrease (1.931,  $p$ -value < 0.0001) of histological score, and a reduction (2.814,  $p$ -value = 0.0639) of paw thickness (inflammation) (Supplemental Figure 5.4, Supplementary Materials). The non-statistically significant decrease of paw thickness by SMD might be due to high inter-study heterogeneity, which is a result of the presence of high standard deviation in some of the included studies(40).

#### **5.4.4 Subgroup analysis**

Clinical scores varied dramatically among the studies, with a  $\tau^2$  value of 0.1542. Thus, we performed further analysis by grouping studies according to the donor species, tissue of origin, transplant types and administration routes of MSC used in treatment (Figures 5.3 – 5.6). Notably, human derived MSC demonstrated more consistent



and effective clinical results, with a further 14.1% reduction in the clinical score compared to the overall effect size (Figure 5.3). The superior treatment effect of human derived MSC is statistically significant compared to mouse derived counterparts, which is indicated by the non-overlapping confidence intervals between human and mouse

Normalised Mean Differences of Clinical Score Increments (MSC Donor Species)

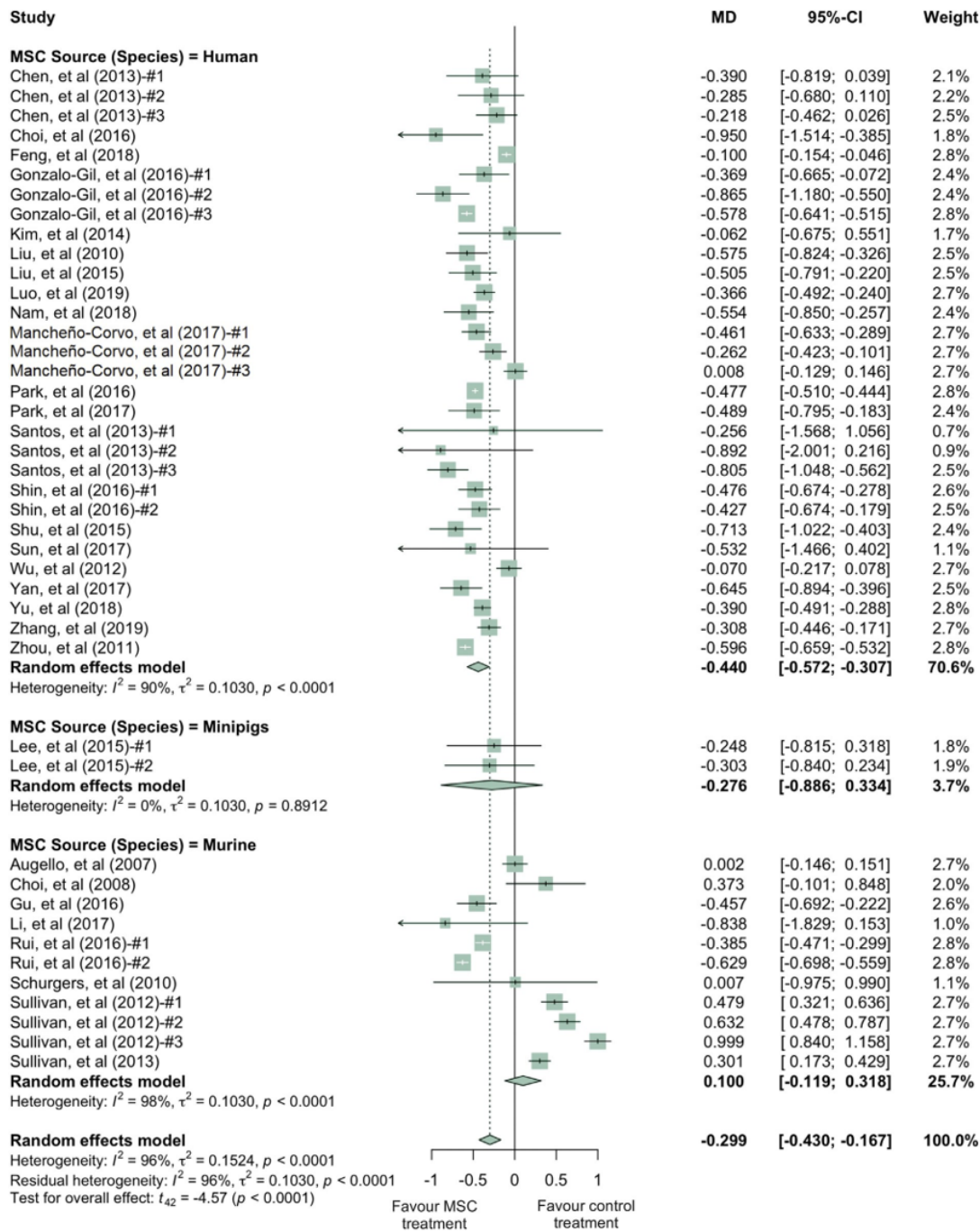


**Figure 5.3. Forest plots showing normalized mean difference (MD) of clinical score changes and 95% CI for the subgroup of MSC donor species.** The graph was generated using the meta package in R. All results were normalized with the sham control group as described in the methods. For all the plots, the vertical line indicates no effect, left hand side indicates favoring MSC treatment while right side indicates favoring PBS control treatment. The size of the box indicates the weighting of each study, and the thin horizontal whisker indicates the 95% CI. Random-effects model was used to summarize the effect sizes. Heterogeneity is denoted by the I<sup>2</sup> and  $\tau^2$ .

Normalised Mean Differences of Clinical Score Increments (Transplant Type)

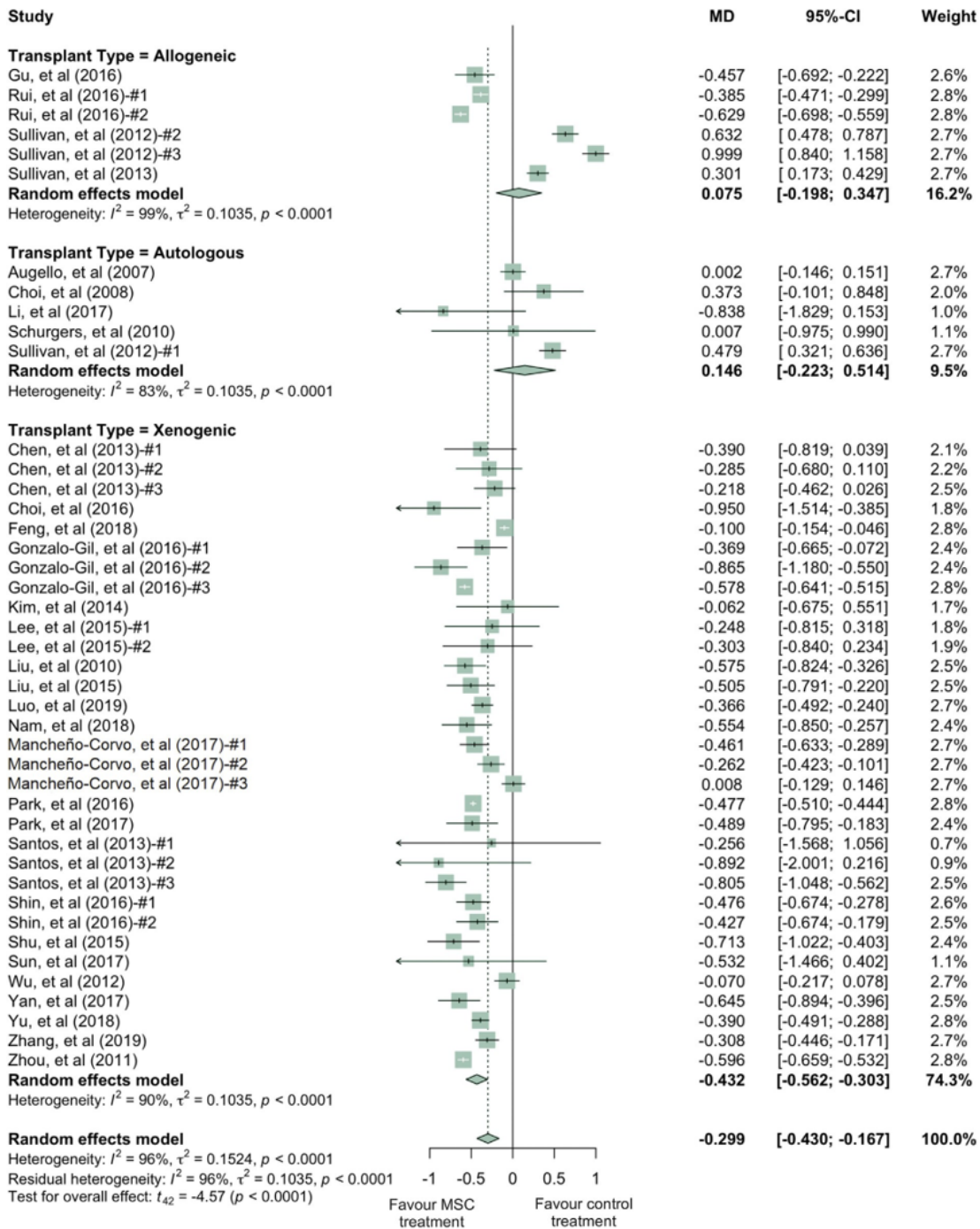


**Figure 5.4. Forest plots showing normalized mean difference (MD) of clinical score changes and 95% CI for the subgroup of transplant types.** The graph was generated using the meta package in R. All results were normalized with the sham control group as described in the methods. For all the plots, the vertical line indicates no effect, left hand side indicates favoring MSC treatment while right side indicates favoring PBS control treatment. The size of the box indicates the weighting of each study, and the thin horizontal whisker indicates the 95% CI. Random-effects model was used to summarize the effect sizes. Heterogeneity is denoted by the  $I^2$  and  $\tau^2$ .

Normalised Mean Differences of Clinical Score Increments (MSC Tissue of Origin)

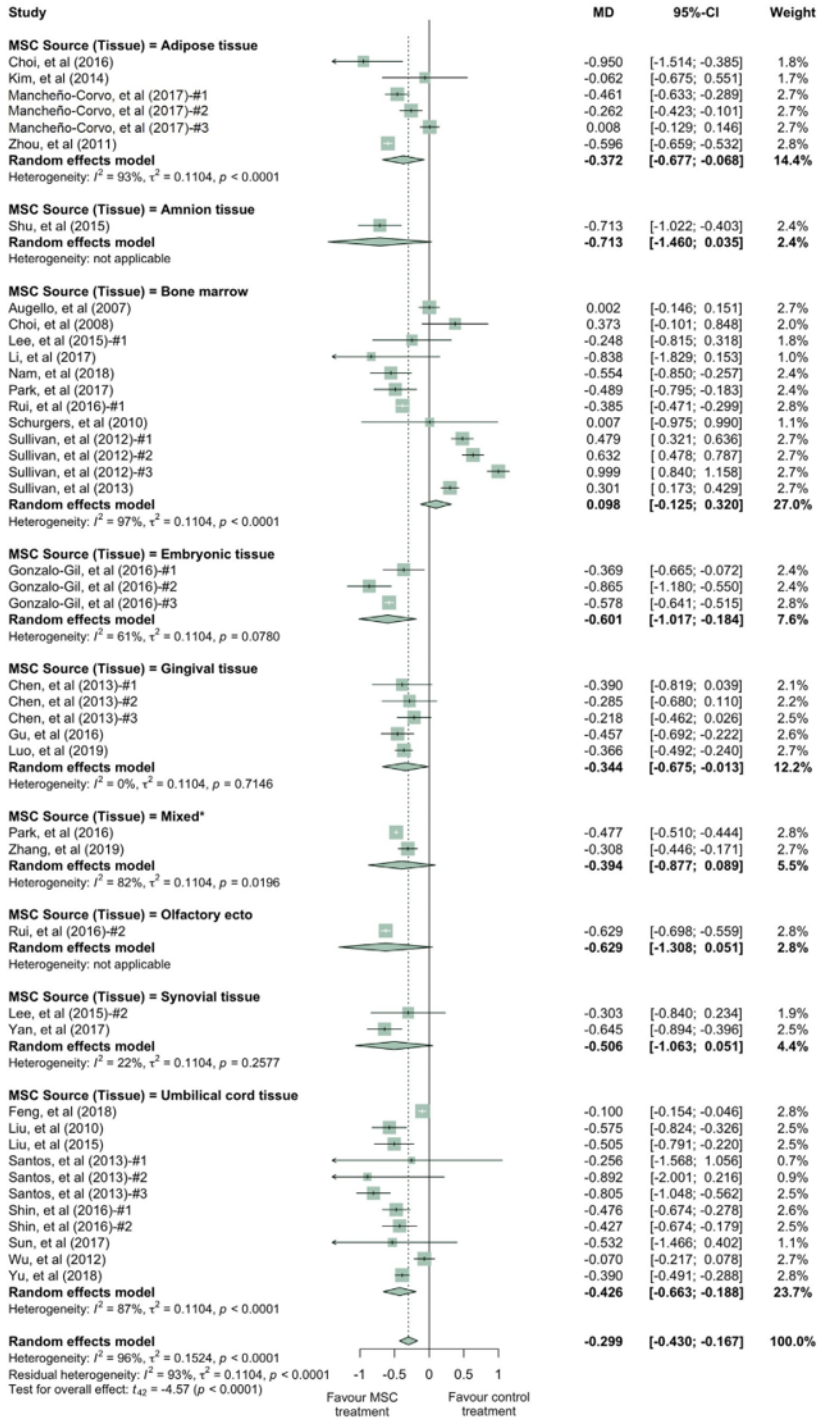
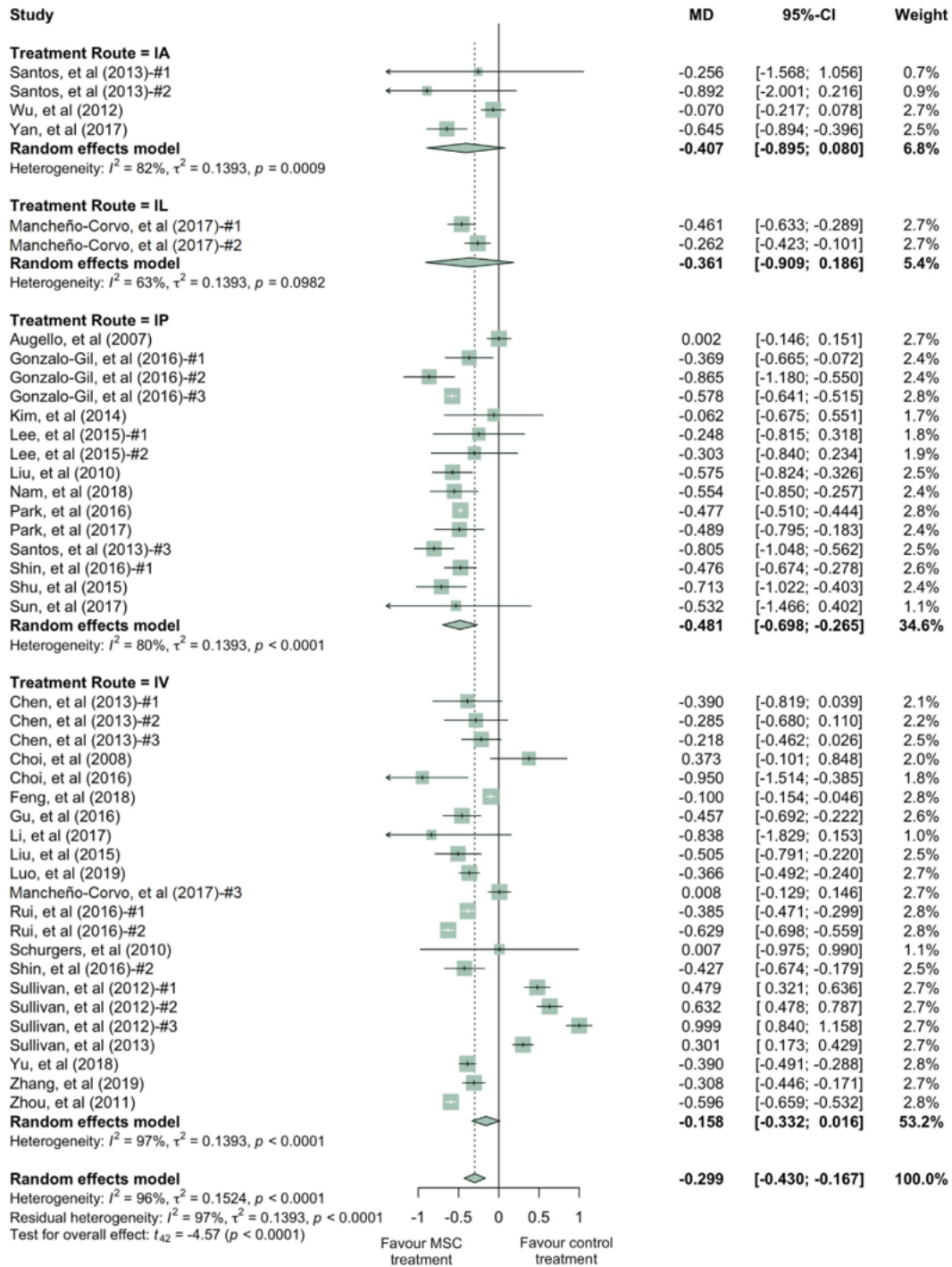


Figure 5.5. Forest plots showing normalized mean difference (MD) of clinical score changes and 95% CI for the subgroup MSC tissue of origin. The graph was generated using the *meta* package in R. All results were normalized with the sham control group as described in the methods. For all the plots, the vertical line indicates no effect, left hand side indicates favoring MSC

treatment while right side indicates favoring PBS control treatment. The size of the box indicates the weighting of each study, and the thin horizontal whisker indicates the 95% CI. Random-effects model was used to summarize the effect sizes. Heterogeneity is denoted by the  $I^2$  and  $\tau^2$ . Mixed\* indicates the treatment arm contains more than one type of MSC tissue of origin.

Normalised Mean Differences of Clinical Score Increments (Routes of Administration)



**Figure 5.6. Forest plots showing normalized mean difference (MD) of clinical score changes and 95% CI for the subgroup of routes of administration.** The graph was generated using the meta package in R. All results were normalized with the sham control group as described in the methods. For all the plots, the vertical line indicates no effect, left hand side indicates favoring MSC treatment while right side indicates favoring PBS control treatment. The size of the box indicates the weighting of each study, and the thin horizontal whisker indicates the 95% CI. Random-effects model was used to summarize the effect sizes. Heterogeneity is denoted by the I<sup>2</sup> and  $\tau^2$ .



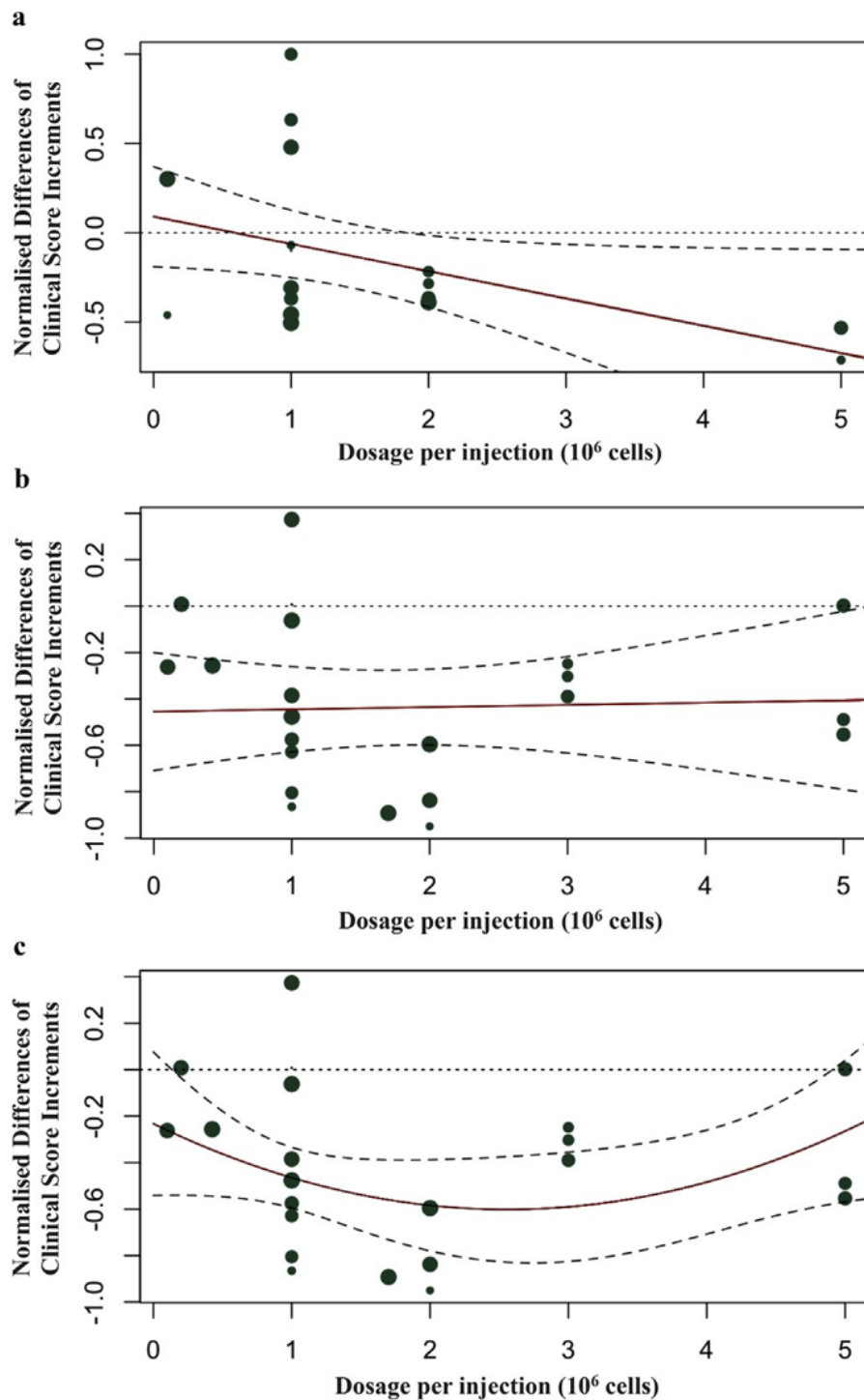


**Figure 5.7. Regression model with regression line is shown in (a) single MSC injection treatment, (b) multiple MSC injections treatment (linear regression), and (c) multiple MSC injections treatment (quadratic regression).** The size of the dot is proportional to number of injections. The dashed lines in (a, b, and c) represent the 95% CIs. The red line represents the trend of interactions between dosage of MSC and normalized difference in clinical score changes. The size of the dot is proportional to the weighting given to the study and the detailed weighting of each study could be found in Figure 5.1.

MSC groups. Interestingly, xenogeneic MSC give significantly better treatment efficacy in terms of clinical score than those from other transplant types (Figure 5.4). MSC from different tissue of origin including umbilical cord, gingiva and adipose showed consistent improvement of clinical score, whereas bone marrow derived MSC showed a trend of favouring PBS control treatment (Figure 5.5). By comparing clinical scores for the donor species and MSC tissue of origin of the MSC simultaneously, we discovered that human MSC, especially MSC derived from adipose tissue and umbilical cord tissue, provided better therapeutic effects, supported by at least four independent studies (Supplemental Figure 5.5, Supplementary Materials). Notably, UC-MSC and gingival tissue derived MSC (G-MSC) showed consistent and robust efficacy as well as the beneficial effect in the subgroup analysis of general histological score (Supplemental Figure 5.6, Supplementary Materials). When comparing the studies by different administration routes, IP injection gave a more significant reduction in clinical score. The decreases in clinical scores with other administration routes, such as IV injection, were not significant (Figure 5.6). Nonetheless, this result might be subject to other factors. For example, most of studies conducting IV injections used bone marrow MSC (BM-MSC), with which inconsistent results were reported among different studies (Figure 5.6, Table 5.1). Specifically, in the studies from Sullivan *et.al.*, which accounts for most of the IV injection treatment arms favouring PBS control treatment, the MSC used have inconsistent cell quality (*e.g.* low CD73 expression), isolation protocols and low dosage ( $1 \times 10^5$  cells).

#### **5.4.5 Meta-regression of effect size**

To address the heterogeneity from different variables and investigate the correlation between experimental parameters and effect size, meta-regression was performed on clinical scores. Predefined potential moderators were tested. We found that either routes of MSC administration or dosage of MSC contributed little heterogeneity, when analysed separately (Supplemental Table 5.2, Supplementary Materials). On the other hand, consistent with the subgrouping results, variation in MSC donor species accounted for 32.43% ( $p$ -value = 0.0006) of the heterogeneity, which was the highest source of variability among tested single moderators (Figure 5.3 and Supplementary Table 5.2, Supplementary Materials).



Regression on transplant types of MSC resulted in a 32.11% reduction in heterogeneity ( $p$ -value = 0.0006) (Supplementary Table 5.2, Supplementary Materials). Moreover, adjusting the tissue of origin of the MSC could reduce the total heterogeneity by 27.58% ( $p$ -value = 0.0315). The interaction between donor species and MSC tissue of origin was significant ( $p$ -value = 0.0413), accounting for 43.94% of the heterogeneity (Supplementary Table 5.2, Supplementary Materials).

The number of injections administered is another parameter that should be considered. When the number of injection (categorised into single or multiple injections) was adjusted separately, the reduction in heterogeneity was significant ( $p$ -value = 0.0147) (Supplementary Table 5.2, Supplementary Materials). Furthermore, there might be interactions between dosage of MSC and number of injection in the treatment protocol. When the interaction between dosage and number of injection was tested, the heterogeneity was decreased by 19.91% (moderator  $p$ -value = 0.0205, interaction  $p$ -value = 0.0722) (Supplementary Table 5.2, Supplementary Materials). A single injection with  $\geq 2 \times 10^6$  cell dosage correlated with better clinical outcomes (Figure 5.7a). However, multiple injections treatment arms did not show any correlation between cell dosage and outcomes in clinical score, when a linear regression was used (Figure 5.7b), but if a quadratic regression was used, there was a better outcome for 2 to  $3 \times 10^6$  cell dosage ( $p$ -value = 0.0391) (Figure 5.7c and Supplementary Table 5.3, Supplementary Materials). By combining the results above, a final model was built with MSC donor species, MSC tissue of origin, transplant types, treatment dosage, and number of injections adjusted. This final model explained 58.04% of the heterogeneity ( $p$ -value = 0.0017) (Supplementary Table 5.2, Supplementary Materials).

#### **5.4.6 Evaluation of publication bias**

Funnel plots for clinical score, histological score, and paw thickness were used to assess the publication bias. There is no significant asymmetry for all the indicators included in this study in which

the *p*-values of the funnel plot asymmetry for clinical score, histological score and paw thickness were 0.2060, 0.4007 and 0.9719 respectively (Figure 5.8). Thus, there is no observable publication bias in this meta-analysis. Multiple studies that reported positive results were out of the  $\pm 1.96$  standard error boundary in the funnel plot for histological score (Figure 5.8b), so we performed a correction using the trim-and-fill method. After correction, the symmetry centre shifted to around +0.0545 (Supplementary Table 5.7b, Supplementary Materials). No obvious change could be also found in the funnel plot for clinical score and paw thickness, after trim-and-fill (Supplementary Table 5.7a and 5.7c, Supplementary Materials).

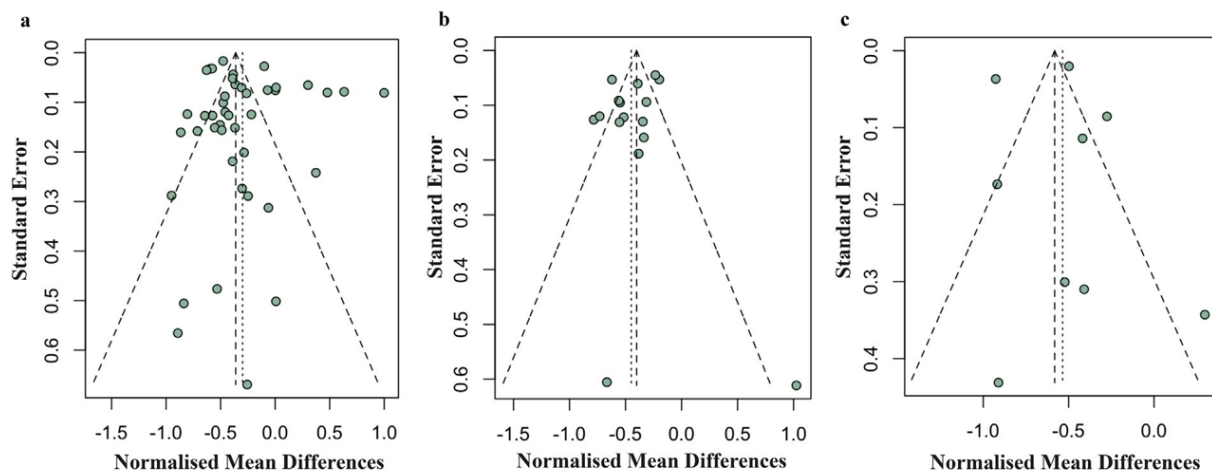


**Figure 5.8. Funnel plot for (a) clinical score, (b) histological score, and (c) paw thickness.** The funnel plots used either a model without regression (horizontal axis is the normalized mean difference), or a model after regression (horizontal axis is the residual value). Each dot in the figure represents a study, with the y-axis signifying study quality and the x-axis showing the study results.

## 5.5 Discussion

This meta-analysis examined preclinical studies of MSC used to treat RA and supports the hypothesis that MSC provide therapeutic benefit with large effect sizes. This work is the meta-analysis article to attempt exploration of study heterogeneity from different MSC study designs, including different donor species, tissues of origin, injection routes and dosages of administration(41). We found that the major contributor of heterogeneity is donor species of MSC, which accounts for 32.43% of the variations (Supplementary Table 5.2, Supplementary Materials).

Number of injections, MSC tissue of origin and transplant types also account for substantial amount of heterogeneity. Notably, when considering MSC treatment dosage and number of injections together, the variation decreased by 19.91% (Supplementary Table 5.2, Supplementary Materials).

This analysis could be used to inform guidelines (*e.g.*, experimental design, power calculation, *etc.*) for the future clinical translation of MSC to the bedside. Even though benefits were significant across species, delivery routes, time of administration in RA treatment, this study has provided evidence that human derived MSC are promising candidates for RA treatment in terms of the efficacy. Our results support further translational studies of human derived MSC in the treatment of RA in human.

The quality of studies and risk of bias were reviewed to investigate their translational potentials. Since most of the published papers related to MSC-based RA treatment did not include double-blinded studies, the overall quality of the studies was lowered with increased risk of bias. Even though most of the studies tried to avoid selection bias and reporting bias, few studies attempted to report their strategies to mitigate the potential performance bias, detection bias or attrition bias. Therefore, the results from this meta-analysis should be interpreted with caution. Instead of excluding potentially biased studies from this review, we tried to increase the sample size, and therefore the statistical power, by including more relevant publications. To improve the overall quality of the studies, we recommend that future studies related to MSC-based RA treatment should include double-blinded studies in their protocols.

Intriguingly, from the meta-regression, a single high dosage ( $\geq 2 \times 10^6$  cells) is associated with a higher effect size in clinical score (Figures 5.7a). Our results also suggest that multiple injections within a range of  $2 \times 10^6$  to  $3 \times 10^6$  cell dosage per injection lead to an optimal treatment outcome (Figure 5.7c). In clinical studies, it is reported that even one injection of MSC would be sufficient for therapeutic benefits, suggesting a single moderate dose of MSC treatment may lead to RA remission, without the need for frequent, routine administrations(30, 31). The results of our meta-analysis agree with the observations from previous clinical studies(30-33). For further studies, especially for early phase clinical trials, exploration of the optimal dosage range (*i.e.*, the range of dosage

that could exert pharmacological effects without significant toxicity) of MSC treatments is needed because few studies have been done on the dose-response relationship of MSC therapy in RA.

Human derived MSC were used in 49 of the total 94 treatment arms, and almost all of them showed therapeutic benefits (Figures 5.3 – 5.6, and Table 5.2). Mouse derived MSC showed therapeutic benefits in 74.3% of the 35 treatment arms, and majority of the studies that favoured PBS control treatment were from mouse derived MSC (9 effects in 35 treatment arms), which suggests that human derived MSC may present better therapeutic effects compared to those from mice, in animal RA models. This observation could be related to the fact that human derived MSC were of xenogeneic implantation in the animal models of RA. These findings also implicate that autologous or donor recipient HLA matching MSC may not be necessary for more effective therapeutic outcomes in human RA treatment. In fact, this finding suggests that an appropriate level of immune incompatibility between donor cells and the host may be beneficial for cell therapy in some context.

We also investigated the effects of different MSC tissue of origin (Table 5.2 and Figure 5.5) and found that UC-MSC (13 out of 13 reported positive effects; all human derived), AD-MSC (13 out of 14 reported positive effects) and G-MSC (5 out of 5 reported positive effects) have shown better RA treatment, compared to other tissue of origin, such as BM-MSC (27 out of 40 reported positive effects, whereas 13 treatment arms reporting negative therapeutic effects). There were no statistically significant differences between UC-MSC, AD-MSC and G-MSC clinical scores found in this study. However, UC-MSC and G-MSC showed better treatment outcomes in regard to histological scores. Additionally, autoantibody levels are considered as an important parameter regarding MSC treatments in RA(21, 42). Our results showed that MSC significantly decreased the serum levels of anti-collagen II (IgG) antibodies (Supplementary Figure 5.8, 5.9 and Supplemental Table 5.1, Supplementary Materials).

Future studies of autoimmune disease animal models treated with stem cells should take into account the inherent problems with having heterogeneity between studies. It would improve the reliability of data coming from these studies if they attempted to minimise variation of comparable data, such as the animal models being used, the methods for evaluating disease levels, the number of experimental groups evaluated in a single study, and the

methods used to prepare cells. Other variables such as the stem cell's species and tissue origin, timing of treatments relative to disease, cell dosage, and delivery routes should be optimised to the parameters that have been previously proven most efficacious, unless further data is provided as to why these optimal methods were not used. In certain cases, one of these parameters may be better than others, but until more studies try to minimise heterogeneity of other parameters, the relative merits of each study will not be clear. The data in this analysis could be used to choose optimum parameters and minimise heterogeneity in future studies. Finally, when the field further progresses in human RA clinical trials of MSC, patient/disease heterogeneity and disease stages are among the most critical variables that can affect MSC's therapeutic efficacy. Note that the consequences and implications of these analyses may be restricted to animal models of arthritis and could not be directly extrapolated to rheumatoid arthritis in human. The differences in the models versus human diseases and the fact that most studies are xenogenic make the relevance to human disease debatable. In the era of precision medicine, therefore, correlations between patient/disease characteristics (*e.g.* based on genetic analyses and biomarkers), clinical outcomes, MSC characteristics as well as preclinical animal data will be critical to define MSC mechanism of actions and identify MSC products for given patient subpopulations.

RA is a debilitating chronic disorder that affects 1.3 million Americans. The current treatments, including NSAIDs, conventional synthetic DMARDs, and biologic DMARDs(43), do not restore immune balance and are associated with side effects. Importantly, 30 - 40% patients are refractory to current treatments(9, 44). Accumulating clinical evidence (Supplementary Table 5.4, Supplementary Materials) has demonstrated that MSC (including AD, BM, UC, or UC blood derived) are potent in modulating the immune system and improving RA symptoms through production of trophic and anti-inflammatory factors, and the induction of self-tolerance(30-33, 45-47). For example, pioneering studies testing hUC-MSC products have been conducted, in several indications including RA. Results of two clinical studies, one in adult refractory RA patients (n = 172) and the other in refractory juvenile idiopathic arthritis (JIA) patients (n = 10), have demonstrated the safety and preliminary efficacy of hUC-MSC products in RA treatment(30, 33).

Both animal and human clinical studies have demonstrated that MSC could modulate the immune system and decrease RA symptoms(30, 34, 35). These studies indicate that the alleviation of disease symptoms are probably caused by the innate ability of MSC to dampen the immune response and induce tolerance(34). For instance, transplantation of hUC-MSC into RA patients led to a significant increase in CD4<sup>+</sup> CD25<sup>+</sup> Foxp3<sup>+</sup> Treg cells, a decrease in IL-6 and TNF-alpha, and induction of disease remission(30). Further analysis on variables, including Treg cells levels, and pro-/anti-inflammatory factors, will be performed to evaluate the treatment effects from MSC on RA. Several factors from preclinical and clinical findings support the conclusion that MSC therapy can be a safe and effective treatment for patients who are refractory to current RA therapies(31, 32). The role and influence of MSC on promoting or inhibiting existing tumour development are controversial(48). Due to mixed results of MSC on tumour relapse(49, 50), toxicology studies including tumorigenicity would be recommended before MSC administration to patients and caution should be taken for patients with existing malignancy due to the unknown effect of MSC on tumours. MSC have an overall positive safety record in hundreds of clinical trials across many different disease indications(51). All in all, this review suggests MSC therapy have a high potential to become a valuable treatment option for human RA disease.

To the best of our knowledge, this meta-analysis is to quantitatively answer whether MSC represent a robust RA treatment option in animal models. It suggests that in preclinical studies in RA animal models, MSC have consistently exhibited therapeutic benefits based on clinical scores, histological scores and paw thickness. These findings were also robust after correction of publication bias. We also found that there were considerable efficacy variations, across donor and recipient species, routes of administration, MSC tissue of origin, timing of MSC introduction, transplant types, dosage of MSC administration and number of injections. These findings demonstrate the need for considering variations in different animal models and treatment protocols in future studies using MSC to treat RA in humans, in order to maximise the therapeutic gains in the era of precision medicine.

## 5.6 Supplemental Materials

### Supplemental Materials and Methods

**Literature search and inclusion criteria.** This meta-analysis review was conducted according to the preferred reporting items for systematic reviews and meta-analysis (PRISMA) guidance(50). We conducted a comprehensive literature search for articles evaluating the therapeutic function of MSC in rheumatoid arthritis. The search terms used were sufficiently broad to capture the majority of the published data using MSC to treat animal models of arthritis. The search terms used were (mesenchymal OR mesenchymal stem cell OR mesenchymal stromal cell OR MSC) AND (rheumatoid arthritis OR rheumatoid OR arthritis OR RA). The electronic search strategy excluded non-English articles, and all studies included in this meta-analysis review were done in animal models of rheumatoid arthritis treated using non-genetic modified native MSC. Only the data documented therapeutic effects on arthritis, which means MSC were administrated at least one day after the initial RA induction, were included in our study. Studies with high risk of any bias were excluded from the meta-analysis if they scored “No” on any one question stated in the SYRCLE’s risk of bias tool (below). In addition, studies that failed to present sample sizes, standard deviations, or missed numerical/graphical results required for evaluating the effect sizes objectively, were also excluded in the parametric meta-analysis.

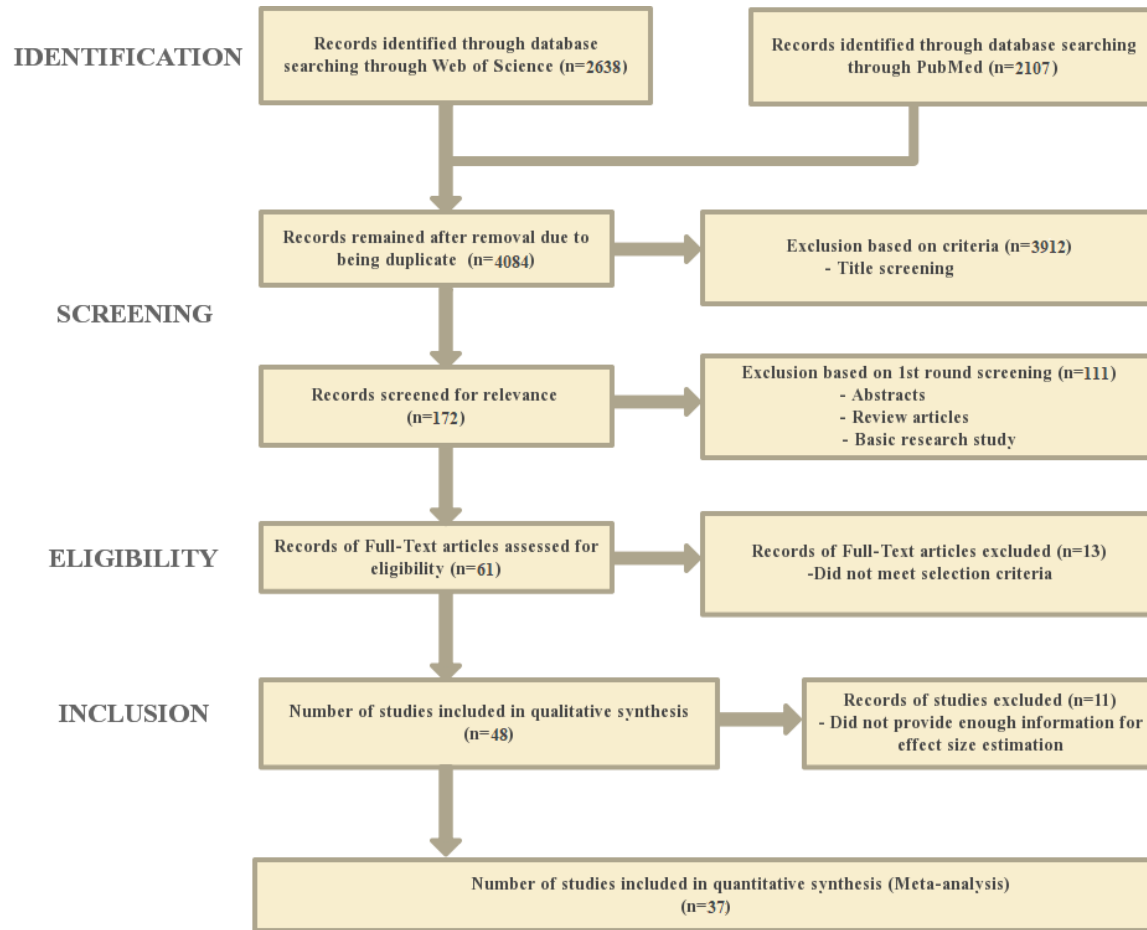
**Data extraction.** Data were extracted from all available sources in each paper, including text and graphs. When only graphical presentation was available, values for mean and SD or SEM were obtained using GraphClick (Arizona Software, Phoenix, AZ) under high magnification by two independent investigators.

**Evaluating the risk of bias.** To evaluate the quality of the studies and risk of any bias, two independent investigators used the SYRCLE’s risk of bias tool, which includes 10 defined criteria:

(1) sequence generation, (2) baseline characteristics, (3) allocation concealment, (4) random housing, (5) blinding against performance bias, (6) random outcome assessment, (7) blinding against detection bias, (8) incomplete outcome data, (9) selective outcome reporting, and (10) other sources of biases including

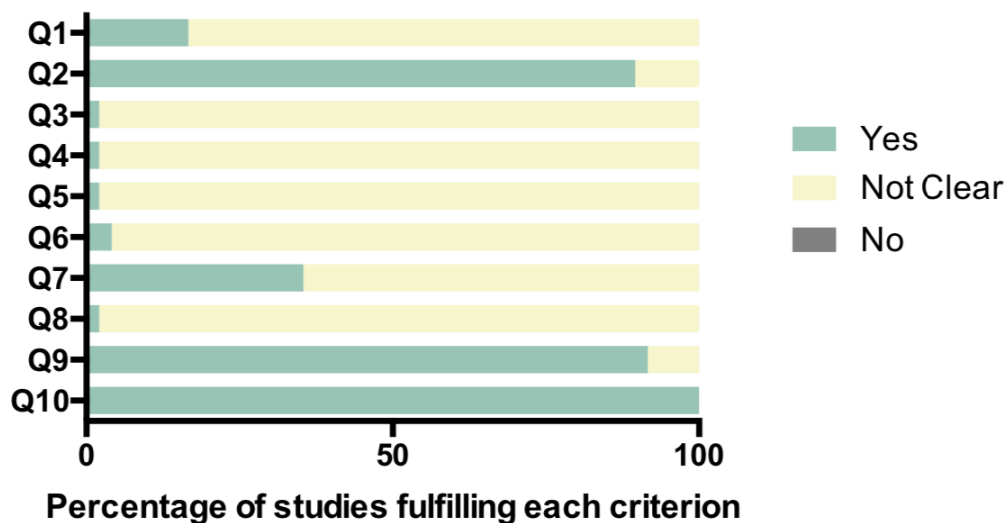
contamination and inappropriate influence of funders(49). In order to assign a judgment of low, high, or unclear risk of bias to each item mentioned in the tool, the following signaling questions were used: Q1: Was the allocation sequence adequately generated and applied? Q2: Were the groups similar at baseline or were they adjusted for confounders in the analysis? Q3: Was the allocation adequately concealed? Q4: Were animals randomly housed during the experiment? Q5: Were the caregivers and/or investigators blinded from knowledge of which intervention each animal received during the experiment? Q6: Were animals selected at random for outcome assessment? Q7: Was the outcome assessor blinded? Q8: Were incomplete outcome data adequately addressed? Q9: Are reports of the study free of selective outcome reporting? Q10: Was the study apparently free of other problems that could result in high risk of bias? A “yes” judgment indicates a low risk of bias, a “no” judgment indicates high risk of bias, and if insufficient details were reported to assess the risk of bias properly, the judgment of bias was recorded as “unclear”(49). As suggested in SYRCLE’s risk of bias tool, we focused on evaluating the potential risk of bias instead of calculating the quality score for each article.





**Supplemental Figure 5.1. Flowchart of meta-analysis search and review process.** Conducted in accordance with PRISMA (preferred reporting items for systematic reviews and meta-analyses) statement criteria. Down arrows indicate the progression of studies that passed the previous criteria (number passed in parentheses). Side arrows indicate the number of studies excluded at each stage, and why they were excluded.

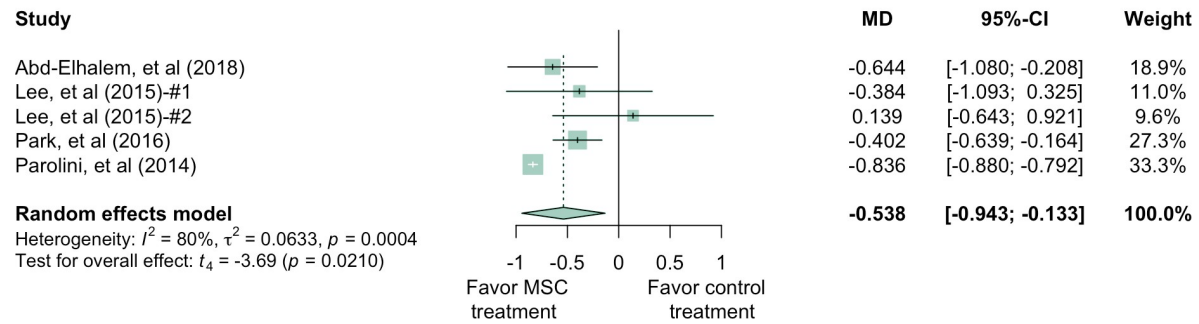
## Quality Assessment



**Supplemental Figure 5.2. Quality assessment of literature.** Horizontal axis indicates percentage of answers to the questions in SYRCLE’s risk of bias tool. Green indicates “Yes”; dark gray indicates “No”; and yellow indicates “Not clear”.

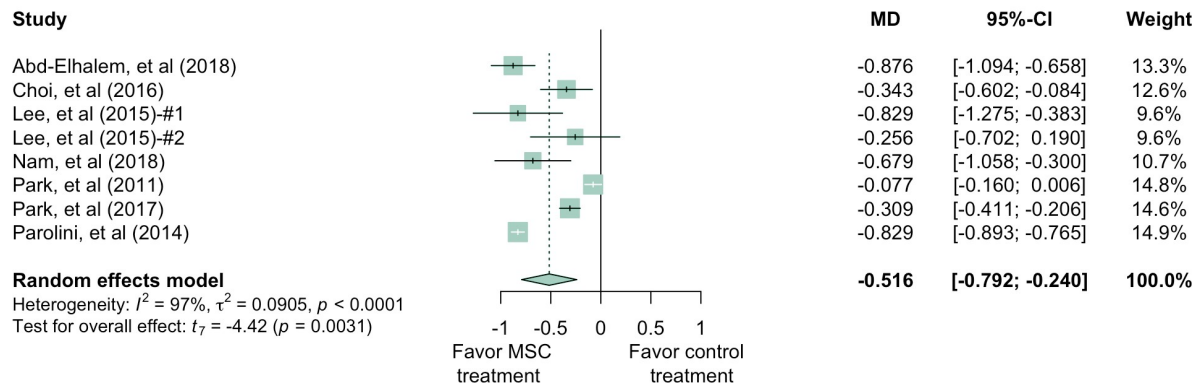
**a**

**Normalised Mean Differences of Histological Score (Bone Erosion)**



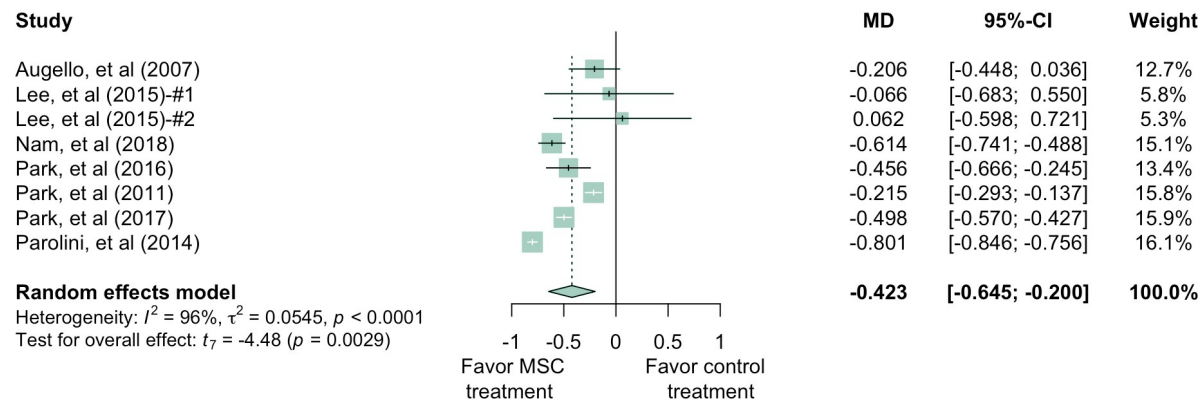
**b**

**Normalised Mean Differences of Histological Score (Cartilage Damage)**



**c**

**Normalised Mean Differences of Histological Score (Inflammation)**

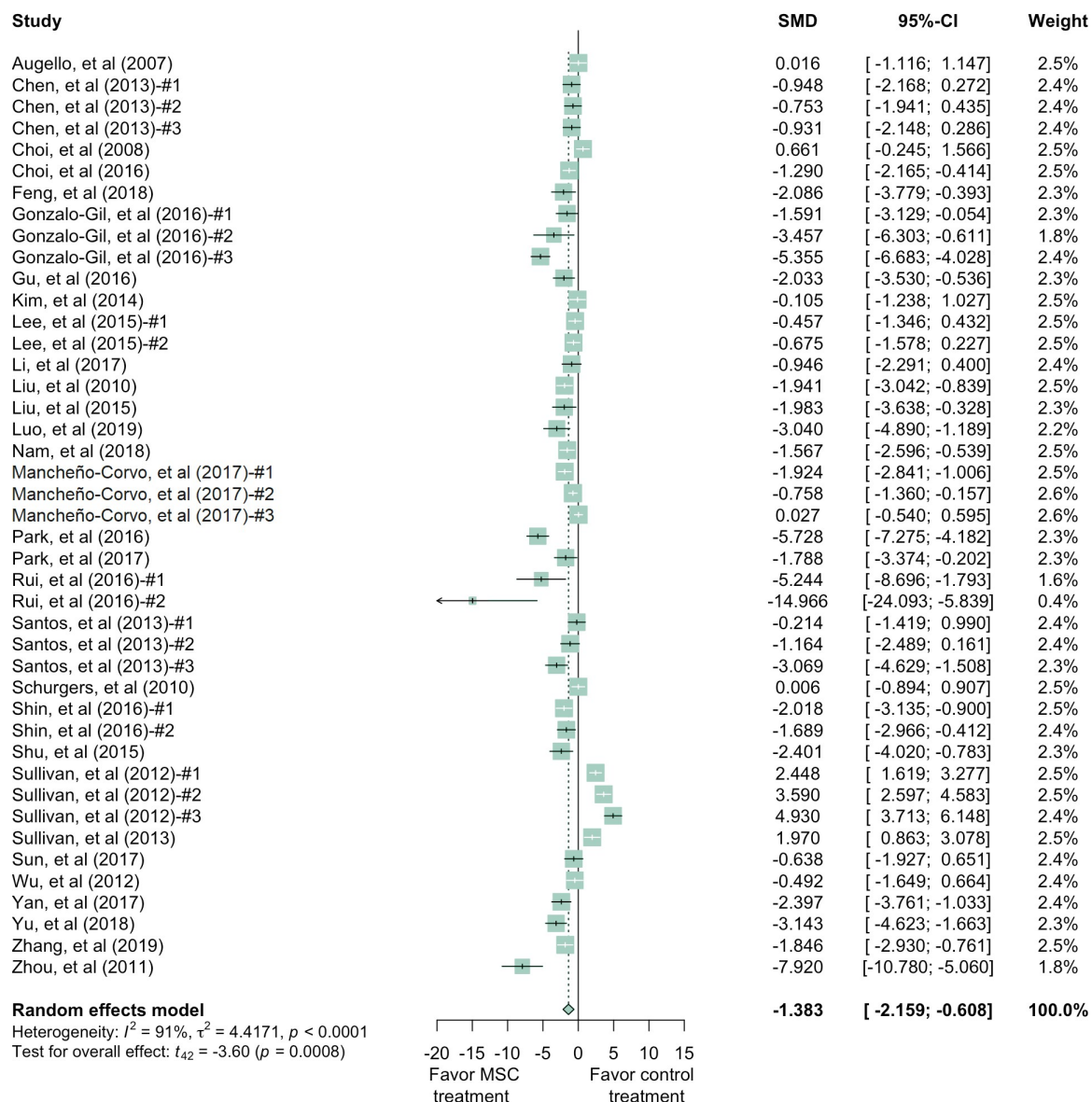


**Supplemental Figure 5.3. Forest plots showing the normalized mean difference (MD) and 95% CI for histological scores with a subgroup of (a) bone erosion; (b) cartilage damage; (c)inflammation. The graphs were**

generated using the *meta* package in R. All results have been normalized with the sham control group as described in the methods. For all the plots, the vertical line indicates no effect, left hand side indicates favoring MSC treatment while right side indicates favoring PBS control treatment. The size of the box indicates the weighting of each study, and the thin horizontal whisker indicates the 95% CI. Random-effects model was used to summarize the effect sizes. Heterogeneity is denoted by the  $I^2$  and  $\tau^2$ .

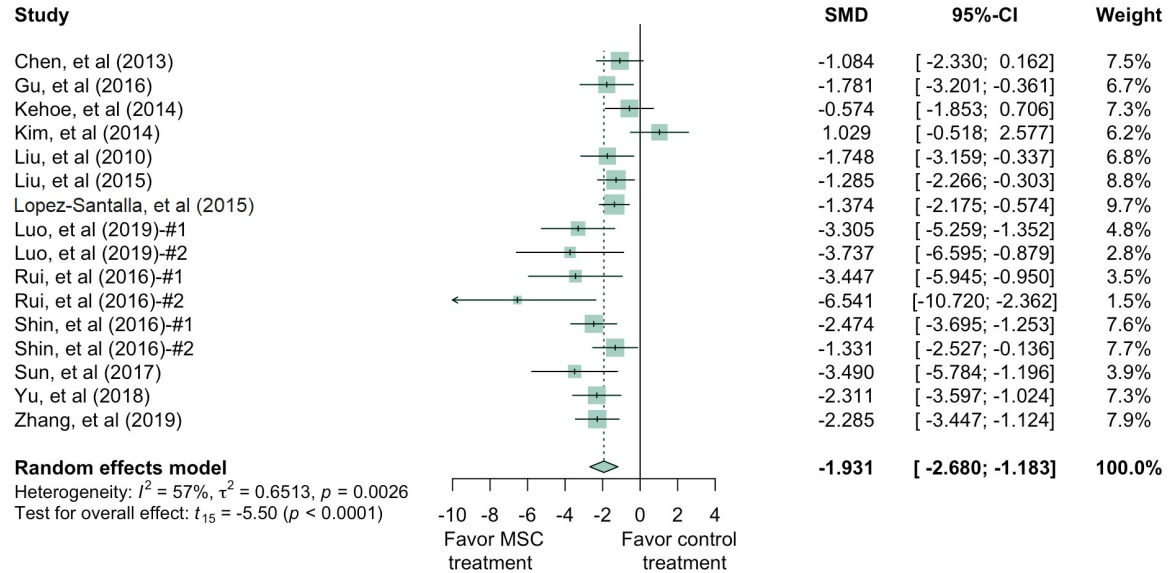
**a**

**Standardised Mean Differences of Clinical Score Increments (General)**



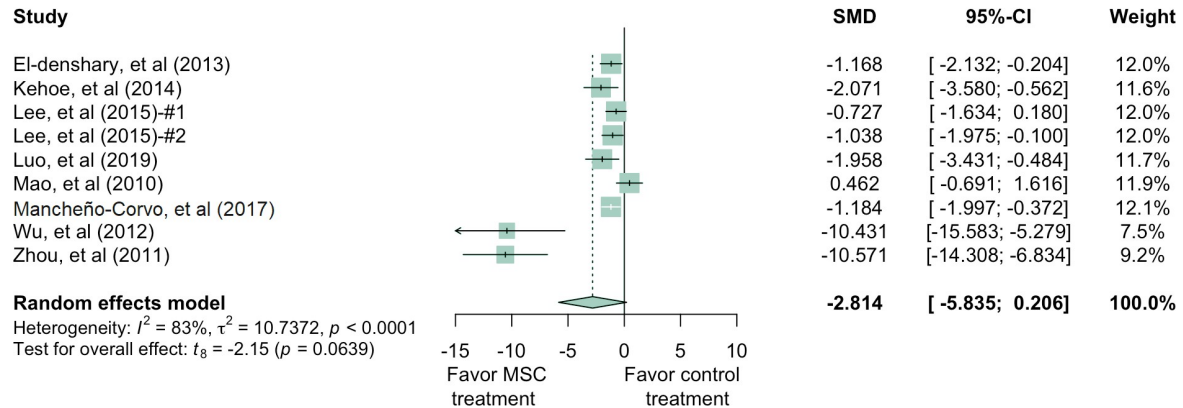
**b**

**Standardised Mean Difference of Histological Score (General)**



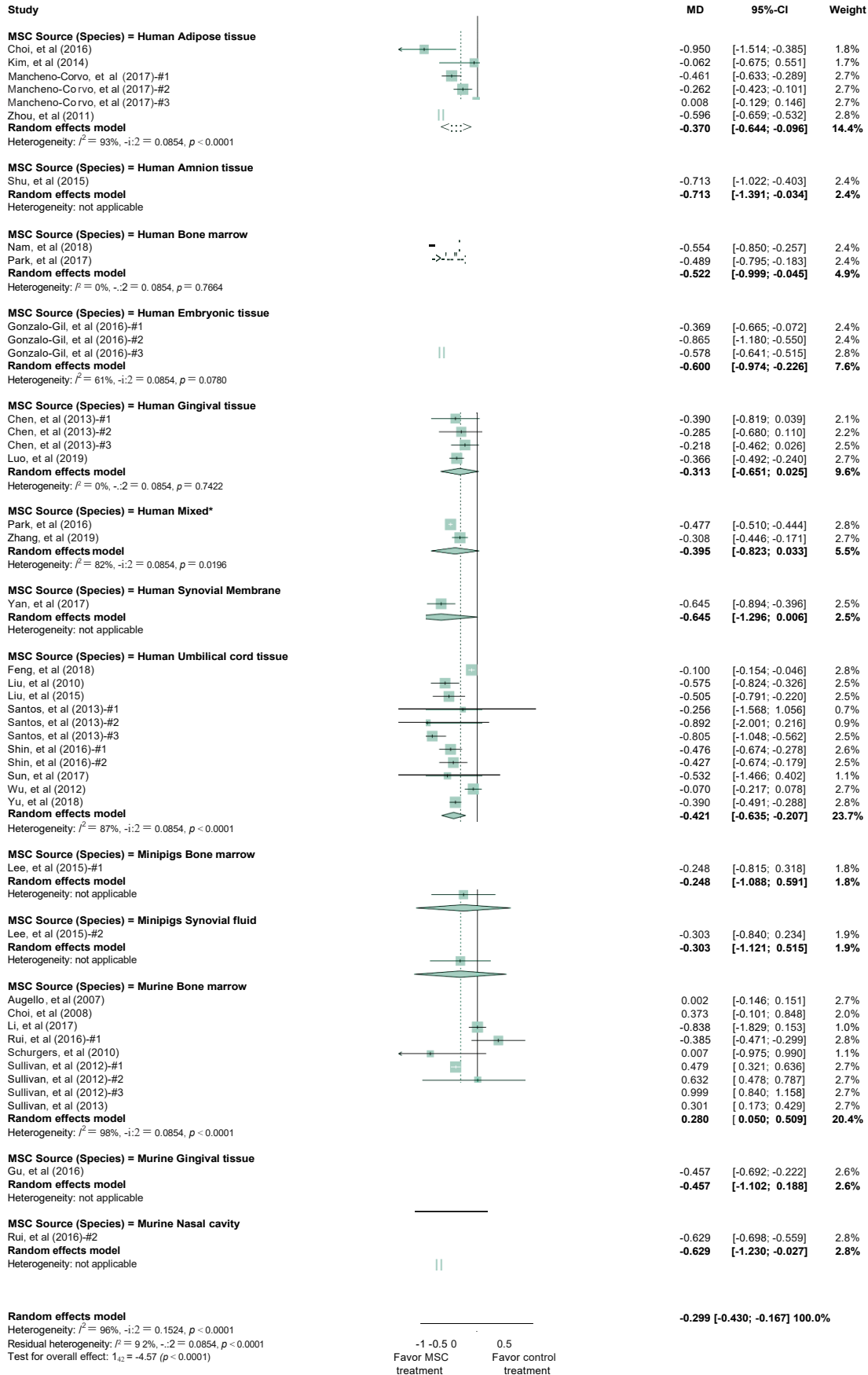
**c**

**Standardised Mean Differences of Paw Thickness Increments**

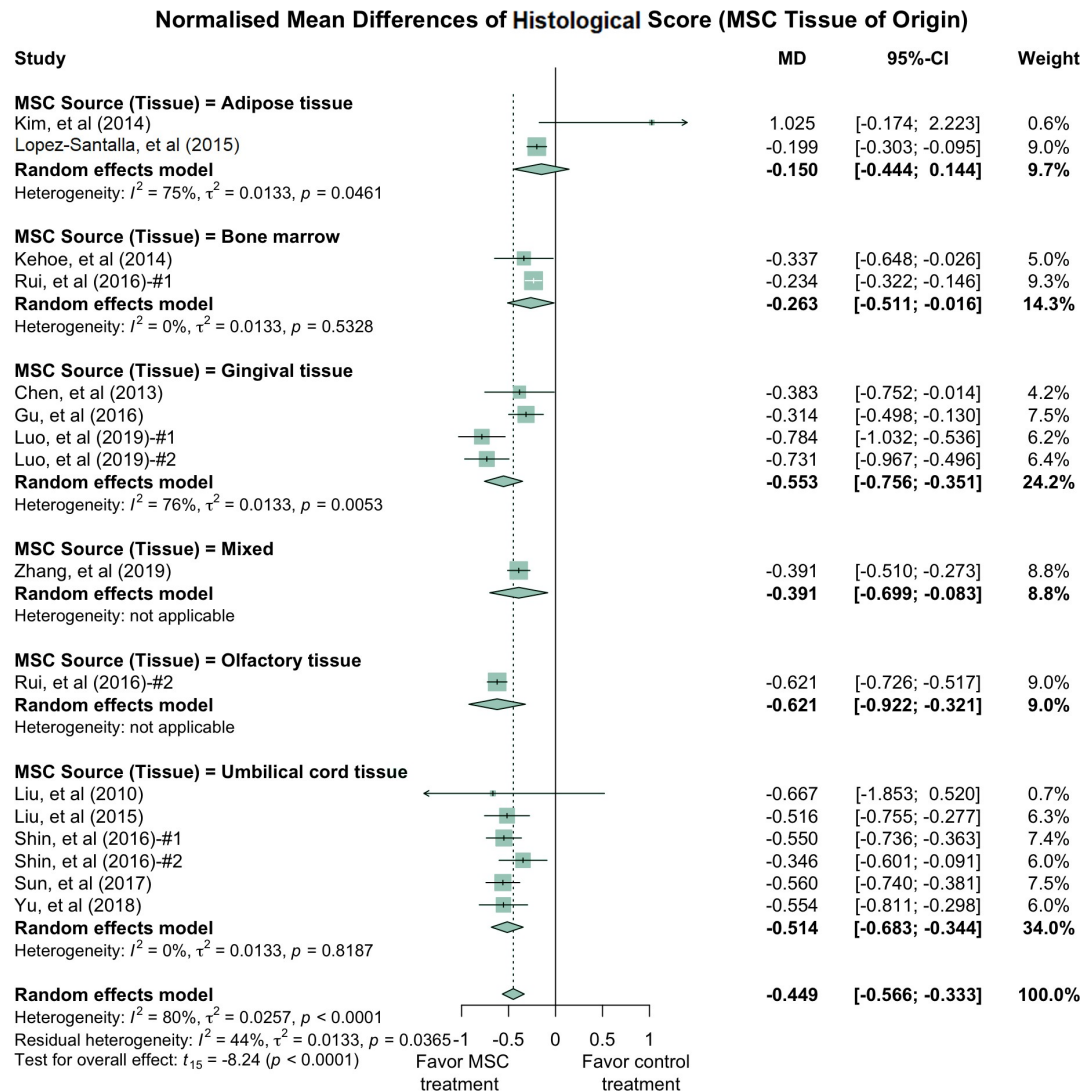


**Supplemental Figure 5.4. Forest plots showing the standardized mean difference (SMD) and 95% CI for (a) clinical score, (b) histological score, (c) paw thickness for each study included in the meta-analysis.** The graphs were generated using the *meta* package in R. All results have been normalized with sham control group as described in the methods. For all the plots, the vertical line indicates no effect, left hand side indicates favoring MSC treatment while right side indicates favoring PBS control treatment. The size of the box indicates the weighting of each study, and the thin horizontal whisker indicates the 95% CI. Random-effects model was used to summarize the effect sizes. Heterogeneity is denoted by the  $I^2$  and  $\tau^2$ .

Normalized Mean Differences of Clinical Score Increments (MSC Donor Species + Tissue of Origin)



**Supplemental Figure 5.5. Forest plots showing the normalized mean difference (MD) and 95% CI for two important MSC donor species, human and mouse, and tissue of origin.** The graphs were generated using the *meta* package in R. All results have been normalized with the sham control group as described in the methods. For all the plots, the vertical line indicates no effect, left hand side indicates favoring MSC treatment while right side indicates favoring PBS control treatment. The size of the box indicates the weighting of each study, and the thin horizontal whisker indicates the 95% CI. Random-effects model was used to summarize the effect sizes. Heterogeneity is denoted by the  $I^2$  and  $\tau^2$ .

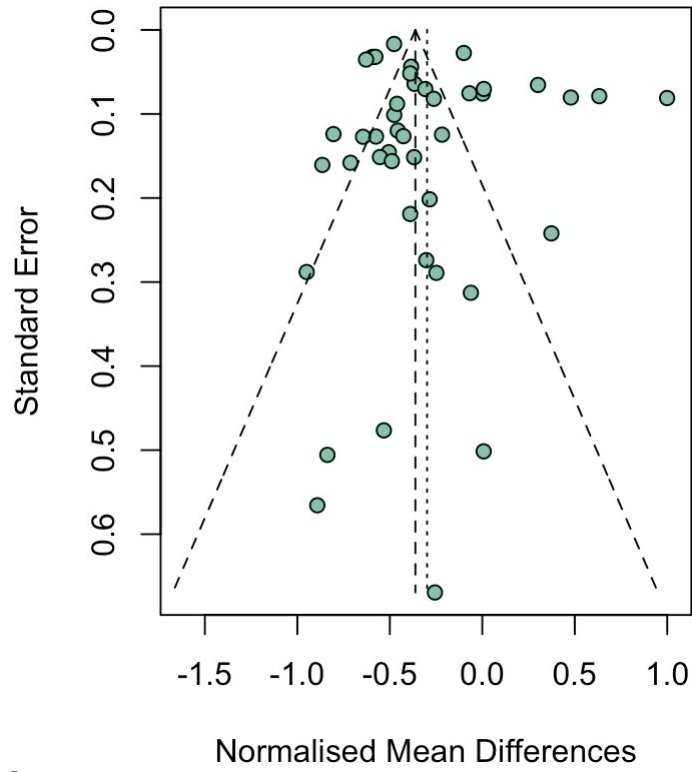


**Supplemental Figure 5.6. A forest plot showing the normalized mean difference (MD) and 95% CI of histological score of MSC tissue of origin.** The graph was generated using the *meta* package in R. All the results have

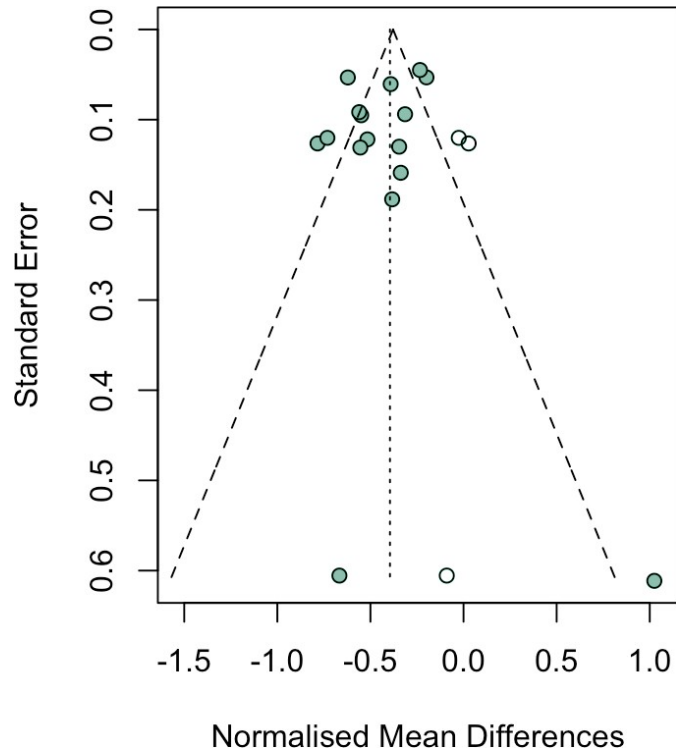
been normalized with the sham control group as described in the methods. The vertical line indicates no effect, left hand side indicates favoring MSC treatment while right side indicates favoring control treatment. The size of the box indicates the weighting of each study, and the thin horizontal whisker indicates the 95% CI. Random-effects model was used to summarize the effect sizes. Heterogeneity is denoted by the  $I^2$  and  $\tau^2$ . Mixed indicates the treatment arm contains more than one type of MSC tissue of origin.

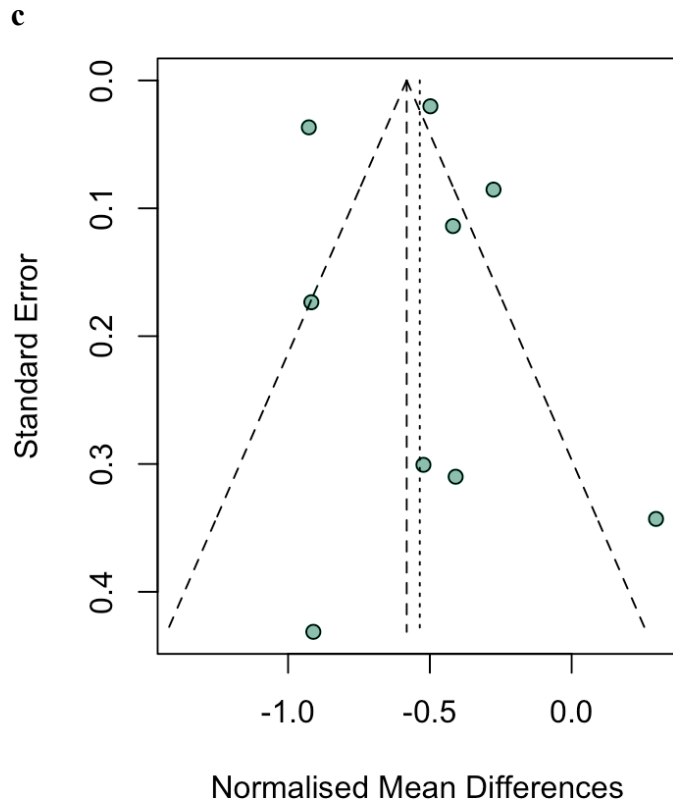


**a**



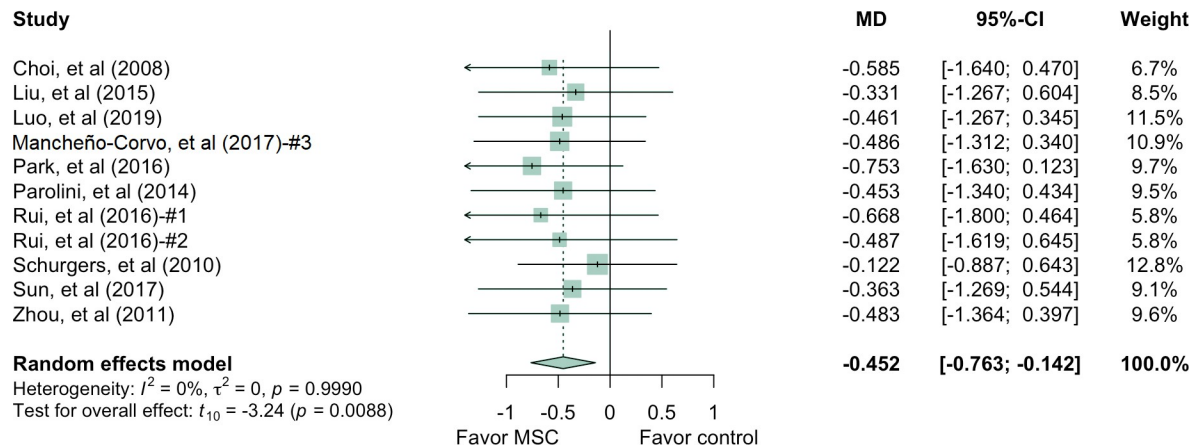
**b**





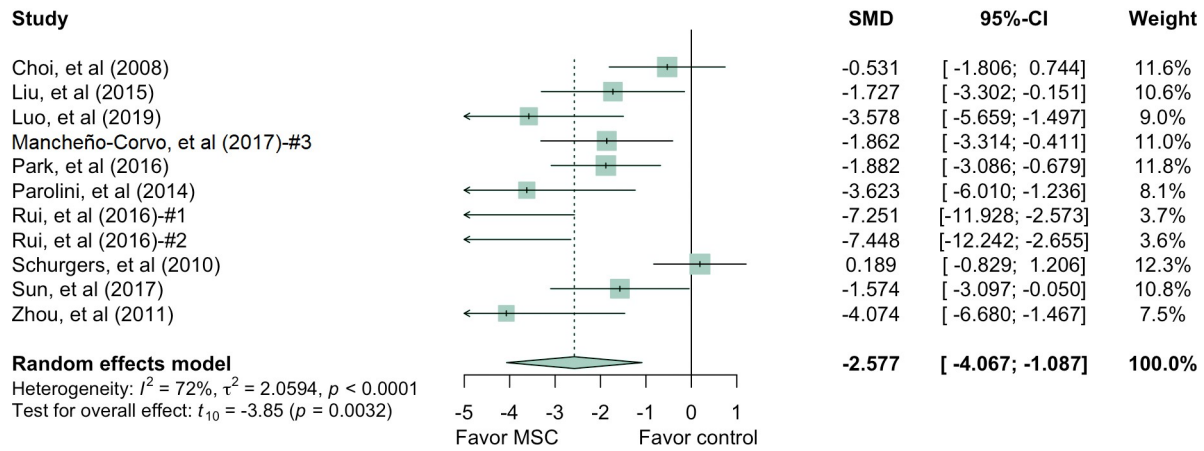
**Supplemental Figure 5.7. Funnel plot for (a) clinical score, (b) histological score and (c) paw thickness, after trim-and-fill correction.** Each dot represents a study with the y-axis representing study quality and the x-axis representing the study results. The original studies are denoted by the green dots, while white dots represent the hypothetical studies added into the analysis.

### Normalised Mean Differences of Autoantibody Levels (IgG)



**Supplemental Figure 5.8. Forest plots showing the normalized mean difference (MD) and 95% CI for clinical scores with a subgroup of autoantibody levels (IgG).** The graphs were generated using the *meta* package in R. All results have been normalized with the sham control group as described in the methods. For all the plots, the vertical line indicates no effect, left hand side indicates favoring MSC treatment while right side indicates favoring PBS control treatment. The size of the box indicates the weighting of each study, and the thin horizontal whisker indicates the 95% CI. Random-effects model was used to summarize the effect sizes. Heterogeneity is denoted by the  $I^2$  and  $\tau^2$ .

### Standardised Mean Differences of Autoantibody Levels (IgG)



**Supplemental Figure 5.9. Forest plots showing the standardized mean difference (SMD) and 95% CI for clinical score, for each study included with subgroup of autoantibody levels (IgG) in the meta-analysis.** The graphs were generated using the *meta* package in R. All results have been normalized with sham control group as described in the methods. For all the plots, the vertical line indicates no effect, left hand side indicates favoring MSC treatment while right side indicates favoring PBS control treatment. The size of the box indicates the weighting of each study, and the thin horizontal whisker indicates the 95% CI. Random-effects model was used to summarize the effect sizes. Heterogeneity is denoted by the  $I^2$  and  $\tau^2$ .

**Supplemental Table 5.1: Autoantibodies summary of the pre-clinical studies using MSC to treat RA in this study**

| Author (year)                              | Arm | <i>P</i> < 0.05 | MSC favor? | Origin     | Donor  | Control    | Transplant type | Treatment protocol              | Rept  | Target                  |
|--|-----|-----------------|------------|------------|--------|------------|-----------------|---------------------------------|-------|-------------------------|
| Zhou, et al (2011) <sup>S1</sup>           | 1   | Y               | Y          | AD         | Human  | PBS/ Other | Xenogenic       | CIA, no booster, IV, Multiple   | Mouse | IgG, IgG2a              |
| #Garimella, et al (2015) <sup>S2</sup>     | 1   | Y               | Y          | AD         | Murine | PBS        | Autologous      | CIA, with booster, IP, Single   | Mouse | IgG                     |
| #Chen, et al (2009) <sup>S6</sup>          | 1   | Y               | N          | BM         | Murine | Nil        | Autologous      | CIA, with booster, IV, Single   | Mouse | IgG                     |
| Rui, et al (2016) <sup>S13</sup>           | 1   | Y               | Y          | BM         | Murine | PBS        | Allogeneic      | CIA, with booster, IV, Multiple | Mouse | IgG                     |
|  | 2   | Y               | Y          | Other (OE) | Murine | PBS        | Allogeneic      | CIA, with booster, IV, Multiple | Mouse | IgG                     |
| Park, et al (2016) <sup>S20</sup>          | 1   | Y               | Y          | BM         | Human  | Other      | Xenogenic       | CIA, with booster, IV, Multiple | Mouse | IgG                     |
|  | 2   | Y               | Y          | BM         | Human  | Other      | Xenogenic       | CIA, with booster, IV, Multiple | Mouse | IgG                     |
|  | 3   | Y               | Y          | BM         | Human  | Other      | Xenogenic       | CIA, with booster, IV, Multiple | Mouse | IgG                     |
| #Gonzalez, et al (2009) <sup>S21</sup>     | 1   | Y               | Y          | AD         | Human  | PBS/ Other | Xenogenic       | CIA, with booster, IP, Multiple | Mouse | IgG, IgG1, IgG2a        |
| #Bouffi, et al (2010) <sup>S23</sup>       | 1   | Y               | Y          | BM         | Murine | N/A        | Allogeneic      | CIA, with booster, IV, Multiple | Mouse | 9-10w                   |
| Schurgers, et al (2010) <sup>S25</sup>     | 1   | N               | N          | BM         | Murine | PBS        | Autologous      | CIA, no booster, IV, Single     | Mouse | IgG                     |
| Liu, et al (2015) <sup>S26</sup>           | 1   | Y               | Y          | UC         | Human  | PBS        | Xenogenic       | CIA, with booster, IV, Single   | Mouse | IgG, Ig M               |
| Choi, et al (2008) <sup>S27</sup>          | 1   | N               | N          | BM         | Murine | PBS        | Autologous      | CIA, with booster, IV, Multiple | Mouse | IgG                     |
| Parolini, et al (2014) <sup>S29</sup>      | 1   | Y               | Y          | Other (AM) | Human  | PBS        | Xenogenic       | CIA, with booster, IP, Multiple | Mouse | IgG, IgG1, IgG2a        |
| Choi, et al (2016) <sup>S32</sup>          | 1   | Y               | Y          | AD         | Human  | PBS        | Xenogenic       | CIA, with booster, IV, Multiple | Mouse | N/A                     |
| #Luz-Crawford, et al (2015) <sup>S33</sup> | 1   | Y               | Y          | BM         | Murine | PBS/ Other | Allogeneic      | CIA, with booster, IV, Multiple | Mouse | IgG2a, IgG1             |
| Luo, et al (2019) <sup>S36</sup>           | 1   | Y               | Y          | Other (GI) | Human  | Nil        | Xenogenic       | CIA, IV, Single                 | Mouse | IgG, IgG1, IgG2a, IgG2b |
|  | 2   | Y               | Y          | Other (GI) | Human  | Nil        | Xenogenic       | CIA, IV, Single                 | Mouse | IgG, IgG1, IgG2a, IgG2b |

|  |   |   |   |    |       |        |           |                                 |       |     |
|--|---|---|---|----|-------|--------|-----------|---------------------------------|-------|-----|
| Mancheño-Corvo, et al, (2017) <sup>S44</sup> | 1 | Y | Y | AD | Human | Ringer | Xenogenic | CIA, with booster, IL, Multiple | Mouse | IgG |
|  | 2 | Y | Y | AD | Human | Ringer | Xenogenic | CIA, with booster, IL, Multiple | Mouse | IgG |
|  | 3 | N | N | AD | Human | Ringer | Xenogenic | CIA, with booster, IV, Multiple | Mouse | IgG |
| Sun, et al, (2017) <sup>S50</sup>            | 1 | N | Y | UC | Human | PBS    | Xenogenic | CIA, with booster, IP, Single   | Mouse | IgG |

**Supplemental Table 5.2: Summary of meta-regression statistics**

| Covariate(s) included                              | $\tau^2$ | R <sup>2</sup> | Test for moderator ( <i>p</i> -value) | Interaction test ( <i>p</i> -value) |
|--|----------|----------------|---------------------------------------|-------------------------------------|
| No regression                                      | 0.1542   | N/A            | N/A                                   | N/A                                 |
| Treatment dosage (A)                               | 0.1505   | 1.25%          | 0.2078                                | N/A                                 |
| Number of injections (B)                           | 0.1294   | 15.08%         | 0.0147                                | N/A                                 |
| MSC tissue of origin (C)                           | 0.1104   | 27.58%         | 0.0315                                | N/A                                 |
| Donor species (D)                                  | 0.1030   | 32.43%         | 0.0006                                | N/A                                 |
| Transplant types (E)                               | 0.1035   | 32.11%         | 0.0006                                | N/A                                 |
| Routes of administration (F)                       | 0.1393   | 8.58%          | 0.1383                                | N/A                                 |
| A and B  | 0.1307   | 14.26%         | 0.0332                                | N/A                                 |
| A and B with interaction                           | 0.1221   | 19.91%         | 0.0205                                | 0.0722                              |
| C and D  | 0.0966   | 36.60%         | 0.0132                                | N/A                                 |
| C and D with interaction                           | 0.0854   | 43.94%         | 0.0052                                | 0.0413                              |
| A and B with interaction, C, D and E (Final model) | 0.0639   | 58.04%         | 0.0017                                | N/A                                 |

A simple mixed-effects model linear regression was used. Normalized clinical score was the dependent variable. Moderators were added to the model through addition, while potential interaction terms were also added if necessary.  $\tau^2$  is the estimation between study variance, and R<sup>2</sup> is the percentage of variance that has been accounted for by the regression model.

**Supplemental Table 5.3: Meta-regression of the effect of treatment dosage with subgroup of number of injections**

| Subgrouping strategy | $\tau^2$ | R <sup>2</sup> | Test for moderator ( <i>p</i> -value) | Significance of adding quadratic term test ( <i>p</i> -value) |
|----------------------|----------|----------------|---------------------------------------|---|
| Single injection     |          |                |                                       |   |
| Linear regression    | 0.1645   | 14.78%         | 0.1043                                | 0.9370  |
| Quadratic regression | 0.1643   | 14.85%         | 0.2786                                |   |
| Multiple injection   |          |                |                                       |   |
| Linear regression    | 0.0520   | 2.34%          | 0.7041                                | 0.0391  |
| Quadratic regression | 0.0346   | 35.03%         | 0.1339                                |   |

Testing the non-linear effect of treatment dosage on normalized clinical score differences with mixed-effects model regression.  $\tau^2$  is the estimation between study variance, and  $R^2$  is the percentage of variance that has been accounted for by the regression model.

**Supplemental Table 5.4: Results of clinical studies using MSC to treat RA**

| Study                                    | Wang, et.al. (2013)   | Wang, et.al. (2016)  | Liang, et.al. (2012)   | Álvaro-Gracia, et.al. (2017)  | Ghoryani, et.al. (2019)   | Park, et.al. (2018)  | Shadmanfar, et.al. (2018)  |
|--|---|--|--|---|---|--|--|
| <b>Clinical Phase</b>                    | 1/2   | Pilot  | Pilot  | 1/2   | N/A   | 1  | 1/2  |
| <b>Study Population</b>                  | Subjects with Active RA   | Subjects with JIA  | Subjects with Refractory RA  | Subjects with Refractory RA   | Subjects with Refractory RA   | Subjects with Active RA  | Subjects with knee involved RA   |
| <b>Primary Objective</b>                 | Safety and Efficacy   | Safety and Efficacy  | Safety and Efficacy  | Safety, Tolerability and Efficacy   | Safety and Efficacy   | Safety and Tolerability  | Safety and Efficacy  |
| <b>Primary Endpoint</b>                  | Primary: Safety (Prevalence of AEs)<br>Secondary: ACR20, ACR50, ACR 70, DAS28, HAQ-DI at month 3, 6 and 8 | Primary: Safety (Prevalence of AEs)<br>Secondary: DAS28, ESR, CRP at month 3 and 6 | VAS pain score, DAS28, EULAR, CRP, ESR at month 1, 3, 6, 12, and then every half year                          | Primary: Safety (Prevalence of AEs)<br>Secondary: ACR20, ACR50, ACR 70, DAS28-ESR, CRP, SF-36 every month until Month 3                             | DAS28-ESR, VAS, ESR, CRP, RF, anti-CCP, measure immunological factors at month 1, 6, 12 | Primary: Safety (Prevalence of AEs)<br>Secondary: DAS28, WOMAC score, VAS at month 3, 6, 12                                    | Primary: Safety (Prevalence of AEs)<br>Secondary: DAS28, HAQ, VAS, ESR at Week 4   |
| <b>Trial Design</b>                      | Open label  | Open label   | N/A  | Randomized, Multicenter, Double blind, Placebo-controlled   | N/A   | Open label   | Randomized, Triple-blind, Single-center, Placebo-controlled  |
| <b>Control Arm</b>                       | Placebo   | None   | None   | Placebo   | None  | None   | Placebo  |
| <b>Random Scheme</b>                     | None  | None   | N/A  | Randomized, 3:1 test article to placebo   | N/A   | None   | Block (Size 4) randomization   |
| <b>Blinding</b>                          | None  | None   | N/A  | Single blinded for safety; Double blinded for efficacy  | N/A   | None   | Triple blinded   |
| <b>Patients Enrolled</b>                 | 172   | 10   | 4  | 67  | 9   | 9  | 30   |
| <b>Patients Treated with Active Drug</b> | 136   | 10   | 4  | 42  | 9   | 9  | 15   |
| <b>Number of sites</b>                   | 1   | 1  | 1  | 18  | 1   | 1  | 1  |
| <b>Route of Delivery</b>                 | IV  | IV   | IV   | IV  | IV  | IV   | Intra-articular  |
| <b>Dose(s)</b>                           | $4.0 \times 10^7$ cells / infusion, single or two IV infusion(s)  | $4.0 \times 10^7$ cells / infusion, two IV infusions                               | $1.0 \times 10^6$ /kg, IV infusions  | $1.0 \times 10^6$ /kg/infusion (Cohort A), $2.0 \times 10^6$ /kg/infusion (Cohort B), $4.0 \times 10^6$ /kg/infusion (Cohort C), three IV infusions | $1.0 \times 10^6$ /kg/infusion, single IV infusion                                      | $2.5 \times 10^7$ cells /infusion, $5.0 \times 10^7$ cells /infusion or $1.0 \times 10^8$ cells /infusion, single IV infusion  | $42 \pm 4 \times 10^6$ cells /injection, single injection to knee joint  |
| <b>Outcomes / Major Findings</b>         | Six cases of 136 patients (4%) showing mild flu-like symptoms during the infusion. No other               | No AEs were observed after MSC infusion. 7 patients (70%, 7/10) achieved           | 3 of 4 patients achieved a reduction in ESR, DAS28, and pain VAS score at 1 and 6 months after administration. | Only 1 of the 8 AE grade 3 from 53 patients is serious. Significant increased ACR 20 response rate  | Significant reduction in DAS28-ESR. VAS score showed significant                        | DAS-28 reduced $1.60 \pm 1.57$ . Reduced levels of IL-1 $\beta$ , IL-6, IL-8, and TNF- $\alpha$ at 24 hours were observed. The | No adverse effects reported. Achieved superior findings according to WOMAC, VAS, time to jelling and pain-free walking distance. The improvement |

|  |   |          |  |  |   |  |  |
|--|---|----------|--|--|---|--|--|
|  | increased ACR 20 response rate and reduction in DAS28, HAQ-DI | ESR, CRP | 2 of 3 had a EULAR moderate response at 6 months but experienced a relapse at 7 and 23 months, respectively. No one achieved DAS28 remission in the follow-up period. No SAEs were reported. |  | significant difference for serum CRP and anti-CCP levels after intervention | HAQ score and pain VAS changes at week 4 were (-0.15 ± 0.48) | cannot be significantly sustained over 12 months |
|--|---|----------|--|--|---|--|--|

### 5.7 Author contributions

L.L. conducted study conception and design, performed data acquisition and interpretation, and drafted the manuscript. C.W.W. participated in study design, performed analysis and interpretation of data, and revised the manuscript. M.H. carried out data acquisition and interpretation, revised the manuscript and coordinated the project. H.P.F. revised the manuscript and participated in data interpretation. G.L. edited the manuscript. Y.L. participated in study design and conception and edited the manuscript. W.L. conducted study conception and design and revised the manuscript. W.Z. was responsible for conception and design of the study, revised the manuscript and supervised overall project. L.L., C.W.W., W.L. and W.Z. had full access to all of the data in the study and take responsibility for the integrity of the data and the accuracy of the data analysis. All authors approved the final version to be published.

### 5.8 Acknowledgments

This work is supported by NIH [1DP2CA195763] and Baylx Inc: BI-206512. H.P.F is in part supported by a pre-doctoral fellowship from the National Institute of Neurological Disorders and Stroke (NINDS/NIH) Training Grant [Award# NS082174].



## 5.9 References

1. Hunt L, Emery P. Defining populations at risk of rheumatoid arthritis: the first steps to prevention. *Nature Reviews Rheumatology*. 2014;10(9):521-30.
2. Smolen JS, Aletaha D, Redlich K. The pathogenesis of rheumatoid arthritis: new insights from old clinical data? *Nature Reviews Rheumatology*. 2012;8(4):235-43.
3. Choy E. Understanding the dynamics: pathways involved in the pathogenesis of rheumatoid arthritis. *Rheumatology (Oxford)*. 2012;51 Suppl 5:v3-11.
4. Scott DL, Wolfe F, Huizinga TW. Rheumatoid arthritis. *Lancet*. 2010;376(9746):1094-108.
5. Smolen JS, Aletaha D. Rheumatoid arthritis therapy reappraisal: strategies, opportunities and challenges. *Nature Reviews Rheumatology*. 2015;11(5):276-89.
6. Choy EH, Kavanaugh AF, Jones SA. The problem of choice: current biologic agents and future prospects in RA. *Nature Reviews Rheumatology*. 2013;9(3):154-63.
7. Weinblatt ME, Keystone EC, Furst DE, Moreland LW, Weisman MH, Birbara CA, et al. Adalimumab, a fully human anti-tumor necrosis factor  $\alpha$  monoclonal antibody, for the treatment of rheumatoid arthritis in patients taking concomitant methotrexate: the ARMADA trial. *Arthritis & Rheumatism*. 2003;48(1):35-45.
8. Lipsky PE, van der Heijde DM, St. Clair EW, Furst DE, Breedveld FC, Kalden JR, et al. Infliximab and methotrexate in the treatment of rheumatoid arthritis. *New England Journal of Medicine*. 2000;343(22):1594-602.
9. Vander Cruyssen B, Van Looy S, Wyns B, Westhovens R, Durez P, Van den Bosch F, et al. Four-year follow-up of infliximab therapy in rheumatoid arthritis patients with long-standing refractory disease: attrition and long-term evolution of disease activity. *Arthritis Res Ther*. 2006;8(4):R112.
10. Curtis JR, Singh JA. Use of biologics in rheumatoid arthritis: current and emerging paradigms of care. *Clin Ther*. 2011;33(6):679-707.
11. Dominici M, Le Blanc K, Mueller I, Slaper-Cortenbach I, Marini F, Krause D, et al. Minimal criteria for defining multipotent mesenchymal stromal cells. The International Society for Cellular Therapy position statement. *Cytotherapy*. 2006;8(4):315-7.
12. Nam Y, Jung SM, Rim YA, Jung H, Lee K, Park N, et al. Intraperitoneal infusion of mesenchymal stem cell attenuates severity of collagen antibody induced arthritis. *PLoS One*. 2018;13(6):e0198740.
13. Park N, Rim YA, Jung H, Kim J, Yi H, Kim Y, et al. Etanercept-Synthesising Mesenchymal Stem Cells Efficiently Ameliorate Collagen-Induced Arthritis. *Sci Rep*. 2017;7:39593.
14. Zhou B, Yuan J, Zhou Y, Ghawji M, Jr., Deng YP, Lee AJ, et al. Administering human adipose-derived mesenchymal stem cells to prevent and treat experimental arthritis. *Clin Immunol*. 2011;141(3):328-37.
15. Lopez-Santalla M, Mancheno-Corvo P, Menta R, Lopez-Belmonte J, DelaRosa O, Bueren JA, et al. Human Adipose-Derived Mesenchymal Stem Cells Modulate Experimental Autoimmune Arthritis by Modifying Early Adaptive T Cell Responses. *Stem Cells*. 2015;33(12):3493-503.
16. Choi EW, Shin IS, Song JW, Lee M, Yun TW, Yang J, et al. Effects of Transplantation of CTLA4Ig-Overexpressing Adipose Tissue-Derived Mesenchymal Stem Cells in Mice With Sustained Severe Rheumatoid Arthritis. *Cell Transplantation*. 2016;25(2):243-59.
17. Liu Y, Mu R, Wang S, Long L, Liu X, Li R, et al. Therapeutic potential of human umbilical cord mesenchymal stem cells in the treatment of rheumatoid arthritis. *Arthritis Res Ther*. 2010;12(6):R210.
18. Liu R, Li X, Zhang ZY, Zhou M, Sun Y, Su DL, et al. Allogeneic mesenchymal stem cells inhibited T follicular helper cell generation in rheumatoid arthritis. *Scient Rep*. 2015;5.
19. Feng Z, Zhai Y, Zheng Z, Yang L, Luo X, Dong X, et al. Loss of A20 in BM-MSCs regulates the Th17/Treg balance in Rheumatoid Arthritis. *Sci Rep*. 2018;8(1):427.

20. Chen M, Su W, Lin X, Guo Z, Wang J, Zhang Q, et al. Adoptive transfer of human gingiva-derived mesenchymal stem cells ameliorates collagen-induced arthritis via suppression of Th1 and Th17 cells and enhancement of regulatory T cell differentiation. *Arthritis Rheum.* 2013;65(5):1181-93.
21. Luo Y, Wu W, Gu J, Zhang X, Dang J, Wang J, et al. Human gingival tissue-derived MSC suppress osteoclastogenesis and bone erosion via CD39-adenosine signal pathway in autoimmune arthritis. *EBioMedicine.* 2019;43:620-31.
22. Ankrum JA, Ong JF, Karp JM. Mesenchymal stem cells: immune evasive, not immune privileged. *Nat Biotechnol.* 2014;32(3):252-60.
23. Galipeau J, Sensebe L. Mesenchymal Stromal Cells: Clinical Challenges and Therapeutic Opportunities. *Cell Stem Cell.* 2018;22(6):824-33.
24. Bianco P, Cao X, Frenette PS, Mao JJ, Robey PG, Simmons PJ, et al. The meaning, the sense and the significance: translating the science of mesenchymal stem cells into medicine. *Nat Med.* 2013;19(1):35-42.
25. Uccelli A, Prockop DJ. Why should mesenchymal stem cells (MSCs) cure autoimmune diseases? *Curr Opin Immunol.* 2010;22(6):768-74.
26. Parekkadan B, Milwid JM. Mesenchymal stem cells as therapeutics. *Annu Rev Biomed Eng.* 2010;12:87-117.
27. Shi X-M, Liu H, Ding J, Wang J, Wang Y, Yang M, et al. Remission of Collagen-Induced Arthritis through Combination Therapy of Microfracture and Transplantation of Thermogel-Encapsulated Bone Marrow Mesenchymal Stem Cells. *Plos One.* 2015;10(3):e0120596.
28. Tyndall A. Mesenchymal stem cell treatments in rheumatology: a glass half full? *Nat Rev Rheumatol.* 2014;10(2):117-24.
29. Gonzalez-Rey E, Gonzalez MA, Varela N, O'Valle F, Hernandez-Cortes P, Rico L, et al. Human adipose-derived mesenchymal stem cells reduce inflammatory and T cell responses and induce regulatory T cells in vitro in rheumatoid arthritis. *Ann Rheum Dis.* 2010;69(1):241-8.
30. Wang L, Wang L, Cong X, Liu G, Zhou J, Bai B, et al. Human umbilical cord mesenchymal stem cell therapy for patients with active rheumatoid arthritis: safety and efficacy. *Stem Cells Dev.* 2013;22(24):3192-202.
31. Álvaro-Gracia JM, Jover JA, García-Vicuña R, Carreño L, Alonso A, Marsal S, et al. Intravenous administration of expanded allogeneic adipose-derived mesenchymal stem cells in refractory rheumatoid arthritis (Cx611): results of a multicentre, dose escalation, randomised, single-blind, placebo-controlled phase Ib/IIa clinical trial. *Annals of the rheumatic diseases.* 2017;76(1):196-202.
32. Liang J, Li X, Zhang H, Wang D, Feng X, Wang H, et al. Allogeneic mesenchymal stem cells transplantation in patients with refractory RA. *Clin Rheumatol.* 2012;31(1):157-61.
33. Wang L, Zhang Y, Li H, Hong J, Chen X, Li M, et al. Clinical Observation of Employment of Umbilical Cord Derived Mesenchymal Stem Cell for Juvenile Idiopathic Arthritis Therapy. *Stem Cells Int.* 2016;2016:9165267.
34. Lee HK, Lim SH, Chung IS, Park Y, Park MJ, Kim JY, et al. Preclinical efficacy and mechanisms of mesenchymal stem cells in animal models of autoimmune diseases. *Immune Netw.* 2014;14(2):81-8.
35. Pers YM, Jorgensen C. Mesenchymal Stromal Cells: Updates and Therapeutic Outlook in Rheumatic Diseases. *J Clin Med.* 2013;2(4):201-13.
36. El-Jawhari JJ, El-Sherbiny YM, Jones EA, McGonagle D. Mesenchymal stem cells, autoimmunity and rheumatoid arthritis. *QJM.* 2014;107(7):505-14.
37. Hooijmans CR, Rovers MM, de Vries RBM, Leenaars M, Ritskes-Hoitinga M, Langendam MW. SYRCLE's risk of bias tool for animal studies. *BMC Medical Research Methodology.* 2014;14(1).
38. Rosloniec EF, Cremer M, Kang AH, Myers LK, Brand DD. Collagen-induced arthritis. *Curr Protoc Immunol.* 2010;Chapter 15:Unit 15 5 1-25.
39. Vesterinen H, Sena E, Egan K, Hirst T, Churolov L, Currie G, et al. Meta-analysis of data from animal studies: a practical guide. *Journal of neuroscience methods.* 2014;221:92-102.

40. Takeshima N, Sozu T, Tajika A, Ogawa Y, Hayasaka Y, Furukawa TA. Which is more generalizable, powerful and interpretable in meta-analyses, mean difference or standardized mean difference? *BMC medical research methodology*. 2014;14(1):30.
41. Hynes K, Bright R, Proudman S, Haynes D, Gronthos S, Bartold M. Immunomodulatory properties of mesenchymal stem cell in experimental arthritis in rat and mouse models: A systematic review. *Semin Arthritis Rheum*. 2016;46(1):1-19.
42. Song YW, Kang EH. Autoantibodies in rheumatoid arthritis: rheumatoid factors and anticitrullinated protein antibodies. *QJM*. 2010;103(3):139-46.
43. Singh JA, Saag KG, Bridges SL, Jr., Akl EA, Bannuru RR, Sullivan MC, et al. 2015 American College of Rheumatology Guideline for the Treatment of Rheumatoid Arthritis. *Arthritis Rheumatol*. 2016;68(1):1-26.
44. Rubbert-Roth A, Finckh A. Treatment options in patients with rheumatoid arthritis failing initial TNF inhibitor therapy: a critical review. *Arthritis Res Ther*. 2009;11 Suppl 1:S1.
45. Ghoryani M, Shariati-Sarabi Z, Tavakkol-Afshari J, Ghasemi A, Poursamimi J, Mohammadi M. Amelioration of clinical symptoms of patients with refractory rheumatoid arthritis following treatment with autologous bone marrow-derived mesenchymal stem cells: A successful clinical trial in Iran. *Biomedicine & Pharmacotherapy*. 2019;109:1834-40.
46. Park EH, Lim Hs, Lee S, Roh K, Seo KW, Kang KS, et al. Intravenous Infusion of Umbilical Cord Blood-Derived Mesenchymal Stem Cells in Rheumatoid Arthritis: A Phase Ia Clinical Trial. *Stem cells translational medicine*. 2018;7(9):636-42.
47. Shadmanfar S, Labibzadeh N, Emadedin M, Jaroughi N, Azimian V, Mardpour S, et al. Intra-articular knee implantation of autologous bone marrow-derived mesenchymal stromal cells in rheumatoid arthritis patients with knee involvement: Results of a randomized, triple-blind, placebo-controlled phase 1/2 clinical trial. *Cytotherapy*. 2018;20(4):499-506.
48. Droujinine IA, Eckert MA, Zhao W. To grab the stroma by the horns: from biology to cancer therapy with mesenchymal stem cells. *Oncotarget*. 2013;4(5):651.
49. 49. Zhao L, Chen S, Yang P, Cao H, Li L. The role of mesenchymal stem cells in hematopoietic stem cell transplantation: prevention and treatment of graft-versus-host disease. *Stem Cell Res Ther*. 2019;10(1):182.
50. 50. Rosland GV, Svendsen A, Torsvik A, Sobala E, McCormack E, Immervoll H, et al. Long-term cultures of bone marrow-derived human mesenchymal stem cells frequently undergo spontaneous malignant transformation. *Cancer Res*. 2009;69(13):5331-9.
51. 51. Kim N, Cho S-G. Clinical applications of mesenchymal stem cells. *The Korean journal of internal medicine*. 2013;28(4):387-402.

# CHAPTER 6

## Preclinical Evaluation of a Single Intravenous Infusion of hUC- MSC (BX-U001) in Rheumatoid Arthritis

**Authors:** Henry P. Farhood<sup>1-3\*</sup>, Linan Liu<sup>8\*</sup>, Menglu Han<sup>1-3</sup>, Guangyang Liu<sup>7</sup>, Jingxia Yu<sup>7</sup>, Lily Nguyen<sup>1-3</sup>, Brenda Nguyen<sup>1-3</sup>, Agnes Nguyen<sup>1-3</sup>, Wenbin Liao<sup>8‡</sup>, and Weian Zhao<sup>1-6‡</sup>

<sup>1</sup> Sue and Bill Gross Stem Cell Research Center, University of California, Irvine, Irvine, CA 92697, USA;

<sup>2</sup> Department of Pharmaceutical Sciences, University of California, Irvine, Irvine, CA 92697, USA;

<sup>3</sup> Chao Family Comprehensive Cancer Center, University of California, Irvine, Irvine, CA 92697, USA;

<sup>4</sup> Edwards Life Sciences Center for Advanced Cardiovascular Technology, University of California, Irvine, Irvine, CA 92697, USA;

<sup>5</sup> Department of Biomedical Engineering, University of California, Irvine, Irvine, CA 92697, USA;

<sup>6</sup> Department of Biological Chemistry, University of California, Irvine, Irvine, CA 92697, USA;

<sup>7</sup> Department of Surgery, University of California, Irvine, Orange, CA 92868, USA;

<sup>8</sup> Baylx, Inc., Irvine, CA 92618, USA.

## 6.1 Abstract

Rheumatoid arthritis (RA) is an inflammatory disease of the joints, which causes severe pain and excessive systemic circulation of harmful inflammatory cytokines. Current treatments are limited, with some patients not responding well, and some experiencing severe and detrimental side effects. Mesenchymal stem cells (MSC) are cell based therapeutic being evaluated as potent immunomodulators in RA and may provide relief to patients not responding well to drug-based treatments. We evaluated the safety and efficacy of BX-U001 human umbilical cord mesenchymal stem cells (hUC-MSC) to treat RA, in support of a successful investigational new drug (IND) application. A collagen-induced arthritis (CIA) mouse model of Rheumatoid Arthritis was established in DBA/1J mice. Mice from the treatment (TA) group were given a tail vein infusion of hUC-MSC 24 days after primary RA induction, while CA group mice were given cell-free carrier solution. All animals were evaluated daily for RA symptoms via clinical scoring, blood was taken periodically for cytokine analysis, and mice were dissected at endpoint for histological analysis. A linear mixed model was used to compare the rate of change among groups. The clinical scores of TA group were significantly reduced compared with CA group ( $p < 0.01$ ), indicating therapeutic effects. The histological scores of the joints in TA group were significantly lower than those in the CA group ( $p < 0.05$ ), but had no significant difference compared with Healthy groups ( $p > 0.05$ ). The concentration of (Interleukin) IL-6 in TA group was significantly reduced by 80.0% ( $p < 0.0001$ ) two days after treatment and by 93.4% at the experimental endpoint compared with levels prior to hUC-MSC injection. A single intravenous infusion of hUC-MSC ( $2 \times 10^6$  cells/mouse), to CIA induced DBA/1J mice, resulted in significant alleviation of RA symptoms and may provide significant therapeutic benefits in humans.

**Keywords: Mesenchymal stem cell, MSC, arthritis, rheumatoid, immunotherapy, immunomodulation, anti- inflammatory, inflammation, umbilical cord**

## 6.2 Introduction

Arthritis affects over 54 million Americans and can lead to Rheumatoid arthritis<sup>1,2</sup>. Rheumatoid arthritis (RA) is an inflammatory disease which affects between 1.5 and 3 million Americans and is characterized by inflammation of the synovial and cartilage tissue, causing damage to the articular cartilage and bone<sup>3-8</sup>. RA can lead to reduced quality of life and serious damage to organ systems, caused by the high level of inflammatory cytokines circulating in the blood<sup>9,10</sup>. The causes of RA are still being elucidated, but there is a clear inflammatory cascade that involves the production of tumor necrosis factor alpha (TNF- $\alpha$ ) and IL-6, following the production of auto-antibodies including “Rheumatoid Factor” (RF) and anti-citrullinated protein autoantibodies (ACPA)<sup>5,6,11</sup>. The pro-inflammatory cytokines and autoantibodies activate macrophages to infiltrate and damage the tissues of the joint, while simultaneously producing more inflammation<sup>12-15</sup>. There are also autoantibody-negative cases of RA, in which disease is characterized by inflammation and fibrosis, developed from the infiltration of fibroblast-like synoviocytes and increased thickening of synovial lining<sup>16,17</sup>. While autoantibody positive RA is associated with worse prognosis, both types of disease result from macrophage dependent inflammation<sup>12-18</sup>.

One of the problems with treating autoimmune diseases, such as RA, is that the immune system is complex and pharmaceutical drugs and biologics tend to target only one or a small subset of the system<sup>19</sup>. The current standard treatment regime varies by country but is generally reliant on methotrexate and biologics (for instance, Antibodies against TNF- $\alpha$ ), but nonsteroidal anti-inflammatory drugs (NSAIDs) and corticosteroids are still common treatments<sup>20</sup>. These treatments are not at all targeted toward the specific causes of RA, cause immunosuppression, and have significant side effects<sup>21,22</sup>. There is great need for more effective therapeutics, and treatments that do not produce systemic immunosuppression<sup>23</sup>.

Stem cell therapies have the potential to treat and manage autoimmune disorders in ways that conventional drugs cannot, because stem cells can harness the complex mechanisms that the body naturally uses to modulate and restore the imbalanced immunity with minimal toxicity<sup>21</sup>. In particular, mesenchymal stem cells (MSC) have been shown to have immunomodulatory effects on many types of immune cells and have limited side effects in past pre-clinical and clinical studies<sup>22</sup>. MSC are multipotent cells that can be

readily isolated from many different adult tissues including fat, bone marrow, blood, and umbilical cord<sup>21</sup>. These cells can then be expanded *in vitro* to serve as “off-the-shelf” therapeutics. Human umbilical cord tissue derived MSC (hUC-MSC) have been shown to have strong immunomodulatory effects and may have higher therapeutic potential for RA than bone marrow derived MSC<sup>22</sup>. Due to MSC’s immune evasive and immunomodulatory properties, they do not have the major graft vs host issues that other cell types do, making them amenable to allogenic transplantation. MSC have been shown to effect CD4+/CD8+ T cells, T regulatory cells (T-reg), B cell, monocytes, natural killer cells and macrophages. The immunomodulatory mechanism of action (MOA) is by direct contact inducing apoptosis of effector lymphocytes, and secretion of soluble mediators such as indoleamine 2,3-dioxygenase (IDO), prostaglandin E2, IL-6, and HLA-G5, which are known to dampen immune response<sup>24</sup>. This multi-pronged immunomodulatory power makes these cells capable of treating diseases caused by many different cell types. Previous preclinical animal studies have consistently shown reduction of RA symptoms upon treatment with MSC, regardless of the animal model used<sup>22</sup>. This preclinical study evaluates the potential of a new MSC product derived from human umbilical cord tissue (BX-U001) to treat a collagen induced arthritis (CIA) mouse model of rheumatoid arthritis and led to the successful filing of an investigational new drug (IND) application with the U.S. Food and Drug Administration (FDA) to initiate a clinical trial.

### **6.3 Materials and Methods**

**Isolation and culture of hUC-MSC:** The hUC-MSC used in this study were isolated and cultured from umbilical cord tissue by a standard tissue explant method<sup>25</sup>. Cells were cultured in hUC-MSC growth medium (BaylX) at 37°C in 5% CO<sub>2</sub>. Cells were used in experiments at passage 6 from tissue harvest.

**hUC-MSC differentiation assays:** For osteogenic and adipogenic differentiations, hUC-MSC were seeded onto 24-well tissue culture plates with  $6 \times 10^4$  cells/well and incubated at 37°C in a humidified atmosphere containing 5% CO<sub>2</sub>. The differentiation induction medium from the Mesenchymal Osteogenesis Differentiation Kit and Mesenchymal Adipogenesis Differentiation Kit (EMD Millipore) were added after the confluence reached 90%. The media was changed every two to three days based on the manufacturer’s

protocol and adipogenic differentiation was confirmed by the deposition of lipid droplets in the cytoplasm using Oil Red O staining (EMD Millipore). The osteogenic differentiation was confirmed by positive staining of the extracellular calcium matrix using Alizarin Red S staining (EMD Millipore). Images of the stained samples were collected using a Nikon Ti-E microscope (Nikon).

**Flow cytometry:** The phenotype of hUC-MSC was analyzed by flow cytometry after trypsinization. MSCs were stained with fluorescein isothiocyanate (FITC)-conjugated antibodies against CD34 and HLA-DR, or phycoerythrin (PE)-conjugated antibodies against CD45, CD90, CD105 and CD73. Mouse isotypic antibodies served as the control. Cells were stained in single label according to the manufacturer's instructions and then analyzed by flow cytometry on a BD Accuri™ C6 flow cytometer (BD Biosciences). Flow cytometry data were processed using FlowJo™ (FlowJo).

**hUC-MSC Potency assay:** hUC-MSC ( $1 \times 10^4$  cells/well) were co-cultured with anti-CD3/anti-CD28/IL-2 treated human peripheral blood mononuclear cells (hPBMC,  $1 \times 10^5$  cells/well) in 96-well tissue culture plates. Activated PBMC cultured alone were used as positive control (Control non-MSC, Secretion inhibition efficiency = 0%). The TNF- $\alpha$  expression was then measured with a LEGEND MAX™ Human TNF- $\alpha$  ELISA Kit (Biolegend) after 3 days' co-culture.

**Animal studies:** A total of 60 male DBA/1J mice (Jackson Laboratories) were randomly labeled and used for two identical experiments. Of that 60, 53 animals were selected randomly for primary induction (26 mice in the first study (Batch 1) and 27 mice in the second (Batch 2)). The remaining 7 mice were assigned to Healthy Groups. On the day of hUC-MSC infusion, 41 mice met the disease onset criteria (*i.e.*, at least one leg reached the clinical score  $\geq 2$  on the day of infusion) and mice were regrouped randomly to ensure no significant differences of clinical scores existed between TA and CA groups. There were 21 mice in TA Group (11 in Batch 1 and 10 in Batch 2), 20 in CA Group (10 in Batch 1 and 10 in Batch 2) and 7 in Healthy Group (4 in Batch 1 and 3 in Batch 2) (Table 6.1). Body weight (17-23 g for Batch 1; 16-24 g for Batch 2) of animals was measured every three days from the start of baseline blood collection (2-3 days before primary induction), to 18 days after the primary induction (Day 18), and was measured every other day



**Table 6.1. Animal Grouping**

| <b>Group</b> | <b>Agent Name</b>          | <b>Dosage (cells)</b>  | <b>Volume of infusion</b> | <b>Animal Number</b> |
|--------------|----------------------------|------------------------|---------------------------|----------------------|
| CA           | Cell-free carrier solution | -                      | 200 $\mu$ L/mouse         | 20                   |
| TA           | hUC-MSC injection          | $2 \times 10^6$ /mouse | 200 $\mu$ L/mouse         | 21                   |
| Healthy      | -                          | -                      | -                         | 7                    |

thereafter (Figure 6.1). The mice were monitored daily and assessed every other day, in a double-blind fashion, for signs of arthritis onset (based on clinical scores) by two independent investigators. Clinical arthritis was scored on a scale of 0–4, where 0 = no swelling, 1 = erythema and mild swelling limited to tarsals or ankle joint; 2 = erythema and mild swelling extending from ankle to tarsal joints; 3 = erythema and moderate swelling extending from ankle to metatarsal joints; 4 = erythema and severe swelling surrounding the ankle, foot, and digits, or ankylosis of the limb. Each limb was graded and the grades from 4 limbs were summed to yield the arthritis score for each animal. The maximal score was 16. Paw thickness (exploratory outcome) was also assessed with a 0–10 mm Thickness Gage (Mitutoyo). All animals were sacrificed 42 days after primary induction (Day 42, endpoint) with CO<sub>2</sub> (or isoflurane) overdose and cervical dislocation. Legs were harvested for further processing, followed by mouse dissection. Notes were taken and a histopathological exam was conducted if any abnormality in the volume, color, texture, *etc.* of organs (brain, heart, liver, spleen, lung, kidney and injection site tissue) was observed. All animal experiments and procedures were performed under permission from the UCI Institution of Animal Care and Use Committee (IACUC protocol number 2016-3212) and conducted per the Animal Welfare Assurance (#A3416.01).

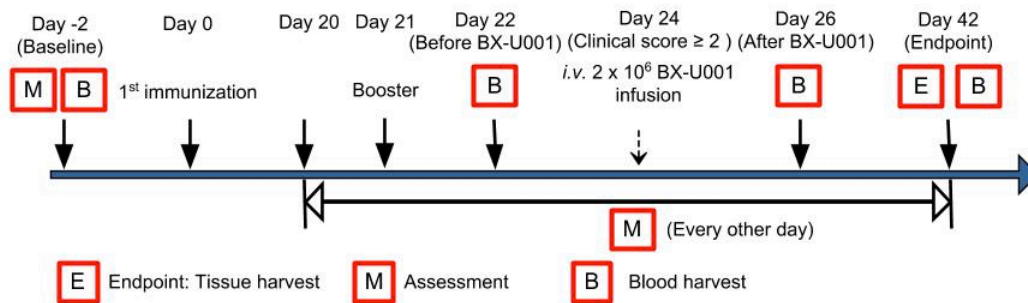


**Figure 6.1. Timeline of using hUC-MSC to treat CIA-induced RA.**

**Arthritis induction:** For collagen-induced arthritis (CIA), DBA/1J mice were immunized with 100 µg of bovine type II collagen (Chondrex), that was emulsified with Freund's complete adjuvant (CFA) containing 200 µg of *Mycobacterium tuberculosis* H37Ra (Sigma-Aldrich), via an intradermal injection at the base of the tail; and a booster emulsion of CII in Freund's incomplete adjuvant (IFA) was administered at 21 days (Day 21) after the primary immunization (Figure 6.1)<sup>26</sup>. Disease onset was defined as at least one leg reached the clinical score  $\geq 2$ .

**MSC administration:** At 24 days (Day 24) after primary induction of CIA (after disease onset), a single infusion of 200 µL carrier solution (Baylx) or 2 million hUC-MSC suspended in 200 µL carrier solution ( $1 \times 10^7$  cells/mL) was intravenously infused via tail vein to each mouse from CA and TA groups. Intravenous infusion via tail vein was used to mimic the clinical administrative route and was done with 1 mL sterile syringes with 30 G  $\times$  ½ disposable needles and an infusion speed of 8-20 µL/second. After drug administration, animals were closely monitored for 2 hours. If any abnormality was observed (e.g., any profound paralysis that inhibits animals' ability to eat or drink, any signs of pain including piloerected/unkept fur, squinted eyes, ataxia, hunched posture, labored breathing, that is not relieved with analgesia), symptoms and their starting time, severity, duration, *etc.* were recorded in detail. Thereafter monitoring was also conducted twice a day with notes taken accordingly.

**Serum cytokine quantification:** Murine blood was collected into EDTA-coated collection tubes (Sai-infusion) at baseline (2-3 days before primary induction), before treatment (Day 22), after treatment (Day

26) and endpoint (Day 42) (Figure 6.1). Then the sera were harvested from blood samples after centrifugation. The pro-inflammatory cytokine levels (including IL-1 $\beta$ , TNF- $\alpha$ , IFN- $\gamma$  and IL-6) were determined by a MILLIPLEX MAP Mouse TH17 Magnetic Bead Panel Luminex assay (EMD Millipore) following the manufacturer's protocol.

**Tissue processing and histology:** Excessive fur and muscle were removed with scissors and tweezers from each mouse's limbs before being fixed in 10% formalin for 2 days. The limbs were decalcified for 3-4 weeks in decalcification solution (14% EDTA, 0.2% of 4% PFA in 1 $\times$  PBS, pH = 7.4); the decalcification solution was changed every two to three days. All limbs were processed in a TP1020-1-1 tissue processor (Leica) using an 18-hour processing protocol. The 10  $\mu$ m paraffin sections were stained using hematoxylin and eosin (EMD Millipore) to assess the difference in tissue morphology among TA, CA and Healthy groups. Stained tissue was imaged on a Nikon Ti Eclipse (Nikon) using a 10 $\times$  objective. Representative images of H&E stained limbs from all three groups were independently scored by two blinded investigators on a scale from 0–4, where 0 = no cell infiltration, cartilage damage, or bone erosion; 1 = mild cell infiltration and synovial membrane hypertrophy, and little to no cartilage damage; 2 = obvious cell infiltration, mild cartilage damage, and little to no bone erosion; 3 = severe cell filtration, cartilage erosion, and bone erosion; and 4 = complete loss of joint integrity and ankylosis.

**Data Analysis and Statistics:** Data were analyzed by Student's two-tailed t test when comparing 2 groups. Data were expressed as the mean  $\pm$  SEM, mean  $\pm$  SD or mean and 95% confidence interval (95% CI), and differences were considered significant at  $p < 0.05$ . CIA mice that did not meet the disease onset criteria for treatment (*i.e.*, at least one leg has a clinical score  $\geq 2$ ) on the infusion day were removed from the study. Samples with readings failed or out of the upper limit of standard curve in Luminex assay were removed from the analysis. Luminex readings out of the lower limit of the standard curve were defined as "0". See Supplementary Materials for detailed information for analysis on clinical scores and paw thickness.

## 6.4 Results

### 6.4.1 Generation and *in vitro* characterization of hUC-MSC

The hUC-MSC used in this study were generated from umbilical cord tissue and were characterized to have standard MSC phenotype according to the International Society for Cellular Therapy (ISCT) criteria (Figure 6.2). We established a laboratory cell bank of hUC-MSC at passage 5. This cell bank was used for *in vitro* characterization and for the animal experiments in our IND-enabling studies. The hUC-MSC cell line displayed appropriate marker expression (Figure 6.2A). The hUC-MSC showed high expression of the key MSC markers CD73, CD90, CD105, while maintaining low expression of non-MSC markers including CD45, CD34, and HLA-DR. Multipotency was displayed via adipogenesis and osteogenesis (Figure 6.2B). When co-cultured with activated PBMC's, the hUC-MSC reduced TNF- $\alpha$  inflammatory cytokines by over ten-fold (Figure 6.2C), indicating an anti-inflammatory functional potency.

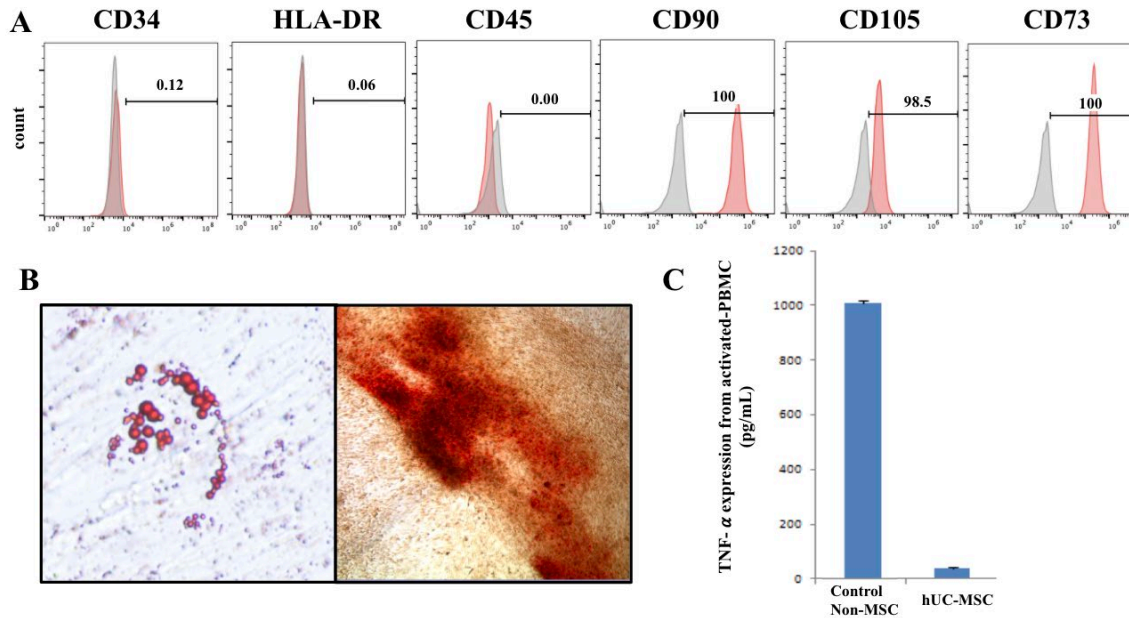


**Figure 6.2. *In vitro* characterization of hUC-MSC.** A) Flow cytometric analysis showed that hUC-MSC were positive for the surface markers CD90, CD105, and CD73, while negative for CD34, HLA-DR, and CD45. B) Oil Red staining (left) showed adipogenic potential of hUC-MSC after adipogenesis differentiation; Alizarin red staining (right) showed mineralization potential of hUC-MSC after osteogenic differentiation. C) hUC-MSC showed a superior TNF- $\alpha$  inhibitive effect when co-cultured with PBMC. TNF- $\alpha$  expression level was analyzed in the presence of hUC-MSC and a non-MSC control following activation of PBMC with anti-CD3, anti-CD28 and IL-2. Data is presented as mean  $\pm$  SD.

#### 6.4.2 hUC-MSc improved arthritis assessment outcomes

Collagen induced arthritis was established in DBA/1J mice to mimic human rheumatoid arthritis. CIA animals were grouped randomly into either a Treatment Assessment (TA) Group, which received a tail vein infusion of 2 million hUC-MSc or a Control Assessment (CA) Group, which received only cell-free carrier solution.

To evaluate disease severity and treatment efficacy, clinical assessments were taken by two independent investigators every other day for 18 days. The averaged clinical score on Day 24 (the day of hUC-MSc infusion) for TA group was 7.08 (95% CI: 6.30, 7.86), 7.51 (95% CI: 6.73, 8.30) for CA Group, and 0.38 (95% CI: -0.57, 1.33) for the Healthy Group, respectively. The Day 24 Healthy Group clinical scores were not significantly greater than zero ( $p = 0.435$ ) and there was no significant difference in clinical scores between TA and CA groups, prior to treatment ( $p = 0.126$ ) (Supplemental Table 6.1). The Day 24 clinical scores of both TA and CA groups were significantly higher than that of the Healthy Group ( $p < 0.0001$ ).

After infusion, a significant difference in clinical scores between TA and CA groups was detected on Day 28, *i.e.*, 4 days after the hUC-MSc infusion (-1.53,  $p = 0.003$ , 95% CI: -2.29, -0.77; with Bonferroni correlation for multiple comparison, Supplemental Table 6.1) which continued to increase until Day 42 (endpoint) (-4.49,  $p < 0.0001$ , 95% CI: -5.97, -3.01; Table 6.2, Figure 6.3 and Supplemental Figure 6.2). In Batch 1, a significant difference in clinical scores between TA and CA groups was observable by Day 32 (-2.82,  $p = 0.036$ , 95% CI: -4.52, -1.12) which continued to increase until Day 42 (endpoint) (-5.44,  $p < 0.0001$ , 95% CI: -7.40, -3.49) (Supplemental Table 6.2). In Batch 2, a significant difference in clinical scores between TA and CA groups started on Day 28 (-1.69,  $p = 0.015$ , 95% CI: -2.59, -0.79) and continued to increase until Day 38 (-3.95,  $p = 0.012$ , 95% CI: -6.02, -1.88) (Supplemental Table 6.3). All baseline clinical scores were zero.

**Table 6.2. Clinical scores after hUC-MSC infusion (Combined batches; Mean and 95% CI)**

| Time point | TA Group          | CA Group           | TA - CA              | P Value  |
|------------|-------------------|--------------------|----------------------|----------|
| Day 26     | 7.17 (6.41, 7.94) | 8.08 (7.31, 8.84)  | -0.90 (-1.56, -0.24) | 0.093    |
| Day 28     | 6.81 (6.26, 7.37) | 8.34 (7.79, 8.90)  | -1.53 (-2.29, -0.77) | 0.003    |
| Day 30     | 6.55 (5.95, 7.15) | 8.50 (7.90, 9.10)  | -1.95 (-2.79, -1.10) | < 0.001  |
| Day 32     | 6.08 (5.04, 7.11) | 8.78 (7.75, 9.81)  | -2.70 (-3.74, -1.66) | < 0.0001 |
| Day 34     | 5.55 (4.55, 6.55) | 8.53 (7.53, 9.53)  | -2.97 (-4.07, -1.87) | < 0.0001 |
| Day 36     | 5.12 (3.50, 6.75) | 8.85 (7.22, 10.48) | -3.73 (-4.98, -2.48) | < 0.0001 |
| Day 38     | 4.78 (3.35, 6.21) | 9.02 (7.59, 10.46) | -4.25 (-5.63, -2.87) | < 0.0001 |
| Day 40     | 4.48 (3.25, 5.72) | 8.79 (7.56, 10.03) | -4.31 (-5.68, -2.94) | < 0.0001 |
| Day 42     | 4.02 (2.95, 5.10) | 8.52 (7.44, 9.59)  | -4.49 (-5.97, -3.01) | < 0.0001 |

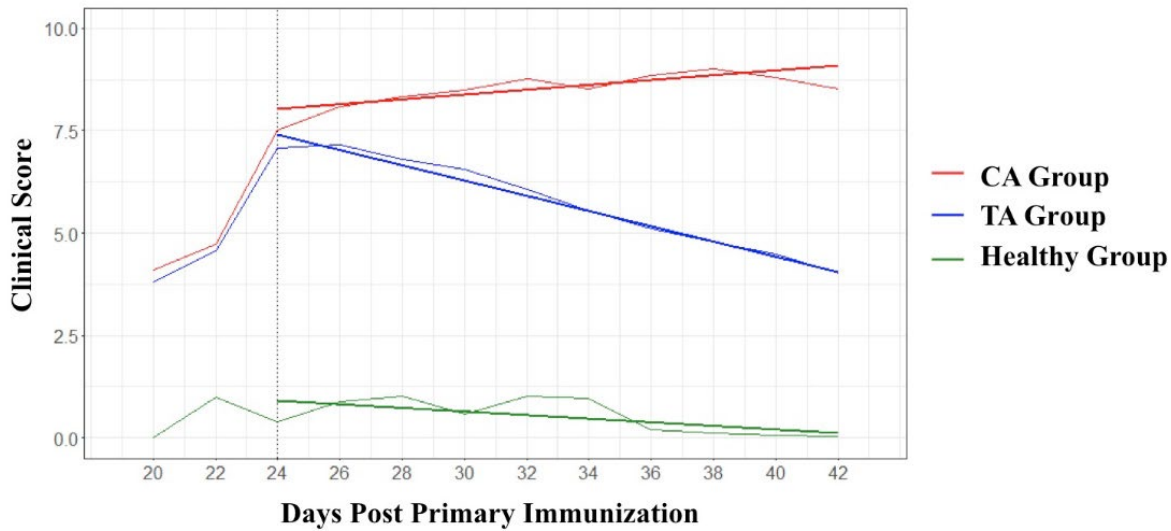


**Figure 6.3. Average clinical score and model-based rate of change for each experimental group from Day20 to Day42 (two batches combined).** TA Group: n = 21, CA Group: n = 20, Healthy Group: n = 7. hUC-MSC was infused on Day 24 (dash line). The three straight bold lines stand for the LMM-fitted linear trends of clinical score in each group.

When comparing the clinical scores between Day 24 and Day 42 (endpoint), a significant decrease of 3.12 ( $p < 0.0001$ , 95% CI: 2.04, 4.20) was observed in TA Group whereas the clinical score was significantly increased by an average of 1.13 ( $p = 0.047$ , 95% CI: 0.05, 2.21) 18 days after hUC-MSC infusion in CA Group (Table 6.3). No significant change of clinical score was detected in Healthy Group ( $p = 0.668$ , 95% CI: -2.18, 1.39; Table 6.4). Importantly, a significant difference in the 18-day clinical score trend was observed between TA and CA groups (-4.25,  $p < 0.0001$ , 95% CI: -5.78, -2.72; Table 6.4). Consistency was observed between both batches (Supplemental Table 6.2 and 6.3).

**Table 6.3. Comparison (TA vs. CA) on clinical score between Day 24 and Day 42 (Estimate = TA - CA)**

| Batch    | Estimate | 95% Confidence Interval | P Value  |
|----------|----------|-------------------------|----------|
| Combined | -4.25    | (-5.78, -2.72)          | < 0.0001 |
| Batch 1  | -5.12    | (-7.02, -3.22)          | < 0.0001 |
| Batch 2  | -3.41    | (-5.90, -0.91)          | 0.015    |

**Table 6.4. Changes of clinical score between Day 24 and Day 42 (Estimate = Day 42 - Day 24)**

| Group   | Batch    | Estimate | 95% Confidence Interval | P Value  |
|---------|----------|----------|-------------------------|----------|
| TA      | Combined | -3.12    | (-4.20, -2.04)          | < 0.0001 |
|         | Batch 1  | -3.40    | (-4.71, -2.09)          | < 0.0001 |
|         | Batch 2  | -2.81    | (-4.62, -1.00)          | 0.007    |
| CA      | Combined | 1.13     | (0.05, 2.21)            | 0.047    |
|         | Batch 1  | 1.72     | (0.34, 3.10)            | 0.024    |
|         | Batch 2  | 0.60     | (-1.12, 2.32)           | 0.502    |
| Healthy | Combined | -0.39    | (-2.18, 1.39)           | 0.668    |
|         | Batch 1  | -0.69    | (-2.76, 1.38)           | 0.522    |
|         | Batch 2  | 0.00     | (-3.14, 3.14)           | 1.000    |

A comparison between TA and CA group clinical scores over the time was also performed (Figure 6.3 and Table 6.3). The model-based rate of change in clinical score was 1.86 decrease (95% CI: 1.58, 2.14) per 10 days in TA Group and 0.60 increase (95% CI: 0.32, 0.88) per 10 days in CA Group. Overall hUC-MSc infusion displayed a significant therapeutic effect on reducing clinical scores in a CIA murine model (-0.25 per day,  $p < 0.0001$ , 95% CI: -0.29, -0.21). Similar results were also observed, showing consistence between batches. The trend detected in Healthy Group was not significantly difference compared to zero (-0.04 per day,  $p > 0.05$ , 95% CI: -0.09, 0.00). Representative pictures of paws are shown in (Supplemental Figure 6.3).

Joint swelling was measured with thickness gages (front and back paws) every other day for 18 days. On the day of hUC-MSc infusion (Day 24), paw thickness between TA and CA groups had no significant difference (-0.01 mm,  $p = 0.874$ , 95% CI: -0.16, 0.14). When analyzed separately, the thickness of neither front paws (0.03 mm,  $p = 0.311$ , 95% CI: -0.03, 0.08) nor hind paws (-0.05 mm,  $p = 0.051$ , 95% CI: -0.11, 0.00) showed significant difference between TA and CA groups.

The mean and 95% CI of paw thickness measured every two days after Day 24 was calculated for front and hind legs separately (Supplemental Table 6.4) and combined (Supplemental Table 6.5). No significant difference was observed in overall, front or hind paw thickness between TA and CA groups from Day 26 to Day 42 (Supplemental Figure 6.4).

### 6.4.3 Microscopic joint inflammation was reduced after hUC-MSC treatment

After endpoint mice were sacrificed, and tissues were harvested so that histological analysis could be performed on the joints. Briefly, at the endpoint (Day 42), mice (Batch 1) were sacrificed and legs were harvested and processed, then assayed with H&E staining. The histological scores of TA Group were significantly lower than those of CA Group ( $p < 0.05$ ) and had no significant difference compared to those of the Healthy Group ( $p > 0.05$ ), demonstrating a significant therapeutic effect of hUC-MSC on RA. A significant difference was also observed between CA Group and Healthy Group ( $p < 0.01$ ; Table 6.5, Figure 6.4). Collectively, arthritis symptoms were successfully established in mice, and hUC-MSC treatment showed improvements in several clinical parameters relating to arthritis.

**Table 6.5. Histological scores (Day 42, Mean  $\pm$  SEM)**

| TA Group (n = 10) | CA Group (n = 9)  | Healthy Group (n = 4) |
|-------------------|-------------------|-----------------------|
| 1.009 $\pm$ 0.243 | 1.826 $\pm$ 0.254 | 0.653 $\pm$ 0.097     |



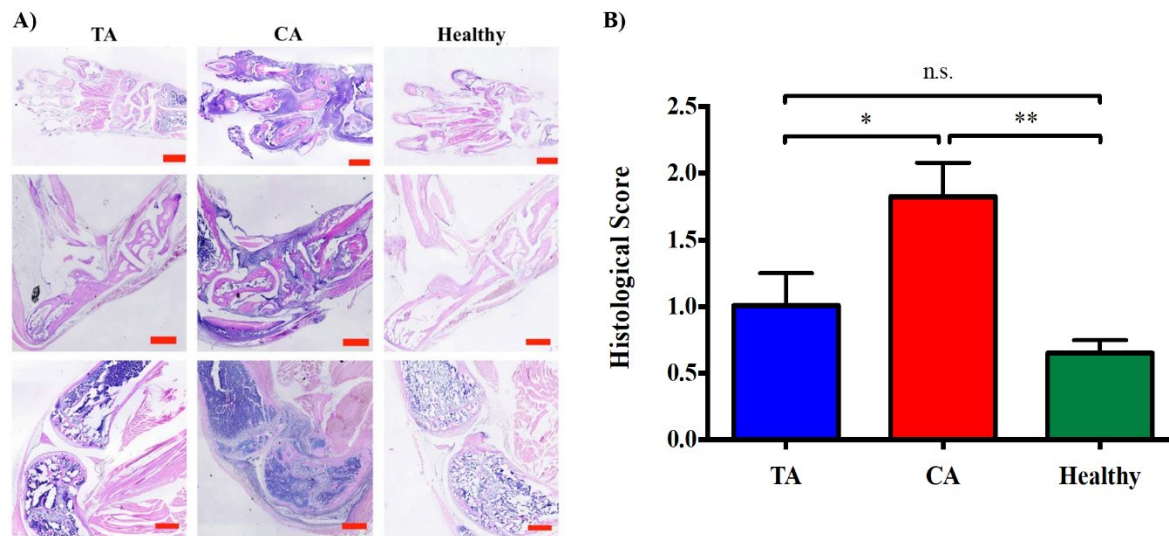


**Figure 6.4. CA group mice had significantly better histological scores than those of TA group.** A) Representative pictures of histological sections. Scale bars = 500  $\mu$ m. B) Comparison of histological scores among three experimental groups at the endpoint (Day 42). Maximum score = 4. Mean  $\pm$  SEM. TA Group: n = 10, CA Group: n = 9, Healthy Group: n = 4. \* $p$  < 0.05, \*\* $p$  < 0.01 and n.s. = not significant.

#### 6.4.4 IL-6 level was declined by hUC-MSC treatment

Blood was taken for cytokine analysis at multiple time points throughout the experiment. Briefly, murine blood (Batch 1) was harvested on the days before (Day 22) and after (Day 26) the hUC-MSC infusion, as well as on the baseline and the endpoint (Day 42). Concentrations of pro-inflammatory cytokines IFN- $\gamma$ , IL-6, TNF- $\alpha$  and IL-1 $\beta$  in plasma were measured with Luminex assay (Table 6.6). At the baseline, the cytokine levels were low and there was no significant difference between TA and CA groups. On Day 22, the concentrations of IFN- $\gamma$ , IL-6 and TNF- $\alpha$  were highly increased with large variation among animals. The concentration of IL-1 $\beta$  also increased but not as high as the other cytokines. No significant difference was shown between TA and CA groups for all the cytokines (Supplemental Table 6.6).

Two days after hUC-MSC infusion (Day 26), the concentration of IL-6 in TA Group was significantly declined by 80.0% ( $p$  < 0.0001) compared with Day 22, whereas no significant change was observed in CA Group. The concentrations of TNF- $\alpha$  in TA Group dropped significantly by 14.3% from Day 22 ( $p$  < 0.05) while a climbing trend was observed in CA Group (increased by 13% compared to Day 22). The

concentrations of IFN- $\gamma$  and IL-1 $\beta$  also decreased compared with Day 22, but there was no significant difference between TA and CA groups.

At the endpoint (Day 42), the concentration of IL-6 was further reduced in both TA and CA groups. The decrease of IL-6 in TA Group (by 93.4% compared to Day 22) was significantly steeper than that of CA Group (by 64.7% compared to Day 22) ( $p < 0.05$ ; Table 6.6 and Figure 6.5A). The concentration of TNF- $\alpha$  was also declined in both TA and CA groups at the endpoint but without significant difference between TA and CA groups. (Table 6.6 and Figure 6.5B). For the concentration of IFN- $\gamma$  and IL-1 $\beta$ , no significant difference was detected between TA and CA groups ( $p > 0.05$ ; Table 6.6, Figure 6.5C and Figure 6.5D).

**Table 6.6. Relative concentrations of cytokines (%), Mean  $\pm$  SEM)**

| Cytokines     | Group | Time point      |                    |                   |
|---------------|-------|-----------------|--------------------|-------------------|
|               |       | Before (Day 22) | After (Day 26)     | Endpoint (Day 42) |
| IFN- $\gamma$ | TA    | 100.0 $\pm$ 0.0 | 37.5 $\pm$ 10.2    | 23.1 $\pm$ 8.3    |
|               | CA    | 100.0 $\pm$ 0.0 | 43.1 $\pm$ 11.3    | 25.2 $\pm$ 11.1   |
| IL-6          | TA    | 100.0 $\pm$ 0.0 | 20.0 $\pm$ 9.5#### | 6.6 $\pm$ 1.3*    |
|               | CA    | 100.0 $\pm$ 0.0 | 50.2 $\pm$ 20.0    | 35.3 $\pm$ 16.5   |
| TNF- $\alpha$ | TA    | 100.0 $\pm$ 0.0 | 85.7 $\pm$ 6.7#    | 42.8 $\pm$ 6.9    |
|               | CA    | 100.0 $\pm$ 0.0 | 113.0 $\pm$ 16.5   | 50.1 $\pm$ 13.9   |
| IL-1 $\beta$  | TA    | 100.0 $\pm$ 0.0 | 85.3 $\pm$ 8.4     | 74.9 $\pm$ 8.1    |
|               | CA    | 100.0 $\pm$ 0.0 | 77.5 $\pm$ 14.4    | 75.6 $\pm$ 13.3   |

# Significant reduction compared with Day 22; \*Significantly lower compared with CA Group

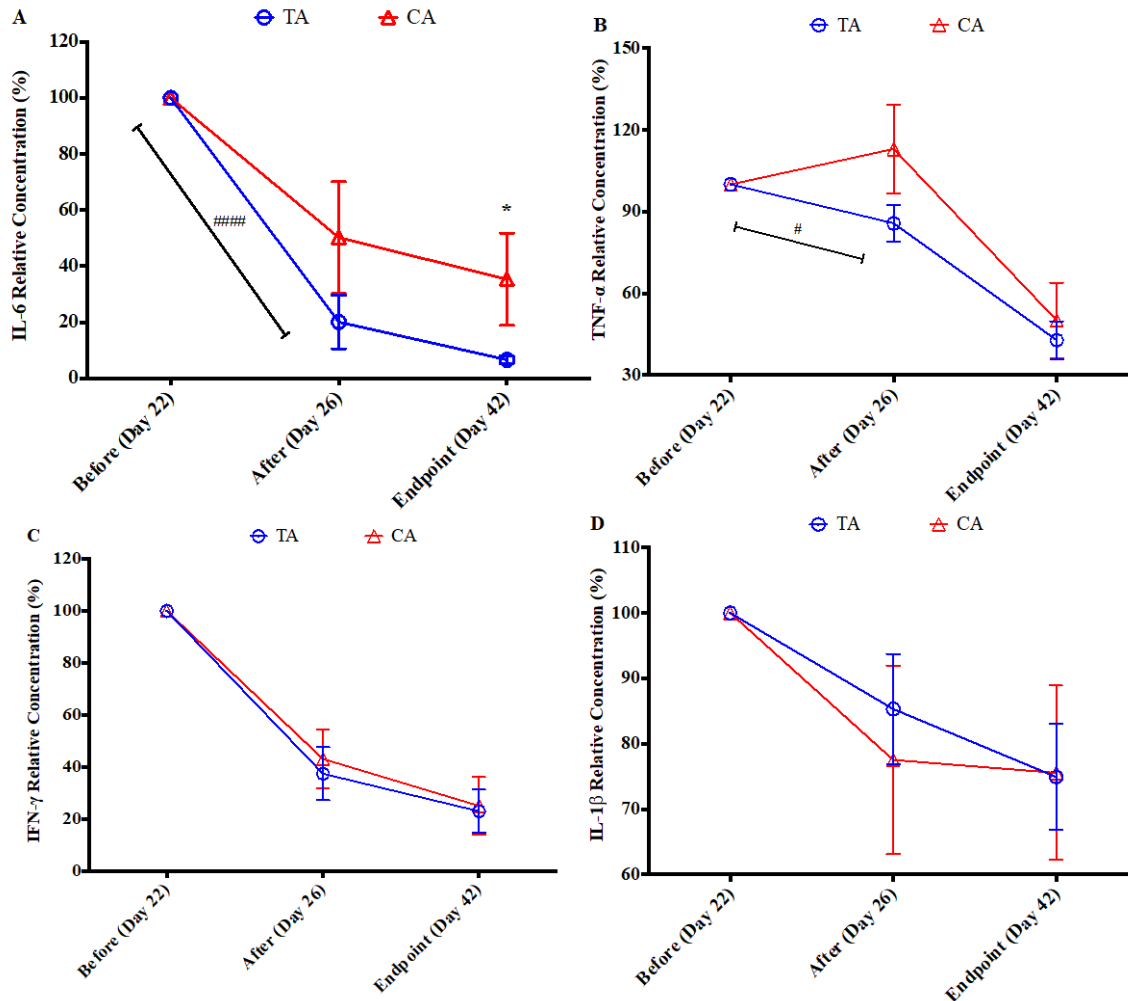


**Figure 6.5. Concentrations of pro-inflammatory cytokines (IL-6, IFN- $\gamma$ , TNF- $\alpha$  and IL-1 $\beta$ ) in each experimental group at baseline, Day 22, Day 26 and endpoint (Day 42).** The concentrations of cytokines were determined by Luminex serology assay. Mean  $\pm$  SEM. \* $p$  < 0.05 (TA Group vs. CA Group); # $p$  < 0.05 and #### $p$  < 0.0001 (Day 22 vs. Day 26).

#### 6.4.5 No side effect was observed after hUC-MSC administration

No abnormalities, including appearance, behavior, secretions and excreta, were observed after infusion of hUC-MSC and no mice died from infusion of test agents. No erythema, edema or exudation was observed at injection site, after infusion of test agent.

Animals were weighed every other day for 18 days. Variations in animal weights prior to CIA disease induction were insignificant (Supplemental Table 6.7). After CIA model induction, all animals lost weight,

and began to recover after two days. No significant difference in body weight was observed at any time points between TA and CA groups ( $p > 0.05$ , Supplemental Table 6.8), but by endpoint, both groups had lower average body weight than healthy mice (Supplemental Figure 6.1).

## 6.5 Discussion

Stem cell therapies have the capacity to treat disease more directly than standard small molecule drugs, which tend to only treat symptoms. Mesenchymal stem cells are a type of adult stem cell with immunomodulatory capabilities and were the active component of the hUC-MSc injection we evaluated in this study. MSC have been investigated for their beneficial therapeutic effects in multiple diseases, including myocardial infarction, connective tissue, autoimmune, inflammatory, lung, and kidney diseases<sup>27,28</sup>. Additionally, MSC have been evaluated in many animal studies and human clinical trials of rheumatic diseases<sup>22,29,30</sup>. There has been great interest in using MSC to treat patients with RA for many years<sup>31,32</sup>. We recently performed a meta-analysis of MSC in the treatment of RA and found that there was much variability between studies, and the origin of MSC may significantly impact treatment outcome<sup>22</sup>. For example, human umbilical cord and adipose derived MSC may be more effective against RA than MSC from other sources. Overall, previous preclinical and clinical studies showed positive efficacy and tolerability and therefore warrant further investigation into the clinical benefits of MSC in RA<sup>22,33</sup>. This study aimed to evaluate the efficacy from a single infusion of hUC-MSc to treat RA in a CIA murine model via tail vein and thereby provide information for preclinical studies of BX-U001.

After a CIA model was established the administration of hUC-MSc significantly reduced clinical scores of TA Group ( $p < 0.01$  starting from 6 days after hUC-MSc administration) compared to CA Group. Clinical scores are a qualitative measure of joint appearance based on comparison to healthy animal joints. Generally, mice induced with a CIA model had swollen joints, and erythema around joints and extremities (especially in the hind legs). While paw thickness measurements alone showed no significant difference

between TA and CA groups, these measurements are limited by the soft tissue surrounding the areas of inflammation and cannot tell us about the underlying joint structure. Clinical scoring includes color and overall appearance (straightness) of the joints, a general macroscopic evaluation which may indicate more about underlying joint health rather than the size of the joint alone.

In many studies of inflammation, histological evaluation can give insight to invasion of the immune system into specific tissue locations, and provide microscopic detail on structural damage, which macroscopic methods cannot achieve<sup>34</sup>. After treatment with hUC-MSC, the histological scores of the joints of TA Group were significantly reduced compared to CA Group ( $p < 0.001$ ). The knee joint had significant inflammation and immune cell invasion in untreated CIA mice (CA group), and there tended to be reduced synovial fluid between the joints. Additionally, bone was clearly eroded in CA group joints, but had been at least partially protected in TA group joints. This type of damage is the typical manifestation of RA inflammation, and directly correlates with pain and overall joint function<sup>35,36</sup>.

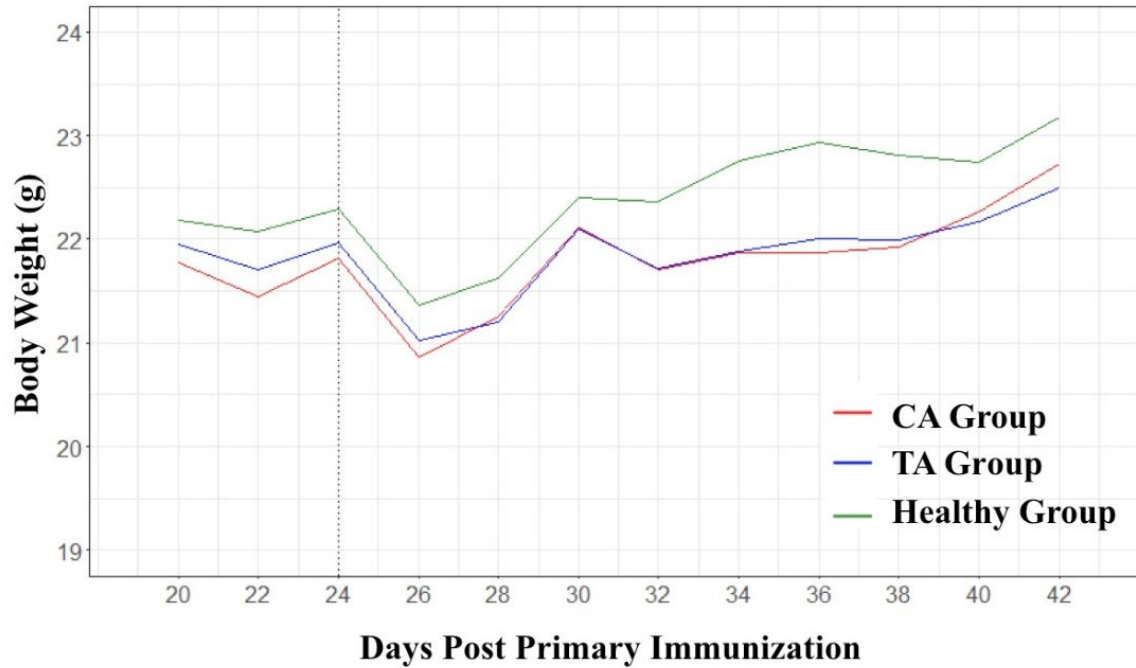
It is essential to evaluate the systemic effects of hUC-MSC treatment in RA, because the high levels of inflammatory cytokines released into the blood during RA pathogenesis can produce damage in the heart, lungs, and other vital organs, despite their geographical distance from inflamed joints<sup>10,37</sup>. In particular, TNF- $\alpha$  and IL-6 are key inflammatory cytokines in both the initial and advanced stages of RA disease<sup>29,30</sup>. The serum levels of these key cytokines were significantly reduced in hUC-MSC treated mice, compared to untreated controls. There was less of an effect of IFN- $\gamma$  and IL-1 $\beta$ , which are also linked to RA pathophysiology. The link between MSC treatment and a reduction in TNF- $\alpha$  and IL-6 is likely attributable to their ability to influence systemic levels of M2 anti-inflammatory macrophages and upregulate the levels of FoxP3<sup>+</sup> T regulatory cells<sup>29,38,39</sup>. Immediately after intravenous injection, many MSC become trapped in the capillaries of the lungs, where they are engulfed by macrophages<sup>40</sup>. The effect MSC have on circulating macrophages, resulting from their engulfment, is heavily linked to the ratio of anti-inflammatory cytokines produced by these macrophages, and their downstream interactions with other immune cells<sup>40-42</sup>. The detailed mechanisms of hUC-MSC action on RA are still being elucidated, but the reduction of TNF- $\alpha$  and

IL-6 cytokines appears to be a key feature.

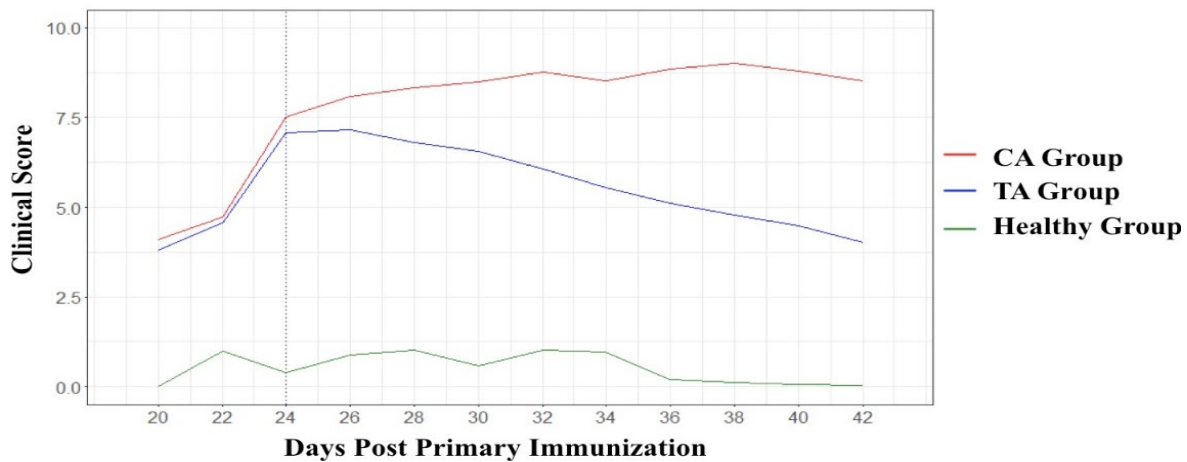
While the hUC-MSC evaluated in this study did not treat every RA disease parameter tested, they did provide significant improvements in macroscopic (clinical scores) and microscopic (histology) pathophysiology, and reduced systemic levels of key inflammatory cytokines related the RA. It is important to consider the application of cell therapies to disease as a supplement rather than a replacement to drug-based treatments. In many drug-resistant cases of autoimmune disease, MSC may provide a chance at treatment, where there is none. In RA patients which respond partially to drug treatments, MSC may provide an additional treatment option or alternative that might be less immunosuppressive or have as severe side effects as the current standard drug treatments Methotrexate and TNF-  $\alpha$  blockers.

A single intravenous infusion of BX-U001 hUC-MSC, can significantly relieve RA disease symptoms, in a CIA mouse model. hUC-MSC decreased clinical scores, histological scores, and reduced serum levels of pro-inflammatory cytokines, indicating they have significant clinical potential. This new cell product showed no signs of adverse effects and will be further tested for safety and efficacy in clinical studies with human patients. The limitations of drug-based treatments may be overcome or at least supplemented by cell therapies, such as hUC-MSC.

## 6.6 Supplemental Materials



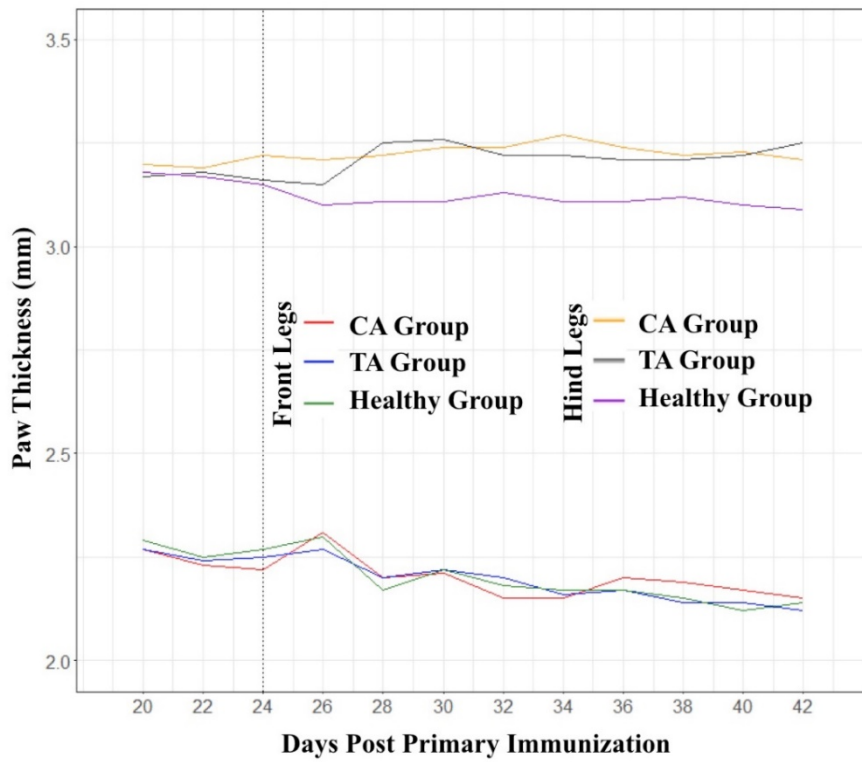
**Supplemental Figure 6.1. Mean body weight of each experimental group from Day 20 to Day 42. TA Group: n = 21, CA Group: n = 20, Healthy Group: n = 7. hUC-MSC were infused on Day 24 (dash line).**



**Supplemental Figure 6.2. Average clinical score of each experimental group from Day 20 to Day 42 (two batches combined). TA Group: n = 21, CA Group: n = 20, Healthy Group: n = 7. hUC-MSC was infused on Day 24 (dash line).**



**Supplemental Figure 6.3. Representative pictures of mouse paws from each experimental group.**



**Supplemental Figure 6.4. Paw thickness of front and hind legs for each experimental group (two batches combined). TA Group: n = 21, CA Group: n = 20, Healthy Group: n = 7. hUC-MSC were infused on Day 24 (dash line).**



**Supplemental Table 6.1. Comparison (TA vs. CA) on clinical score on Day 24 (Estimate = TA - CA).**

| Batch    | Estimate | 95% Confidence Interval | P Value |
|----------|----------|-------------------------|---------|
| Combined | -0.43    | (-0.98, 0.11)           | 0.126   |
| Batch 1  | -0.56    | (-1.39, 0.26)           | 0.194   |
| Batch 2  | -0.30    | (-1.04, 0.44)           | 0.435   |

**Supplemental Table 6.2. Batch 1 Clinical scores (Mean  $\pm$  SD).**

| Time point | TA Group (n = 11) | CA Group (n = 10) | Healthy Group (n = 4) |
|------------|-------------------|-------------------|-----------------------|
| Baseline   | 0 $\pm$ 0         | 0 $\pm$ 0         | 0 $\pm$ 0             |
| Day 20     | 4.93 $\pm$ 1.06   | 5.39 $\pm$ 0.75   | 0 $\pm$ 0             |
| Day 22     | 6.40 $\pm$ 1.03   | 6.22 $\pm$ 0.96   | 2.06 $\pm$ 2.38       |
| Day 24     | 7.40 $\pm$ 0.83   | 7.72 $\pm$ 0.59   | 0.75 $\pm$ 1.50       |
| Day 26     | 7.38 $\pm$ 1.02   | 8.11 $\pm$ 0.79   | 1.50 $\pm$ 1.91       |
| Day 28     | 6.98 $\pm$ 1.38   | 8.36 $\pm$ 0.78   | 1.69 $\pm$ 2.11       |
| Day 30     | 6.68 $\pm$ 1.76   | 8.69 $\pm$ 1.09   | 0.94 $\pm$ 1.09       |
| Day 32     | 6.38 $\pm$ 2.35   | 9.19 $\pm$ 1.05   | 1.88 $\pm$ 2.07       |
| Day 34     | 5.90 $\pm$ 2.24   | 9.06 $\pm$ 1.35   | 1.25 $\pm$ 1.50       |
| Day 36     | 6.05 $\pm$ 2.60   | 9.67 $\pm$ 1.27   | 0.38 $\pm$ 0.25       |
| Day 38     | 5.33 $\pm$ 2.92   | 9.92 $\pm$ 1.26   | 0.31 $\pm$ 0.24       |
| Day 40     | 4.65 $\pm$ 2.77   | 9.83 $\pm$ 1.02   | 0.19 $\pm$ 0.38       |
| Day 42     | 4.00 $\pm$ 2.92   | 9.44 $\pm$ 1.48   | 0.06 $\pm$ 0.13       |

**Supplemental Table 6.3. Batch 2 Clinical scores (Mean  $\pm$  SD).**

| Time point | TA Group (n = 10) | CA Group (n = 10) | Healthy Group (n = 3) |
|------------|-------------------|-------------------|-----------------------|
| Baseline   | 0 $\pm$ 0         | 0 $\pm$ 0         | 0 $\pm$ 0             |
| Day 20     | 2.54 $\pm$ 0.98   | 2.22 $\pm$ 0.57   | 0 $\pm$ 0             |
| Day 22     | 2.75 $\pm$ 0.79   | 2.94 $\pm$ 1.04   | 0.13 $\pm$ 0.18       |
| Day 24     | 6.69 $\pm$ 0.92   | 7.11 $\pm$ 0.81   | 0 $\pm$ 0             |
| Day 26     | 6.97 $\pm$ 0.92   | 7.61 $\pm$ 0.79   | 0.25 $\pm$ 0.35       |
| Day 28     | 6.56 $\pm$ 0.78   | 8.36 $\pm$ 1.32   | 0.25 $\pm$ 0.35       |
| Day 30     | 6.41 $\pm$ 1.80   | 8.58 $\pm$ 0.59   | 0 $\pm$ 0             |
| Day 32     | 5.81 $\pm$ 1.80   | 8.67 $\pm$ 0.86   | 0 $\pm$ 0             |
| Day 34     | 5.28 $\pm$ 2.36   | 8.33 $\pm$ 0.95   | 0.50 $\pm$ 0.71       |
| Day 36     | 4.38 $\pm$ 3.00   | 8.06 $\pm$ 1.35   | 0 $\pm$ 0             |
| Day 38     | 4.59 $\pm$ 3.34   | 8.36 $\pm$ 1.08   | 0 $\pm$ 0             |
| Day 40     | 4.69 $\pm$ 3.45   | 7.92 $\pm$ 1.21   | 0 $\pm$ 0             |
| Day 42     | 4.41 $\pm$ 3.73   | 7.64 $\pm$ 1.29   | 0 $\pm$ 0             |

**Supplemental Table 6.4. Paw thickness (front vs. hind) after hUC-MSC infusion (Mean and 95% CI)**

| Front      |                   |                   |                     |         |
|------------|-------------------|-------------------|---------------------|---------|
| Time point | TA Group (mm)     | CA Group (mm)     | TA – CA (mm)        | P Value |
| Day 26     | 2.27 (2.09, 2.46) | 2.31 (2.13, 2.50) | -0.04 (-0.10, 0.02) | 0.218   |
| Day 28     | 2.20 (2.14, 2.26) | 2.20 (2.13, 2.26) | 0.00 (-0.09, 0.09)  | 0.992   |
| Day 30     | 2.22 (2.15, 2.29) | 2.21 (2.14, 2.28) | 0.01 (-0.07, 0.09)  | 0.794   |
| Day 32     | 2.20 (2.06, 2.33) | 2.15 (2.02, 2.29) | 0.04 (-0.05, 0.14)  | 0.404   |
| Day 34     | 2.16 (2.04, 2.29) | 2.15 (2.03, 2.28) | 0.01 (-0.10, 0.12)  | 0.879   |
| Day 36     | 2.17 (1.98, 2.35) | 2.20 (2.01, 2.39) | -0.03 (-0.13, 0.07) | 0.525   |
| Day 38     | 2.14 (1.98, 2.31) | 2.19 (2.02, 2.36) | -0.05 (-0.16, 0.06) | 0.390   |
| Day 40     | 2.14 (1.98, 2.29) | 2.17 (2.02, 2.32) | -0.03 (-0.15, 0.08) | 0.560   |
| Day 42     | 2.12 (1.98, 2.27) | 2.15 (2.01, 2.30) | -0.03 (-0.15, 0.09) | 0.632   |
| Hind       |                   |                   |                     |         |
| Time point | TA Group (mm)     | CA Group (mm)     | TA – CA (mm)        | P Value |
| Day 26     | 3.15 (2.97, 3.34) | 3.21 (3.02, 3.40) | -0.06 (-0.12, 0.01) | 0.085   |
| Day 28     | 3.25 (3.19, 3.31) | 3.22 (3.16, 3.28) | 0.03 (-0.05, 0.12)  | 0.474   |
| Day 30     | 3.26 (3.19, 3.33) | 3.24 (3.17, 3.31) | 0.01 (-0.07, 0.09)  | 0.715   |
| Day 32     | 3.22 (3.09, 3.36) | 3.24 (3.10, 3.37) | -0.01 (-0.11, 0.08) | 0.819   |
| Day 34     | 3.22 (3.10, 3.35) | 3.27 (3.14, 3.39) | -0.04 (-0.15, 0.07) | 0.451   |
| Day 36     | 3.21 (3.02, 3.40) | 3.24 (3.05, 3.43) | -0.03 (-0.13, 0.07) | 0.598   |
| Day 38     | 3.21 (3.04, 3.38) | 3.22 (3.05, 3.38) | 0.00 (-0.11, 0.10)  | 0.935   |
| Day 40     | 3.22 (3.07, 3.38) | 3.23 (3.07, 3.38) | 0.00 (-0.12, 0.11)  | 0.932   |
| Day 42     | 3.25 (3.11, 3.39) | 3.21 (3.06, 3.36) | 0.04 (-0.08, 0.16)  | 0.512   |

**Supplemental Table 6.5. Paw thickness after hUC-MSC infusion (Mean and 95% CI)**

| Time point | TA Group (mm)     | CA Group (mm)     | TA – CA (mm)        | P Value |
|------------|-------------------|-------------------|---------------------|---------|
| Day 26     | 2.71 (2.52, 2.91) | 2.76 (2.56, 2.96) | -0.05 (-0.19, 0.09) | 0.509   |
| Day 28     | 2.72 (2.61, 2.84) | 2.71 (2.59, 2.83) | 0.02 (-0.15, 0.19)  | 0.854   |
| Day 30     | 2.74 (2.62, 2.86) | 2.72 (2.60, 2.85) | 0.01 (-0.16, 0.18)  | 0.874   |
| Day 32     | 2.71 (2.55, 2.87) | 2.69 (2.54, 2.85) | 0.02 (-0.16, 0.19)  | 0.860   |
| Day 34     | 2.69 (2.55, 2.84) | 2.71 (2.56, 2.86) | -0.02 (-0.20, 0.17) | 0.871   |
| Day 36     | 2.69 (2.49, 2.89) | 2.72 (2.51, 2.92) | -0.03 (-0.21, 0.15) | 0.746   |
| Day 38     | 2.68 (2.50, 2.86) | 2.70 (2.52, 2.88) | -0.03 (-0.21, 0.15) | 0.785   |
| Day 40     | 2.68 (2.51, 2.85) | 2.70 (2.53, 2.87) | -0.02 (-0.20, 0.17) | 0.845   |
| Day 42     | 2.69 (2.53, 2.85) | 2.68 (2.52, 2.84) | 0.01 (-0.18, 0.19)  | 0.946   |

**Supplemental Table 6.6. Difference in TA vs TA mean body weights prior to CIA induction (Day 24).**

| Estimate (g) | 95% Confidence Interval | P Value |
|--------------|-------------------------|---------|
| 0.15         | (-0.83, 1.12)           | 0.769   |

**Supplemental Table 6.7. Comparison of body weight in TA and CA groups after hUC-MSc infusion (Mean and 95% CI).**

| Time point | TA Group (g)         | CA Group (g)         | TA – CA (g)         | P Value |
|------------|----------------------|----------------------|---------------------|---------|
| Day 26     | 21.03 (19.31, 22.74) | 20.86 (19.14, 22.59) | 0.16 (-0.77, 1.10)  | 0.735   |
| Day 28     | 21.20 (19.78, 22.61) | 21.26 (19.84, 22.68) | -0.06 (-0.96, 0.83) | 0.890   |
| Day 30     | 22.10 (21.04, 23.15) | 22.11 (21.04, 23.18) | -0.01 (-0.93, 0.90) | 0.976   |
| Day 32     | 21.72 (20.63, 22.81) | 21.70 (20.60, 22.80) | 0.01 (-0.87, 0.90)  | 0.977   |
| Day 34     | 21.89 (21.15, 22.64) | 21.87 (21.11, 22.62) | 0.03 (-0.93, 0.98)  | 0.955   |
| Day 36     | 22.01 (20.84, 23.18) | 21.87 (20.69, 23.05) | 0.13 (-0.79, 1.06)  | 0.776   |
| Day 38     | 21.99 (20.46, 23.52) | 21.93 (20.39, 23.46) | 0.06 (-0.81, 0.93)  | 0.887   |
| Day 40     | 22.17 (21.24, 23.09) | 22.27 (21.34, 23.20) | -0.10 (-0.94, 0.74) | 0.812   |
| Day 42     | 22.50 (21.48, 23.51) | 22.73 (21.70, 23.75) | -0.23 (-1.16, 0.69) | 0.625   |

**6.7 Acknowledgements**

This work was supported by the NIH (R21CA219225 to W.Z.), the DOD (W81XWH-17-1-0522 to W.Z.), and a contract with Baylx Inc. (BI-206512). H.P.F. was supported by the National Institute of Neurological Disorders and Stroke of the NIH (T32NS082174). The content of this paper is solely the responsibility of the authors and does not necessarily represent the official views of the National Institutes of Health.

**6.8 References**

1. Barbour KE. Vital Signs: Prevalence of Doctor-Diagnosed Arthritis and Arthritis-Attributable Activity Limitation — United States, 2013–2015. *MMWR Morb Mortal Wkly Rep.* 2017;66.
2. Hootman JM, Helmick CG, Barbour KE, Theis KA, Boring MA. Updated Projected Prevalence of Self-Reported Doctor-Diagnosed Arthritis and Arthritis-Attributable Activity Limitation Among US Adults, 2015-2040. *Arthritis & Rheumatology (Hoboken, NJ).* 2016;68(7):1582-1587.
3. Gabriel SE, Crowson CS, O'Fallon WM. The epidemiology of rheumatoid arthritis in Rochester, Minnesota, 1955-1985. *Arthritis Rheum.* 1999;42(3):415-420.
4. Costenbader KH, Chang S-C, Laden F, Puett R, Karlson EW. Geographic Variation in Rheumatoid Arthritis Incidence among Women in the United States. *Arch Intern Med.* 2008;168(15):1664-1670.
5. Feldmann M, Brennan FM, Maini RN. Rheumatoid Arthritis. *Cell.* 1996;85(3):307-310.
6. Scott DL, Wolfe F, Huizinga TW. Rheumatoid arthritis. *The Lancet.* 2010;376(9746):1094-1108.
7. Ropes MW, Bennett GA, Cobb S, Jacox R, Jessar RA. 1958 Revision of diagnostic criteria for rheumatoid arthritis. *Arthritis & Rheumatism.* 1959;2(1):16-20.

8. Arnett FC, Edworthy SM, Bloch DA, McShane DJ, Fries JF, Cooper NS, Healey LA, Kaplan SR, Liang MH, Luthra HS. The American Rheumatism Association 1987 revised criteria for the classification of rheumatoid arthritis. *Arthritis Rheum.* 1988;31(3):315-324.
9. Smolen JS, Aletaha D, Redlich K. The pathogenesis of rheumatoid arthritis: new insights from old clinical data? *Nat Rev Rheumatol.* 2012;8(4):235-243.
10. Choy E. Understanding the dynamics: pathways involved in the pathogenesis of rheumatoid arthritis. *Rheumatology (Oxford).* 2012;51(suppl\_5):v3-v11.
11. van der Linden MPM, van der Woude D, Ioan-Facsinay A, Levarht EWN, Stoeken-Rijsbergen G, Huizinga TWJ, Toes REM, van der Helm-van Mil AHM. Value of anti-modified citrullinated vimentin and third-generation anti-cyclic citrullinated peptide compared with second-generation anti-cyclic citrullinated peptide and rheumatoid factor in predicting disease outcome in undifferentiated arthritis and rheumatoid arthritis. *Arthritis Rheum.* 2009;60(8):2232-2241.
12. Kinne RW, Bräuer R, Stuhlmüller B, Palombo-Kinne E, Burmester G-R. Macrophages in rheumatoid arthritis. *Arthritis Res.* 2000;2(3):189-202.
13. Sun W, Zhang H, Wang H, Chiu YG, Wang M, Ritchlin CT, Kiernan A, Boyce BF, Xing L. Targeting Notch-Activated M1 Macrophages Attenuates Joint Tissue Damage in a Mouse Model of Inflammatory Arthritis. *J Bone Miner Res.* 2017;32(7):1469-1480.
14. Culemann S, Grüneboom A, Nicolás-Ávila JA, Weidner D, Lammle KF, Rothe T, Quintana JA, Kirchner P, Krljanac B, Eberhardt M, Ferrazzi F, et al. Locally renewing resident synovial macrophages provide a protective barrier for the joint. *Nature.* 2019;572(7771):670-675.
15. Paoletti A, Rohmer J, Ly B, Pascaud J, Riviere E, Seror R, Le Goff B, Nocturne G, Mariette X. Monocyte/Macrophage Abnormalities Specific to Rheumatoid Arthritis Are Linked to miR-155 and Are Differentially Modulated by Different TNF Inhibitors. *J Immunol.* 2019;203(7):1766-1775.
16. Oosterhout M van, Bajema I, Levarht EWN, Toes REM, Huizinga TWJ, Laar JM van. Differences in synovial tissue infiltrates between anti-cyclic citrullinated peptide-positive rheumatoid arthritis and anti-cyclic citrullinated peptide-negative rheumatoid arthritis. *Arthritis & Rheumatism.* 2008;58(1):53-60.
17. Vossenaar ER, Smeets TJM, Kraan MC, Raats JM, Venrooij WJV, Tak PP. The presence of citrullinated proteins is not specific for rheumatoid synovial tissue. *Arthritis & Rheumatism.* 2004;50(11):3485-3494.
18. van der Helm-van Mil AH, Verpoort KN, Breedveld FC, Toes RE, Huizinga TW. Antibodies to citrullinated proteins and differences in clinical progression of rheumatoid arthritis. *Arthritis Res Ther.* 2005;7(5):R949-R958.
19. Bjarnason I, Hayllar J, MacPherson AJ, Russell AS. Side effects of nonsteroidal anti-inflammatory drugs on the small and large intestine in humans. *Gastroenterology.* 1993;104(6):1832-1847.
20. Le Blanc K, Frassoni F, Ball L, Locatelli F, Roelofs H, Lewis I, Lanini E, Sundberg B, Bernardo ME, Remberger M, Dini G, et al. Mesenchymal stem cells for treatment of steroid-resistant, severe, acute graft-versus-host disease: a phase II study. *The Lancet.* 2008;371(9624):1579-1586.
21. Fan C-G, Zhang Q, Zhou J. Therapeutic Potentials of Mesenchymal Stem Cells Derived from Human Umbilical Cord. *Stem Cell Rev and Rep.* 2011;7(1):195-207.
22. Liu L, Wong CW, Han M, Farhoodi HP, Liu G, Liu Y, Liao W, Zhao W. Meta-analysis of preclinical studies of mesenchymal stromal cells to treat rheumatoid arthritis. *EBioMedicine.* 2019;47:563-577.
23. Chandrashekhara S. The treatment strategies of autoimmune disease may need a different approach from conventional protocol: A review. *Indian J Pharmacol.* 2012;44(6):665-671.
24. Ghannam S, Bouffi C, Djouad F, Jorgensen C, Noël D. Immunosuppression by mesenchymal stem cells: mechanisms and clinical applications. *Stem Cell Res Ther.* 2010;1(1):2.
25. Lu LL, Liu YJ, Yang SG, Zhao QJ, Wang X, Gong W, Han ZB, Xu ZS, Lu YX, Liu D, Chen ZZ, Han ZC. Isolation and characterization of human umbilical cord mesenchymal stem cells with hematopoiesis-supportive function and other potentials. *Haematologica.* 2006;91(8):1017-1026.
26. Pietrosimone KM, Jin M, Poston B, Liu P. Collagen-Induced Arthritis: A model for Murine Autoimmune Arthritis. *Bio Protoc.* 2015;5(20).
27. Liu H, Ding J, Wang J, Wang Y, Yang M, Zhang Y, Chang F, Chen X. Remission of Collagen-Induced Arthritis through Combination Therapy of Microfracture and Transplantation of Thermogel-Encapsulated Bone Marrow Mesenchymal Stem Cells. *PLOS ONE.* 2015;10(3):e0120596.
28. Tyndall A. Mesenchymal stem cell treatments in rheumatology—a glass half full? *Nature Reviews Rheumatology.* 2014;10(2):117-124.

29. Wang L, Wang L, Cong X, Liu G, Zhou J, Bai B, Li Y, Bai W, Li M, Ji H, Zhu D, et al. Human Umbilical Cord Mesenchymal Stem Cell Therapy for Patients with Active Rheumatoid Arthritis: Safety and Efficacy. *Stem Cells and Development*. 2013;22(24):3192-3202.
30. Wang L, Zhang Y, Li H, Hong J, Chen X, Li M, Bai W, Wang J, Liu Y, Wu M. Clinical Observation of Employment of Umbilical Cord Derived Mesenchymal Stem Cell for Juvenile Idiopathic Arthritis Therapy. *Stem Cells International*.
31. Liang J, Li X, Zhang H, Wang D, Feng X, Wang H, Hua B, Liu B, Sun L. Allogeneic mesenchymal stem cells transplantation in patients with refractory RA. *Clin Rheumatol*. 2012;31(1):157-161.
32. Álvaro-Gracia JM, Jover JA, García-Vicuña R, Carreño L, Alonso A, Marsal S, Blanco F, Martinez-Taboada VM, Taylor P, Martin-Martin C, DelaRosa O, et al. Intravenous administration of expanded allogeneic adipose-derived mesenchymal stem cells in refractory rheumatoid arthritis (Cx611): results of a multicentre, dose escalation, randomised, single-blind, placebo-controlled phase Ib/IIa clinical trial. *Annals of the Rheumatic Diseases*. 2017;76(1):196-202.
33. Zhou B, Yuan J, Zhou Y, Ghawji M, Deng YP, Lee AJ, Lee AJ, Nair U, Kang AH, Brand DD, Yoo TJ. Administering human adipose-derived mesenchymal stem cells to prevent and treat experimental arthritis. *Clinical Immunology*. 2011;141(3):328-337.
34. Garimella MG, Kour S, Piprode V, Mittal M, Kumar A, Rani L, Pote ST, Mishra GC, Chattopadhyay N, Wani MR. Adipose-Derived Mesenchymal Stem Cells Prevent Systemic Bone Loss in Collagen-Induced Arthritis. *J Immunol*. 2015;195(11):5136-5148.
35. Welsing PMJ, Gestel AMV, Swinkels HL, Kiemeny LALM, Riel PLCMV. The relationship between disease activity, joint destruction, and functional capacity over the course of rheumatoid arthritis. *Arthritis & Rheumatism*. 2001;44(9):2009-2017.
36. Ødegård S, Landewé R, Heijde D van der, Kvien TK, Mowinckel P, Uhlig T. Association of early radiographic damage with impaired physical function in rheumatoid arthritis: A ten-year, longitudinal observational study in 238 patients. *Arthritis & Rheumatism*. 2006;54(1):68-75.
37. Smolen JS, Aletaha D, Redlich K. The pathogenesis of rheumatoid arthritis: new insights from old clinical data? *Nature Reviews Rheumatology*. 2012;8(4):235-243.
38. Vasandan AB, Jahnvi S, Shashank C, Prasad P, Kumar A, Prasanna SJ. Human Mesenchymal stem cells program macrophage plasticity by altering their metabolic status via a PGE 2 -dependent mechanism. *Scientific Reports*. 2016;6(1):38308.
39. Weiss ARR, Dahlke MH. Immunomodulation by Mesenchymal Stem Cells (MSCs): Mechanisms of Action of Living, Apoptotic, and Dead MSCs. *Front Immunol*. 2019;10.
40. De Witte SFH, Luk F, Parraga JMS, Gargasha M, Merino A, Korevaar SS, Shankar AS, O'Flynn L, Elliman SJ, Roy D, Betjes MGH, et al. Immunomodulation By Therapeutic Mesenchymal Stromal Cells (MSC) Is Triggered Through Phagocytosis of MSC By Monocytic Cells. *STEM CELLS*. 2018;36(4):602-615.
41. Luk F, De Witte SFH, Korevaar SS, Roemeling-van Rhijn M, Franquesa M, Strini T, van den Engel S, Gargasha M, Roy D, Dor FJMF, Horwitz EM, et al. Inactivated Mesenchymal Stem Cells Maintain Immunomodulatory Capacity. *Stem Cells and Development*. 2016;25(18):1342-1354.
42. Gonçalves F da C, Luk F, Korevaar SS, Bouzid R, Paz AH, Lopez-Iglesias C, Baan CC, Merino A, Hoogduijn MJ. Membrane particles generated from mesenchymal stromal cells modulate immune responses by selective targeting of pro-inflammatory monocytes. *Sci Rep*. 2017;7.

# **CHAPTER 7**

## **Summary**

### **Developing a highly effective and consistent mouse model of bone metastasis.**

Due to the limitations of other injection routes, to develop bone metastasis in mice, the caudal artery delivery method described by Kuchimaru et al. should become the new standard of delivering cells to the bones via the circulatory system. Here I described, in more detail, a simple and effective way to generate syngeneic breast cancer bone metastasis in a mouse model. For perfectly executed caudal artery model inductions, I was able to get bone metastasis rates over 95%. These metastases were not only consistent in their sizes, but also in their locations. There were few metastases to vital organs, which further improved the experimental consistency, since mice maintained their health longer and did not need sacrificing before the planned experimental endpoint. The consistency of this model allows a reduction in both the total number of animals used, and the costs relating to syngeneic bone metastasis studies. Consistency also increases the robustness of therapeutic studies, because it allows more homogenous grouping of experimental animals.

### **Developing a combinatorial method to treat bone metastasis and the tumor micro-environment.**

This research demonstrates a new strategy using mRNA-engineered stem cells for combinatorial targeting and delivery of multiple factors to interrogate both cancer cells and the metastatic niche in treating bone metastases. This technology for combinatorial targeting could be extended to other types of systemic bone metastases and skeletal disorders including prostate cancer bone metastasis, multiple myeloma, and osteoporosis. As a platform technology, our system can be used to deliver other pro-drug systems, or combinations of pro-drug systems shown to be synergistic. As a facile RNA delivery tool, this technology could potentially be used for simultaneous delivery of next-generation genome editing components (e.g., Cas9 mRNA and guide RNAs in CRISPR) in molecular biology and gene therapy.

### **Evaluating Human Umbilical Cord MSC (hUC-MSC) to treat inflammatory bowel disease.**

A single tail vein injection of BX-U001 hUC-MSC is efficacious for the treatment of TNBS-induced murine colitis, a classic animal model for IBD in humans. The results from this preclinical study

supported an FDA IND submission, and the therapeutic potential and safety of an hUC-MSc infusion to treat IBD patients will be further evaluated in a future clinical trial.

### **Meta-analysis of MSC treatment studies for rheumatoid arthritis.**

A meta-analysis of pre-clinical treatment studies using MSC to treat rheumatoid arthritis. To the best of my knowledge, this meta-analysis is to quantitatively answer whether MSC represent a robust RA treatment option in animal models. It suggests that in preclinical studies in RA animal models, MSC have consistently exhibited therapeutic benefits based on clinical scores, histological scores and paw thickness. These findings were also robust after correction of publication bias. There were considerable efficacy variations, across donor and recipient species, routes of administration, MSC tissue of origin, timing of MSC introduction, transplant types, dosage of MSC administration and number of injections. These findings demonstrate the need for considering variations in different animal models and treatment protocols in future studies using MSC to treat RA in humans, to maximize the therapeutic gains in the era of precision medicine.

### **Evaluating Human Umbilical Cord MSC (hUC-MSc) to treat rheumatoid arthritis.**

A single intravenous infusion of BX-U001 hUC-MSc, can significantly relieve RA disease symptoms, in a CIA mouse model. hUC-MSc decreased clinical scores, histological scores, and reduced serum levels of pro-inflammatory cytokines, indicating they have significant clinical potential. This new cell product showed no signs of adverse effects and will be further tested for safety and efficacy in clinical studies with human patients. The limitations of drug-based treatments may be overcome or at least supplemented by cell therapies, such as hUC-MSc.